Paleomagnetic studies of hyaloclastite mountains, indications of duration of buildup

Einar Ragnar Sigurðsson

Faculty of Earth Sciences
University of Iceland
2019

Paleomagnetic studies of hyaloclastite mountains, indications of duration of buildup

Einar Ragnar Sigurðsson

60 ECTS thesis submitted in partial fulfillment of a
Magister Scientiarum degree in Geophysics

Advisors
Leo Kristjansson
Magnus Tumi Gudmundsson

Master's Examiner
Haraldur Audunsson

Faculty of Earth Sciences
School of Engineering and Natural Sciences
University of Iceland
Reykjavik, October 2019

Paleomagnetic studies of hyaloclastite mountains, indications of duration of buildup

60 ECTS thesis submitted in partial fulfillment of a *Magister Scientiarum* degree in Geophysics

Faculty of Earth Sciences
School of Engineering and Natural Sciences
University of Iceland
Sturlugata 7
101 Reykjavik
Iceland

Telephone: 525 4000

Bibliographic information:
Einar Ragnar Sigurðsson, 2019. *Paleomagnetic studies of hyaloclastite mountains, indications of duration of buildup*. Master's thesis, Faculty of Earth Sciences, University of Iceland, pp.166.

Printing: Háskólaprent
Reykjavik, Iceland, October 2019

Abstract

Paleomagnetic measurements were used to estimate the buildup time of hyaloclastite mountains such as tuyas. Tuyas are in general built up of a pillow lava under hyaloclastite, both formed in an underwater eruption. Above the hyaloclastite is a flow-foot breccia and a cap lava formed in a subaerial eruption. From the difference of measured paleomagnetic directions in the lava formations it is possible the estimate the minimum build-up time of the mountain.

The research was done on the tuya Hlöðufell in Icelandic West Volcanic Zone, south of Langjökull. Results showed a considerable difference of paleomagnetic directions, or a 36° cumulative change from the pillow lava to the highest cap lava. Considering that the likely maximum 5° change of magnetic direction in one century, this indicates a minimum of 700 years for the formation of Hlöðufell. However, the results are not unambiguous since most of the difference occurs between the pillow lava at the base to the lowermost cap lava and from there to the higher cap lavas. Other explanations for the changes in measured paleomagnetic directions are possible, such as rotation of the lava blocks. More paleomagnetic measurements could help in narrowing the range of possible scenarios. However, the inaccessibility of the unmeasured lavas would make such surveys very difficult.

Prior to this research, only two lava benches had been identified. In this research a clear lava bench was identified on the north terrace of the mountain underlain by what appears to be a flow-foot breccia. Several other, not as clear, smaller lava benches were also identified. This includes the south terrace where detailed analysis of the formations is required to decide on the true nature of these suspected lava benches.

Útdráttur

Í þessari rannsókn voru bergsegulmælingar notaðar til að varpa ljósi á hve langan tíma myndun móbergsstapa getur tekið. Móbergsstapar eru almennt byggðir upp af bólstrabergi og móbergi þar ofan á sem myndast við eldgos undir vatni. Ofan á móberginu er hraunfótsbreksía og hraunskjöldur sem hefur runnið þegar eldgosið hefur náð uppúr vatninu. Út frá mun á mældum segulstefnum í hraununum má meta líklegan lágmarks myndunartíma fjallsins.

Bergsegulmælingar voru gerðar á móbergsstapanum Hlöðufelli á vestara gosbeltinu, sunnan Langjökuls. Niðurstöður sýndu talsverðan mun á segulstefnum eða 36° uppsafnaða breytingu í misvísun frá bólstraberginu til efsta hraunlagsins. Miðað við að segulstefna breytist um 5° á öld, má gera ráð fyrir að Hlöðufell hafi myndast á a.m.k. 700 árum. Niðurstöður eru samt ekki ótvíræðar því stærstur hluti breytinga á segulstefnum er frá bólstraberginu og að neðri hluta neðri hraunstalls fjallsins og aftur að efri hraunlögum þess. Aðrar orsakir fyrir þessum breytingum á bergsegulstefnum eru mögulegar svo sem að hraunblokkir hafi færst til. Til að ganga úr skugga um það væri hægt að gera víðtækari bergsegulmælingar á neðri hluta neðri hraunstalls Hlöðufells en þó er á það bent að þau hraunlög eru ekki aðgengileg til slíkra mælinga.

Áður hafði Hlöðufelli verið lýst svo að þar væru tveir hraunstallar. Í athugunum sem voru gerðar í þessari rannsókn komu fram einn mjög greinilegur hraunstallur að auki á norðurhluta fjallsins ásamt líklegri hraunfótsbreksíu. Þar komu einnig fram nokkrar minna áberandi hraunbrúnir. Á suðurstalli fjallsins má einnig greina sambærilegar hraunbrúnir.

Dedication

This work is dedicated to my parents:
Hrefna Einarsdóttir and Sigurður Gunnarsson.

Table of Contents

List of Figures

List of Tables

Acknowledgements

My work on this thesis would not have been possible without great help from other people. First I would like to thank my supervisors, Leó Kristjánsson and Magnús Tumi Guðmundsson for their generous support through the project, their patience and the fact that they never lost their believe in me to finish this work.

From the comprehensive field work I thank Gunnar Sigurðsson, Haraldur Gunnarsson and Höskuldur Björnsson for all their support. They had to carry most of the heavy equipment for me up to the mountain several times, when I was injured and not able to carry the equipment with me. I also thank Ragnhildur Hrönn Sigurðardóttir for assistance in field work in Undirhlíðar and Hrefna Einarsdóttir who rescued me when my my car broke down in one of the field trips.

Then I thank Marteinn Sigurðsson for allowance to use his maps from iskort.is, used in the thesis.

Finally I would like to thank the external examiner, Haraldur Auðunsson for his contribution during the MS exam and very helpful suggestions for final corrections and improvements of the thesis.

1 Introduction

The main research question in this study is to find out if it is possible to estimate the minimum build up time of a hyaloclastite mountain from difference of measured paleomagnetic directions in the mountain's lava formations.

Paleomagnetic research has mostly be done in lava fields where several lavas are accessible in stratigraphical order and also sediment rock. In this research, paleomagnetic research was done in a hyaloclastite volcano, trying to find out if it was possible to get some indication of the duration of buildup of the mountain.

The main research area was the tuya Hlöðufell in the west volcanic zone in Iceland, south of the glacier Langjökull but study area was also in a quarry in Reykjanes peninsula volcanic belt. The part taken place in Undirhlíðar was mostly to get familiar with the methods of paleomagnetic core sampling, measurements and calculation of the paleomagnetic directions. The results of the paleomagnetic measurements in Undirhlíðar are in Appendix L.

The work in Undirhlíðar took place in the summer 2014 and the fieldwork in Hlöðufell area began in the autumn, same year. A couple of accidents I had in the following month were affecting the speed of the research work but total number of field trips to Hlöðufell was 15 on 20 days in total.

Remanent magnetization of the sample cores was measured with equipment in the paleomagnetic laboratory in the University of Iceland.

2 Magnetic theory

2.1.1 The magnetic field, formulas

An electric current **i** in a straight wire produces magnetic field **H** in a distance r_w from the wire as shown in Figure 2-1, described by Ampere's law:

$$H = \frac{i}{2\pi r_w} \qquad \textit{eq. 2-1}$$

Since the current **i** is in Amperes and radius r_w is in meters, the dimensions of the SI unit for magnetic field **H** are A/m,

If the wire is bent in a loop as shown in Figure 2-1 (B) it produces a dipole magnetic field as a permanent magnet. The magnitude of the dipole moment is proportional to the current, number of loops (n) and the area of the loop (πr^2):

$$m = ni\pi r^2 \quad , \qquad \textit{eq. 2-2}$$

with SI unit for magnetic moment m: Am^2 (Tauxe, 2010).

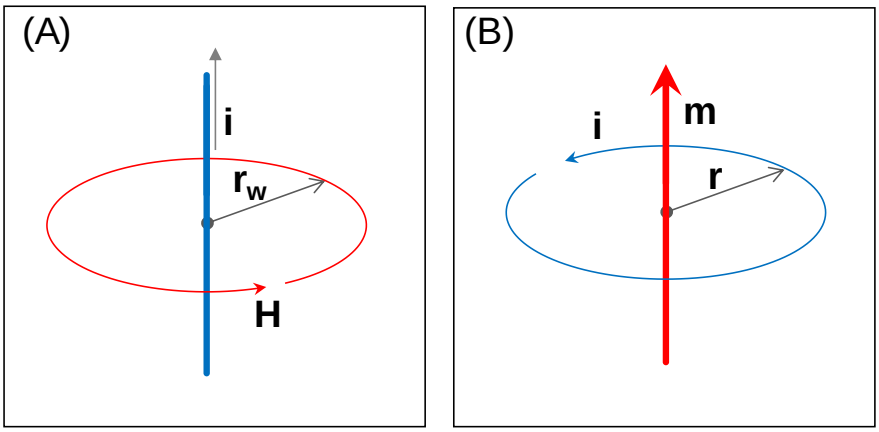

*Figure 2-1. (A) Electric current i in a straight wire creating a magnetic field, **H**. (B) A wire with a current i bent in a loop producing a magnetic moment, **m**. Figures modified from Tauxe (2010).*

The magnetic field is a vector field since it has both magnitude and direction in each point as shown in Figure 2-2. The magnetic field lines represent the magnetic flux Φ which is measured in its own unit Weber (Wb, equals Volt seconds) but the density of the lines represents the strength of the magnetic field, the magnetic induction, **B**.

The unit of magnetic induction **B** is called Tesla (T) and can be described from an electric conductor that is moving at a steady speed in a magnetic field leading to induced electric potential in the conductor. The unit Tesla is the strength of induced magnetic field required to make 1 Volt electric potential in a 1-meter long conductor moving at 1 m/s speed. So, the unit Tesla is equivalent to $[\,V/(m \cdot m/s)\,] = [\,V\,s\,m^{-2}\,] = [\,T\,]$ (Tauxe, 2010).

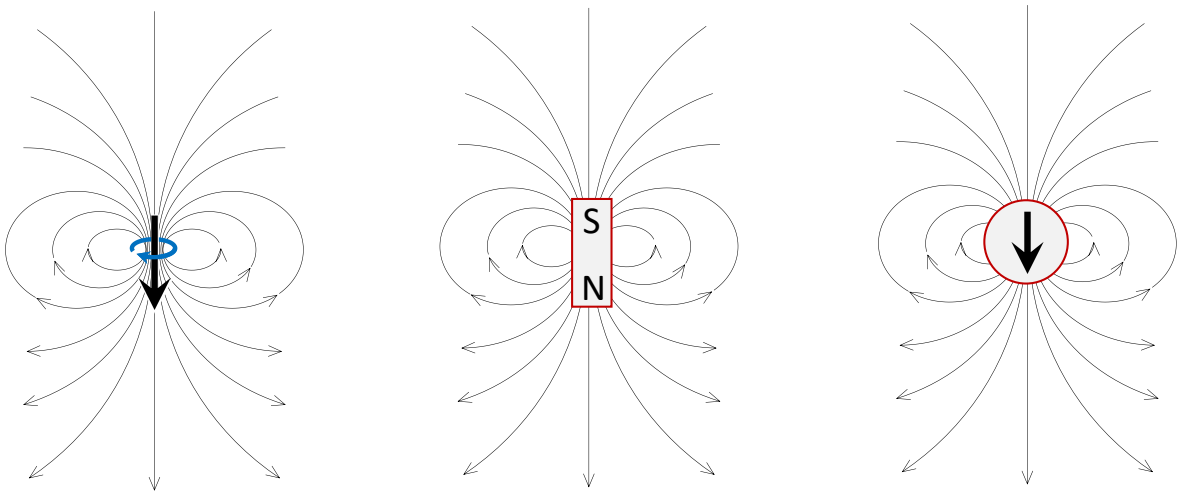

Figure 2-2. The magnetic dipole, showing how the magnetic field lines are identical to that of a magnetic dipole for (a) a small electric current loop, (b) small bar magnet and (c) uniformly magnetized sphere, when all have the same magnetic dipole moment. Figures modified from Lowrie (2007), Kearey, Brooks and Hill (2002) and Sharma (1986).

The magnetization, **M,** is magnetic moment of a body normalized with volume and is given by:

$$\boldsymbol{M} = \frac{\boldsymbol{m}}{V} \qquad \textit{eq. 2-3}$$

From that equation unit for magnetization (**M**) is [Am^2 / m^3] = [A/m] but that is the same unit as was used for the magnetic field, **H**. The magnetization is induced in the material ($\mathbf{M_I}$) or remanent ($\mathbf{M_R}$). The letter **J** may also occasionally be used as a symbol for magnetization.

The relation between magnetization of a material **M** and the magnetic field **H** is that when a magnetic material is in an external magnetic field, the charges in the atoms of the material, the protons and the electrons respond to the external field. This is described with magnetic susceptibility, χ:

$$\boldsymbol{M_I} = \chi \boldsymbol{H} \qquad \textit{eq. 2-4}$$

Since the units for magnetization and magnetic field are the same, the bulk susceptibility χ is non-dimensional. Magnetic moment can also be normalized by mass but mass susceptibility is no longer dimensionless.

The induced magnetic field inside a medium is **B** and **H** describes how **B** is modified by the magnetization **M**. The relationship between them is given by the equation:

$$\boldsymbol{B} = \mu_0(\boldsymbol{H} + \boldsymbol{M}) = \mu \boldsymbol{H} \qquad \textit{eq. 2-5}$$

where μ is permeability, a physical constant of the medium. The field **H** has been referred to as the *magnetizing field*. (Lowrie, 2007). For most cases in paleomagnetic studies, the field is measured outside the magnetized material where **M** = 0, and the permeability is that of vacuum μ_0. The equation then simplifies to

$$\boldsymbol{B} = \mu_0 \boldsymbol{H} \qquad \textit{eq. 2-6}$$

The permeability of vacuum has the value $\mu_0 = 4\pi\times10^{-7}$ H/m, where H stands for the unit Henry. Also, to be noticed that H/m can be expressed as Wb/A.

2.2 Magnetization of rocks

2.2.1 Types of magnetism

Magnetism of a material is caused by the movement of the electrons in the atoms. There are two sources of magnetism at atomic level that derive respectively from the orbital movement of the electrons and from the spin movements of electrons.

Diamagnetism

According to classical theory, all electrons in an atom have orbital angular momentum and a corresponding magnetic moment. The movement of each electron gives magnetic moment ($\mathbf{m_b}$) but while they are randomly oriented they do not give any net magnetic moment of the material.

On the other hand, if the material is placed in an external magnetic field the angular movement of the orbiting electron starts to precess around the magnetic directions like a spinning top precesses around the direction of gravity. This changes the magnetic moment of the electron so that it opposes the applied field. This is called diamagnetism and is a property of all materials. It is negative (opposite direction to the applied external magnetic field), temperature independent property of all materials but very small. It can be expressed by the equation:

$$\boldsymbol{M}_I = \chi_d \boldsymbol{H} \ , \qquad \textit{eq. 2-7}$$

where χ_d is *diamagnetic susceptibility*. Some rock forming minerals have only this type of magnetism, such as quartz and calcite. Their susceptibility is close to -10^{-6} in SI units (Tauxe, 2010; Lowrie, 2007).

Paramagnetism

The spin of each electron generates also a magnetic moment. Most of the electrons are paired with magnetic moments from spin in opposite directions so the net magnetic moment will be zero from each pair. Depending on various conditions electrons can be unpaired and then have an uncompensated magnetic moment. While the directions of the moments are randomly distributed, they will give no net magnetic moment. But as with the orbital movement they respond to an external magnetic field creating a net magnetic moment,

$$\boldsymbol{M}_I = \chi_p \boldsymbol{H} \ , \qquad \textit{eq. 2-8}$$

where χ_p is *paramagnetic susceptibility*. The paramagnetic susceptibility varies inversely with temperature, with $\chi_p = C/T$ where T is temperature in Kelvin and C is a constant for the material. At room temperature, paramagnetic susceptibility of common minerals such as chlorite, amphibolite, pyroxene and olivine is around 10^{-5} to 10^{-4} in SI units, which is 10 to 100 times larger than the negative value of diamagnetism (Tauxe, 2010; Lowrie, 2007).

Ferromagnetism

In some metals and metal oxides, the lattice crystal structure places the atoms so close to each other that the magnetic moments of the atoms can interact with each other. The energy involved is called *exchange energy* which is minimized when the spins are aligned parallel or anti-parallel depending on the details of the crystal structure.

In metals such as iron, nickel and cobalt the magnetic moments align exactly parallel and create very strong total magnetic moment, known as *true ferromagnetism* or *ferromagnetism sensu stricto*, see Figure 2-3a.

The 3d orbitals of atoms are particularly susceptible to the exchange interactions both because of the shape of the orbits and the amount of unpaired spins occurring in some oxides. The oxygen atoms can form a bridge between neighboring cations which are otherwise too far apart for direct overlap of the 3d orbitals but become coupled through the oxygen atom. While the atoms connected are not with the same charges the coupling will be antiparallel. Then the magnetic moments will point in opposite directions and cancel each other out, see Figure 2-3b. The material does not have net magnetic moment from the spins of electrons and is called *antiferromagnetic*. Ilmenite ($FeTiO_3$) is an important example of antiferromagnetic mineral (Lowrie, 2007; Tauxe, 2010).

In some minerals there are the magnetic moments from the spins are not exactly antiparallel but inclined at a small angle. The net magnetic moment of that kind of a material will be sidewise and referred to as *parasitic antiferromagnetism* or *spin-canted antiferromagnetism*, see Figure 2-3c. An important example of parasitic antiferromagnetic mineral is Hematite (Fe_2O_3).

If an antiferromagnetic material has defects in the crystals there can be unpaired spins, creating a very weak net magnetic moment parallel to the direction of the moments of the spins, known as *defect ferromagnetism* (Lowrie, 2007; Tauxe, 2010).

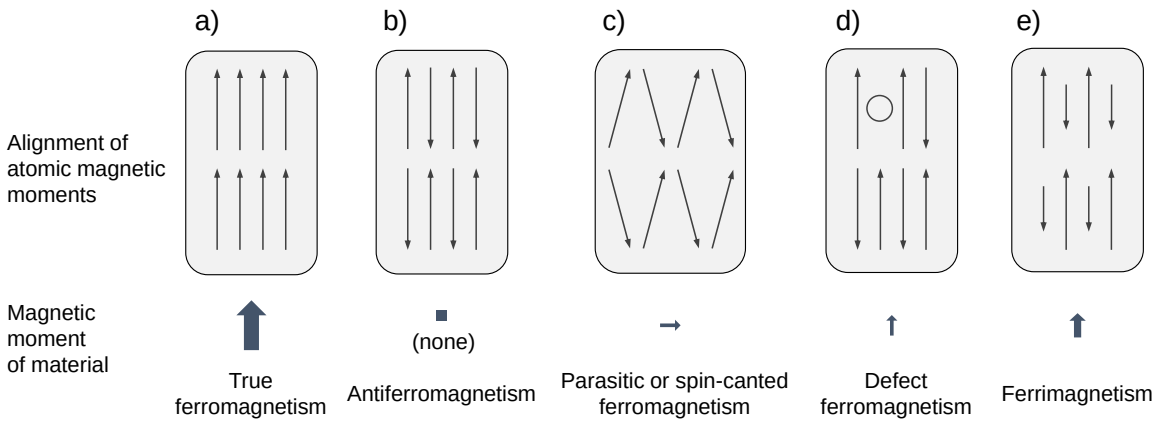

Figure 2-3. Different types of ferromagnetism. A schematic diagram showing the alignment of magnetic moments of the atoms and the resulting magnetic moment of the material. Modified from Tauxe (2010) and Lowrie (2007).

In some minerals two types of cations with different coordination to the surrounding anions. This is the case with the inverse spinel structure described with the general formula: $X^{2+}\ Y_2^{3+}\ O_4^{2-}$ for 2-3 spinel (or $X^{4+}\ Y_2^{2+}\ O_4^{2-}$ for 4-2 spinel), where X^{2+} (or X^{4+}) and Y^{3+} (or X^{2+}) stand for cations and O^{2-} stands for oxygen anions (Bosi, Hålenius & Skogby, 2009). The spinel structure consists of both octahedral and tetrahedral coordination. In normal spinel structure both X^{2+} and Y^{3+} ions are in octahedral and tetrahedral coordination. The inverse spinel structure on the other

hand has tetrahedral oxygen coordination surrounding half of the Y^{3+} ions but no X^{2+} ions and octahedral coordination surrounding equal amount of Y^{3+} and X^{2+} ions while the corresponding number of tetrahedral sites are empty. For antiferromagnetic materials, this difference of coordination of different metallic cations leads to different magnitudes of the opposing magnetic moments known as *ferrimagnetism*, see Figure 2-3e. The very important magnetic mineral, magnetite (Fe_3O_4) is of this kind (Lowrie, 2007; Tauxe, 2010; Gasparov, Rush, Pekarek, Patel, & Berger, 2009; Perkins, 2011).

2.2.2 Remanent magnetization in rocks

The hysteresis loop

If a rock sample containing ferromagnetic minerals is placed in a slowly increasing strong magnetic field, H, the material becomes more and more magnetic going from point 1 to 2 in Figure 2-4 until it reaches its maximum value, the *saturation magnetization* M_s. If the magnetic field is reduced from point 2 to 3 in Figure 2-4, there is some magnetization left when the magnetic field H reaches zero. That is the *saturation remanence magnetization*, M_{rs} or *isothermal remanent magnetization*, IRM (Lowrie, 2007).

If the magnetic field is now increased again in different direction, going from point 3 to 4 in Figure 2-4 the magnetization of the material is reduced further until it reaches zero at point 4, where the value of the field H is called *coercive force*, H_c. At point 5 *coercivity of remanence*, H_{cr} is reached where zero magnetic field would be observed if the field were to be reduced to zero, returning to point 1 again. If the applied field increases further and reaches point 6 saturation is again achieved (Lowrie, 2007).

The hysteresis curve defines characteristic attributes of the material such as M_s, M_{sr}, H_c and H_{cr}. Their ratios, M_{rs}/M_s and H_{cr}/H_c are also characteristic for the material. They depend on the grain size of the minerals as well as on anisotropy effects (Lowrie, 2007).

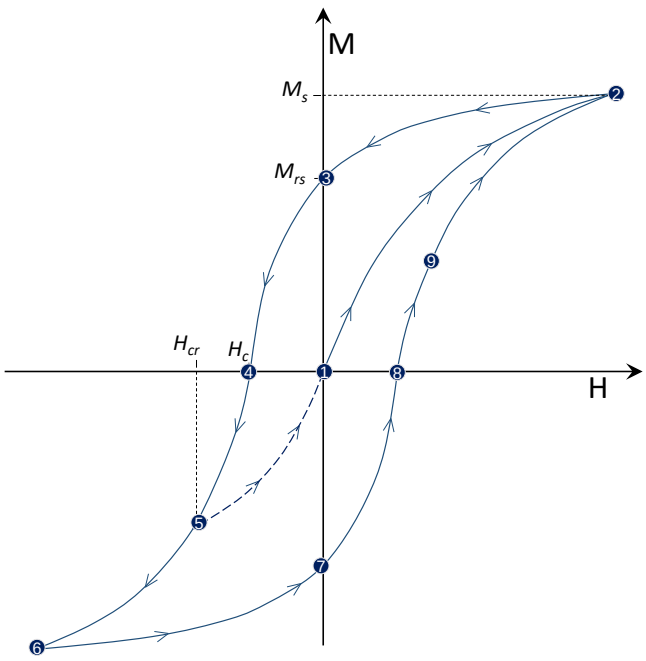

Figure 2-4. Magnetic hysteresis loop of an arbitrary ferromagnetic material. Modified from Lowrie (2007)

Relaxation time, τ

If a magnetic rock is placed in a weak external magnetic field, the magnetization of the particles slowly starts to align with the external field. This process takes a long time but after the relaxation time an equilibrium is reached. There is an equation describing the relaxation time of a small magnetic grain of a single domain grain with volume v:

$$\tau = \frac{1}{C}\, e^{\left(\mu_0 H_c M_s\, v / 2kT\right)} \left(1 - \frac{H}{H_c}\right)^2 , \qquad \textit{eq. 2-9}$$

where C is a frequency factor of the order of magnitude 10^{10} s^{-1}, H is the applied field, H_c is the coercivity field, M_s is the saturation magnetization of the material, T is the temperature and k is the Boltzmann's constant. Note also that some of the parameters are also function of each other since the saturation magnetization is a function of temperature (Tauxe, 2010).

In stable natural condition on earth, the applied field (Earth's magnetic field) is much lower than the coercive field, the above equation becomes:

$$\tau = \frac{1}{C}\, e^{\left(\mu_0 H_c M_s\, v / 2kT\right)} . \qquad \textit{eq. 2-10}$$

Graphs for relaxation time versus temperature for different grain-sizes of elliptical magnetite grains are shown in Figure 2-5. Calculated from the above formulas, material properties of magnetite and grains of elliptical shape in length to width ratio 1.3:1 (Tauxe, 2010).

Curie temperature and Néel temperature

With increased temperature, the thermal motion of the atoms increases and causes the exchange forces to weaken. Eventually the cooperative spin behavior disappears entirely, and the material becomes paramagnetic. This temperature is called Curie temperature T_c for true ferromagnetic material but Néel temperature (T_N) for antiferromagnetic materials. Those temperatures are characteristic for each material (Tauxe, 2010).

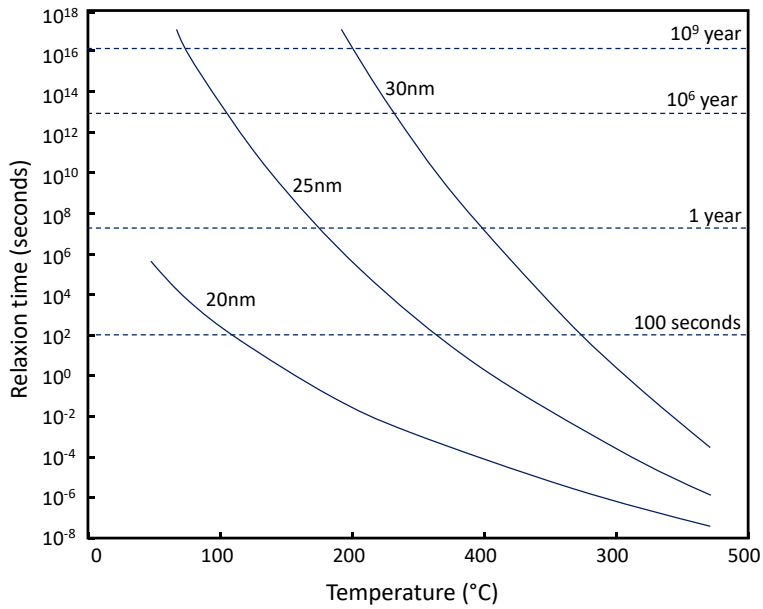

Figure 2-5. Graph showing the effects of temperature and grain size on relaxation time. Relaxation time versus temperature for magnetite ellipsoids of different widths. Modified from Tauxe (2010).

Different types of remanent magnetization

Natural remanent magnetization, NRM

Magnetic rock in nature has *natural remanent magnetization* (NRM) which is a combination of remanence acquired by various processes. Some of these main processes are described briefly below.

Viscous remanent magnetization, VRM

If a magnetic rock is placed in a constant external magnetic field, the net magnetic moments of particles start to slowly align with the external field as described before. The effect on the remanent magnetization is known as *viscous remanent magnetization*, VRM. The VRM is then a function of both time and the strength of the external field, the temperature and various properties of the material (Tauxe, 2010).

Thermal remanent magnetization, TRM

The relaxation time is also a function of environmental parameters such as temperature. At normal temperature the relaxation time is commonly millions of years or more. In high temperature, close to Curie temperature (T_c), the relaxation time shortens rapidly. The temperature where relaxation time is just hundreds of seconds is defined as *blocking temperature* (T_b). Above the blocking temperature but below Curie temperature it is not possible to define remanent magnetization and the material becomes what is called *superparamagnetic* see Figure 2-6.

When cooling lava is still at a temperature above the Curie temperature it cannot be ferromagnetic. When it reaches the Curie temperature it becomes superparamagnetic and its magnetic grains will take up the surrounding magnetic field. If the lava is not stationary it will have unstable magnetization while changing its orientation to the external field. When the lava cools down below the blocking temperature, the relaxation time grows very fast and the external magnetic field will be remanent in the magnetic grains of the lava.

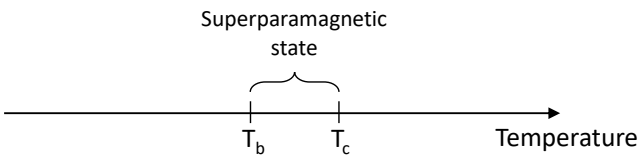

Figure 2-6. Blocking temperature and Curie temperature of magnetic grains. Temperature in arbitrary units. Figure based on Tauxe (2010).

Chemical remanent magnetization, CRM

Chemical processes can slowly change the magnetization of the magnetic particles of a rock, known as *chemical remanent magnetization*, CRM. Two main processes are taking part. First it can be due to alteration or other chemical changes of minerals where minerals (ferromagnetic mineral or not) originally in the rock change into other minerals (ferromagnetic or not). Secondly it can be due to growth of new ferromagnetic minerals in the rock.

Since magnetite can be out of chemical equilibrium in many environments on Earth it can transform to other ferromagnetic mineral, maghemite, see Figure 2-7. When this happens the magnetization of the maghemite becomes a complicated relationship between the original magnetization of the rock and the ambient magnetic field while the transformation is taking place.

For growing minerals in the rock, the mineral grains are at first very small. Taking notice of how volume influences the relaxation time see eq. 2-10, it is clear the relaxation time is small while the grains are small so the minerals are superparamagnetic in the beginning. As they grow, the relaxation time grows as well and it is possible to define a blocking volume similar as the blocking temperature. Based on these principles, the process of CRM due to growth of minerals is should behave similar as the process of TRM described before (Tauxe, 2010).

Detrital remanent magnetization, DRM

When magnetized particles are falling down in water and building up sediment layers, they have a slight tendency to align their magnetic moments with the direction of the ambient field. The sediments and the sedimentary rocks become magnetized this way through the process called *detrital remanent magnetization*, DRM. How this happens is an important study for magnetic measurements in sedimentary rocks but since this study is mainly about magnetic measurements in igneous rocks it is omitted here.

Isothermal remanent magnetization, IRM

Looking at eq. 2-9 one can see that if the applied field becomes larger than the coercive field, the relaxation time will be short. This does not happen in normal stable condition of the Earth's magnetic field but happens when a lightning strikes a rock outcrop. Then the lightning makes instantly very strong magnetic field, larger than the coercive field for the rock. This introduces a remanent magnetization into the rock known as *isothermal remanent magnetization*, IRM (Tauxe, 2010).

Note also this is the same process as was described for the hysteresis loop, see page 6.

Thermo-viscous remanent magnetization, TVRM

A magnetized rock that is at a high temperature for some period of time can change its remanent magnetization in the process known as *thermo-viscous remanent magnetization*, TVRM. Taking notice of the effect which temperature has on the relaxation time, see eq. 2-10 one can see that if the temperature is higher than normal temperature, the relaxation time becomes shorter (Tauxe, 2010). This can happen if the rock is buried deep in the uppermost crust close to igneous intrusions.

Königsberger ratio, Q

Defined as the ratio between remanent and induced magnetism of a material, usually when it is in a field of ~ 50μT.

$$Q = \frac{M_R}{M_I}. \qquad \textit{eq. 2-11}$$

2.2.3 Minerals

Fe-Ti oxides

The most important ferromagnetic minerals in geology are the Fe-Ti oxides which can be described through a rutile (TiO_2) – hematite (Fe_2O_3) – wüstite (FeO) ternary diagram, see Figure

2-7. More Ti rich minerals are to the top while Fe rich is in the lower part. Fe^{2+} on the left-hand side and Fe^{3+} on the right-hand side, representing increasing oxidation towards right.

Red lines are representing three isomorphic exsolution series: titanomagnetites, titano-hematites and pseudobrookites, see Figure 2-7. The first two are ferromagnetic but the last one is paramagnetic.

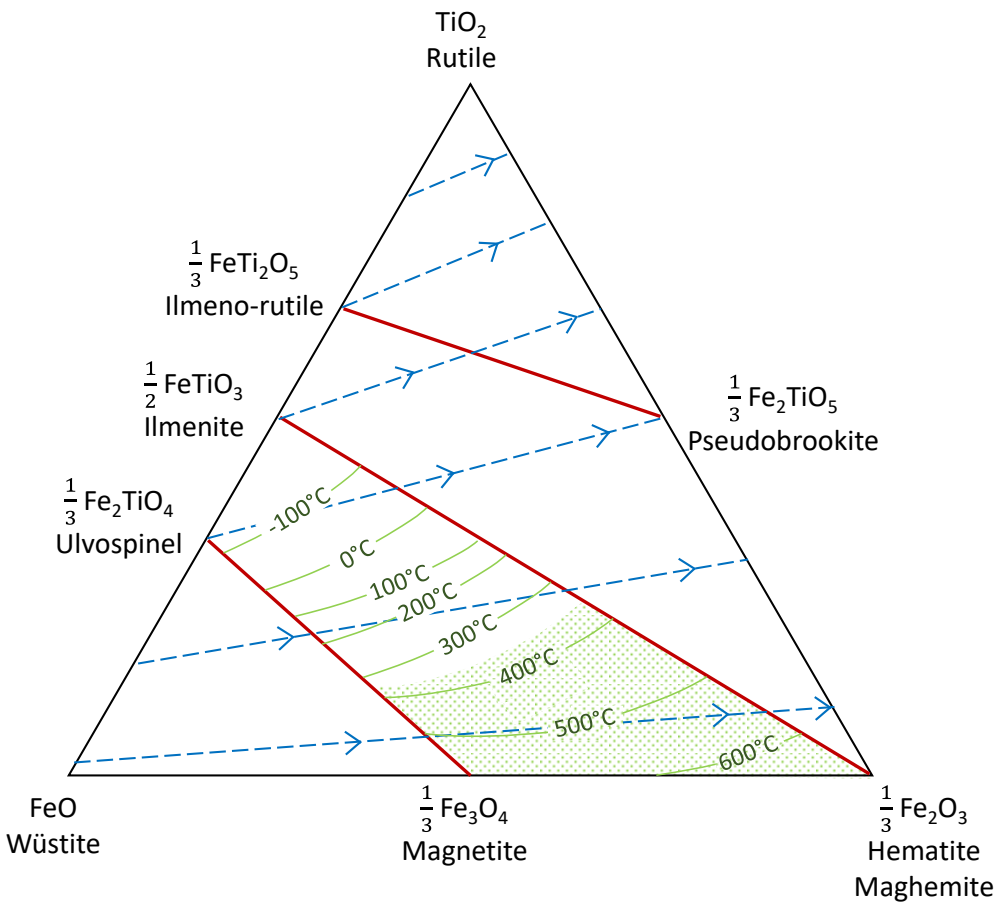

Figure 2-7. Rutile (TiO_2) – hematite (Fe_2O_3) – wüstite (FeO) ternary diagram. The blue dotted lines represent increasing degree of oxidation while red lines represent isomorphic series. Green lines and degrees in Celsius represent Curie and Néel temperature. Green shaded area represents the field of titanomaghemite. Modified from Lanza and Meloni (2006), Reynolds, Rosenbaum, Hudson and Fishman (1990) and Tauxe (2010).

Titanomagnetites

The end members of the solid solution of titanomagnetites are magnetite and ulvöspinel. Although they both crystallize in the cubic system and have inverse spinel structure, the ulvöspinel does not have Fe^{3+} ions and the Fe^{2+} ions are equally distributed in the tetrahedral and octahedral construction while the Ti^{+4} ions have no net moment. Hence, ulvöspinel becomes antiferromagnetic with no magnetization, while magnetite is ferrimagnetic as described before and highly magnetic. Saturation magnetization (M_s) varies considerably from 480kA/m for pure magnetite to 0 kA/m for ulvöspinel. Curie (Néel) temperature varies also, from 575°C for magnetite to -153°C for ulvöspinel, see also Figure 2-7 (Bosi et al., 2009; Lanza & Meloni, 2006; Tauxe, 2010).

Titanohematites

The terms of the solid solution of titanohematites are hematite and ilmenite. The magnetic moments of hematite are not coupled exactly antiparallel against each other but deviated of 0.2° resulting in canted antiferromagnetic behavior. Ilmenite is on the other hand antiparallel but with very low Néel temperature so in natural condition it is paramagnetic (Lanza & Meloni, 2006).

Titanomaghemites

The spinel structure of maghemite (Fe_2O_3) with the same chemical formula as hematite forms by low temperature oxidation of magnetite. Some not very well understood environmental factors can also form hematite from oxidation of magnetite (Reynolds et al., 1990).

Ferromagnetic minerals in rock in nature

Ferromagnetic minerals are never abundant in rock in natural conditions but are only present as accessory minerals, less than 5%. Still their extremely high susceptibility with a content as low as 0.1% of magnetite can mask out effects of other minerals in the rock, see Figure 2-8 (Lanza & Meloni, 2006).

Because of the relatively low concentration of the ferromagnetic minerals in most natural conditions, the rock can be considered to be formed by a diamagnetic and/or paramagnetic matrix, within which ferromagnetic grains are distributed far enough from each other to do not interact with each other. But the magnetic interactions between individual grains are effective over distances up to a few times their diameter (Lanza & Meloni, 2006).

As a rule of thumb, one can read from Figure 2-8 that if a rock has susceptibility of 0.03 in SI units (or 2.5×10^{-3} in cgs) if corresponds to 1% concentration of magnetite in the rock by volume.

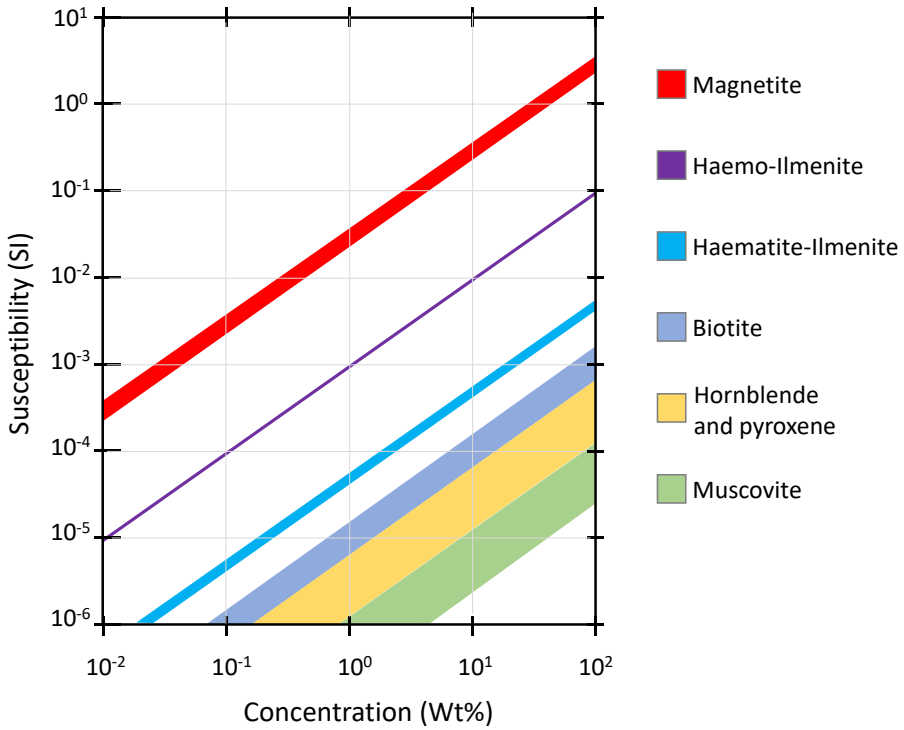

Figure 2-8. Susceptibility from some ferromagnetic and other minerals in rock versus their concentration. Modified from Lanza and Meloni (2006)

2.3 Earth's magnetic field

2.3.1 The elements of the Earth's magnetic field

The Earth is characterized by a strong magnetic field relative to other planets. The total magnetic field of Earth is composed of contributions from several different sources, external and internal (Lanza & Meloni, 2006; Flóvenz, Hersir, Sæmundsson, Ármannsson & Friðriksson, 2012):

a) the main geomagnetic field, with its origins in the outer core of the Earth;
b) the crustal field, generated by magnetized rocks in the Earth's crust;
c) the atmospheric field, produced by thunderstorms and other aspects in atmosphere;
d) the external field, produced by electric currents in the ionosphere and the magnetosphere, from energy directly from the sun;

The main geomagnetic field is of most importance in paleomagnetic studies, cannot be produced by magnetic materials since most of the interior of Earth is above the Curie temperature of the materials involved. The main geomagnetic field instead is assumed to be mostly produced by the geodynamo convection of the liquid outer core of Earth, which is among other materials composed of iron and nickel (Tauxe, 2010; Lanza & Meloni, 2006).

The simplest form describing the magnetic field of earth is one tilted magnetic dipole (Figure 2-9) whose location in year 2015 was 80.31°N 72.62°W and the opposite south geomagnetic pole at 80.31°S 107.38°E (NOAA, 2016). That dipole can describe 90% of the observed total magnetic field of Earth (Kearey, Brooks, & Hill, 2002). If this dipole field is subtracted from the observed field, the residual field can be fitted by another dipole giving better result and so on (Kearey et al., 2002).

By spherical harmonic analysis and least squares fitting by inverse modeling, models are made for the main magnetic field, called International geomagnetic reference field (IGRF) and have been calculated for year 1590 AD to present. This reference field defines magnitude and direction of the magnetic field vector for all places on earth and can be accessed at the National Centers for Environmental Information from National Oceanic and Atmospheric Administration web page: www.ngdc.noaa.gov.

The dipole and the locations of the geomagnetic poles are not measurable directly. However, at two places on approximately opposite sides of the Earth the total magnetic field of Earth is vertical, at one location pointing downwards and the opposite side pointing upwards. Those points can be located from observations of the magnetic field and are known as the *magnetic poles* or *dip poles* of Earth, see Figure 2-9. Based on models, the 2015 location of the north magnetic pole is 86.27°N 159.18°W and the south magnetic pole is 64.26°S 136.59°E (NOAA, 2016).

From the dipole it is possible to calculate the *geomagnetic equator*. There is also a *magnetic field equator* where the measured magnetic field is parallel to the surface of the earth, or horizontal, see Figure 2-9.

From the direction of the magnetic field-vector observed at a given location of earth it is possible to calculate the location of the dipole magnetic poles that would give the measured magnetic field. Those poles are known as *virtual geomagnetic poles, VGPs*.

2.3.2 Calculation of the dipole

When measuring the remanent magnetization, the result is a vector with direction and magnitude. If the vector is measured in Cartesian coordinates where x is to the geographic north, y is to the geographic east and z is vertically down to center of Earth, then (see Figure 2-10) the magnitude of the total field (F), horizontal component H, declination (D) and inclination (I) is (Tauxe, 2010; Lanza & Meloni, 2006):

$$F = \sqrt{X^2 + Y^2 + Z^2}\,, \quad H = \sqrt{X^2 + Y^2}\,, \quad D = \tan^{-1}\frac{Y}{X} \quad \text{and} \quad I = \sin^{-1}\frac{Z}{B} \qquad \textit{eq. 2-12}$$

We also have: (Lanza & Meloni, 2006) with F as the total field.

$$H = F \cos I\,; \quad Z = F \sin I\,; \quad Z = H \tan I\,; \quad X = H \cos D\,; \quad Y = H \sin D \qquad \textit{eq. 2-13}$$

The virtual geomagnetic pole can be calculated from geometry (see Figure 2-11) where λ_s and ϕ_s are respectively the latitude and longitude of the observation point. The location of the virtual geomagnetic pole (λ_p ; ϕ_p) is then obtained from measured declination (D) and inclination (I), based on a method described by McElhinny (1973).

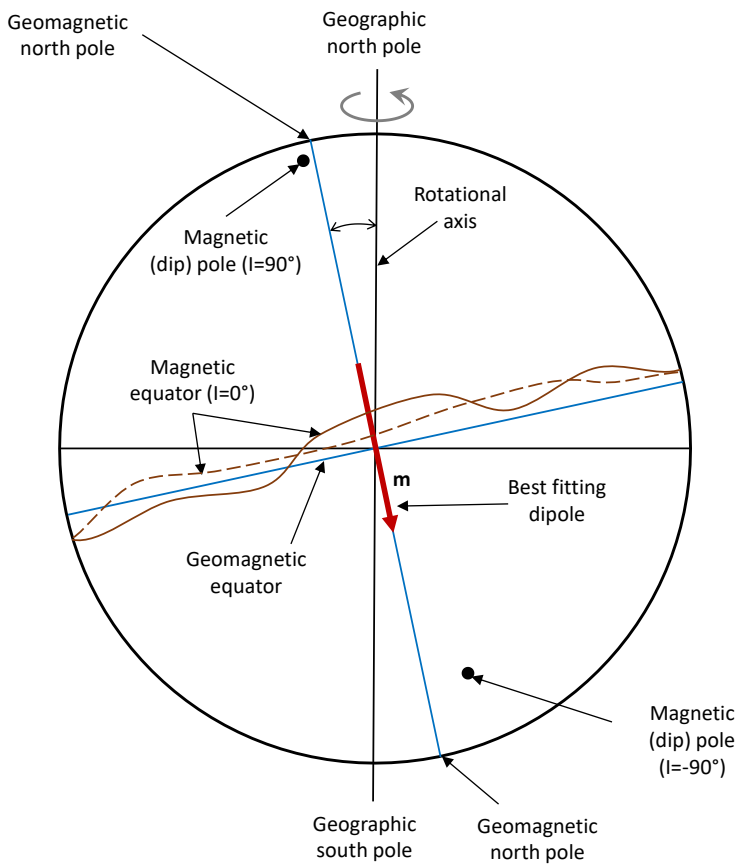

Figure 2-9. Schematic description of geographical poles, geomagnetic poles, magnetic (dip) poles and equator lines. Modified from Lanza and Meloni (2006).

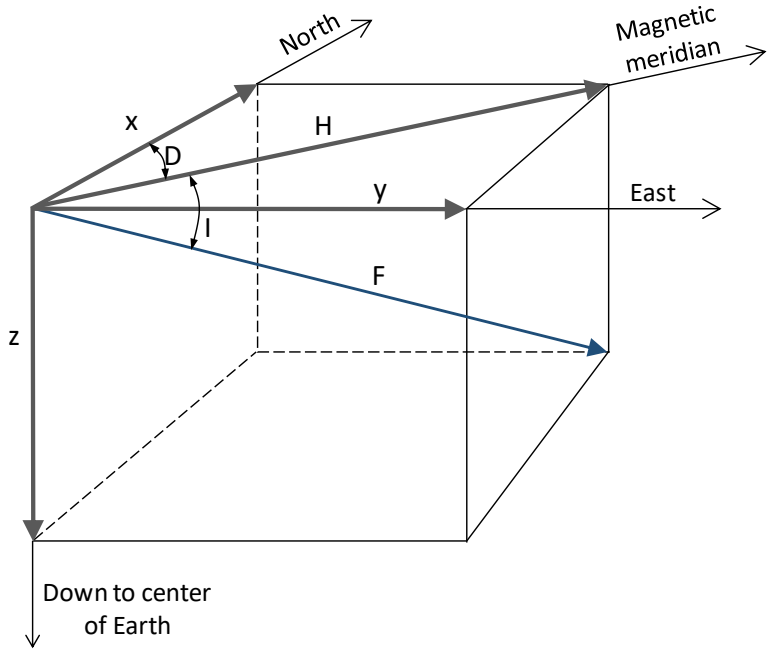

Figure 2-10. The elements of the magnetic field. Modified from Opdyke and Channell (1996).

From the dipole formula the arc distance from the site to the pole, here defined as A, where:

$$\tan I = 2\cot A \quad \Leftrightarrow \quad A = \cot^{-1}\left(\frac{\tan I}{2}\right), \qquad \textit{eq. 2-14}$$

Note that the arc distance A can never be more than 180°, corresponding to the most distant point possible, on the opposite place on the Earth. The laws of sinuses and cosines give:

$$\sin\lambda_p = \sin\lambda_s \cos A + \cos\lambda_s \sin A \cos D \;;\; -90° \le \lambda_p \le +90°, \qquad \textit{eq. 2-15}$$

$$\Leftrightarrow \quad \lambda_p = \sin^{-1}(\sin\lambda_s \cos A + \cos\lambda_s \sin A \cos D) \;;\; -90° \le \lambda_p \le +90° \qquad \textit{eq. 2-16}$$

providing the latitude of the virtual geomagnetic pole, λ_p.

We also have:

$$\phi_p = \phi_s + \beta \quad when \quad \cos A \ge \sin\lambda_s \sin\lambda_p$$

and

$$\phi_p = \phi_s + 180° - \beta \quad when \quad \cos A < \sin\lambda_s \sin\lambda_p \qquad \textit{eq. 2-17}$$

where

$$\sin\beta = \frac{\sin A \sin D}{\sin\theta_p} \quad \Leftrightarrow \quad \beta = \sin^{-1}\left(\frac{\sin A \sin D}{\sin\theta_p}\right), \qquad \textit{eq. 2-18}$$

giving us the longitude of the virtual geomagnetic pole, ϕ_p since λ_p is already known.

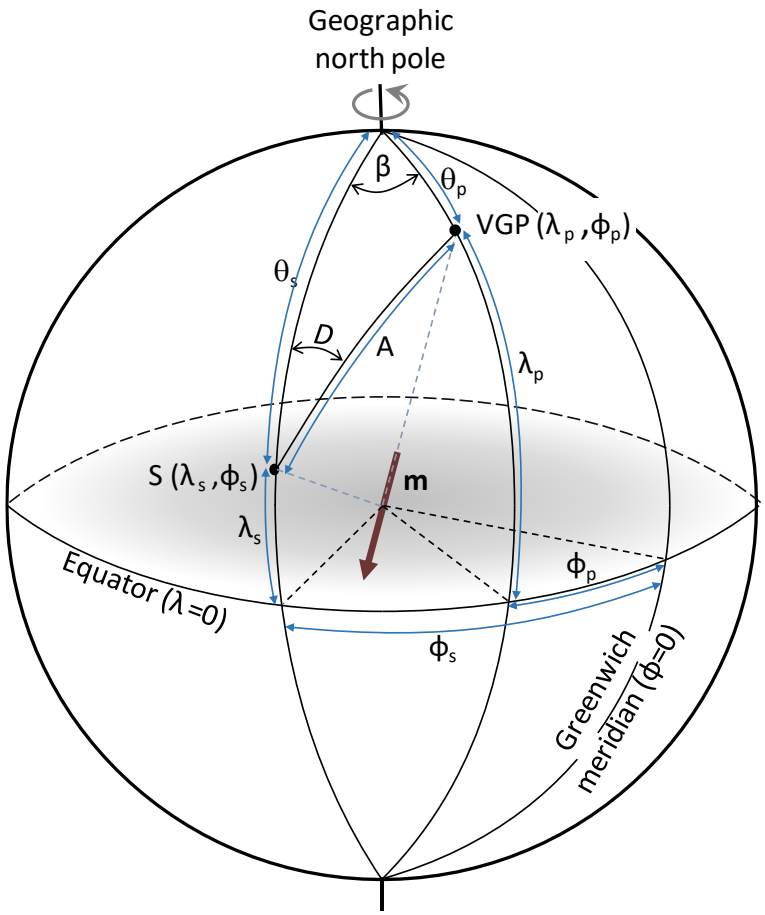

Figure 2-11. Symbols for angles and points to calculate virtual paleo-geomagnetic pole position from measurements of inclination and declination at a site S pointing at a pole P. Figure modified from McElhinny (1973), Tauxe (2010) and Lowrie (2007).

The declination and inclination for a given site location can be calculated from already known location of geomagnetic poles. From eq. 2-14:

$$I = \tan^{-1}(2 \cot A) \qquad \textit{eq. 2-19}$$

where

$$A = \cos^{-1}\left(2 \cos\theta_s \cos\theta_p + \sin\theta_s \sin\theta_p \cos\beta\right)$$

eq. 2-20

and $\beta = \phi_p - \phi_s$

Declination is obtained from:

$$D = \sin^{-1}\left(\frac{2 \sin\beta \cos\lambda_p}{\sin A}\right) \quad \text{when} \quad \cos A \geq \sin\lambda_s \sin\lambda_p$$

and

eq. 2-21

$$D = \sin^{-1}\left(\frac{2 \sin(180° - \beta) \cos\lambda_p}{\sin A}\right) \quad \text{when} \quad \cos A < \sin\lambda_s \sin\lambda_p$$

2.3.3 Variation of the Earth's magnetic field

Variations of Earth's magnetic field occur at very different frequencies and are produced by different processes. Variation of longer time periods, secular variation (number 4 to 7 in Table 2-1) are produced by processes inside the Earth. Shorter terms variations (number 1 to 3) are produced in the atmosphere and ionosphere, partly from the activity of the sun (Opdyke & Channell, 1996; Lanza & Meloni, 2006). The secular variation and longer-term variations can be researched through paleomagnetic study but the shorter time periods are important in geophysical exploration notably in magnetotelluric (MT) soundings (Flóvenz et al., 2012). The focus in this project is on longer term variations, mostly secular variations.

Table 2-1. Scales of geomagnetic variability (Opdyke & Channell, 1996; Lanza & Meloni, 2006)

Geomagnetic behavior	Duration
1. Pulsations or short-term fluctuation	minutes
2. Daily magnetic variations	hours
3. Magnetic storms	hours to days
4. Geomagnetic jerks	10^0 - 10^2 yr.
5. Secular variations	10^1 - 10^3 yr.
6. Magnetic excursions	10^3- 10^4 yr.
7. Reversal transition	10^3- 10^4 yr.
8. Interval between reversals	10^5- 10^6 yr.

Information about variations in the paleomagnetic directions is available from several different sources.

IGRF12 model from NOAA

Information for geomagnetic field is available from the IGRF12 model that are presented on the NOAA web page, http://www.ngdc.noaa.gov/geomag-web/. For given location declination and inclination for each year from 1590 to the present day is provided. The declination and inclination have been calculated by equations described in the previous chapter for location Iceland (Figure 2-12). The difference in magnetic direction, the differential angle (DEL) has also been calculated over one century using Eq. 2-24 described better in chapter 2.4.1 (Figure 2-13).

The maximum change in magnetic direction (DEL) over 100 years according to this is 4.9° and the rate goes down to 2.7° over 100 year time period. On average for all 100 year time periods from year 1590, the average change is 3.7° over 100 years.

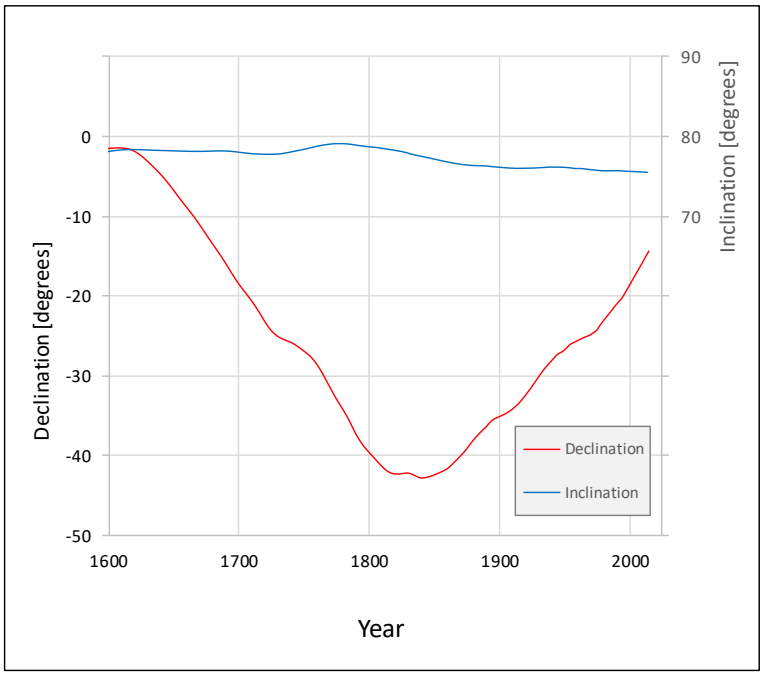

Figure 2-12. Calculated declination and inclination for the Hlöðufell area between 1590 and 2015 corresponding to the movement of the Geomagnetic north pole according to the IGRF12 model. Graph from the author.

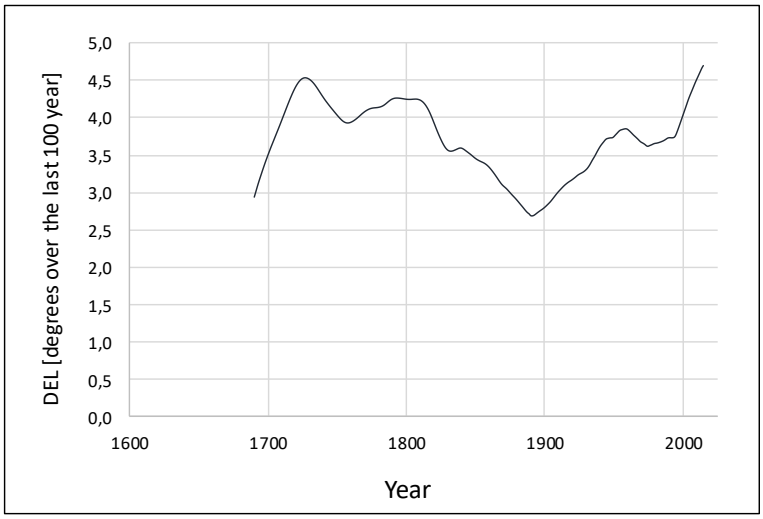

Figure 2-13. The differential angle (DEL) over the last 100 years calculated from information of geomagnetic north pole according to the IGRF12 model, from the data shown on the previous figure. Graph from the author.

Model CALS7K.2, data for last 7000 years

Another model from Korte and Constable (2005), available at https://www.gfz-potsdam.de/en/section/earths-magnetic-field/topics/sources-of-the-earths-magnetic-field/core-field/magnetic-poles-and-dipole-tilt-variation/ and retrieved on 07 Jul 2018 for this study covers much longer time period. That model is a continuous model of archaeomagnetic and lake sediment data of 7 thousand years. It covers the calendar years from 5000 BC to 1950 AD.

In the same way as for the data in IGRF12 model, the data from the CALS7K.2 model was used to calculate the declination and inclination for location Iceland and then from that, the differential angle, DEL (Figure 2-14). The change according to this model is much slower, with minimum change of 0.02° over one century and maximum change of 2.0°. The average change is 0.8°.

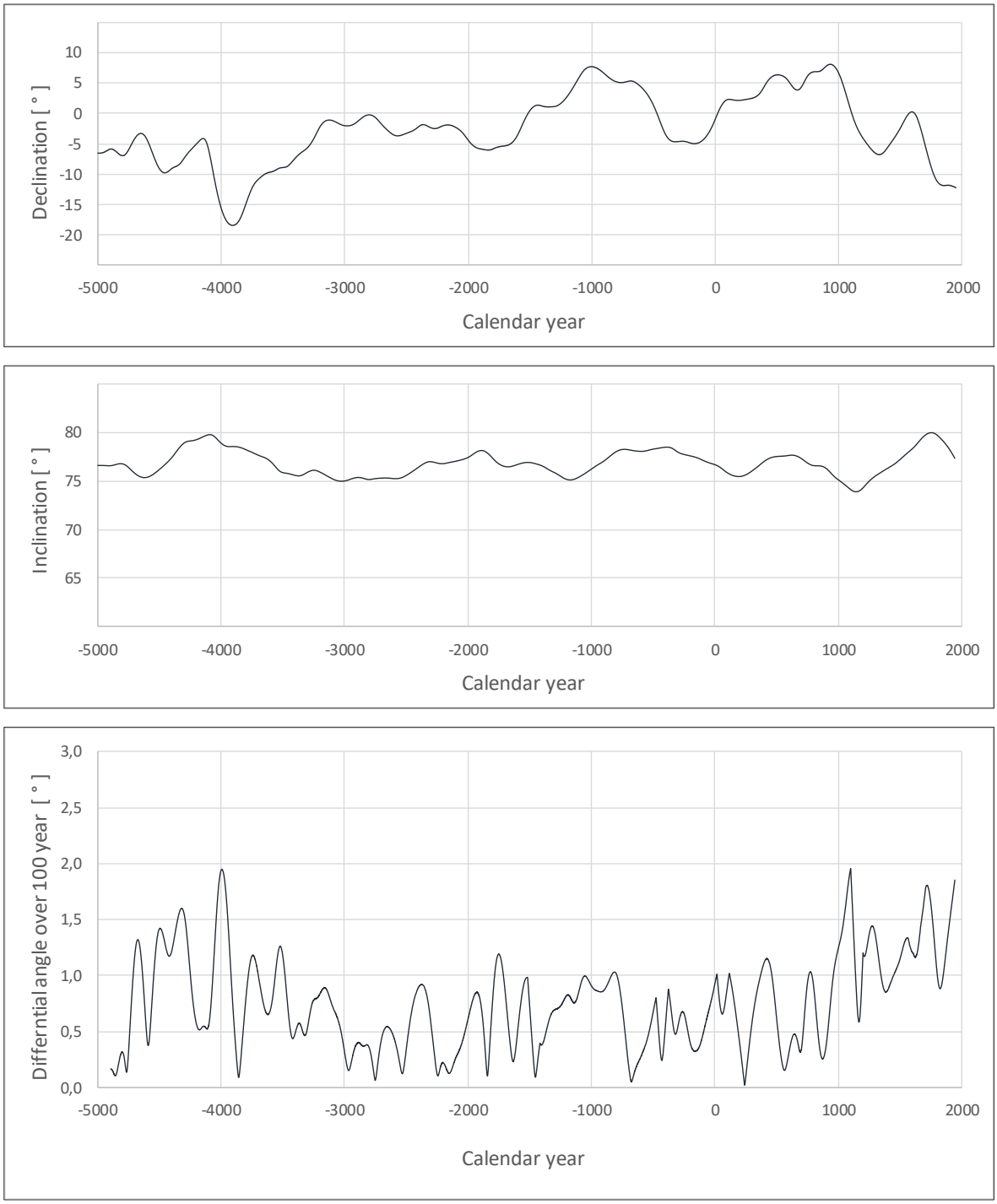

Figure 2-14. Calculated declination and inclination for the last 7000 years according to the CALS7K.2 model. Also on the last diagram, the calculated 100 years change in direction, the differential angle (DEL). Graph from the author.

Here should be noted that this is not accurate measured change of the magnetic directions in Iceland but only data from a model based on archaeomagnetic and lake sediment data. That kind of paleomagnetic data is not as reliable as data from measured lavas.

Magnetic information from Leirvogur

Magnetic results from Leirvogur (Leirvogur Magnetic Results, 2016) shows total change in declination in years 1958-2016. Calculated change in magnetic direction from year 1958 to 2016 with eq. 2-24 is then 2.9° and then 5.1° over one century. This is actual measured data but the time frame we have here is very limited.

Other research

Champion, Hodges, Davis and Lanphere (2011) concluded that the local geomagnetic field vector usually varies with an average angular motion of 4 to 5 degrees per 100 years in latest Pleistocene and Holocene basalt lava flows, with extreme variance from 0 to 10 degrees per 100 years. Mankinen, Prévot, Grommé and Coe (1985) assumed the average cumulative change in virtual paleomagnetic pole angle to be 6° over 100 years' time. Those numbers are mostly based on measurements in lavas.

Overview and what will be used here

Overview of the research described above is in Table 2-2 and it is clear that the assumed average change varies a lot. The average of the averages is 4.0°. However, since Leirvogur with actual data and the measurements on lavas indicate a bit higher value, the best estimate assumed here is 5° change over 100 years' time. The confidence interval of those could be ± 2.5°, also just a rough estimate. Also note that it is very unlikely that the change rate is higher than 7 or 8 degrees but it could easily be lower than 2 or 3 degrees for some centuries.

Table 2-2. Overview of research and data for a change in magnetic direction over 100 years.

	Change in direction over 100 years		
Research or source of data	**Average**	**Minimum**	**Maximum**
IGRF12	3.7°	2.7°	4.9°
CALS7K.2	0.8°	0.02°	2.0°
Leirvogur	5.1°	NA	NA
Champion et al, 2011	4-5°	0°	10°
Mankinen er al, 1985	6°	NA	NA

2.4 Calculations of magnetization and data analysis

2.4.1 Measurements of remanent magnetization of a sample core

The magnetometer used in this research (see Chapter 3.2) gives mV readings, corresponding to the three dimensions of the coordinate system fixed in the core, see Figure 2-15. The x direction of the coordinate system is the vertical direction with positive upward. Direction z is along the

axis of the cylinder and with positive direction inside the rock. Direction y is horizontal and orthogonal to the other axes with positive sense to the right.

Measured declination of the remanent magnetization of the sample core in its own coordinate system is in clockwise direction from x axis. Inclination is the deviation from the xy-plane with positive direction down.

The magnetometer gives mean measurement in mV for the signal in each direction x, y and z with the amplitude as:

$$Ampl = \sqrt{x^2 + y^2 + z^2} \qquad \textit{eq. 2-22}$$

With adjusted magnification of the magnetometer (normally adjusted between 0.1 and 2.0 for different magnetization strength of the core measured), known calibration of the magnetometer and volume of the measured core, we have the magnetization of the core:

$$M = \frac{Ampl * \ magnification * calibration}{volume\ of\ the\ core\ measured} \qquad \textit{eq. 2-23}$$

For the equipment used in the research we have the calibration constant of 48 and using volume of the core in cm^3 the outcome will be magnetization in A/m.

The declination and inclination in the coordinate system of the core is calculated in the same way as before (see eq. 2-12) that is $D = tan^{-1}(y/x)$ and $I = sin^{-1}(z/(\sqrt{x^2+y^2+z^2}))$.

The angular difference between two measurements of directions in the same sample core, called DEL is calculated from their scalar product, using the well known formula:

$$DEL = \cos^{-1}\left(\frac{\boldsymbol{M}_1\boldsymbol{M}_2}{M_1M_2}\right) = \tan^{-1}\left(\frac{\sqrt{1 - CDE^2}}{CDE}\right)$$

where

eq. 2-24

$$CDE = \left(\frac{X_1X_2 + Y_1Y_2 + Z_1Z_2}{Ampl^2}\right)$$

For small angles a simplified formula can be used:

$$DEL = \sqrt{(\Delta I)^2 + (\Delta D\ cosI_m)^2} \qquad \textit{eq. 2-25}$$

where ΔI and ΔD is the difference in inclination and declination respectively between the two measurements and I_m is the mean of the two inclinations. Those equations will be used to define how different paleomagnetic directions are between sampling sites or geological units.

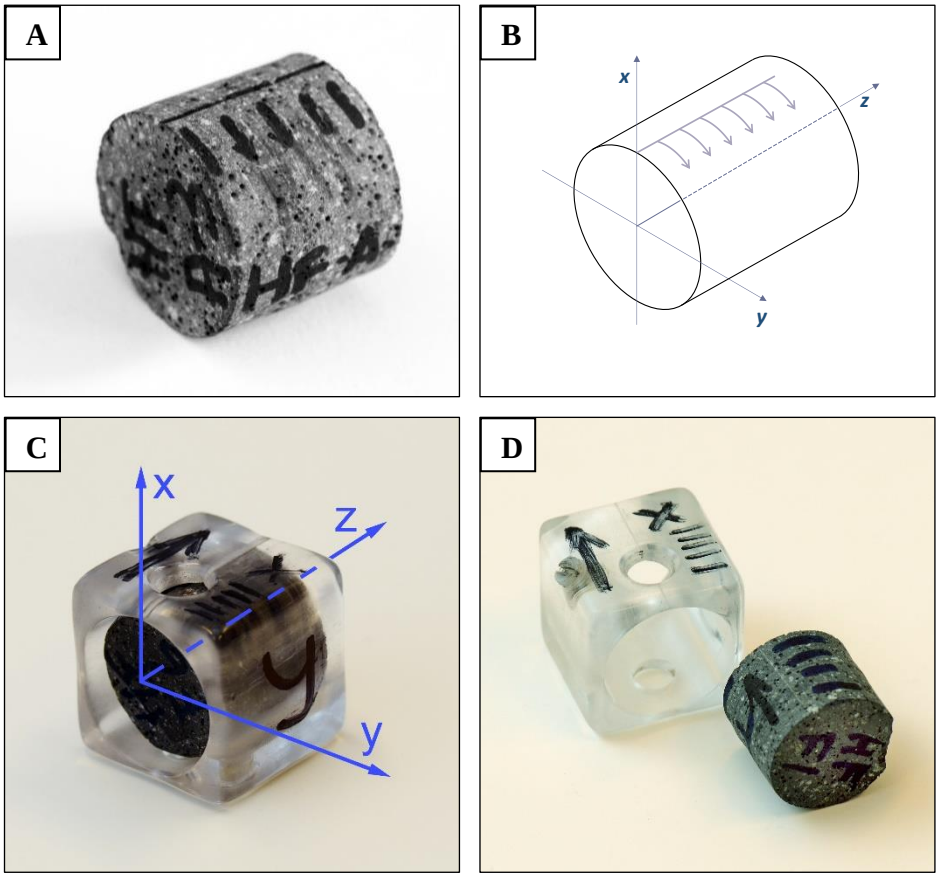

Figure 2-15. A sample core with a sample holder and the coordinate system fixed in the core for magnetic measurements of a core. Photos and drawing by author.

2.4.2 Magnetic field transformed to geographical coordinate system

The magnetic moment of the specimen described above is measured in the coordinate system of the specimen itself. The difference between the sample core coordinate system (x,y,z) and the geographical coordinate system (here referred to with x', y', z') is described with the azimuth (Az) angle between the inward direction of the sample and direction to the geographical North and the plunge (Pl) angle of the sample core. Then the geographical coordinates will be (Tauxe, 2010):

$$\begin{aligned} x' &= x\cos(Pl)\cos(Az) - y\sin(Az) - z\sin(Pl)\cos(Az) \\ y' &= x\cos(Pl)\sin(Az) + y\cos(Az) - z\sin(Pl)\sin(Az) \\ z' &= x\sin(Pl) + z\cos(Pl) \end{aligned} \qquad \textit{eq. 2-26}$$

In the above equation, the Azimuth is the geographical direction of the z axis of the sample while plunge is the slope of the x axis of the sample, see Figure 2-16, where we have: *Plunge angle = Dip angle – 90°*.

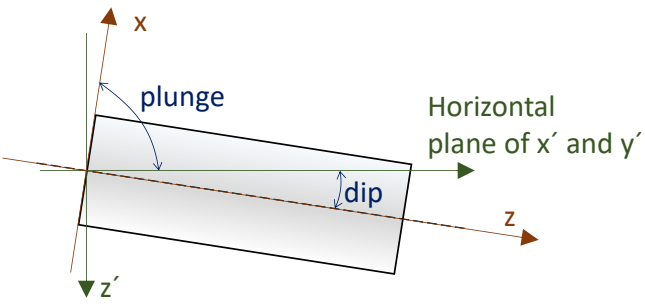

Figure 2-16. Plunge and measured dip angle of a sample core

Inclination and declination in the geographical Earth coordinate system is then (as described before, see eq. 2-12) $D = tan^{-1}(y'/x')$ and $I = sin^{-1}(z'/\sqrt{((x')^2+(y')^2+(z')^2)})$. But here it is important if used for example in computer programs, to take notice of in which quadrant the vector is. If x' and y' is both positive, then $D = tan^{-1}(y'/x')$, if x´ is negative, then we have $D = 180° + tan^{-1}(y'/x')$, if x´ is positive but y´ is negative, we can use $D =360 + tan^{-1}(y'/x')$ to have the declination D, going from 0° to 360°.

2.4.3 Fisher statistics methods used

Usually we have more than one sample from each site, yielding directions that are scattered around some true value. The scatter can be due to various factors, such as (Tauxe, 2010; Kristjansson, 2002):

- uncertainty in the measurement in the field from orienting of the sample;
- uncertainty in the measurement in the lab;
- natural variations of secondary magnetization and its removal;
- uncertainty caused by the process of magnetization;
- rotation and fractures of blocks within the sampled site and
- uncertainty caused by local anomalies on length scales of meters to tens of km, generated by lateral magnetization inhomogeneities in all underlying rocks as well as in the lava itself (including effects of irregularly shaped boundaries).

The probability distribution of the calculated magnetic field vector can be described with (Fisher, 1953; Tauxe, 2010):

$$P_{dA} = \frac{\kappa}{4\pi \ \sinh \kappa} \, e^{\kappa \cos \alpha} \qquad \textit{eq. 2-27}$$

where α is the angle between the true direction and measured direction and κ is a precision parameter. When κ has a large value, the measured directions are more concentrated around the true direction, while lower κ value means more scattering. If κ is equal to 0 then the distribution is uniform over the sphere.

If we have N measurements then we have N vectors, giving the total length of:

$$R = \sqrt{(\Sigma x)^2 \ + \ (\Sigma y)^2 \ + \ (\Sigma z)^2} \qquad \textit{eq. 2-28}$$

and mean direction components of the unit vector $(\bar{x}, \bar{y}, \bar{z})$ with:

$$\bar{x} = \frac{\Sigma x}{R} \quad , \quad \bar{y} = \frac{\Sigma y}{R} \quad , \quad \bar{z} = \frac{\Sigma z}{R} \qquad \textit{eq. 2-29}$$

It has then been shown by Fisher (1953) that κ can be approximated with:

$$\kappa \cong k = \frac{N-1}{N-R} \qquad \textit{eq. 2-30}$$

and also, that there is *1 - P* probability that <u>the true mean direction</u> of a population of N directions lies within a circular cone whose axis is the observed mean direction and whose semi vertical angle $\alpha_{(1-P)}$ is given by the equation (Fisher, 1953; Sharma, 1986):

$$\alpha_{1-P} = \cos^{-1}\left[1 - \frac{N-R}{R}\left(\left(\frac{1}{P}\right)^{\frac{1}{N-1}} - 1\right)\right] \qquad \textit{eq. 2-31}$$

In most cases for paleomagnetic studies P is taken to be 0.05, so there will be 95% probability that the true mean direction of the vector to be within angle alpha95 degrees from the mean direction calculated from observations, reducing the above equation to:

$$\alpha_{95} = \cos^{-1}\left[1 - \frac{N-R}{R}\left(20^{1/(N-1)} - 1\right)\right] \qquad \textit{eq. 2-32}$$

A simplified equation for alpha95 can also be given by an estimate which is reliable for k larger than 25 (Tauxe, 2010):

$$\alpha_{95} \cong \frac{140}{\sqrt{kN}} \qquad \textit{eq. 2-33}$$

Then the estimated angular (or circular) standard deviation can be approximated in degrees by,

$$ASD = \frac{81}{\sqrt{k}}\ , \qquad \textit{eq. 2-34}$$

which is then the radius of a circle around the mean direction containing 63% of the data (Tauxe, 2010).

The statistic δ is also an approximation for ASD (Tauxe, 2010), given by:

$$\delta = \cos^{-1}\frac{R}{N} \qquad \textit{eq. 2-35}$$

3 Equipment and methods

3.1 Field work

3.1.1 Core sampling

Drilling, orienting and equipment used

For core sampling a portable gasoline-powered drilling machines were used with standard 2.5-cm-diameter drills, see Figure 3-1. The cores were water-cooled during drilling. For all cores a Brunton compass was used with the orienting equipment shown in Figure 3-2. Most often it was cloudy in the area so there was not an opportunity for using the sun to correct the local declination. Instead 'known directions' from maps and using GPS measured locations for sampling sites were used for correction. For improved accuracy for reading of the compass, a magnifying glass was usually used for that reading. For the few instances when it was possible to use both the sun and direction to nearby mountains, both were used and the average used if the measured local declination was not the same from both methods. Usually the difference was not more than 1°.

Azimuth of the sun

A Garmin manual GPS clock with reading accuracy +/- 30 seconds was used and the Garmin GPS 60 when available. The clock was checked with the web page: http://time.is/GMT. For calculation of the true azimuth angle of the sun a NOAA Solar Calculator was used (http://www.esrl.noaa.gov/gmd/grad/solcalc/).

Equipment used for location and maps

For GPS locations a Garmin GPS 60 CSx with WAAS/Egnos correction enabled was used. When location was taken, an average method built into the Garmin GPS60 was used. The uncertainty of the Garmin GPS is not well known but could be 5-10 meters or even more in vertical position. This is not assumed to have any serious effect on the research since the position or elevation data is not used in that way it would influence the results of the research.

Maps for locations of nearby mountains were found out with the Garmin Mapsource software and Basecamp software. That software was also used for calculations of true directions from sample sites to the nearby mountains used. Distance to these nearby mountains was usually in the range 5 - 10 km.

Terminology

In this work the following terminology is used:

- *Sample* is one peace of rock which can be measured in the lab.
- *Sample core* is one drilled core and usually one sample can be made from the core.
- *Sampling site* is a place in a unit with several sample cores.
- *Unit* or *geological unit* is a part of a formation stage that one or more sampling sites are used represent.
- *Stage* represent one or more formations in the volcano that have formed in the same or similar situations during the eruption that built the mountain.

Figure 3-1. Drilling equipment: consisting of a pressurized water-tank connected to the gasoline-powered drilling machine. A drill bit is already installed in the drilling machine in the photo.

Figure 3-2. Setup while orienting at sample site HF-A in Hlöðufell

3.1.2 Sampling strategy

The pre-project in Undirhlíðar was used as an exercise for the main project and for that purpose the first sample cores there were taken under the supervision of Leo Kristjansson. For each sampling site, all samples were usually taken from the same pillow, see Figure 3-3 (A) as an example. No other sampling strategy was set up in the beginning of the project and the first samples even from cap lavas in Hlöðufell were first taken in the same way, as shown for HF-D in Figure 3-3 (B). In the later stages of the research the sample cores were distributed better within the sampling site as shown in Figure 3-3 (C) for sampling site HF-O.

Here it should also be noted that sampling at Hlöðufell was in most cases rather difficult and in many cases, it would not have been possible to distribute the sampling locations more evenly over each sampling site. HF-R and HF-S are examples of sampling sites on the western side of the mountain from stage I units, for location see Figure 6-1. The outcrops were covered as thoroughly as possible with samples, see photos in appendix on pages 124 and 125 of the sampling sites HF-R and HF-S respectively.

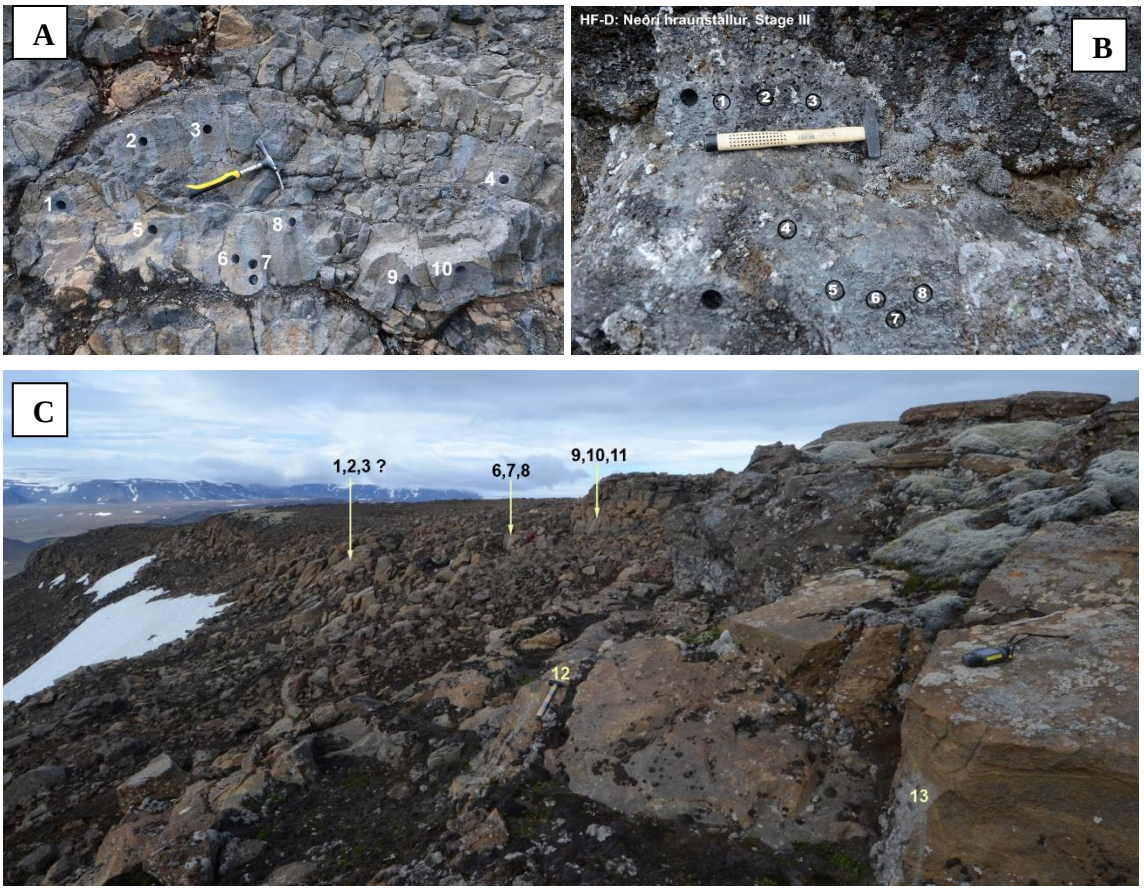

Figure 3-3. Examples how samples were taken in some sampling sites during this research. (A) sampling from one pillow samples in Undirhlíðar. (B) Samples taken in lower cap lava at sampling site HF-D. All samples are taken within a very small area in the lava. (C) Samples taken in sampling site HF-O, one of the later samples in lava and better distributed over the site.

This led to clustering of some sampling sites. An example of this are the sampling sites from pillow lavas in Rani in stage I (Figure 3-5). The pillows in Rani should be considered as one unit but the result using 95% confidence interval indicates that the paleomagnetic directions differ between the sampling sites. A decision has then been made to use 99% confidence interval, that is alpha99 when comparing paleomagnetic directions of different sampling sites within a unit. This is done to be on the safe side when interpreting the results.

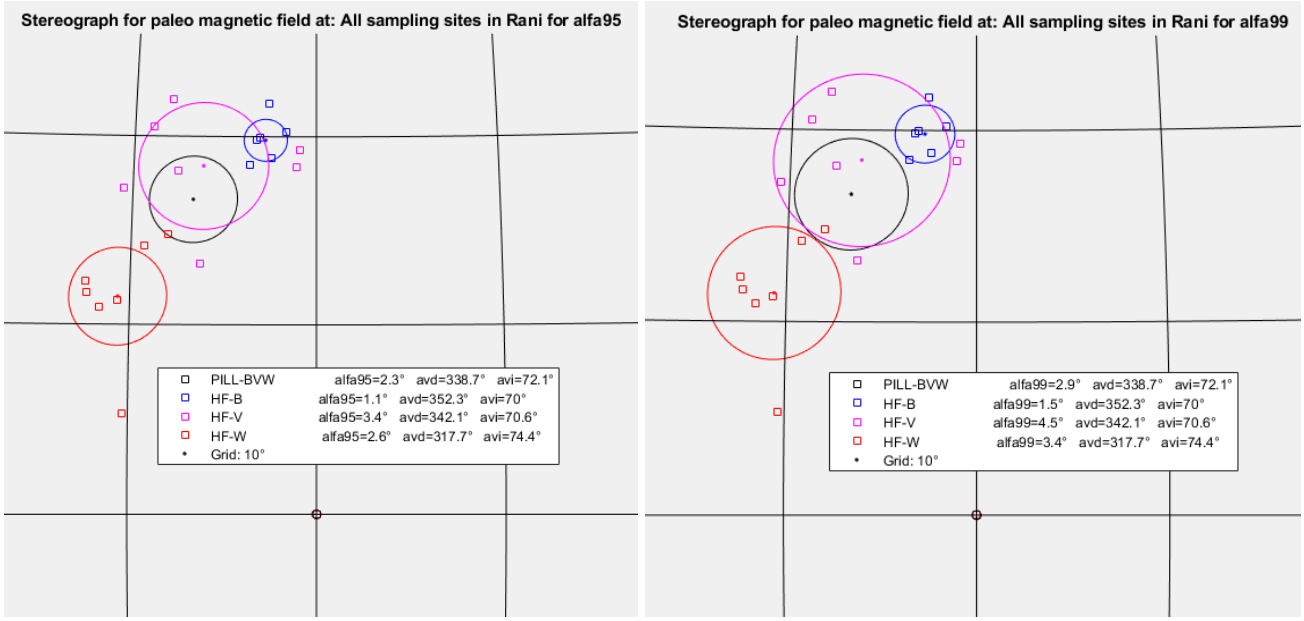

Figure 3-4. Comparison of 95% confidence interval and 99% confidence interval for all sampling sites in Rani. The black circle in both images is the confidence interval calculated if using all 21 samples in the 3 sampling sites.

3.1.3 Final finish of the samples prior to magnetic measurements

After each field trip, the samples were marked and approximately 2.2 cm long cylinders for measurements were made using a rock saw (Figure 3-5). Figure 2-15 provides another example of a sawed core.

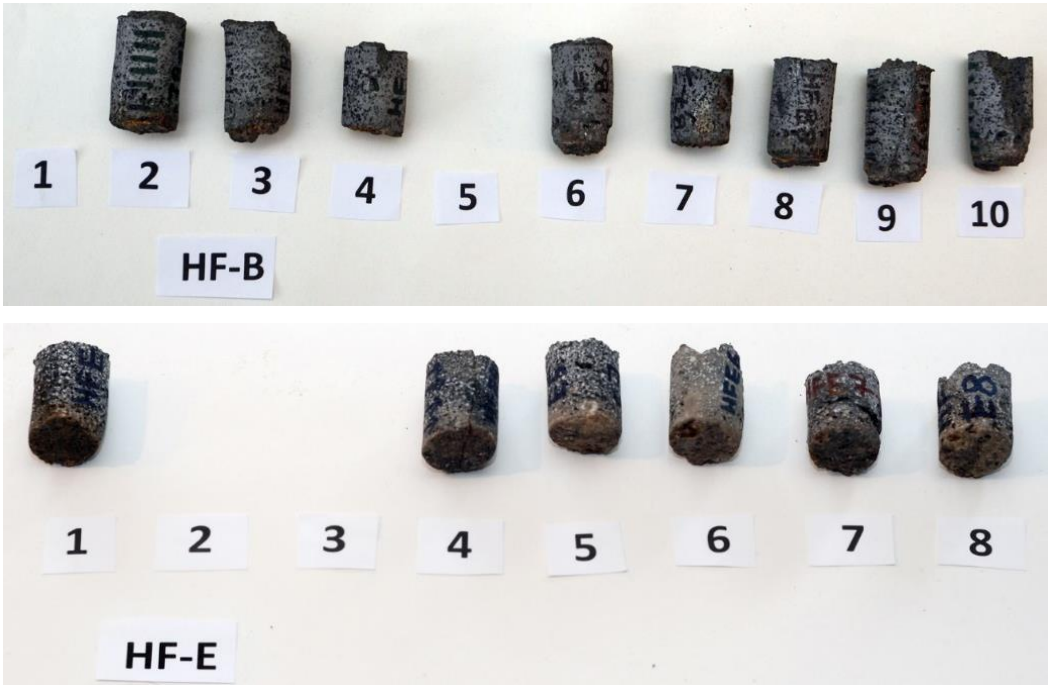

Figure 3-5. Examples of sample cores from two of the sampling sites. For increased precision when finishing the cores, in some instances a geology magnifying-loupe was used to find out marks on them from field work. The photos are showing sample cores prior to sawing. An example of a samples to be measured is shown on Figure 2-15.

3.2 Laboratory work

Figure 3-6. The laboratory in Askja.

The magnetometer

The magnetometer used for all remanence measurements was a fluxgate instrument made by Institut Dr. Förster, Reutlingen, Germany. A fluxgate probe basically contains a coil wound around a long core and fed with a purely sinusoidal audio-frequency current. The core is made of a magnetic alloy (e.g. so-called µ-metal) which saturates very easily, i.e. has a narrow hysteresis loop, see Figure 2-4 (Sharma, 1986). The a-f voltage induced in another coil wound on the same core, will be distorted, i.e. it consists of the original frequency plus an overtone signal. With proper arrangement, the amplitude of the overtone signal is proportional to the component of the magnetic field parallel to the core.

The Förster magnetometer has four approximately identical fluxgate probes, the signal from which is combined. They surround the cylindrical rock specimen to be measured. Two of the probes are "end-on" so that they measure the field caused by that component of the specimen´s dipole moment which is parallel to the axis of the setup. Two probes are at the sides of the specimen, measuring field lines which go the other way (Figure 2-2). This combination of the four probes eliminates external field variations, such as from ionospheric currents, traffic, elevators, etc. The output of the magnetometer is 0 to +/- 1500 millivolts d-c.

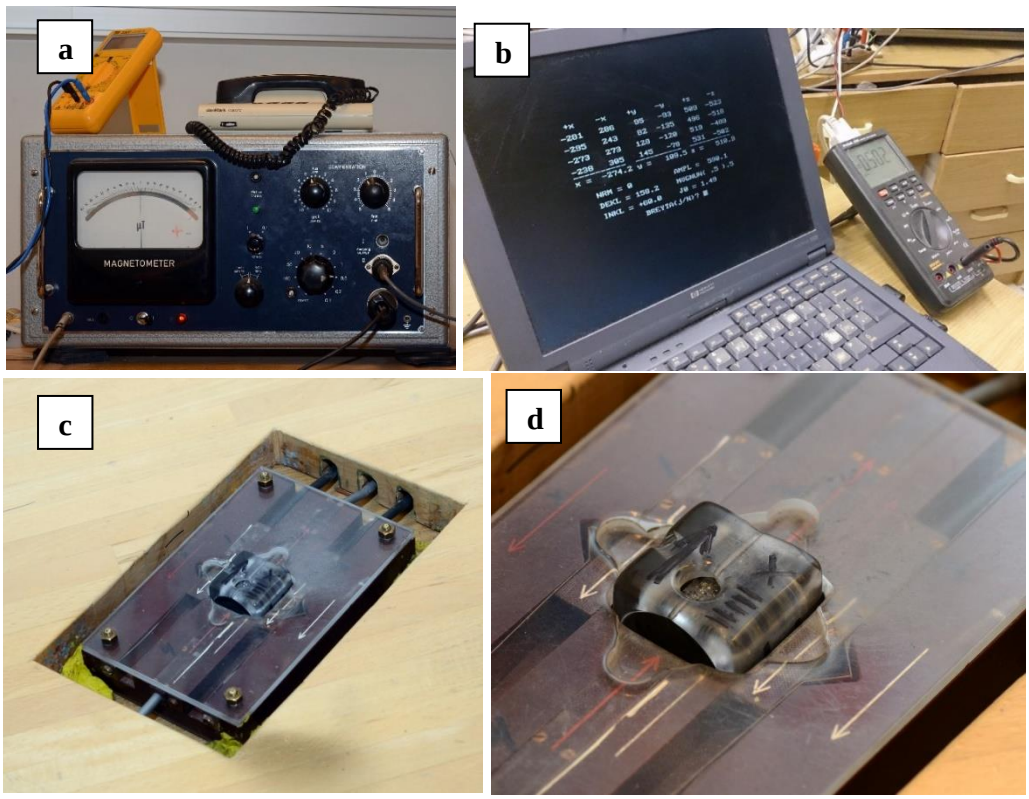

Figure 3-7. The magnetometer used in this research.

A specimen is measured in all 24 possible orientations, that is 4 times for the +x component, 4 for -x and so on. The values for each of the three components are averaged, which largely cancels out effects from the non-spherical shape of the sample and inhomogeneities in its magnetization. A simple computer program converts the readings to a spherical coordinate system in the specimen. The magnetometer is very stable, the reproducibility of a direction measurement being better than 0.2°. It was calibrated monthly with a 19-turn d-c coil of the same dimensions as a specimen, fed with a few mA. This (eq. 2-2) gives a factor for converting the magnetic dipole moment m of the specimen from millivolts (eq. 2-28) to Am^2.

The error in the magnetization value M = m/V of a specimen is a few %, due to errors in V.

Demagnetization

Basalt lavas tend to contain various magnetizations of different origin. The main one is the primary thermoremanent magnetization (TRM) acquired during initial cooling. There is also viscous magnetization (VRM) built up during recent thousands of years. Most often it is small compared to the TRM but can occasionally exceed it in magnitude. In a few cases, lava outcrops are also affected by lightning, making isothermal remanent magnetization (IRM) which can be very intense. However, these two and other secondary magnetizations are in most cases of relatively low coercivity and can be eliminated by treatments which only affect the TRM slightly. The main treatments used in practice are thermal and alternating-field (AF) demagnetizations. The former which involves heating specimens in steps and measuring them in between is time-consuming and cumbersome, and it causes undesirable chemical changes to the magnetic minerals. It has not been used here and is rarely employed on Icelandic rocks.

In AF demagnetization, a specimen is subjected to a sinusoidally varying magnetic field, generally of frequency < 100 Hz. Its amplitude is increased in a few seconds to a maximum peak and then decreases to zero in a minute or so. This treatment is performed in a field-free environment created either within a set of large d-c coils or in a μ-metal can. In order to avoid introducing a certain disturbing magnetization component (anhysteretic remanence, ARM). the specimen is rotated about two axes simultaneously during the treatment. Sometimes also, it must be demagnetized and measured twice at the same peak field, with the results being averaged to eliminate so-called rotational remanence (RRM). Our equipment for this purpose (Figure 3-8) was made by Molspin Ltd. of Newcastle-on-Tyne, England.

The usual demagnetization steps for Icelandic lavas have peak fields of 5, 10, 15, 20, 25, 30 mT. From over 60 years of experience with these lavas it has been found that the VRM has usually been removed by the 10 mT step. This improves the within-lava agreement of sample directions, even dramatically. The treatment was stopped at 20 mT in many early studies. More recently it has been extended to 25 or 30 mT although the reduction in alpha95 values at these fields has turned out to be quite marginal (Sæmundsson, Kristjansson, McDougall, & Watkins, 1980; Kristjansson, 2002, 2013). In the present work the AF treatment has been carried out to 30 mT in all samples, sometimes up to 40 or 50 mT (Appendix B). The AF peak field which has wiped out a half of the remanence, referred to as the median demagnetizing field (MDF) is on average 20 mT. The value of MDF varies for the samples in Hlöðufell from below 10 mT to more than 50 mT. Higher values indicate relatively anisotropic magnetite grains, for instance needle-shaped ones.

The equipment used for demagnetization in this project displays the strength of the peak field in oersted (oe) or Örsted which has the same dimensions as Tesla and in some cases in this research the unit oe is used for that reason. The conversion between Örsted and Tesla is such that 1 oe equivalences 0.1 mT.

Figure 3-8. The equipment for demagnetization used in this research.

The initial room-temperature magnetic susceptibility of samples can yield clues about their magnetic stability and other properties. This parameter is essentially the slope of curve 1-2 in Figure 3-4 near point 1. As shown in Figure 2-8, a susceptibility value of 0.03 in SI units roughly corresponds to 1% of pure magnetite per volume. Titanomagnetites however have lower susceptibilities. Average susceptibility values of about 0.025 are common in older lavas in Iceland which contain magnetite exsolved from titanomagnetites by oxidation (Kristjansson, 2015). In pillow lavas and other rapidly cooled rocks, the titanomagnetite grains did not have time to exsolve into pure magnetite and titanium minerals. Hence, they generally have low values

of susceptibility. This is also the case in our samples, whose average susceptibility is 0.0078 SI cf. section 6.1. It leads to high values of the Königsberger ratio Q, which is generally considered to be a good qualitative indicator of magnetic stability.

The susceptibility meter used here is an MS-2 instrument from Bartington Ltd., Oxford, England (Figure 3-9). It employs the fact that the self-inductance L of a coil increases when a piece of non-conducting para- or ferromagnetic material is placed inside it. If the coil and a capacitor C form an LC-circuit with relatively small resistance, its resonance frequency is $1/2\pi\sqrt{(LC)}$ Hz. The frequency is here of the order of 0.5 kHz, and changes in it are easily measured. From these changes, the susceptibility value for a 10 cc standard size sample is displayed by the meter.

The susceptibility meter can also be used to measure the Curie temperature of a sample, in a water-cooled sensor within an electric furnace monitored by a thermocouple (Figure 3-10). The temperature where the ferromagnetic susceptibility of the main magnetic carrier disappears (by straight-line extrapolation to zero of the steepest part of the thermomagnetic curves), reflects the composition of the titanomagnetites of the sample, cf. Figure 2-7. A few samples of basalts from Hlöðufell were measured, their number being limited because of instability which developed in the instrument. The results which are shown in Appendix D, indicate that the magnetic material consists chemically of a solid solution of about 60-70% ulvöspinel, 30-40% magnetite. This is a typical composition for fresh basalts.

Figure 3-9. Equipment for susceptibility measurements

Figure 3-10. Setup of equipment for Curie point measurements.

3.3 Data processing and computer programs

3.3.1 General

Custom made computer programs were used for the data processing. Some programs were used without much modifications from the computer of the magnetic measurement lab in Askja. As several of the existing programs were old, had limitations due to old storage media that is no longer used and did not support any graphical presentation, many of them were rewritten by the author or new made for this project.

3.3.2 Programs for calculation of paleomagnetic field and demagnetization

A computer in Askja with old custom made Basic computer program (Figure 3-6 and Figure 3-7) gave result for magnetization of the specimen measured in the coordinate system of the specimen, using the equations described in Chapter 2.4.1 both on printed paper and in a file. The result from that was then put in another computer with an old Fortran computer program, for calculation of paleomagnetic directions: declination and inclination of the rock. The Basic program was used in this research as it was but the Fortran program was rewritten by the author completely in MATLAB. The new program gave graphical results (Figure 3-11 and Figure 3-12) that made the data analysis done in this research possible.

For calculations of the remanent magnetization and getting paleomagnetic directions in the geographical coordinate system, a custom made MATLAB program was written using equations described in Chapter 2.4.2 for transformation of coordinate systems. Then equations described in Chapter 2.4.3 for Fisher distribution are used as well. Then the virtual paleomagnetic pole is calculated among other things, (Chapter 2.3.2) and making a map showing the location of the paleopole as jpg-image. MATLAB functions from Allmendinger, Cardozo and Fisher (2012) for graphical representation of paleomagnetic data in stereographic equal area net projection.

These images such as Figure 3-12 (C) show how it is possible to analyze the demagnetization process of each sample. The programs made as well figures that were used to compare different sampling sites and units, see Figure 3-4 as an example and also Chapter 7 where result is analyzed and Appendix K.

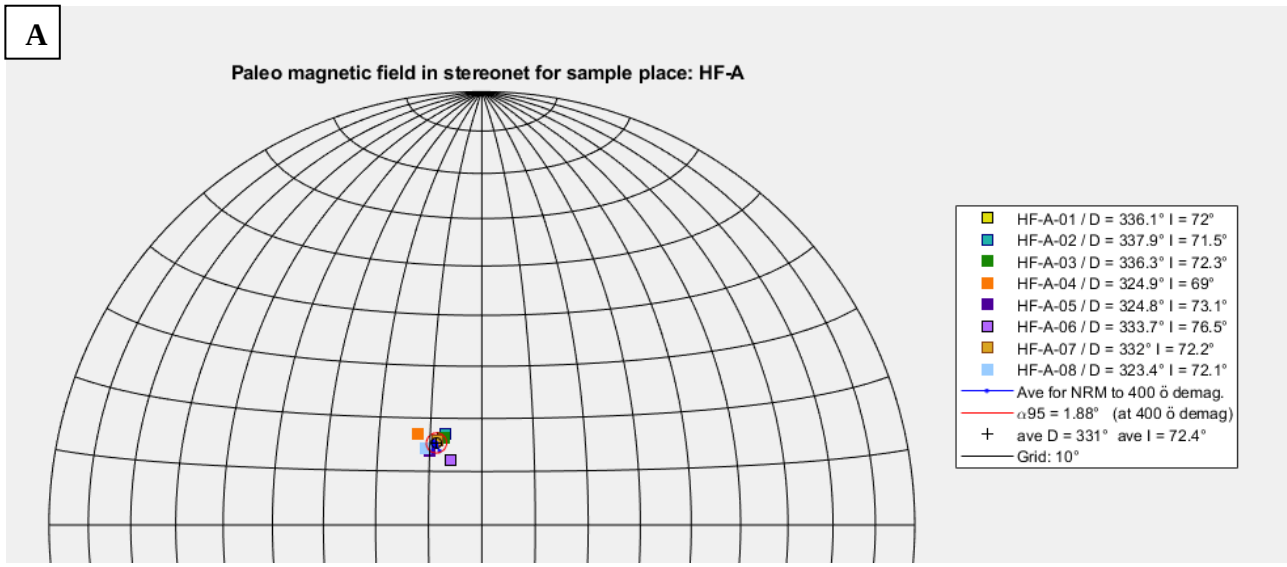

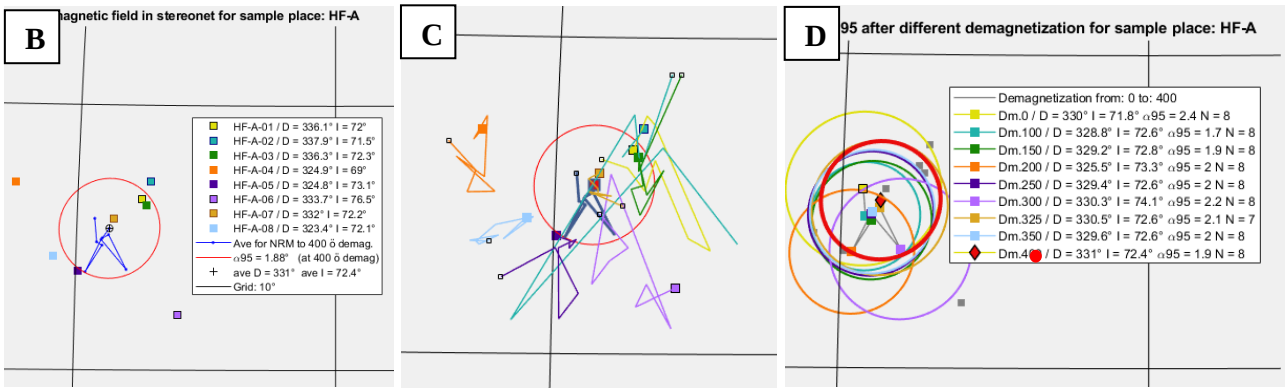

E

CALCULATED PALEO DECLINATION AND INCLINATION IN COORDINATE SYSTEM OF THE SAMPLE CORE:

	TNB Az	Dip	PaleoDecl	PaleoIncl	PaleoDecl	PaleoIncl	PaleoDecl	PaleoIncl	PaleoDecl	PaleoIncl	PaleoDecl
ATION (orsted):			0	0	100	100	150	150	200	200	250
HF-A-01	341.4	+36.0	332.9	+71.8	334.9	+72.4	335.5	+73.3	337.8	+72.6	337.9
HF-A-02	344.4	+31.5	342.2	+70.2	336.0	+72.6	337.6	+71.0	314.9	+74.2	339.0
HF-A-03	344.4	+34.5	343.0	+70.3	335.7	+72.7	336.3	+72.3	335.6	+73.1	334.2
HF-A-04	355.4	+30.5	322.0	+68.6	322.3	+69.9	320.4	+70.3	322.5	+70.8	321.7
HF-A-05	344.4	+20.0	317.4	+73.0	323.9	+73.4	322.9	+75.0	319.1	+75.3	324.2
HF-A-06	334.4	+15.0	330.0	+73.3	330.9	+74.7	328.2	+74.7	324.9	+75.0	333.0
HF-A-07	-15.6	+29.5	332.6	+73.4	330.7	+72.7	332.1	+73.0	330.2	+72.5	330.3
HF-A-08	335.4	+19.5	318.9	+71.9	317.6	+71.5	320.1	+72.0	318.0	+71.8	318.0
AVD & AVI:			330.0	+71.8	328.8	+72.6	329.2	+72.8	325.5	+73.3	329.4
Alfa 90:				2.092		1.473		1.612		1.682	
Alfa 95:				2.450		1.725		1.887		1.970	
Alfa 99:				3.234		2.277		2.491		2.601	
R (Total length of vector):				7.986		7.993		7.992		7.991	
N (Number of measurements):				8		8		8		8	
k (Estimate of kappa):				512.3		1032.2		862.4		791.5	

CALCULATED PALEOPOLE According to location of the sample place Latitude: 64.40115 °N Longitude: -20.55046 °E

Sample	Lat	Lon	Lat	Lon	Lat	Lon	Lat	Lon	Lat	Lon	Lat
Demagnetization (orsted):	Mean values		0	0	100	100	150	150	200	200	250
HF-A-01	77.4	232.7	74.8	231.8	76.2	231.9	77.3	235.9	77.5	228.2	79.9
HF-A-02	67.9	205.3	76.4	209.2	76.9	231.3	75.7	220.8	69.3	259.8	77.7
HF-A-03	77.0	230.8	76.8	207.9	76.8	231.9	76.7	229.1	77.2	234.8	76.6
HF-A-04	68.3	236.5	66.9	235.1	68.4	238.2	68.0	241.3	69.4	240.7	67.4
HF-A-05	72.5	251.4	69.3	253.2	72.5	249.1	73.3	257.8	71.9	261.5	72.6
HF-A-06	76.2	254.3	75.0	242.5	76.5	249.5	75.4	252.2	74.2	256.5	75.4
HF-A-07	74.9	238.0	76.2	240.3	74.8	238.8	75.6	238.5	74.4	238.4	74.5
HF-A-08	69.4	246.7	69.0	247.9	68.0	247.8	69.5	247.1	68.4	248.3	68.3
Mean values from AVI and AVD:			73.6	235.5	73.8	240.5	74.2	241.1	73.1	247.2	74.1

Date of calculations: 21.07.2018 Time: 23:12
Matlab program: paleostefnur.m (function)

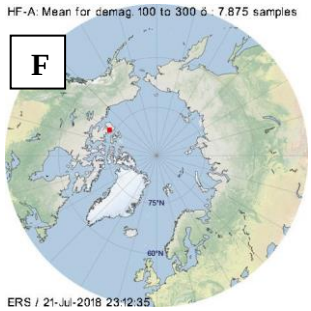

Figure 3-11. An example of output from the sampling site HF-A in Hlöðufell. (A): All samples in a simple stereonet graph with alpha95 circle. All graphs are resizable. (B) Similar graph as in A but in colors for each sample and enlarged. It also shows the path of demagnetization for the average values for paleo declination and inclination. (C) Same as in figure B but also showing paths for demagnetization of all samples. It provides opportunities to see if some samples are showing unexpected behavior in demagnetization. (D) Figure showing development of alpha95 circles for a demagnetization path. (E) main table with values for the remanent magnetization, inclination and declination and the virtual magnetic paleo-pole calculated. (F) Map showing location of the paleopole, a mean value after demagnetization (10 mT to 30 mT).

About stereograph images

In the stereonet graphs used in this work, one can imagine being located above the middle of a bowl, having a vector sloping down (the inclination) and pointing into a direction (the declination). If the inclination angle is the slope angle of the vector so if the inclination is let's say 80° then it is pointing almost straight down to the middle of the bowl. If the declination angle is let's say +45° then it is point half way to the right.

Here the stereograph are set up on a Schmidt net with equal area circles. That gives the opportunities to draw alpha95 confidence limits as circles on the diagrams as is shown in Figure 3-11 as an example.

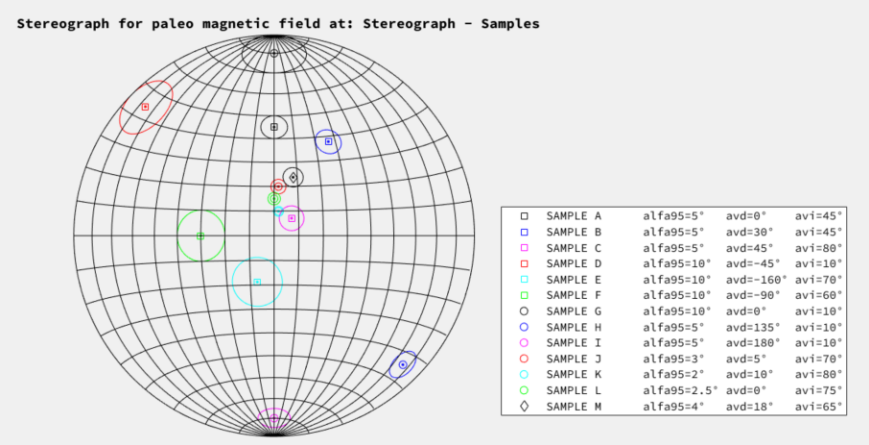

Figure 3-12. A stereonet diagram as used in this research. Several samples for different declination, inclination and alpha95 confidence limits shown as circles.

Demagnetization process

Data from the file made by the Basic program from the measurements of remanent magnetization was used for analysis of the demagnetization process. A MATLAB program made by the author for graphical representation of the datafile, showing the demagnetization process (Figure 3-13) and also calculating characteristics for the samples such as the median demagnetizing field (MDF).

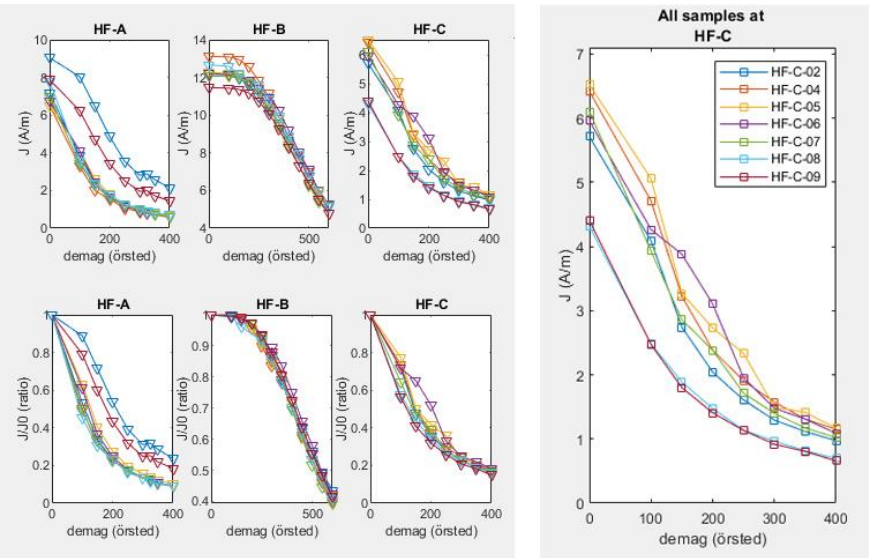

Figure 3-13. An examples of the graphical representation of the demagnetization data from the programs made by the author. Note the difference in demagnetization behavior of the samples. Discussion about that is in Appendix B.

4 Geological setting

4.1 Geology of Iceland

The volcanic activity of Iceland is mostly considered to be a product of the interaction of the spreading plate boundary between North-Atlantic plate and Eurasian plate and a mantle plume with its axis located close to the center of the island. The mean tectonic features are shown in Figure 4-1, with the Mid-Atlantic ridge entering Iceland in the southwest on the Reykjanes peninsula, crosses Iceland as volcanic zones and then continues to the north. The volcanic zones are characterized by volcanic systems with fissure swarms that in the rift zones trend roughly perpendicular to the direction of rifting. Many of the volcanic systems have a central volcano and some of these host one or more caldera structures (Thordarson & Larsen, 2007).

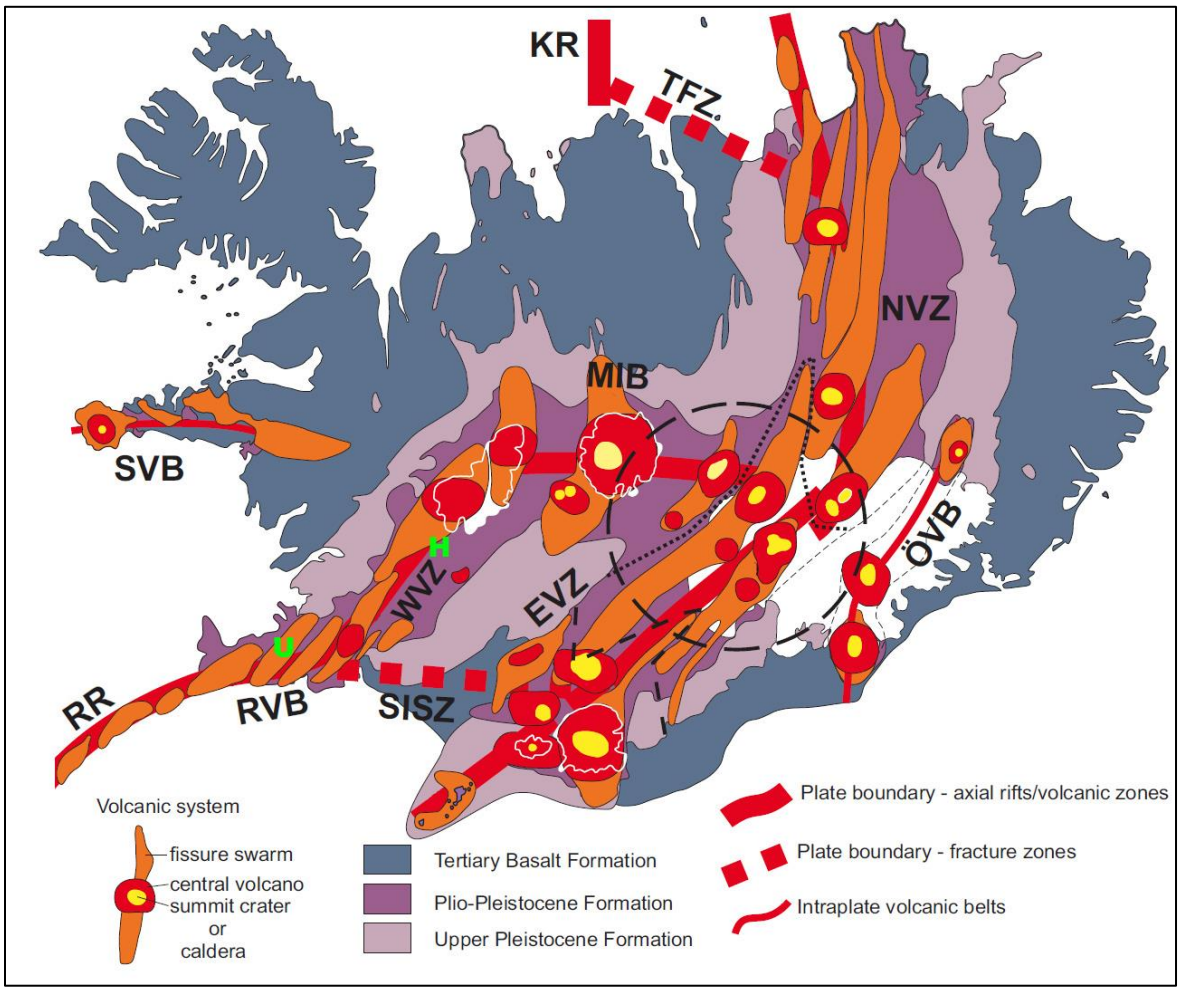

Figure 4-1. Volcanic zones and volcanic systems in Iceland with location of study areas. Abbreviations are: ***RR****, Reykjanes Ridge;* ***RVB****, Reykjanes Volcanic Belt;* ***SISZ****, South Iceland Seismic Zone;* ***WVZ****, West Volcanic Zone;* ***MIB****, Mid-Iceland Belt;* ***EVZ****, East Volcanic Zone;* ***NVZ****, North Volcanic Zone;* ***TFZ****, Tjörnes Fracture Zone;* ***KR****, Kolbeinsey Ridge;* ***ÖVB****, Öræfi Volcanic Belt;* ***SVB****, Snæfellsnes Volcanic Belt;* ***U****, location of Undirhlíðar study area; and* ***H****, location of Hlöðufell study area. Broken circles show approximate location of the Icelandic mantle plume. Figure after Thordarson and Höskuldsson (2008).*

The West Volcanic Zone (WVZ) is a N25° striking lineament extending from the Hengill triple junction, which lies at the WVZ intersection of the Reykjanes Volcanic Belt (RVB) and the South Iceland Seismic Zone (SISZ). The spreading rate of the WVZ has been approximately 1 cm/yr (Luxey, Blondel & Parson, 1997) over the last few thousand years, which is about half the total spreading rate in Iceland.

The study areas of this research are at two locations. The quarry at Undirhlíðar in the Reykjanes Volcanic Belt was used as a pre-project to learn the sampling methods and the magnetic measurement. The main research area (Figure 4-1) is the tuya Hlöðufell in the West-Volcanic Zone. Undirhlíðar is marked as "U" and Hlöðufell is marked as "H".

4.2 Hyaloclastite mountains

The hyaloclastite mountains are a very prominent landform in the active volcanic zones of Iceland. From the research of M.A. Peacock in the first decades of the 20th century it became clear that the hyaloclastite formations in Iceland have their origins from lacustrine eruptions, usually subglacial (Jakobsson & Gudmundsson, 2012).

When an eruption happens in a water, a normal lava cannot form because of rapid cooling and solidification of the magma. We have this situation when an eruption starts in an ocean or in a lake, but this also happens when an eruption starts under a glacier. Then the heat from the lava starts to melt the glacier and forms a lagoon inside the glacier. The development of a tuya forming under a glacier is shown in Figure 4-2. The main units of a tuya after the glacier has melted away is shown in Figure 4-3 (Sigmundsson et al., 2013; Jakobsson & Gudmundsson, 2012).

The formation of the tuya, Hlöðufell has previously (Skilling, 2009) been described in four different stages and those stages will be used in the description here.

Stage I, pillow lava

The base of the construction of hyaloclastite mountains is a *pillow lava* from eruption in deep water where the pressure is high, so the magma solidifies and cools without fragmentation. This can happen in a lake or in an ocean and this can also happen under a glacier as shown in Figure 4-2 A. If the eruption ends here, the result will be a rather low *pillow lava ridge* or *pillow lava mound*. Undirhlíðar is an example of this.

Within the pillows are commonly found sheets of *cube-joint basalt* also called small-jointed columnar sheet lavas or kubbaberg (Jones, 1968; Werner & Schmincke, 1999). Those cubes are usually at least partly irregular and often curvy, and they are assumed to be evidence of fast cooling lava due to water. The formations are usually of limited horizontal extent. In hyaloclastite mountains most of them are probably formed during the effusive deep-water phase but may in some cases be intruded at a later stage of the eruption (Jakobsson & Johnson, 2012).

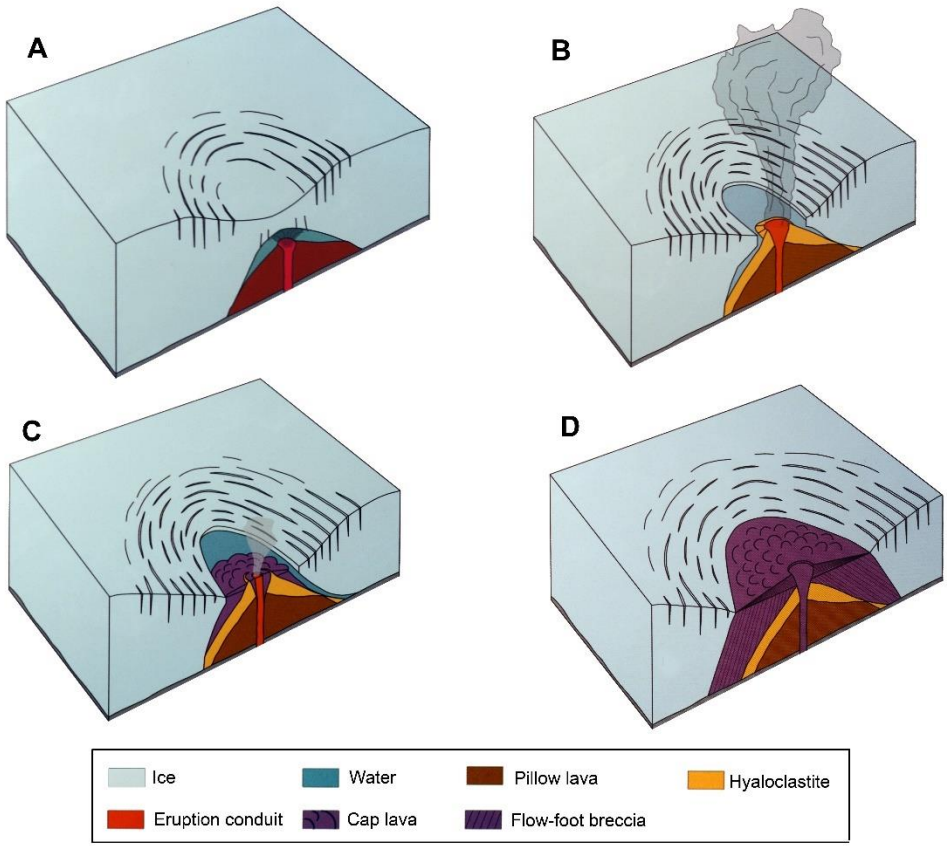

Figure 4-2. The development of a hyaloclastite mountain (tuya) forming in an eruption under a glacier. (A) An eruption under a glacier forming a pillow lava mound. Melting of the glacier begins forming circular crevasses on the glacier but has not reached the surface of it. (B) The melting of the glacier has reached the surface of it, forming a lake in the glacier. The eruption becomes phreatomagmatic when the pillow lava mound comes closer to the surface of the lake. (C) The eruption has reached the surface of the lake, forming a crater and subaerial flows from the crater. (D) The lava continues to flow building up cap lava above a cross-bedded flow-foot breccia lying on the hyaloclastite. Figures after Sigmundsson et al. (2013)

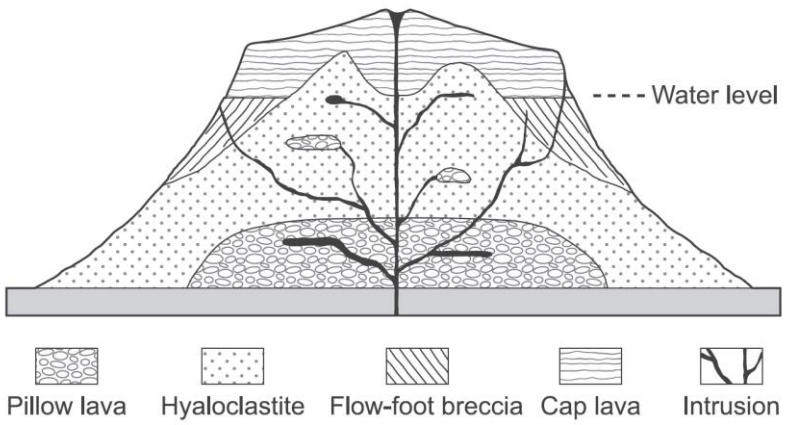

Figure 4-3. Main units of a hyaloclastite mountain, tuya (Jakobsson & Gudmundsson, 2008).

Figure 4-4. An example of cube joint basalt in Hlöðufell within pillow lava or breccia. This formation is in the western side of the ravine, Hlöðuvallagil.

Stage II, hyaloclastite

As the pillow lava continues to pile up, the volcanic vent reaches lower water pressure, the lava starts to fragment and a phreatomagmatic explosive eruption begins, forming clastic, glassy material, the hyaloclastite (Figure 4-2B). Research in the West-Volcanic Zone in Iceland suggests that this effusive-explosive transition in basaltic eruptions can occur at 150-200 m water depth (Jakobsson, 1978; Jakobsson & Gudmundsson, 2012).

If the eruption ends in this stage, the result will be a hyaloclastite mountain usually called hyaloclastite ridges, tindar or móbergshryggir (Jakobsson & Gudmundsson, 2012). Hyaloclastite ridges have been defined as linear ridges of hyaloclastite usually without a cap lava (Jones, 1969; Jakobsson & Gudmundsson, 2008, 2012; Russell, 2014). Þórólfsfell north of Hlöðufell is an example of this.

Intrusions occur in hyaloclastite mountains and are most common in the hyaloclastite, see Figure 4-6 as an example from Hlöðufell. These intrusions are commonly dykes, less than 1m in diameter. They can be irregular with pillow-like formations connected with them. Field research and chemical analysis of the intrusions indicates that they may develop late in the formation of the mountain. Those intrusions may play a role in the solidification of the hyaloclastite, by raising the temperature of the edifice, as proposed for the marine-emergent eruption of Surtsey in 1963-1967 (Jakobsson & Gudmundsson, 2012).

The interaction of water and magma does not necessarily happen at the vent and the tephra can either be unconsolidated or form a consolidated deposit. The term *hyaloclastite* is used as a collective term for volcaniclastic deposits which formed by explosive magma-water fragmentation and non-explosive granulation of glassy lava rims. If the hyaloclastite becomes consolidated it is called *tuff* (Fisher & Schmincke, 1984; Jakobsson & Gudmundsson, 2008).

If clasts as fragments of pillows or lava is in the hyaloclastite, it is commonly called *tuff-breccia* or pillow-breccia, see Figure 4-7. If the hyaloclastite (with or without isolated pillows and pillow fragments) forms a large relatively flat layer it can be called *moberg sheet* (Walker & Blake, 1966; Loughlin, 2002; Jakobsson & Gudmundsson, 2008, 2012).

Stage III, cap lava

If the volcanic edifice builds up to the lake surface, eventually the eruption may become effusive again as water no longer has access to the vents. As a result, lava may again flow from the vents. The lava advances over the hyaloclastite top as a *cap lava* and as the lava flow into the surrounding water in the ice-confined lake the lava fragments and cascades down the slopes, forming a *flow-foot breccia*. This breccia is cross-bedded, commonly with the layers dipping by 25-35° consisting mostly of angular clasts larger than 1 cm. The breccia is composed of hyaloclastite, pillows and pillow fragments. The interface between the flow foot breccia and the cap lava is called a *passage zone* and indicates the water-level from the eruption. An example of a passage zone indicating the water-level from an eruption from Hlöðufell is shown in Figure 4-5. A flow-foot breccia has also been referred to as a foreset breccia and a lava-fed delta (Jakobsson & Gudmundsson, 2008, 2012; Skilling, 2009; Jakobsson, 1978; Jones, 1970).

If the eruption reaches this final stage, we have what is called a *tuya* while the Icelandic word used is stapi or móbergsstapi.

Repeated stages in hyaloclastite mountains

The stages can be repeated in the hyaloclastite mountains. That is the case in Hlöðufell where two cap lavas have previously been identified by Skilling (2009) above two separate flow foot breccias and have been referred to as Stage III and Stage IV (Figure 4-9).

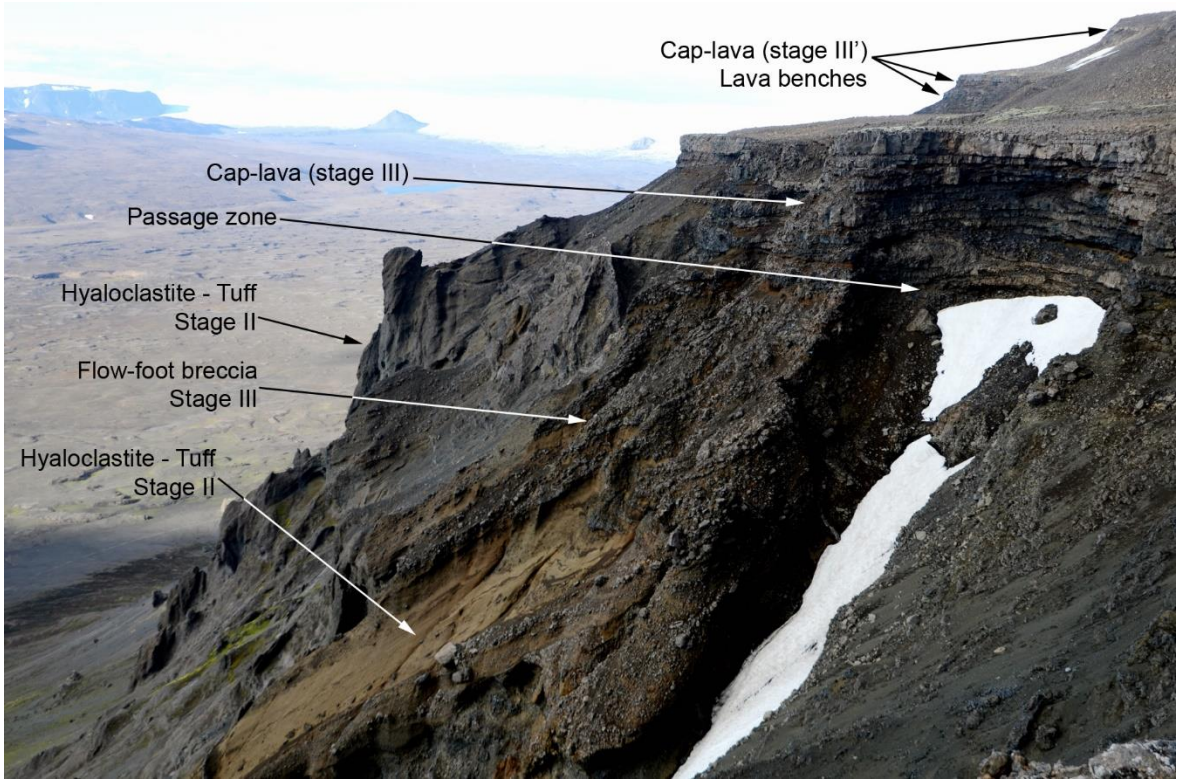

Figure 4-5 Some of the typical units in hyaloclastite mountains, Hlöðufell, North west part, photo taken from northern lower terrace. The flow-foot breccia is from the stage of an eruption when a lava advanced into a glacial lake and the passage zone between the cap lava and the flow-foot breccia indicates the water-level when this was happening. Note that several cap lavas are indicated in the photo.

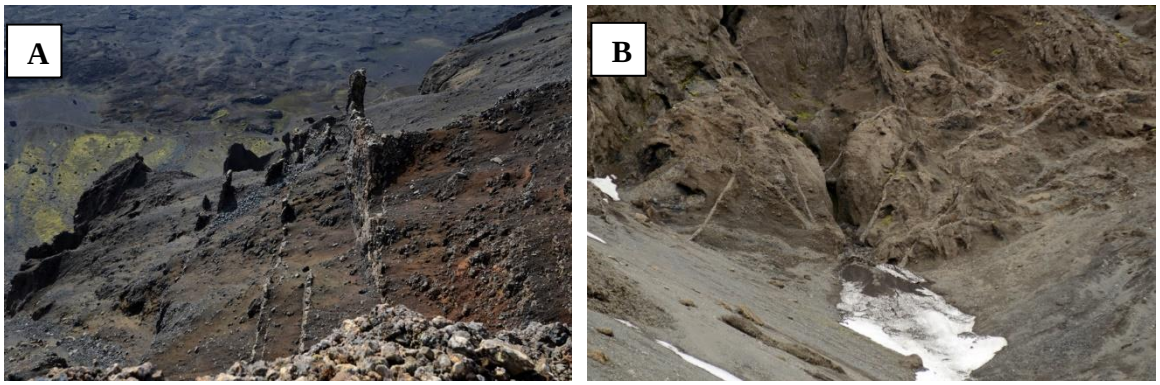

Figure 4-6. Dykes in hyaloclastite in Hlöðufell. ***A****: NW part of the Hlöðufell, photo taken from above stage III.* ***B****: Dykes in east part of Hlöðufell, photo taken from the road around the mountain.*

Figure 4-7. Tuff-breccia (above the yellow hammer) on top of pillow-lava in Rani at Hlöðufell Area.

Paleomagnetic measurements in hyaloclastite mountains

Paleomagnetic measurements have not been done often in hyaloclastite mountains. Since they can best be done in lavas or crystalline intrusions the focus of this research is the paleomagnetism of the pillow lava forming the base of the mountains and the subaerial lava forming the top part. The only known paleomagnetic measurements in Icelandic hyaloclastite mountains are unpublished measurements made in year 2003 in Hlöðufell by Leo Kristjansson and Magnus Tumi Gudmundsson, see Appendix C. Several studies have also been made in the hill Skálamælifell in the Reykjanes peninsula, and nearby volcanoes (Jicha et al., 2011).

4.3 Hlöðufell and Hlöðufell area

Hlöðufell is one of the most prominent tuyas in Iceland located in the West-Volcanic zone, south of Langjökull see maps on Figure 4-1 and Figure 4-8 showing its location, sideview photos in Figure 4-9 and a map of the mountain in Figure 4-10 showing the stages in the building of the mountain among other things. Hlöðufell is in an area of several postglacial lavas and it is surrounded completely with two of them: Lambahraun 4000 years old east of the mountain and Sköflungur lava aged 5300 years in west and north side of the mountain (Sinton, Grönvold &

Sæmundsson, 2005). Hlöðufell itself has been dated 172 kyr (Jakobsson, Gudmundsson & Duncan, 2003).

The region around Hlöðufell hosts several other large hyaloclastite mountains. These include the tuyas: Skriða, Högnhöfði and Rauðafell, and the hyaloclastite ridges Þórólfsfell, Skriðutindar and Kálfstindur.

Topographical characteristics of Hlöðufell are in Table 4-1.

Table 4-1. Topographical characteristics of Hlöðufell

Element aspect	Data	Note	Reference
Altitude	1186m a.s.l.	Highest point of the mountain, reading from a map	(Mál og menning / Forlagið, 2009)
Altitude of the surroundings	447m a.s.l.	Reading from a map, lowest point in a mudflat close to Hlöðuvellir to find altitude of area under the lava forming after the formation of the mountain.	(Mál og menning / Forlagið, 2009)
Relative height of the mountain	740 m	Estimate of the relative height of the mountain before the formation of the surrounding lavas, lowest point taken close to the mountain. 1186-447 = 739 ≈740 m. Note however that the mountain rises only 660-720 m above the lavas surrounding the mountain.	(Mál og menning / Forlagið, 2009; Gudmundsson, Hognadottir, Jakobsson, 2000)
Estimated volume of the mountain	3.3 km^3	Estimate of volume of Hlöðufell is done in Appendix E.	Appendix E
Location	N64.42° W20.54°	Approximate center of the mountain.	(Mál og menning / Forlagið, 2009)

4.3.1 General description of the edifice construction

The general structure and formation of Hlöðufell has been described by Skilling (2009), who divided it into four stages. Skilling's definitions are adopted here. Approximate location of the stages is shown in Figure 4-9 and the map in Figure 4-10.

Stage I: Sub-Ice pillow lava complex

The initial stage of the construction of Hlöðufell is the formation of subaqueous pillow lava. The pillow lava formation is mostly hidden under hyaloclastite, breccias and talus on the slope of the mountain (Figure 4-9) but is visible in several gullies and other natural outcrops around the mountain so most likely the pillow lavas form a basement under the whole mountain. The pillow lavas are best exposed in the ravine on the south of the mountain. Here the name Hlöðuvallagil is used for this ravine. In general it is not possible to define how thick the Stage I formation is, since it is mostly covered by thick talus in the side of the mountain (Figure 4-9). However, in previous research of Skilling (2009) the Stage I formation was measured to be up to 240 m thick in Hlöðuvallagil (Figure 4-10).

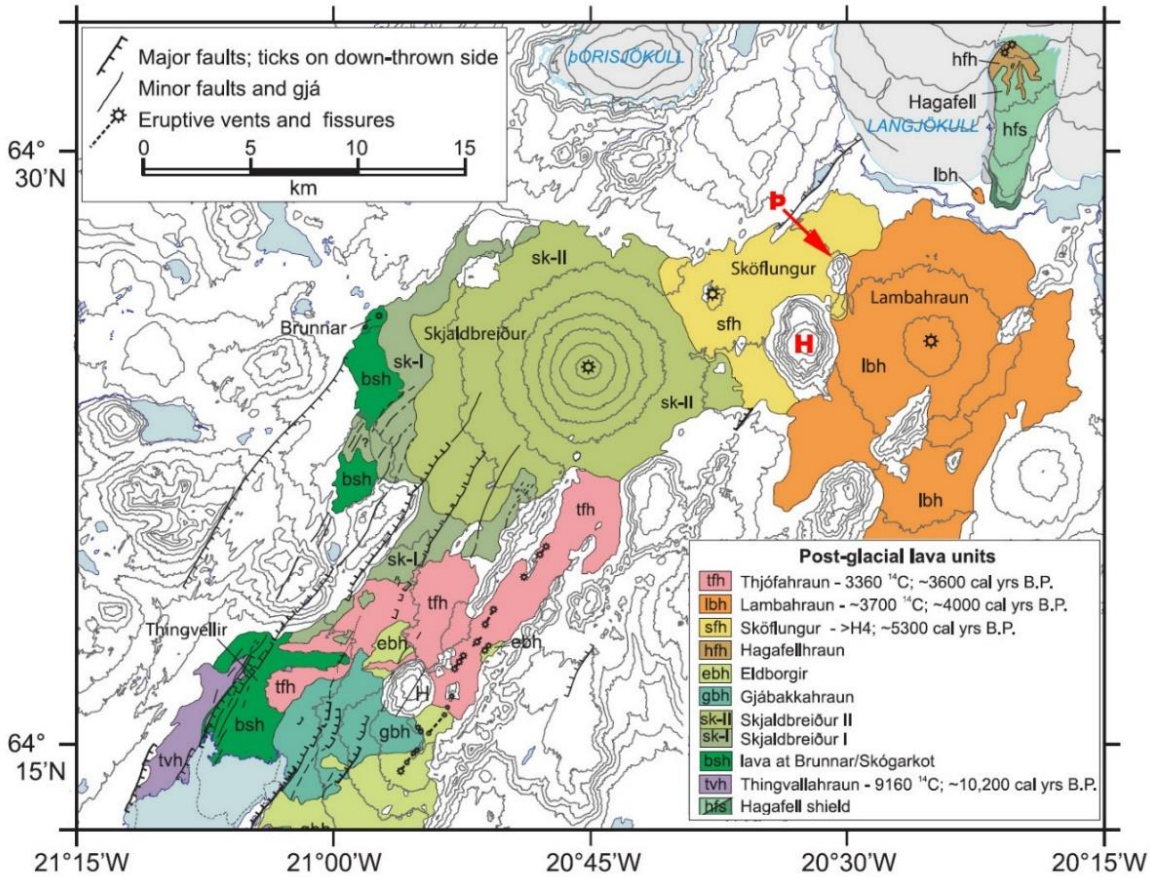

*Figure 4-8. Geology map showing the area around Hlöðufell in West-Volcanic Zone. Hlöðufell marked with **H** is located between Lambahraun and Sköflungur. Þórólfsfell, north of Hlöðufell is marked with **Þ**. Map modified from Sinton et al. (2005).*

Rani, a peninsular snout extending outwards from the SE corner of Hlöðufell, forms a part of the Stage I formation. Rani is mostly made of pillow lava but has a draping of hyaloclastite tuffs (Figure 4-11). It is about 70 m high relative to the flats to the west, east and south.

Stage II

The stage II formation is made of phreatomagnetic, Surtseyan water-lain tephra, appearing as hyaloclastite, tuff and tuff-breccia in the lower half of the cliffs and visible in some places of the sides of the mountain (Figure 4-9). Dykes are also commonly seen in these Stage II tuffs. Many of these dykes extend higher up into the Stage III and even IV formations. In the Rani area (Figure 4-11) water-lain tuff as stage II formation drapes the pillow lavas from stage I formation in places showing cross-bedded flow structures.

The main vent for the Stage II part of eruption that formed the mountain has been assumed to be the cone in the south-east end of the mountain (Skilling, 2009), here called Suðurgígur (Figure 4-10).

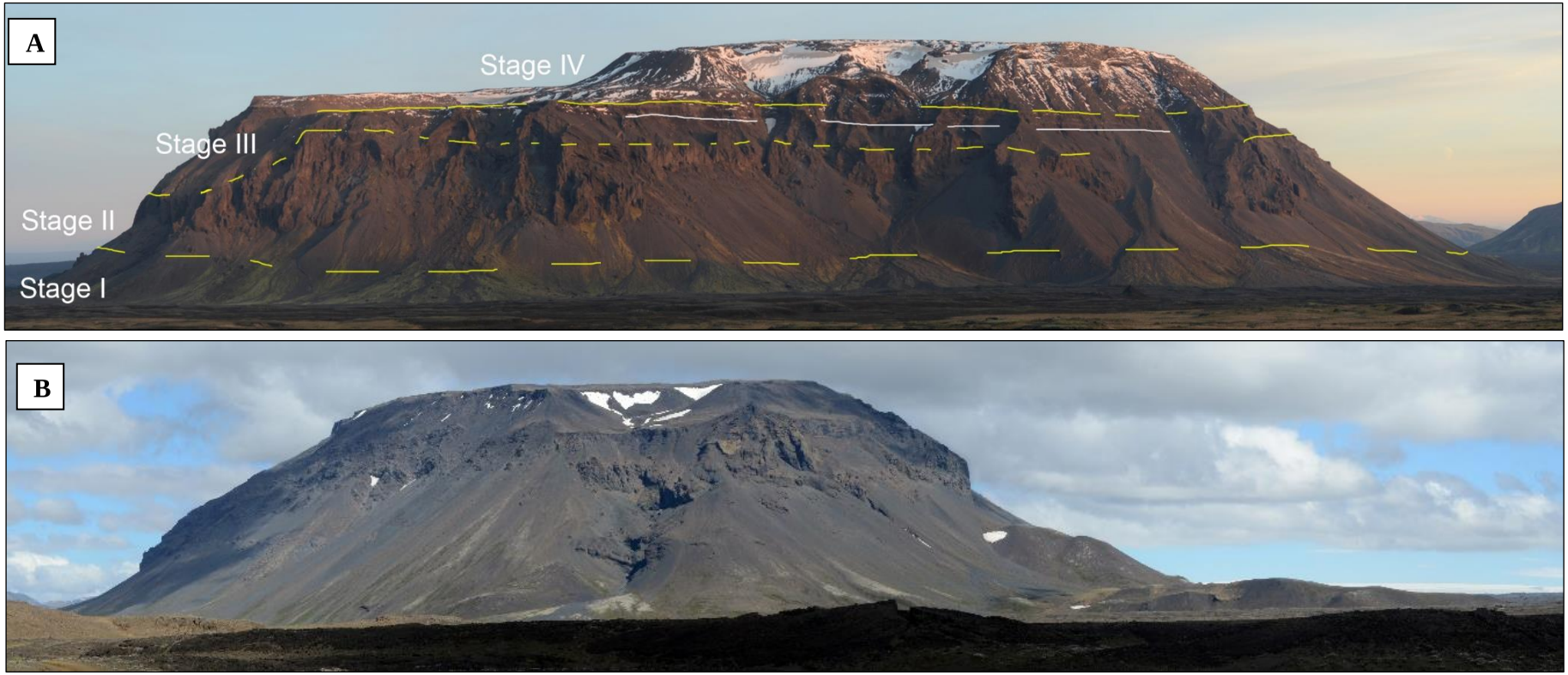

Figure 4-9. Hlöðufell. A talus is covering most of the pillow lavas in in the lower areas of the mountain. A tuff for a couple of hundreds of meters is above the talus area and then there are easily visible the two main lava-units. (A) A view from Sköflungur, north-west of the mountain. The northern terrace is on the left-hand side of the photo. (B) A view from south of the mountain from the road from Laugarvatn. The ravine in the middle of the mountain is here called Hlöðuvallagil. On the right-hand side (south-east) of the mountain is one mound visible. The ridge, Rani is leading more to the right-hand side of the mountain.

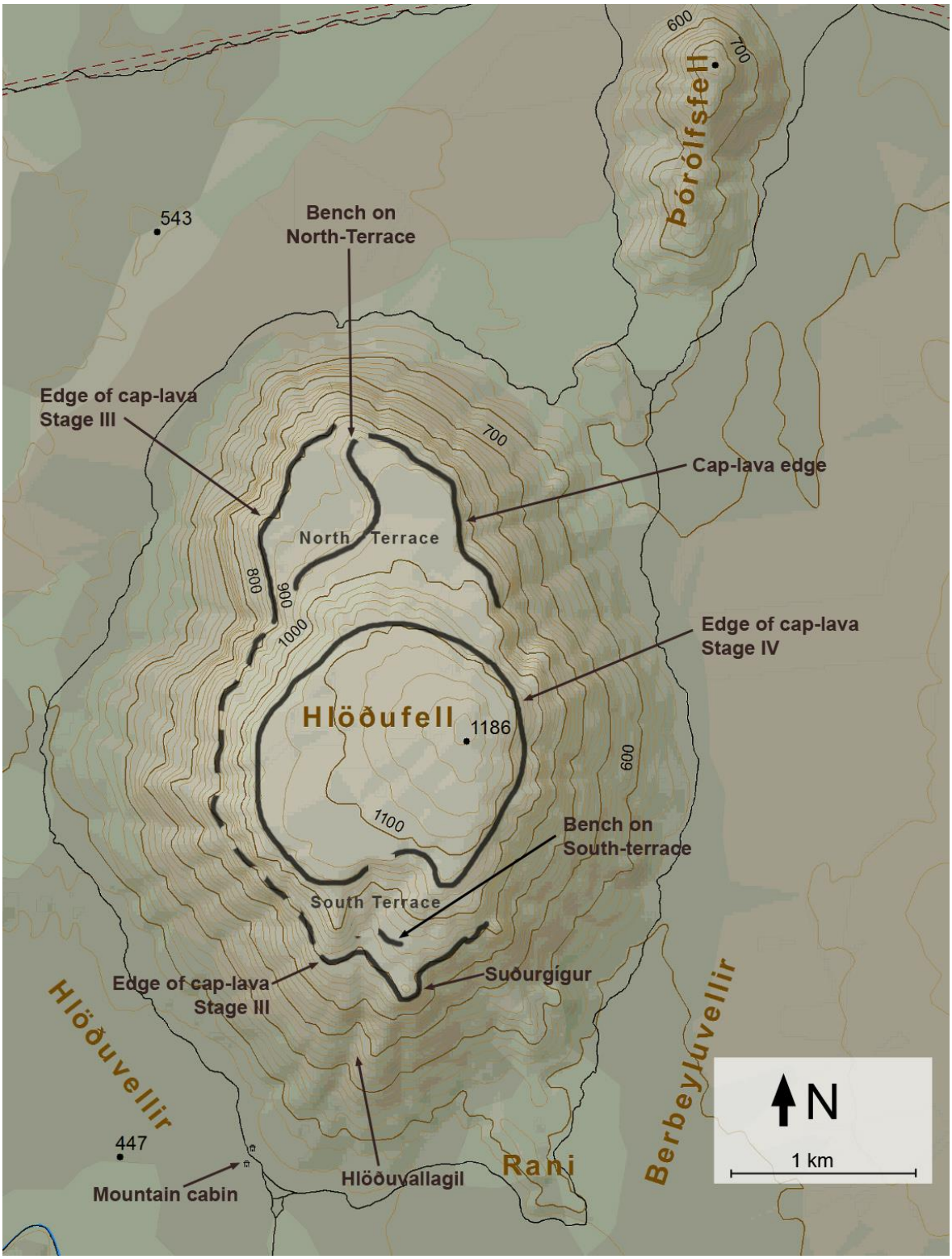

Figure 4-10. Maps of the area, Hlöðufell and Þórólfsfell. Cap lava edges of Stages III and IV in Hlöðufell are shown and lava benches described in Chapter 5 are shown.

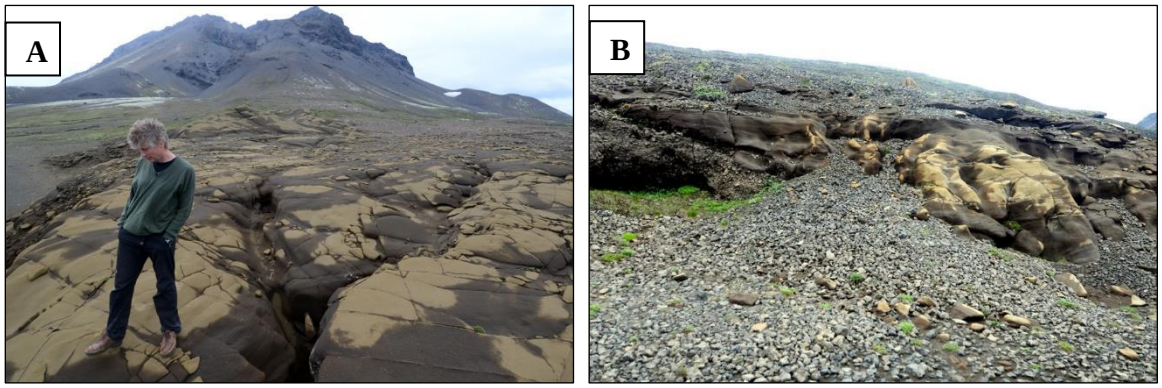

Figure 4-11. From Rani, a broad low ridge extending south east from Hlöðufell. (A) In Rani area, water-lain hyaloclastite-tuff on surface, Hlöðufell in the background. (B) Tuff-breccia in Rani and water-lain hyaloclastite-tuff on top of the breccia.

It is difficult to measure the thickness of the hyaloclastite in stage II formation but the formation could be 150 m thick and in some places almost reach the passage zone below the cap lava of stage III formation.

Stage III

Stage III is formed by the first or lowest part of subaerial lava flows. It consists of flow-foot breccia underlying a pahoehoe cap-lava. The passage zone has been described to be sub horizontal and not displaying any obvious steps between places on the mountain, indicating stable water-level during that stage of the eruption (Skilling, 2009).

The passage zone of stage III formation was measured 810 m a.s.l. in the south part of Hlöðufell in Hlöðuvallagil. The upper part of the bench there is about 50 m higher, that is 860 m a.s.l. (Figure 5-6).

Stage IV

Stage IV has been referred to as the upper cap lava. It also has a clear flow-foot breccia, as is does the Stage III formation. The Stage IV lava does not cover the whole area of Stage III cap-lava so it leaves terraces or benches in both the south and north parts of the mountain. The north terrace is much larger (Figure 4-9A). The main crater for the Stage IV formation is the summit of the mountain. There is also obvious secondary crater, here called Austurgígur and there is also a possible small crater, marked Vesturgígur.

The difference in altitude between the passage zones of Stages III and IV formations is about 150 m, indicating the rise of the water-level before the onset of Stage IV. Former research has not identified any significant time gap between Stage III and IV formation, indicating relatively rapid change in the rise of water-level (Skilling, 2009). The height of the mountain is 1186 m a.s.l. so according to this 150 m, the stage IV formation is from approximately 1040 m height of the passage zone a.s.l.

5 Stratigraphic observations at Hlöðufell

Previous research of Hlöðufell has only identified two sets of cap-lavas (Stage III and IV) with separate flow foot breccias for each cap lava. However, during the paleomagnetic sampling of Hlöðufell observations of the stratigraphy and in particular the area between Stage III and Stage IV lava caps indicate that small additional lava caps exist between the two main ones. The evidence for this is presented below. The map in Figure 4-10 marks the lava layers observed in the mountain.

5.1 Lava benches, cap lava on the north terrace of Hlöðufell

There are additional benches that can be clearly seen on both the north and the south terrace. The main lava bench on the north terrace is so large it can be seen on a map (Figure 4-10) and there are also several smaller benches higher up in the terrace (Figure 5-1). The main bench on the north terrace have previously been assumed to be formed from glacial erosion (Skilling, 2009). However, they could also have formed by a rise in the water level, possibly accompanied by thickening of the glacier during the eruption, with or without discontinuity in eruptive activity during this possible rise in water level.

Since no clear signs of glacial erosion were observed in relation to the benches and since that it looks like a flow-foot breccia is part of the bench (Figure 5-2), it is here assumed more likely that the benches were formed during the eruption. Figure 5-2 is taken from the lower level of the north terrace. It indicates the existence of flow-foot breccias between the benches. However, those formations were not investigated in detail. On the east part of the north terrace are also some more complex flow-foot breccias (Figure 5-3), also indicating some change in water level during the eruption.

5.2 Lava benches, cap lava on the south terrace of Hlöðufell

On the south terrace one clear lava bench is above the main cap lava of Hlöðuvallagil (Figure 5-4). There was a sampling site taken from this lava bench (HF-K) and it is more than 50 m higher than the highest sampling site of the main cap lava of stage III (HF-Y).

No flow foot breccia was noticed in connection to that lava bench in this location. However, west of the south terrace a flow foot breccia is at a higher altitude than the main cap lava of stage III, see Figure 5-5. Those photos show a cap lava somewhat higher and what looks like flow-foot breccia also at an elevation slightly above 900 m. Note also the flow-foot breccia from the superimposed cap lava from Stage IV that looks like it has been flowing down previously eroded cliffs of the underlying cap lava.

In this research Stage III will be referred to as clearly the lowest cap lava with surely just one flow-foot breccia underneath and Stage IV will be referred to as clearly the highest cap lava with clearly no flow-foot breccia above. Cap lavas with possible more than one flow foot breccia underneath and still one or more flow-foot breccias above, will be referred to as Stage III'.

Figure 5-1. Photos taken on the north terrace of Hlöðufell providing a view over the terrace which can be split into two levels. (A) From the slope of Stage IV over the bench on the terrace, the photo is taken from close to the sampling site HF-P and it is showing the most prominent bench on the terrace that HF-O is taken from. (B) View over the slope of the bench of the north terrace, showing three small benches.

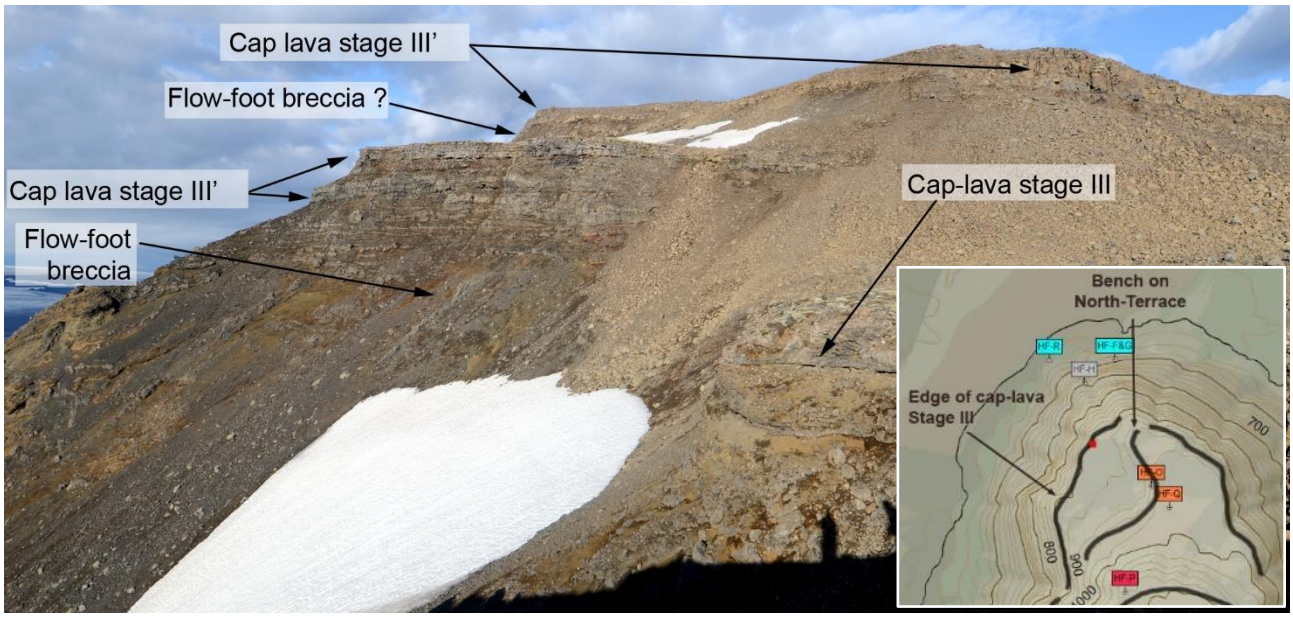

Figure 5-2. Lava benches in stage III' on the north terrace, east side. Photo taken from location: N64.43324 W20.55267 in ENE direction, location is marked with a red square on the inset map.

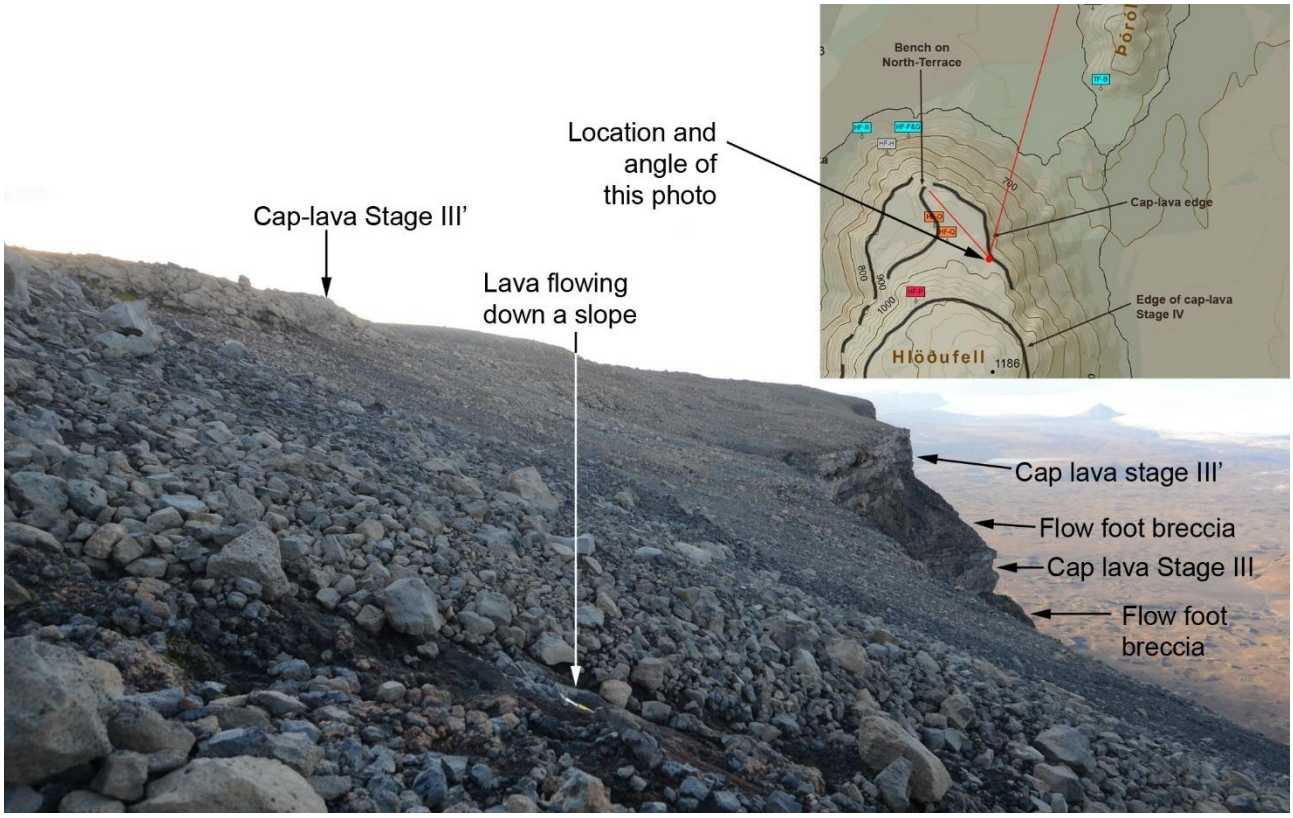

Figure 5-3. Lava benches in stage III' on the north terrace, west side. The photo is taken in WNW direction, location and angle of photo are marked with a red dot on the inset map. All the area on this photo is much lower than Stage IV cap lava.

Figure 5-4. Lava bench on the south terrace, above the cap lava in stage III. Here referred to as stage III'. Sampling site HF-K is from this lava bench.

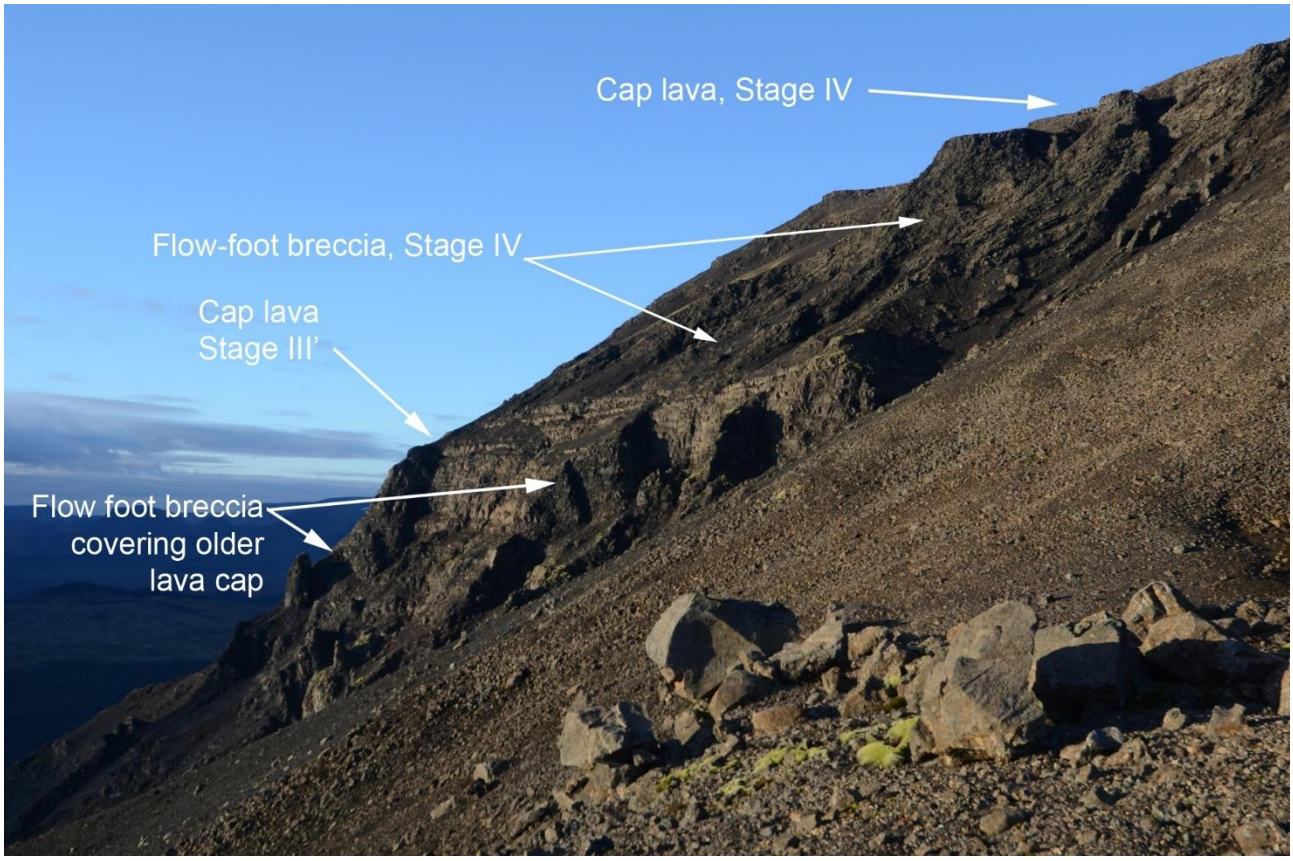

Figure 5-5. Photo taken from the south bench or terrace along the western side of the mountain. The photo is taken from altitude at least 50 m higher than the cap lava stage III in the south of Hlöðufell (sampling site HF-Y). But also note here that there is no visible lower stage III cap lava on this photo.

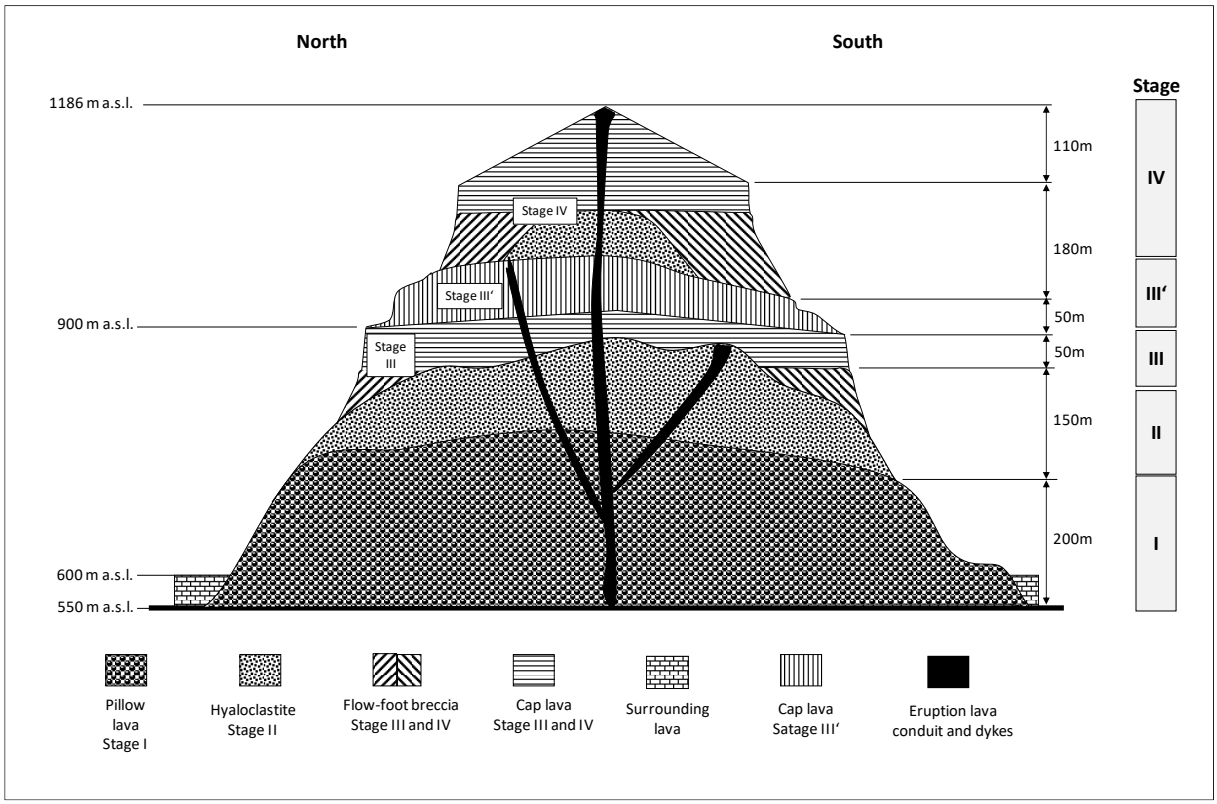

Figure 5-6. Schematic diagram of Hlöðufell based on observations done in this project and previous research made by Skilling (2009). Note that since most of the slopes of the mountain are covered by talus and elevation measurements are from maps and hand-held GPS, all elevation and thickness data on this diagram is uncertain at least with +/- 20 m confidence limit.

Those observations have been taken together on a schematic diagram (Figure 5-6) showing estimated altitude and thickness of various units.

5.3 Lava on the lower slopes on the western part of the mountain

In the south-western part of Hlöðufell (location on map in Figure 5-7 E) are several outcrops which looked from distance as pillows but upon closer look they are subaerial lavas that have advanced down the slope of the mountain. It is not easy to connect them with the cap lavas from Stage III or Stage IV, since they lie much lower than the flow foot breccia of stage III and its lowest passage zone (Figure 5-7). These lavas were not sampled or studied in detail and no sampling site is from those lavas. It is possible that they are Stage III lavas that have flowed down the slope with their upper parts now covered by talus.

This lava could be described by fluctuations when leakage of a volcanic glacial lake can be triggered by opening of fissures resulting from volcanic activity. After closing the fissures, the water level can rise again by melting (Werner, Schmincke & Sigvaldason, 1996). From fluctuations of that kind we could have partly subaerial lavas forming during a stage that has otherwise dominating explosive eruption in water, forming hyaloclastite.

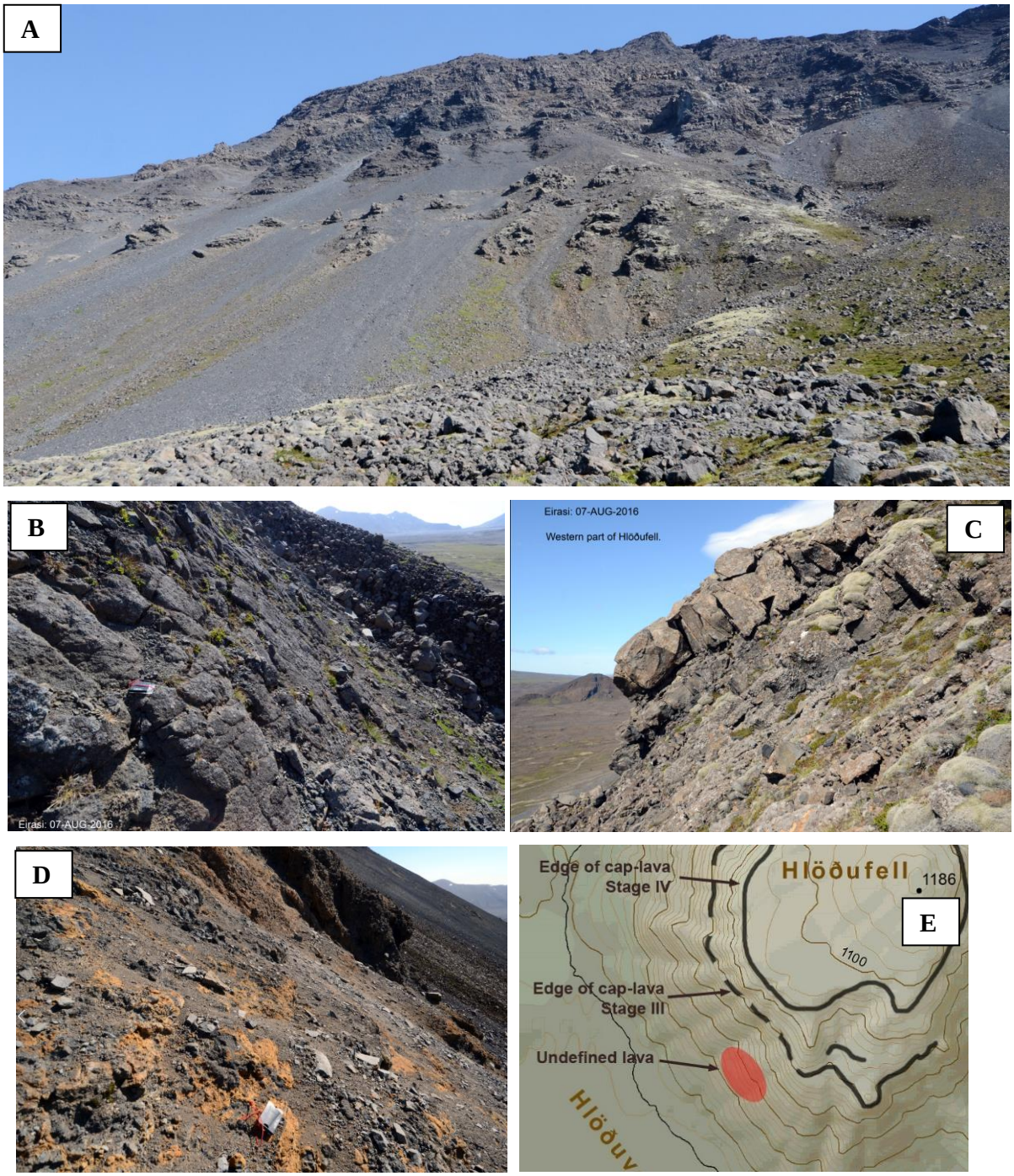

Figure 5-7. Lava in the west slope of Hlöðufell. (A) The lava does not clearly connect to the Stage III cap lava above. (B) Lava, that looks like subaerial lava at an altitude (close to 600 m a.s.l.) much lower than the passage zone of lowest stage III lava. (C) Columnar jointed lava not showing clear signs of rapid cooling by water in similar altitude, close to of 600 m a.s.l. (D) Breccia under Stage III lava at altitudes about 750 m a.s.l. (E) Location of the undefined lava formation.

6 Sampling locations at Hlöðufell area

6.1 Overview

Sampling for paleomagnetic measurements is difficult in hyaloclastite mountains. It is not possible with the technology used in this research to measure directions of the magnetic field from the hyaloclastite itself due to its low magnetization and difficulty of obtaining good cores. Thus, the focus in core sampling was on the pillow lava and cube joint basalt from Stage I and the cap lavas from Stage III and Stage IV. It is also possible to use samples from dykes, but the relative age of dykes compared to the pillows or the cap lavas can be difficult to decide. The breccias are not good for sampling as is not possible to decide with confidence whether the material has cooled and magnetized before or after deposition.

Hlöðufell is a relatively steep mountain with only one good location where the upper parts in stage III can be reached. Because of this, the lower parts are more accessible for core sampling than the higher areas. Therefore, the majority of samples are from Stage I pillow lavas. The outcrops close to Hlöðuvallagil are the most sampled. The lower cap-lavas are mostly inaccessible and during this research it was only possible to get samples from that formation from the south part if the mountain, close to the walking path to the summit, west of Hlöðuvallagil. For overview of location of all sampling sites, see Table 6-1 and a map in Figure 6-1. Then three sampling sites are from the lava benches on north and south terraces, from stage III' as described in previous chapter.

Table 6-1. Overview of sampling sites in Hlöðufell area

Unit		Stage	Number of sites	Sampling sites
Upper cap lava	LAVA-ELP	IV	3	HF-E;L;P;HL-3 *
Cap lava benches on north terrace	LAVA-OQ	III'	2	HF-O; Q
Cap lava benches on south terrace	LAVA-K	III'	1	HF-K
Lower cap lava	LAVA-DJNY	III	4	HF-D; J; N; Y;HL-2 *
Cube joint basalt-lava in Hlöðuvallagil	CJB-C	I	1	HF-C
Pillow lavas west side of Hlöðufell, higher	PILL-FG	I	2	HF-FG
Pillow lavas west side of Hlöðufell, lower	PILL-RS	I	2	HF-R; S
Pillow lavas east side of Hlöðufell	PILL-X	I	1	HF-X
Pillow ridge at Hlöðuvallagil	PILL-AMTU	I	4	HF-A; M; T ; U; HL- 4*
Pillow lava in Rani	PILL-BVW	I	3	HF-B; V; W
Dykes	DYKES-HI	NA	2	HF-H; I
Pillow lava in Þórólfsfell		NA	2	TF-A; B
			29	

* Additional samples (HL) are from previous research from Leo Kristjansson, see Appendix C.

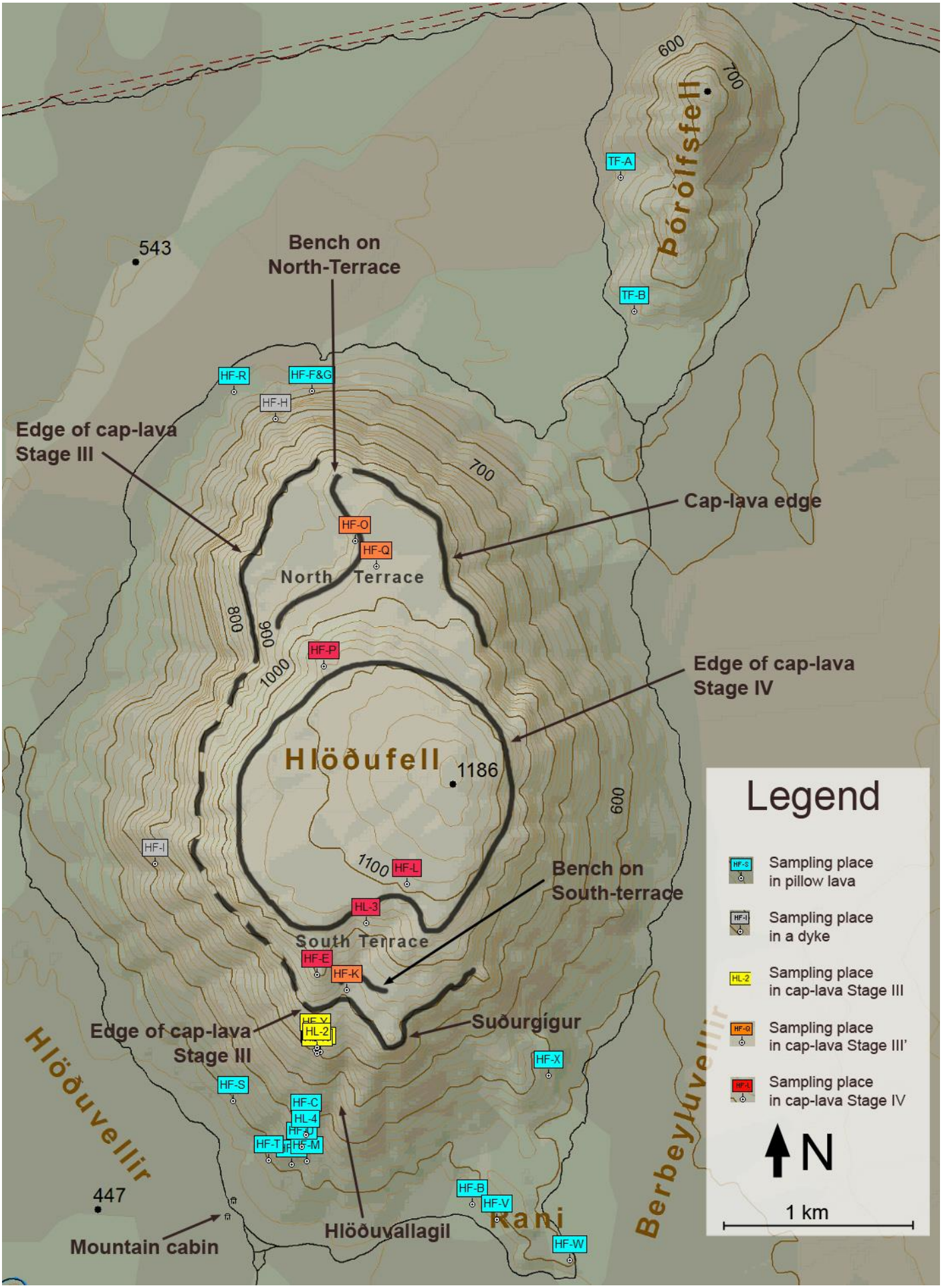

Figure 6-1. Maps showing all sampling sites in Hlöðufell and Þórólfsfell.

Samples from Hlöðufell in this research are all named HF and a letter in alphabetical order, indicating the sampling site. So, the letter after HF has no connection to the stage or unit the sampling site is from but can tell if sampling and orienting in the site began early or late in the research. HF-A is then the first sampling site, taken in year 2014 and HF-Y is the sampling site that was last oriented in the autumn 2016. Overview of all field trips is in Appendix H and basic information about all sampling sites are in Appendix J.

In addition to the sampling in this research from Hlöðufell are two sampling sites named TF that are from the small hyaloclastite ridge Þórólfsfell, north of Hlöðufell. Three sampling sites, named HL are from previous research made by Leo Kristjansson and Magnus Tumi Gudmundsson in year 2003, see Appendix C.

6.2 Stage I: Pillow lavas

6.2.1 General about paleomagnetic measurements of pillow lavas

The material in pillow lavas is in general small jointed basalt full of small fractures. Partly it is irregularly jointed as well and very often could parts of it be referred to as breccia. To have a sample core for magnetic measurements it is necessary to have large enough piece of rocks without fractures to make one sample core. The rocks must be strong enough to not to crack apart when drilling and orienting. This is a difficult condition for paleomagnetic core sampling and in overall, within 50% of the drill holes gave usable sample cores for paleomagnetic measurement in the laboratory.

6.2.2 Pillow ridges

Pillow lava in Rani: HF-B, HF-V and HF-W

There are three sampling sites in Rani, all the samples are from pillow lava. Sampling sites. For location, see maps in Figure 6-1 and Figure 6-3.

Pillow ridge at Hlöðuvallagil: HF-A, HF-M, HF-T, HF-U and HL-4.

Several sampling sites are from the pillow ridge at Hlöðuvallagil, close to Hlöðuvellir from stage I of the formation of Hlöðufell (Skilling, 2009). All sampling sites are from pillows or pillow-like lavas. For precise location, see the map in Figure 6-3.

The altitudes of those sampling sites are all rather similar. Altitudes of HF-A, HF-M and HF-T from about 510 m to 560 m a.s.l. Sampling site HL-4 would then also be from the same unit (Figure 6-2).

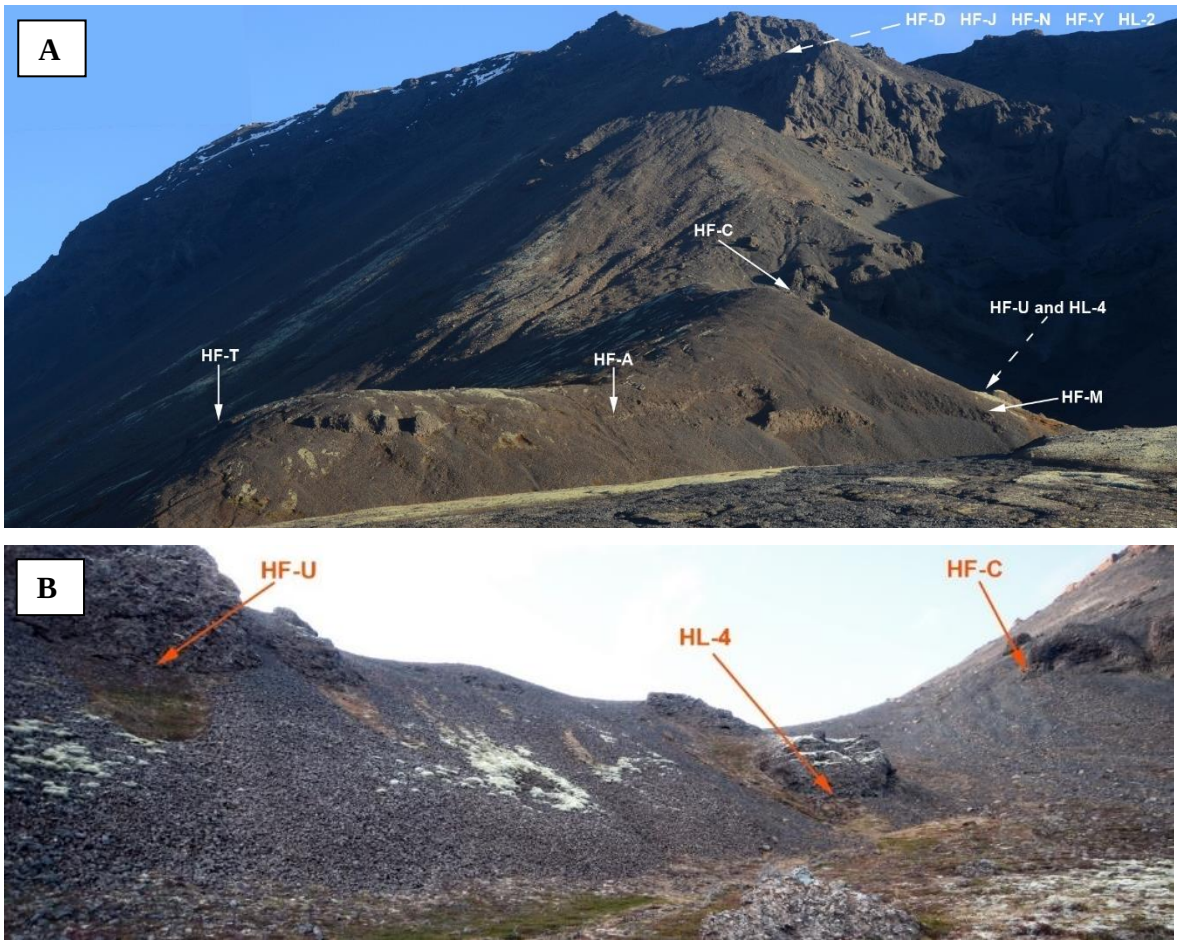

Figure 6-2. Sampling sites in south part of Hlöðufell stage I, pillow ridge close to the mountain hut at Hlöðuvellir. (A) Overview of the sampling sites in the pillow ridge at Hlöðuvellir. (B) Sampling sites HF-U and HL-4 with HF-C which is not necessarily part of the ridge

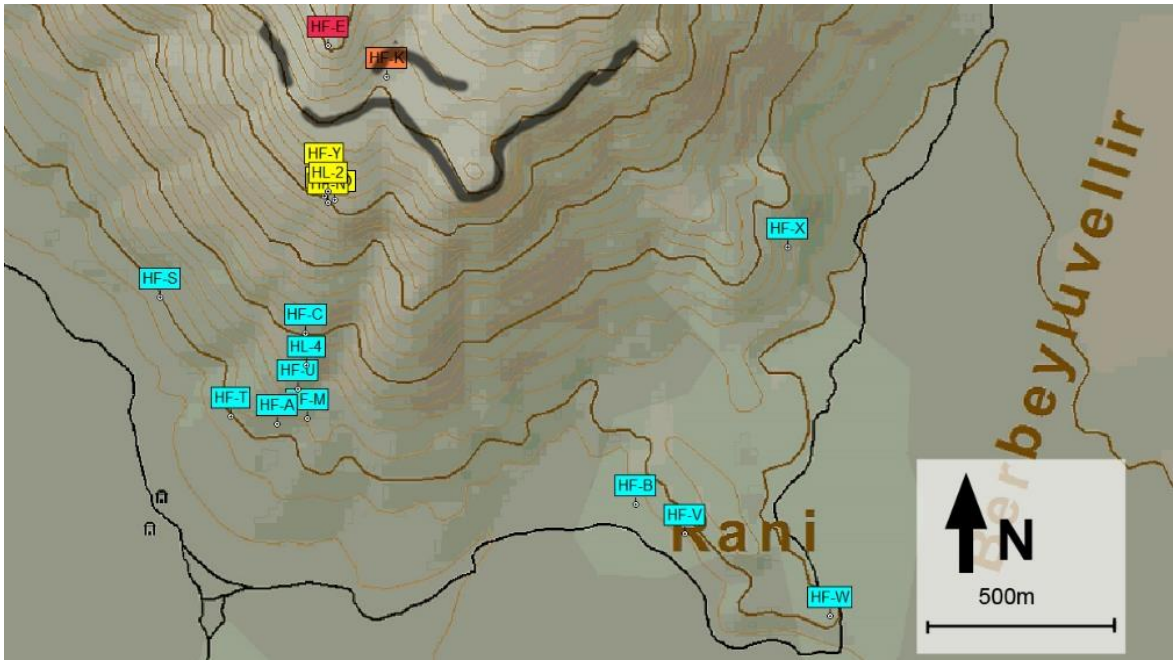

Figure 6-3. A map showing location of sampling sites for Stage I in the south part of Hlöðufell.

6.2.3 Pillow lava in the main mountain

A map showing location of all sampling sites in the main mountain is in Figure 6-5. All those sampling sites are from the lower part of the mountains, from outcrops and ravines. Altitude ranging from little bit more than 500 m a.s.l. to almost 600 m a.s.l.

East side of Hlöðufell, HF-X

There are several ravines in the east side of the mountain where possible sampling sites where but most of them perhaps not very good for paleomagnetic core sampling. Only one sampling site is from this part of the mountain and it is in the south-east part of the mountain, HF-X. Altitude of that sampling site is similar as HF-R. For location, see the maps in Figure 6-1 and Figure 6-3.

West side of Hlöðufell, HF-FG, HF-R and HF-S

Sampling sites HF-F and HF-G are from the same formation which is referred to as the cavity formation (Skilling, 2009). The samples were taken from the outer surface of two pillows, one pillow for each of the two sampling sites. Since they are very close to each other, they are taken as one sampling site, HF-FG.

Most part of the lower western side of Hlöðufell is covered by talus from the higher areas of the mountain so there are not many opportunities for sampling sites there. Two sampling sites were used, HF-R and HF-S from pillow-like lava and they are similar as some of the sampling sites in the pillow ridge at Hlöðuvellir. First it was HF-R which is in the north-west part of the mountain. The second one is HF-S, which is close to the pillow ridge at Hlöðuvellir and Hlöðuvallagil. Of those two, HF-S is several tens of meters lower than HF-R, but they are both lying low in the mountain. For location, see the map in Figure 6-1.

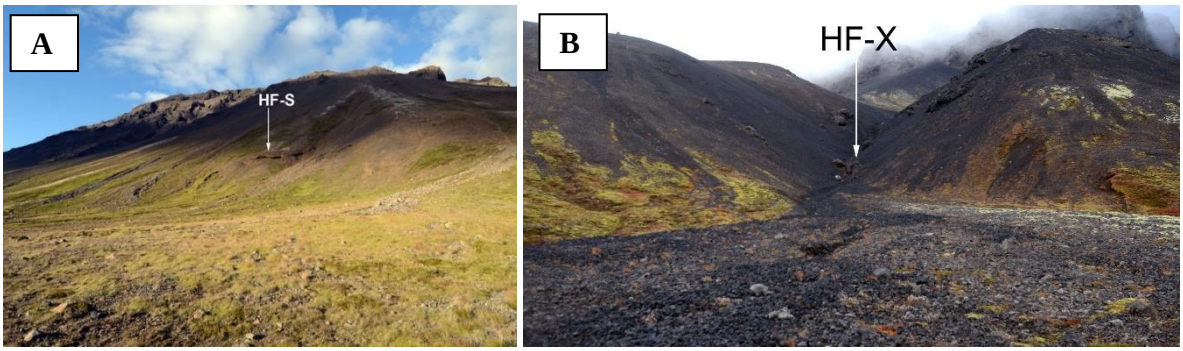

Figure 6-4. (A) Sampling site HF-S in the south-west side of Hlöðufell from stage I. Sampling site HF-R was similar. The pillow ridge at Hlöðuvallagil is farther in the righthand side out of the photo. (B) Sampling site HF-X in a ravine in the east part of the mountain.

West side of Hlöðufell, HF-C

Sampling site HF-C is from cube-joint lava above the pillow ridge above Hlöðuvellir in Hlöðuvallagil, see Figure 6-6 and also Figure 6-2 and the maps in Figure 6-1 and Figure 6-3. It was only possible at the time of sampling in this site to take those samples from rather small area of the formation. Although this sampling site is very close to the sampling sites in the pillow ridge at Hlöðuvellir (Figure 6-2B) it should be clear from Figure 6-6 that the cube joint lava is a part of the main mountain rather than the pillow ridge itself.

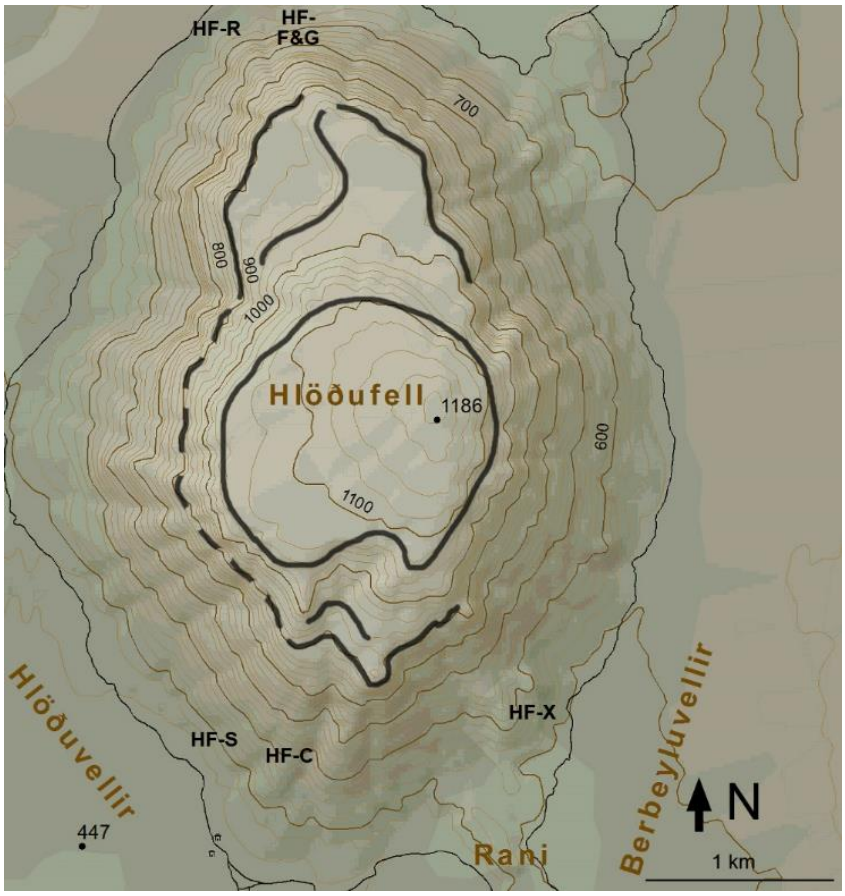

Figure 6-5. A map showing sampling sites in the main mountain.

Figure 6-6. The sampling site HF-C from a cube joint lava in Hlöðuvallagil. The formation is considered to be a part of the main mountain.

6.3 Stage III: Lower cap lava

Lower cap lava, south part: HF-D, HF-J, HF-N, HF-Y and HL-2.

The main part of the lower cap lava in stage III is only easily accessible for sampling in the south part of the mountain were the walking path to the summit goes through in or above Hlöðuvallagil. Samples were gathered in several sampling sites in that area, east of the walking path. All samples are from subaerial lavas. For location of samples see the map in Figure 6-1 and close-up of the map to see relative location of each sampling site in Figure 6-7.

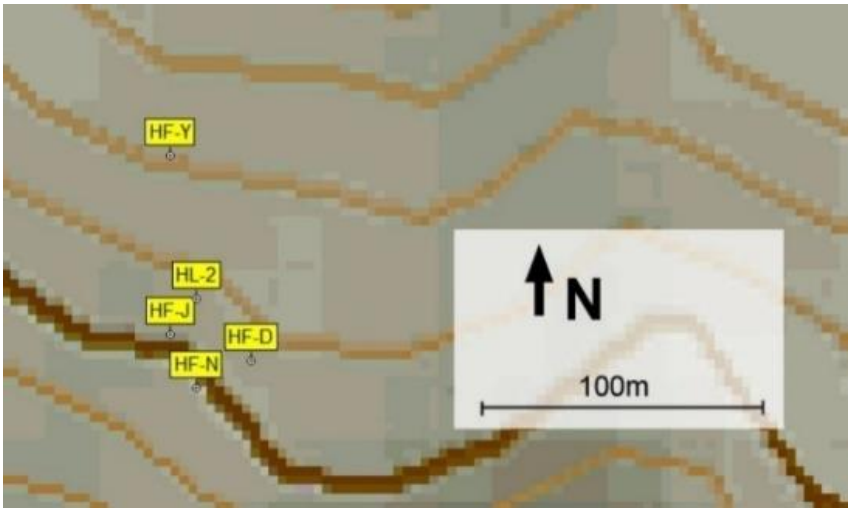

Figure 6-7. Map showing relative location of the sampling sites in lower cap lava, Stage III. See Figure 6-1 and Figure 6-3 for location in the mountain.

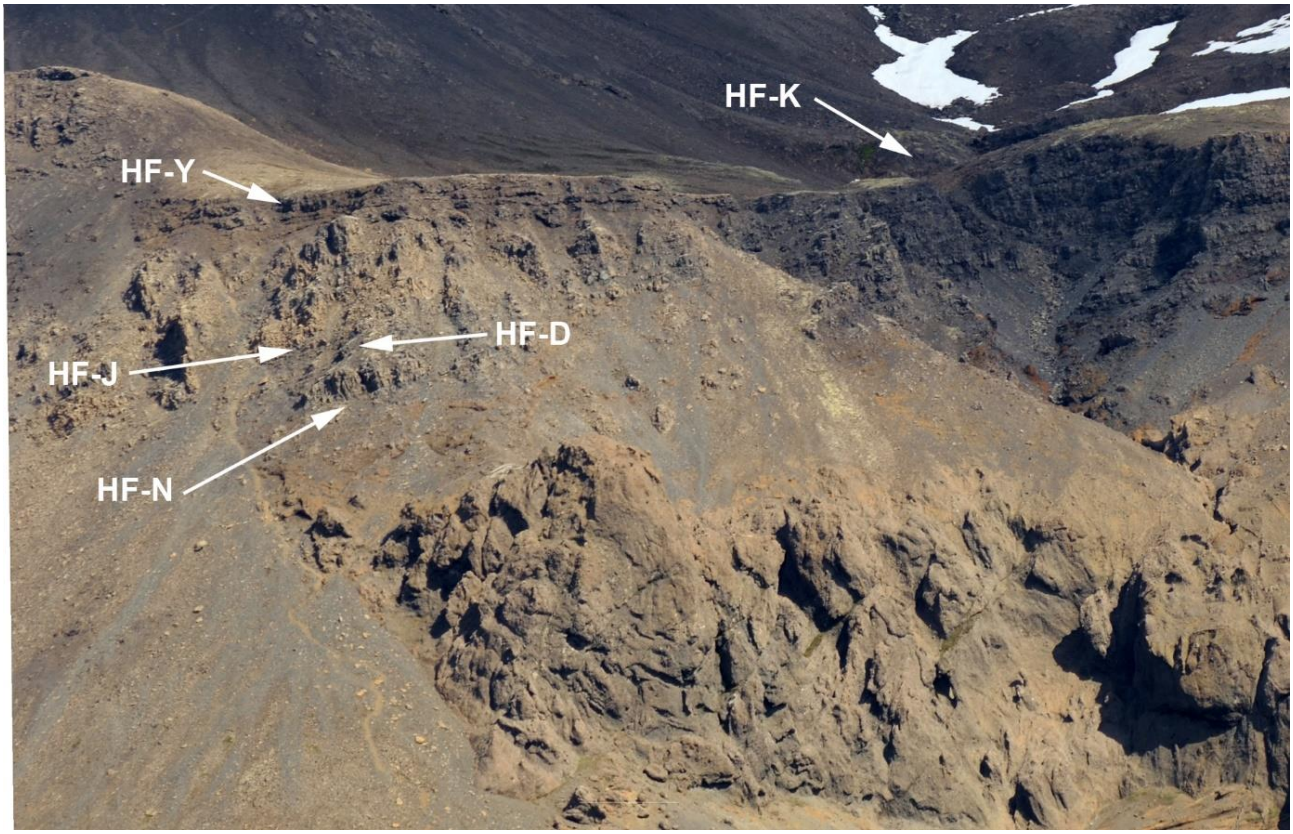

Figure 6-8. Sampling sites in the south part of stage III, lower cap lava, HF-D, HF-J, HF-N, HF-Y.

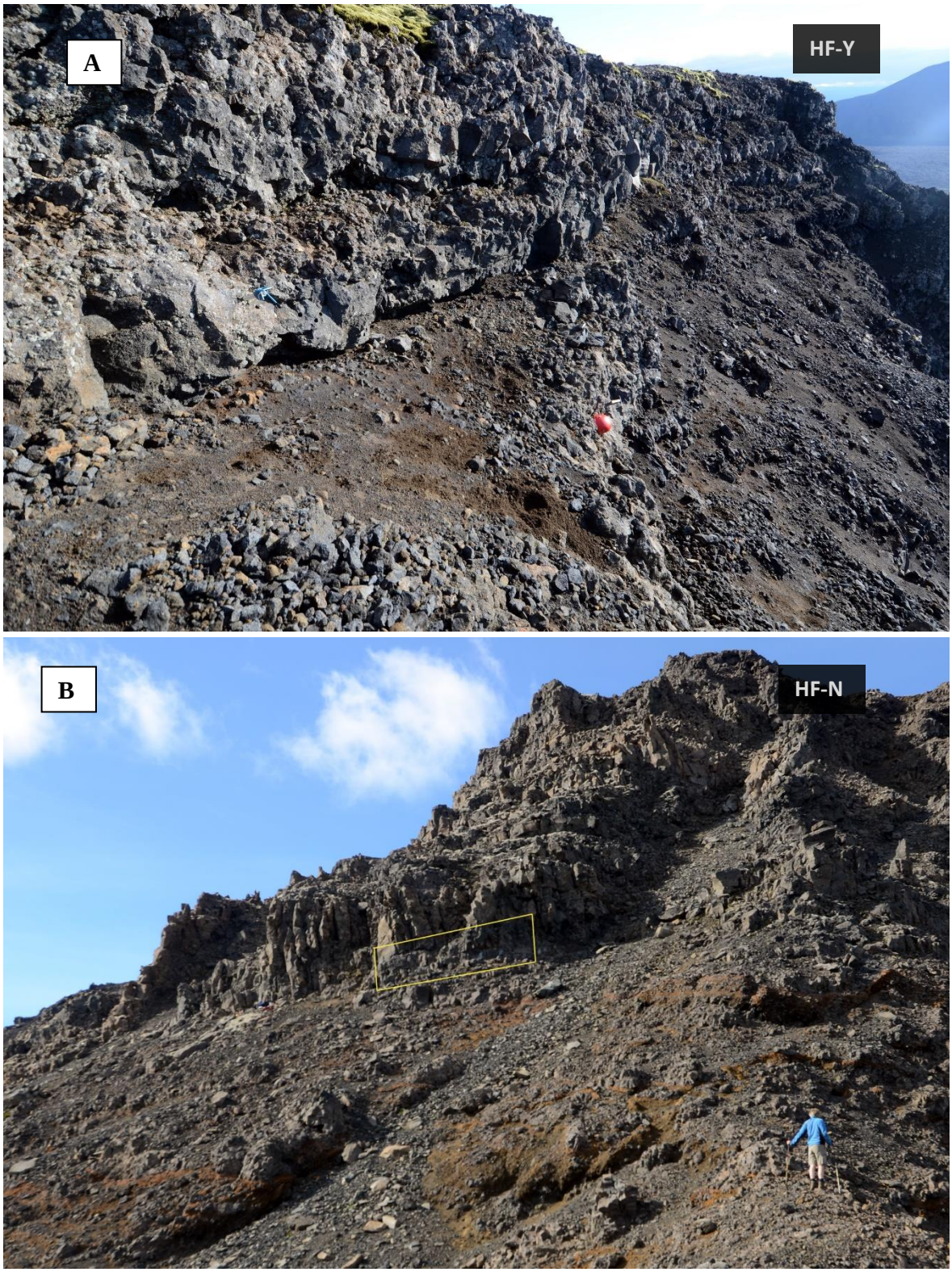

Figure 6-9. Sampling sites in Unit III, lower cap lava. (A) Sampling site HF-Y which is the highest sampling site in the lava cap from unit III. (B) Sampling site HF-N which is the lowest sampling site in the lava cap from unit III, standing on the flow-foot breccia.

As shown on Figure 6-8 and in the map in Figure 6-7, sampling sites HF-D, HF-J and HF-N are close to each other. Sampling site HF-N is lowest, and it is just above the flow-foot breccia and the passage zone. It was measured in altitude of 817 m a.s.l. Sampling site HF-Y is on the other hand just below the edge of the cap lava in stage III as it could be described. According to the GPS measurements of altitudes, the cap lava in Stage III is more than 40 meters thick and, in several places, there are visible some junction that could possibly be between two layers of lava. However, such junctions were not investigated thoroughly in this research but will be considered for the magnetic measurements in this lava.

6.4 Stage III': Lava benches (cap lava) on terraces above Stage III cap lava

As described in Chapter 5 , there are additional lava benches between Stage III and Stage IV and they are here taken separately from the lavas from Stage III and Stage IV and here referred to as Stage III'. One sampling site from those benches is in the south part and two in the north part.

Lava bench, cap lava stage III' on south terrace (HF-K)

Sampling site HF-K is in a low lava bench above the lava bench of unit III, see Figure 6-10. Location of HF-K can be seen the map in Figure 6-1. How it is located in relation with the sampling sites in the lava below the edge of the lava cap of stage III can best be seen on Figure 6-8.

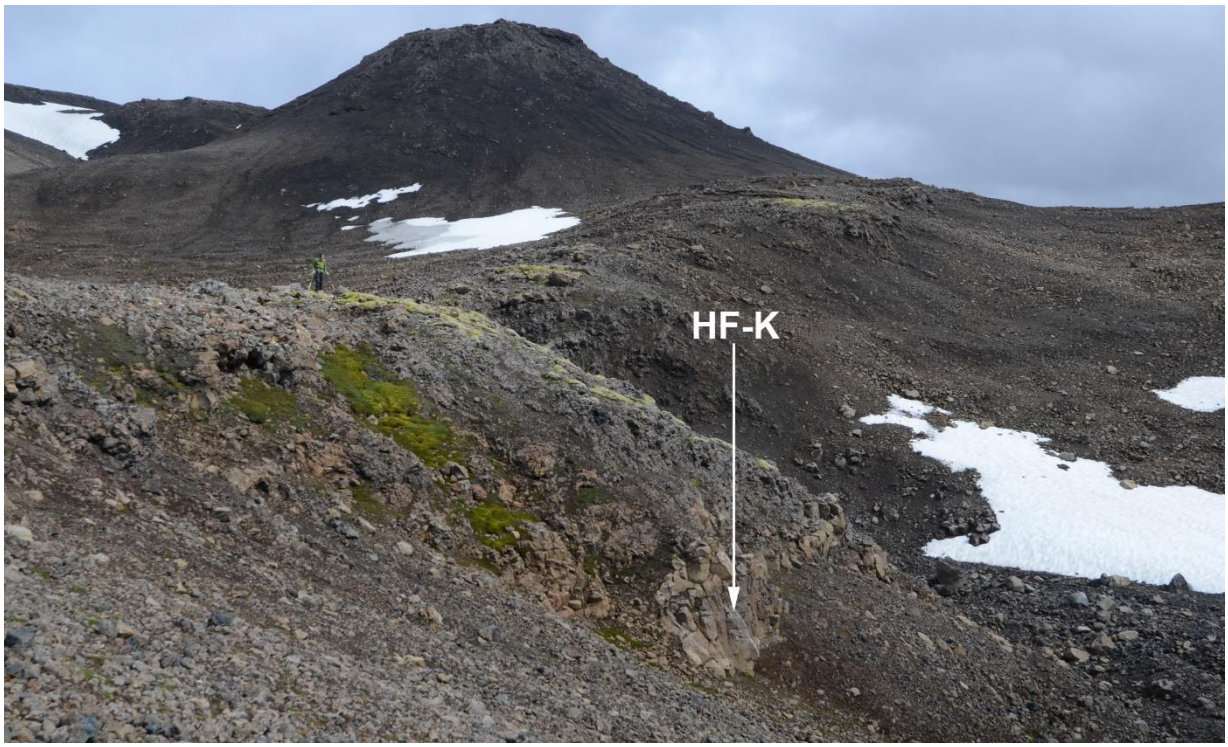

Figure 6-10. Sampling site HF-K in lava bench, cap lava on south terrace, stage III'.

Lava bench, cap lava stage III' on north terrace (HF-O, HF-Q)

In the north terrace where samples taken in two sampling sites, HF-O and HF-Q, see in Figure 6-1 and Figure 6-11. See also Figure 5-1 and Figure 5-2 with discussion about the lava benches on the north terrace. Sampling site HF-O includes quite many samples and was taken from the edge of the lava bench and samples rather well distributed over 50 m wide area. Sampling site HF-Q was a little bit higher up in the same formation in an outcrop making drilling possible.

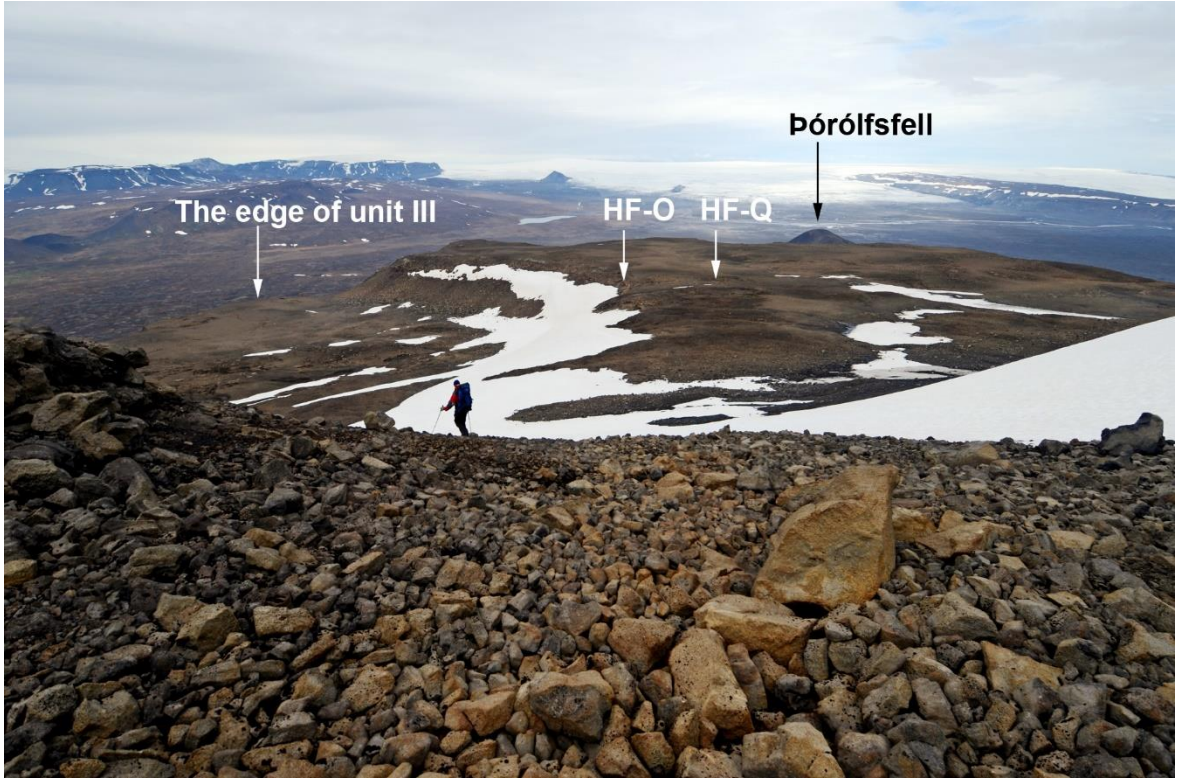

Figure 6-11. A view over the North terrace. Sample sites HF-O and HF-Q on the north middle lava bench, stage III', a view over the north lava bench of Hlöðufell seen from a point close to HF-P of cap lava Stage IV.

6.5 Stage IV: Upper cap lava

Upper cap lava (HF-E, HF-L, HF-P, HL-3)

In the upper cap lava where samples taken in three places, see the map in Figure 6-1. Conditions for paleomagnetic core sampling from the upper cap lava were not very good since the top was rather flat with not many opportunities of sub-horizontal drilling and the edge were in many cases fragmented or too steep for drilling. Sampling site HF-E is from the south edge of the cap lava and HF-P is from the north edge. HF-L is from the top of the cap lava.

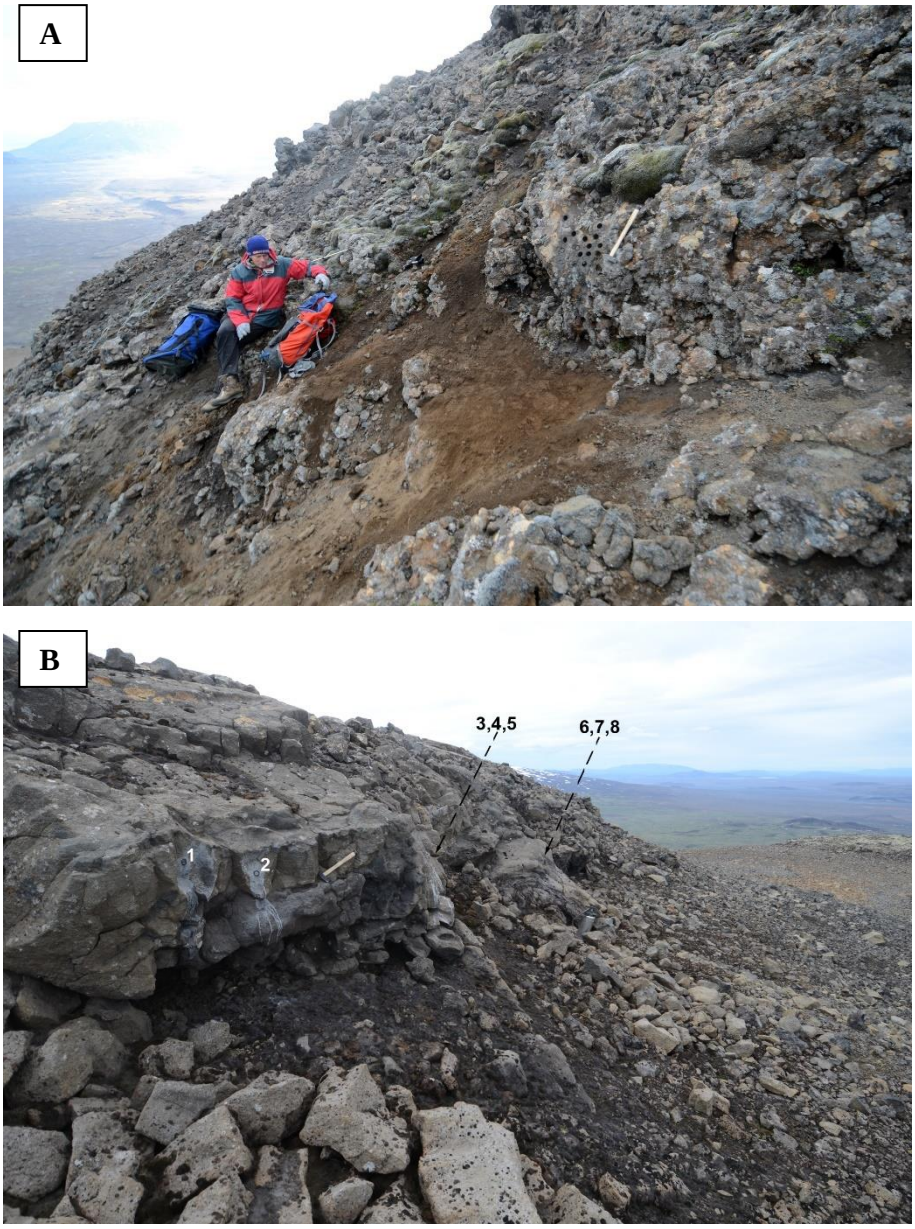

Figure 6-12. Examples of the sampling sites from the highest cap lava, Stage IV. (A) Sampling site HF-E from the south part of the highest cap lava. (B) Sampling site HF-P from the north part of the highest cap lava.

6.6 Dykes

As described before dykes are common in hyaloclastite mountains, so there are dykes in several places in Hlöðufell. Since dykes are not in stratigraphic order they are somewhat less useful in magnetic measurements than lavas, but still, two sampling sites in dykes where taken in this research. Location of the dykes with their directions are shown on map in Figure 6-13.

The sampling site HF-H is from a dyke in a ravine in the north-west part of the mountain. Measured thickness of the dyke was 60 cm. Strike: 134°T ± 5° and dip-angle: 85° ± 5°. The dyke was going forward up to the hyaloclastite. it was not clear how high it went. Sampling site HF-I is from a dyke from a dyke swarm in west part of Hlöðufell. Strike of the dyke: 110°T ± 5° and dip: 90° ± 5°.

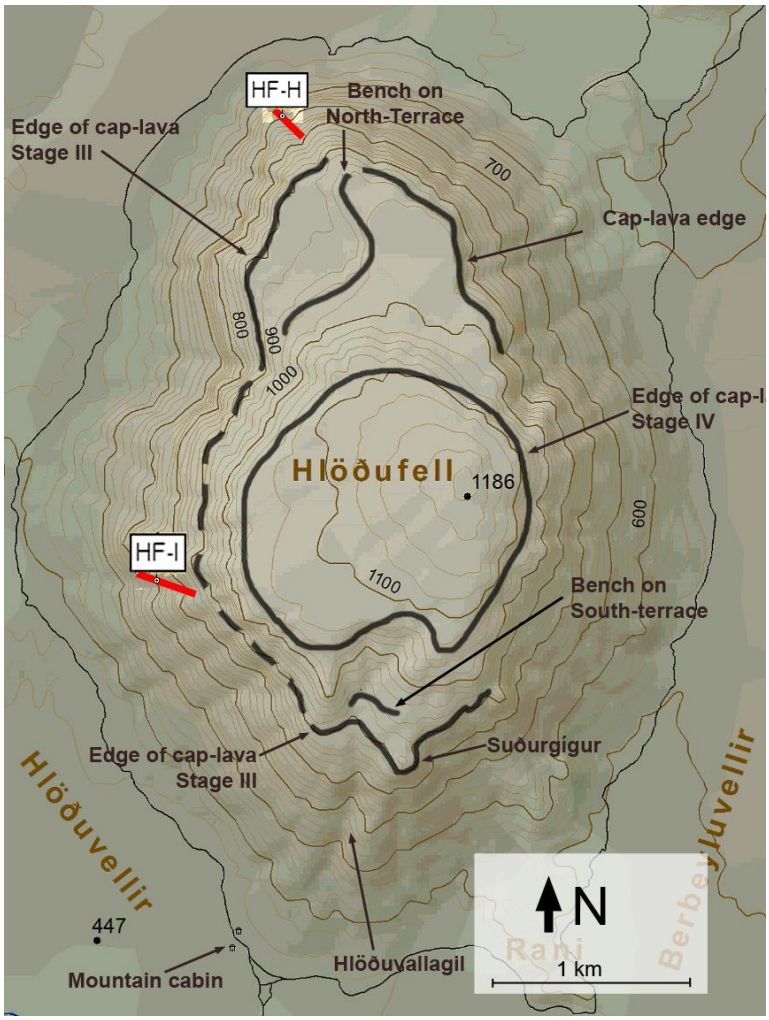

Figure 6-13. Map showing location and direction of the dykes of sampling sites HF-H and HF-I.

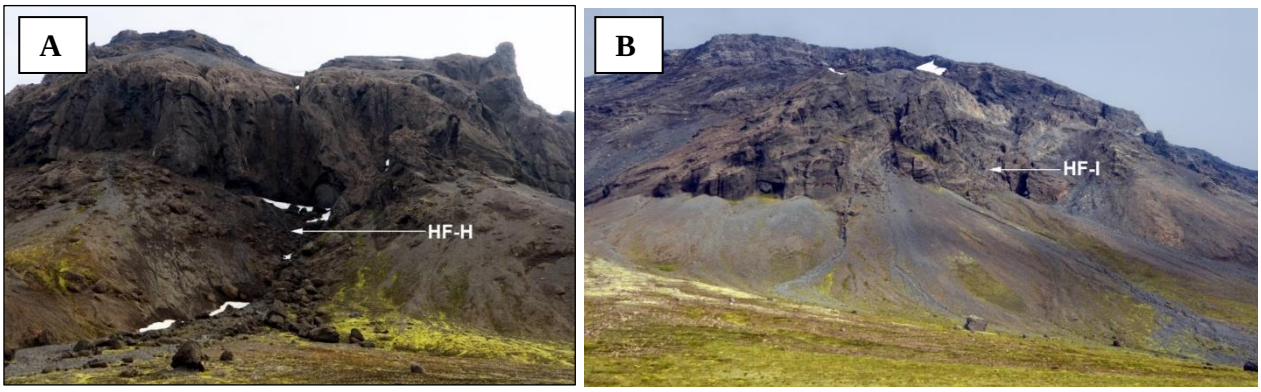

Figure 6-14. Sampling sites from dykes in Hlöðufell. (A) HF-I from a dyke in the north-west side of Hlöðufell. (B) HF-H from a dyke in the south side of Hlöðufell.

6.7 Þórólfsfell

6.7.1 Þórólfsfell, pillow ridges

Two sampling sites are in the neighboring mountain Þórólfsfell, north of Hlöðufell. They are both from pillow lava in outcrops in the lower most area of the mountain. Samples were taken in year 2014 at the beginning of the research. For location, see the map in Figure 6-1.

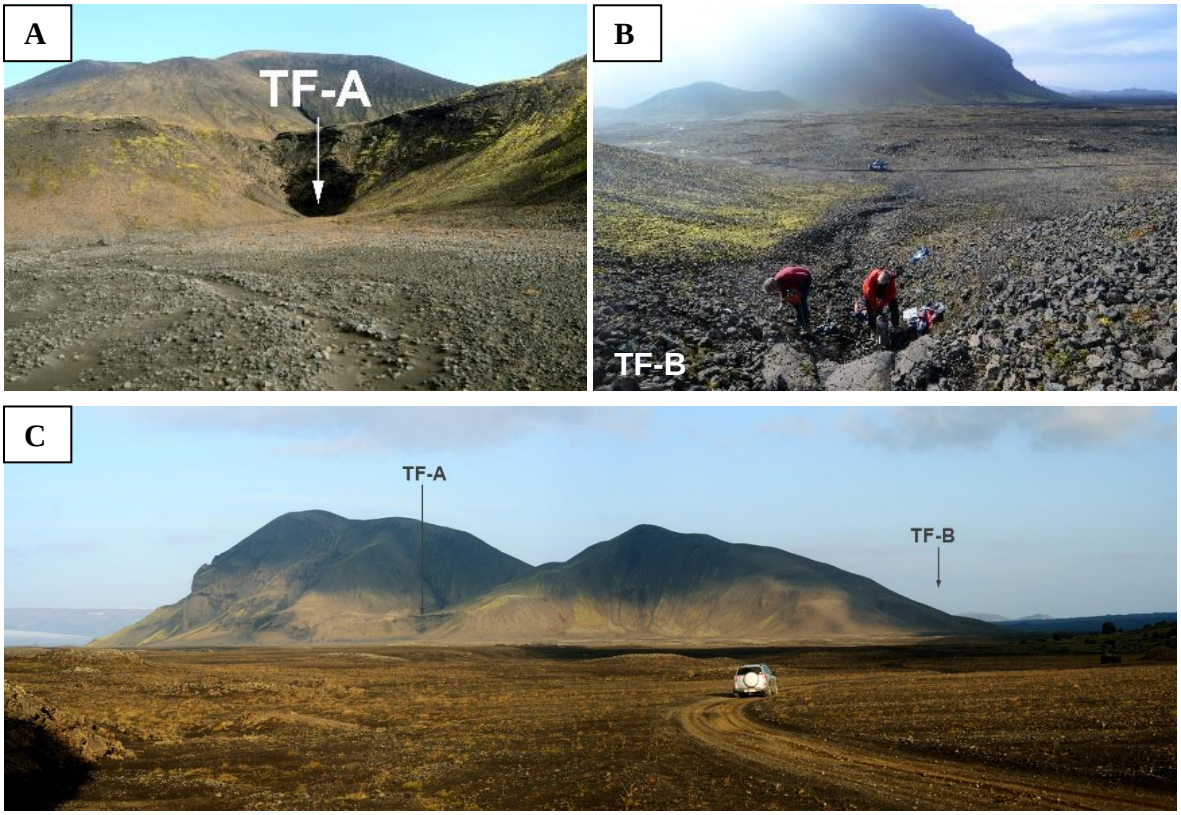

Figure 6-15. Sampling sites in Þórólfsfell. (A) TF-A; (B) TF-B; (C) Location of the sampling sites (TF-A and TF-B) in Þórólfsfell seen from the big rock NW of Hlöðufell. For location see map in Figure 6-1.

7 Results

7.1 General

From measured remanent magnetization of all sample cores, paleomagnetic field, inclination and declination have been calculated with the methods and the MATLAB programs described in Chapters 2.3.2 and 3.3.2. Stereonet diagrams from the programs will be used to present the results.

Main numerical results from the measurements are in Table 7-1 and more detailed results in tables are in a table in Appendix A. Results for each stage will be presented in this chapter and each stage possible divided into geological units if the paleomagnetic results give a reason for that.

7.2 Results for different stages and units

7.2.1 Stage I: Pillow lavas

Overall results for paleomagnetic directions are shown on a stereonet diagram in Figure 7-1. A rather clear pattern in the magnetic directions measured appears when the sampling sites in Stage I are categorized as has been described in the previous chapter: (1) pillow ridge at Hlöðuvellir, leading south-west from Hlöðufell; (2) pillow ridge in Rani area, leading south-east from Hlöðufell and (3) pillow samples from the main mountain. This categorizing is primary based on the location of the sampling sites in the main mountain and in the two pillow ridges leading from the mountain. Altitude is similar however, the sampling sites in Rani ridge (HF-B,V,W) are a somewhat lower than the sampling sites in the ridge at Hlöðuvellir. Most of the sampling sites in the main mountain are higher.

The paleomagnetic directions from most of the pillow ridge samples coincide while the directions from the sampling sites in the main mountain coincide separately. The only clear outlier is the sampling site HF-T. If that sampling site is excluded, the measured average declination angle of the sampling sites in the pillow ridges, calculated with Fisher statistics is ranging from -42.3° to -7.7° (or 317.7° to 352.3°). The declination angles for the sampling sites in pillow lavas in the main mountain are ranging from 1.5° to 7.8°.

A possible explanation for the outlier, HF-T is that it is known from previous paleomagnetic measurements in the area from year 2003, that a sampling site very close to the sampling site HF-T was heavily affected by a lighting, see information about sampling site HL-1 in Appendix C. Also noted here is that the location of the sampling site HF-T is at the end of the ridge so it is more likely to have rotated somewhat than other samples in the ridge. More detail analysis of that sampling site is in Appendix K, see page 142. As described there, a rotation of a block in the pillow lava ridge with the sampling site HF-T is assumed more likely, since the demagnetization process of the sampling site was normal in every respect.

The difference becomes clear if all samples in Stage I are divided in two units. One unit with all samples from the pillow ridges at Hlöðuvellir (HF-AMTU) and the pillow ridge in rani area (HF-BVW) and other unit with all the remaining sampling sites representing the main mountain (HF-CFGRSX). The result of this is shown in Figure 7-2. The alpha 99 confidence level circles for those two units are securely separated. The differential angle between the two units, calculated with eq. 2-24, is 6.5°.

Table 7-1. Main results for all sampling sites in alphabetical order. See more detail results in tables in Appendix A.

Name	Location (GPS)	Altitude [m]	Number of samples	DECL [°]	INCL [°]	Demag [mT]	Alpha95 [°]	Stage	Unit
HF-A	N64.40115 W20.55046	518	8	-29	72.4	40	1.9	I	PILL-AMTU-BVW
HF-B	N64.39941 W20.53045	475	7	-7.7	70	20	1.1	I	PILL-AMTU-BVW
HF-C	N64.40331 W20.54896	610	7	8.7	73.3	35	1.7	I	PILL-CFGRSX
HF-D	N64.40654 W20.54755	830	7	58.5	70	20	1.3	III	LAVA-DJN
HF-E	N64.41020 W20.54815	1009	6	-8.3	75.8	35	1.9	IV	LAVA-ELP
HF-FG	N64.43795 W20.55031	595	12	1.5	74.9	20	1.4	I	PILL-CFGRSX
HF-H	N64.43658 W20.55424	636	5	-4.5	73.4	25	1.8	NA	DYKE
HF-I	N64.41526 W20.56618	724	7	-4.8	73.8	30	2.1	NA	DYKE
HF-J	N64.40662 W20.54813	829	6	29.8	72.4	15	1.7	III	LAVA-DJN
HF-K	N64.40950 W20.54482	908	11	12.1	74.6	25	1.2	III '	LAVA-KOQY
HF-L	N64.41461 W20.53851	1115	6	-12.6	71.4	30	1.7	IV	LAVA-ELP
HF-M	N64.40130 W20.54876	527	9	-24.8	64.9	30	1.7	I	PILL-AMTU-BVW
HF-N	N64.40644 W20.54791	817	8	38.1	65.4	20	4.7	III	LAVA-DJN
HF-O	N64.43087 W20.54511	974	15	1.3	71.1	20	2.0	III '	LAVA-KOQY
HF-P	N64.42490 W20.54816	1081	8	-1.2	73.9	15	2.6	IV	LAVA-ELP
HF-Q	N64.42965 W20.54270	991	8	1	74.1	15	1.5	III '	LAVA-KOQY
HF-R	N64.43781 W20.55889	543	9	7	72.7	15	1.0	I	PILL-CFGRSX
HF-S	N64.40409 W20.55708	507	11	3.8	70.5	30	1.5	I	PILL-CFGRSX
HF-T	N64.40130 W20.55296	510	8	15.8	70.7	25	1.2	I	PILL-AMTU-BVW
HF-U	N64.40201 W20.54929	558	8	-15.4	72.5	15	1.1	I	PILL-AMTU-BVW
HF-V	N64.39875 W20.52769	480	7	-17.9	70.6	25	3.4	I	PILL-AMTU-BVW
HF-W	N64.39687 W20.51954	505	7	-42.3	74.4	30	2.6	I	PILL-AMTU-BVW
HF-X	N64.40567 W20.52242	551	5	3.6	67.5	10	3.8	I	PILL-CFGRSX
HF-Y	N64.40719 W20.54816	859	7	-2.8	72.7	15	0.9	III '	LAVA-KOQY
TF-A	N64.44850 W20.51689	544	10	18.7	72.1	300	1.8	NA	TF-PILL
TF-B	N64.44211 W20.51501	536	7	-5.6	71.5	600	2.9	NA	TF-PILL

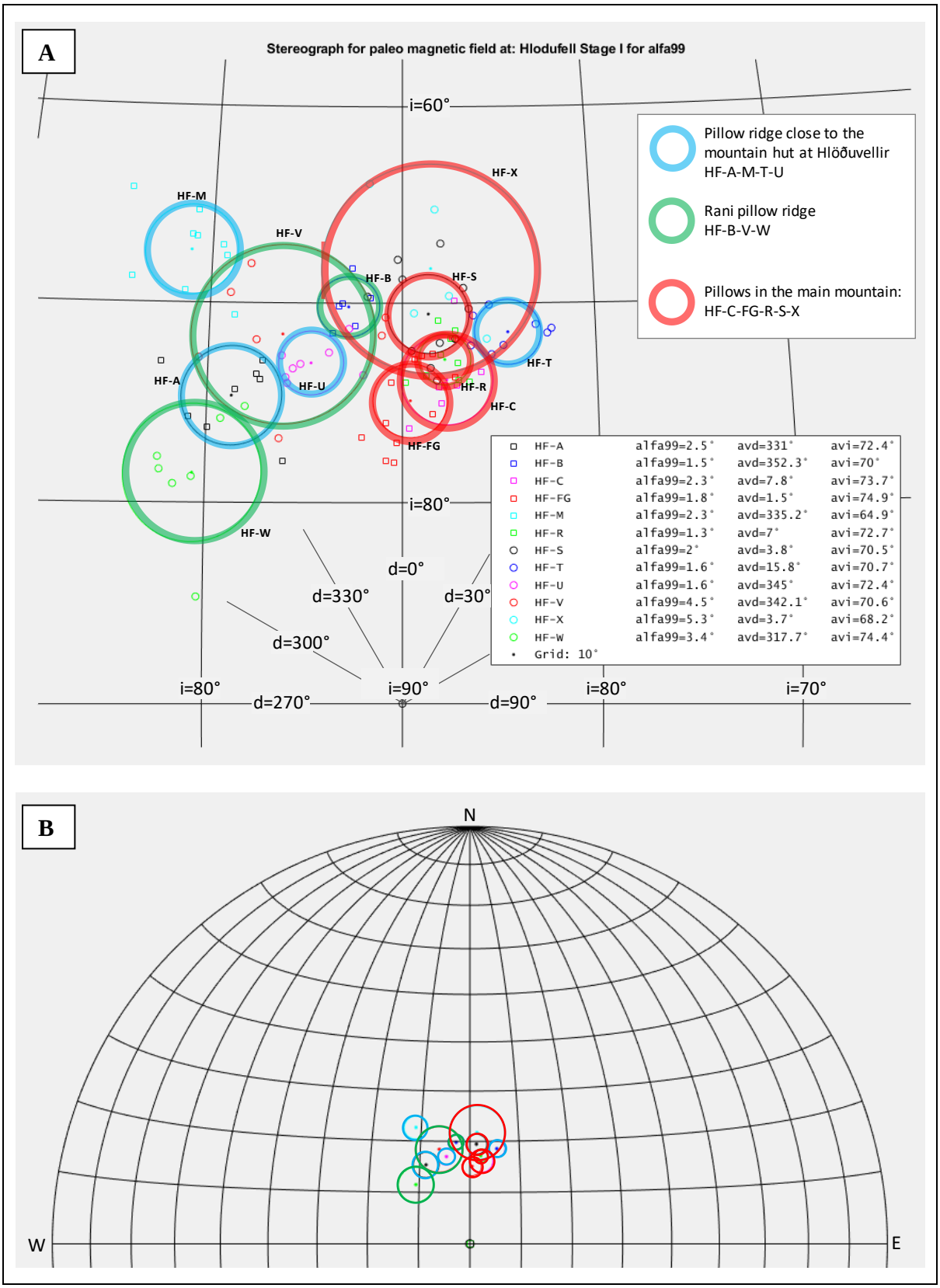

Figure 7-1. Paleomagnetism directions for all samples in pillow lavas, shown on stereonet diagram. (A) Enlarged part of figure B showing paleomagnetic field directions with alpha99 confidence circles. (B) Showing direction of the paleomagnetic field on large scale.

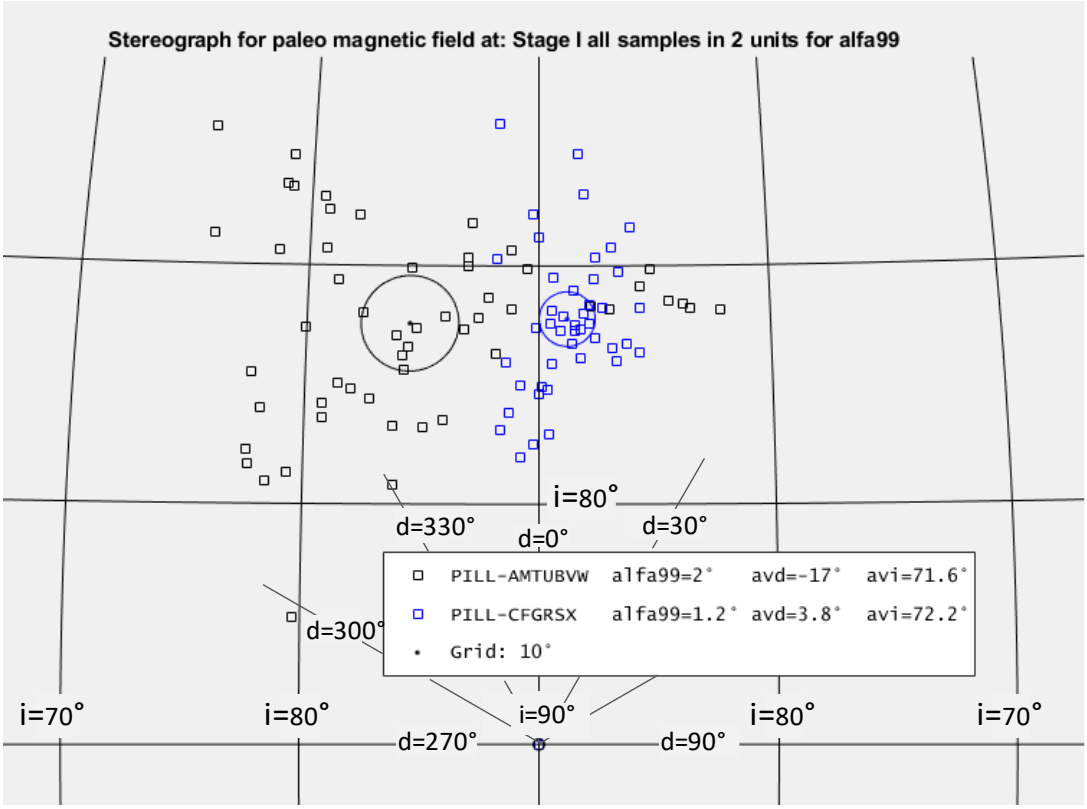

Figure 7-2. Paleomagnetism directions for Stage I, all sampling sites from pillow lavas, shown on stereonet diagram.

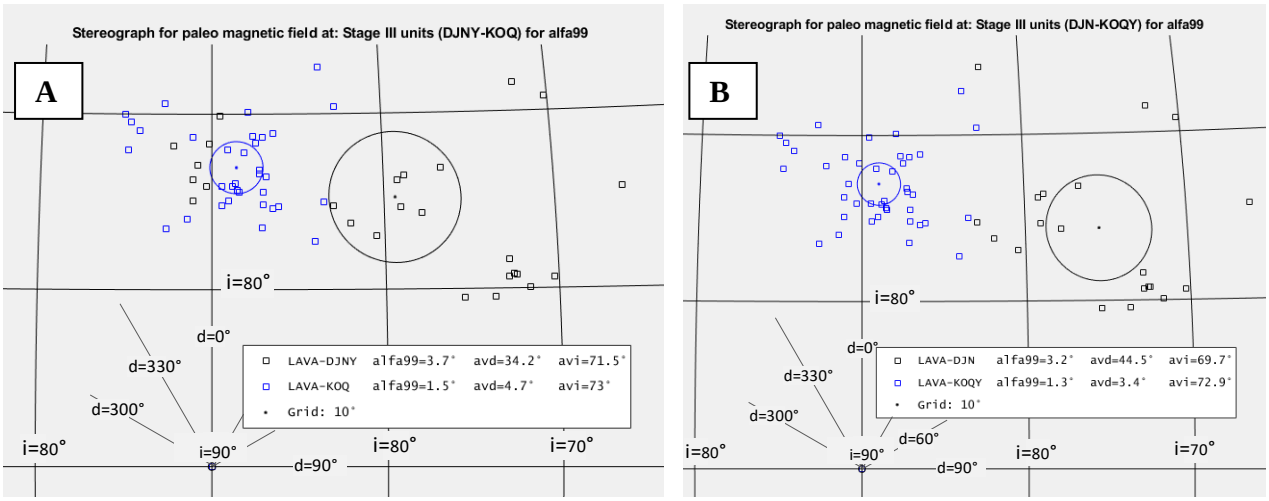

Figure 7-3. Sampling sites in stage III, shown on stereonet diagram. (A) Sampling site HF-Y taken with other sampling sites in the lower part of the cliffs, south of Hlöðufell, (Stage III). Differential angle between the directions is 9.0° (B) Sampling site HF-Y taken with the upper part sampling sites in north and south part of Hlöðufell (Stage III'). Differential angle between the directions is 13.3°.

7.2.2 Stage III: Lower cap lava

As discussed before (Chapter 5), the cap lava in Stage III can be more complicated than be just from one eruption happening at one time so the results here will be analyzed with that in mind. The main results of the paleomagnetic measurements are shown on a stereonet diagram (Figure 7-4). The paleomagnetic directions measured indicate some differences between the sampling sites and some pattern not possible to ignore. The samples from the upper part of Stage III, that has been referred to as III' make one cluster with declination angles ranging from 1° to 12.1° while most of the sampling sites in the lower part of Stage III have declination angles ranging from 33.1° to 58.5°.

The sampling site HF-Y does not fit the paleomagnetic directions measured in the sampling sites HF-DJN but the paleomagnetic direction of HF-Y fits very well with the sampling sites from Stage III', that is sampling sites HF-KOQ. Now, with closer look at a photo of the cap lavas, see Figure 6-8 it is possible to see some interface below HF-Y, separating HF-Y from the sampling sites HF-DJN, so it could be possible to link HF-Y with the samples referred to as stage III'. Both cases (HF-Y with HF-DJN and HF-Y with HF-KOQ) have been calculated and are shown on Figure 7-3. In both cases the difference of paleomagnetic directions is obvious. If HF-Y is taken with HF-DJN, then the differential angle calculated with eq. 2-24 is 9.0° but if HF-Y is taken with HF-KOQ, the differential angle between the two is 13.3°. Hence, in the discussion after this, the sampling site HF-Y will be taken with the units referred to as Stage III', that is sampling sites HF-K that is in the south terrace close to but considerably above HF-Y and the two sampling sites on the north terrace, HF-O and HF-Q. The three sampling sites, HF-D, HF-J and HF-N will then represent the lowest cap lava, referred to as Stage III.

Note however that the primary reason for taking the sampling site HF-Y from its neighbor, HF-D;J;N is the result of the paleomagnetic measurements but not its location.

7.2.3 Stage IV: Upper cap lava

Only three sampling sites were taken in the uppermost cap lava, Stage IV, HF-ELP. No special pattern is obvious when looking at all the samples from the three sampling sites and all three confidence interval circles intersect, see Figure 7-5. They seem to form one rather uniform distribution and will here be taken as one unit.

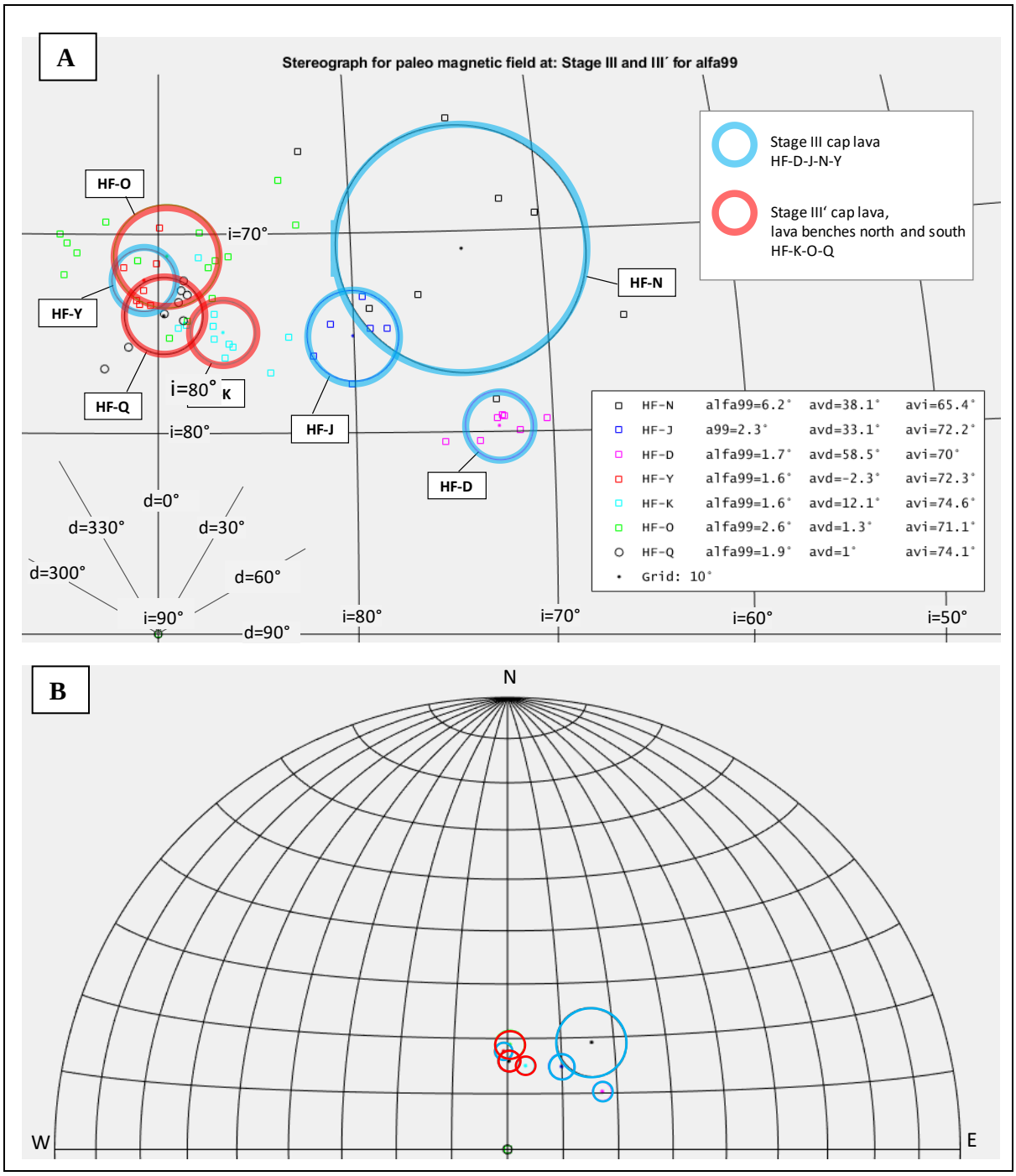

Figure 7-4. Paleomagnetic directions for all samples in lower cap lava, Stage III and Stage III', shown on stereonet diagram. (A) Enlarged part of figure B showing paleomagnetic field directions with alpha99 confidence circles. (B) Showing direction of the paleomagnetic field on large scale.

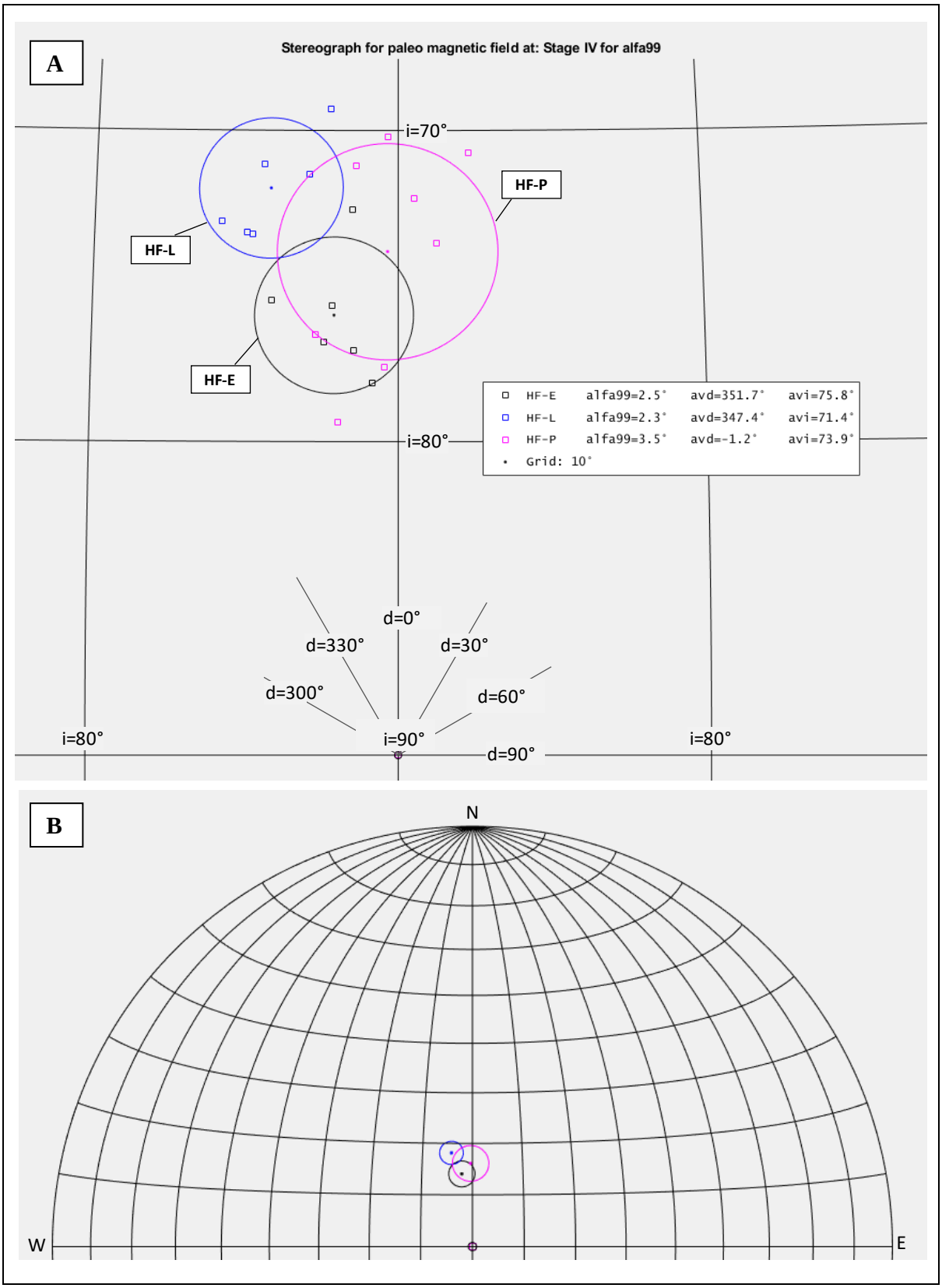

Figure 7-5. Paleomagnetic directions for all samples in upper cap lava, Stage IV, shown on stereonet diagram. (A) Enlarged part of figure B showing paleomagnetic field directions with alpha99 confidence circles. (B) Showing direction of the paleomagnetic field on large scale.

7.3 Overall results

7.3.1 All units on a stereonet diagram

The overall results are shown in Table 7-2 and on a stereonet diagram in Figure 7-6 for the geological units already described in this chapter. The units in the table are ranked by estimated mean altitude of each unit and calculated differential angle for each unit is presented there. Both differential angle from the previous (lower) unit and differential angle from the pillow ridges which are taken as the initial stage of the mountain with lowest altitude of all units.

Paleomagnetic directions as a function of altitude are presented on two following graphs. On Figure 7-7 is showing the differential angle for each sampling site from the sampling site HF-W. Showing clearly how the differential angle increases with altitude up to the lower cap lava of stage III and then decreasing again in the cap lavas above that. The same pattern is visible on Figure 7-8 where the differential angle for each unit is shown in the same way. The green line shows the differential angle between each unit and the pillow ridge unit. The red line shows how the differential angle cumulates from the pillow lava ridges.

Table 7-2. Main results for all units, calculated from all samples in each unit

Description	Sampling sites	Stage	Number of sampling sites	Estimated mean location	Estimated mean altitude [m]	Number of samples total	Decl [°]	Incl [°]	Alpha95 [°]	Alpha99 [°]	Demag [mT]	DEL relative to last	DEL relative to first	DEL cumula-tive
Lower pillows	PILL-AMTU-BVW	I	7	64.4005 °N 20.5370°W	510	54	-17.0	71.6	1.6	2.0	25	0	0	0
Upper pillows	PILL-CFGRSX	I	5	64.4190 °N 20.5420°W	560	44	3.8	72.2	0.9	1.2	30	6.5	6.5	6.5
Lower cap lava	LAVA-DJN	III	3	64.40673 °N 20.54795 °W	825	20	44.5	69.7	2.5	3.2	20	13.2	19.6	19.7
Middle cap lava	LAVA-KOQY	III '	3	64.42965°N 20.5427°W	935	41	3.4	72.9	1.0	1.3	20	13.3	6.3	33.0
Upper cap lava	LAVA-ELP	IV	3	64.4102°N 20.54815°W	1070	20	-6.9	73.8	1.5	1.9	30	3.1	3.7	36.1

7.3.2 Comparison

The results already described will now be compared with other results that is available. That is: (1) Measurements of dykes in this research; (2) Measurements in Þórólfsfell in this research (3) Measurements from Leo Kristjansson and Magnus Tumi Gudmundsson from year 2003.

Dykes

Samples were taken from dykes in two separated places in the mountain, see Figure 6-1 and Chapter 6.6. The two dykes measured showed almost the same declination and inclination directions with their alpha circles coinciding almost completely, see Appendix K on page 155. The mean paleomagnetic directions of the dykes then coincides very well with the uppermost cap lava of stage IV, see Figure 7-9.

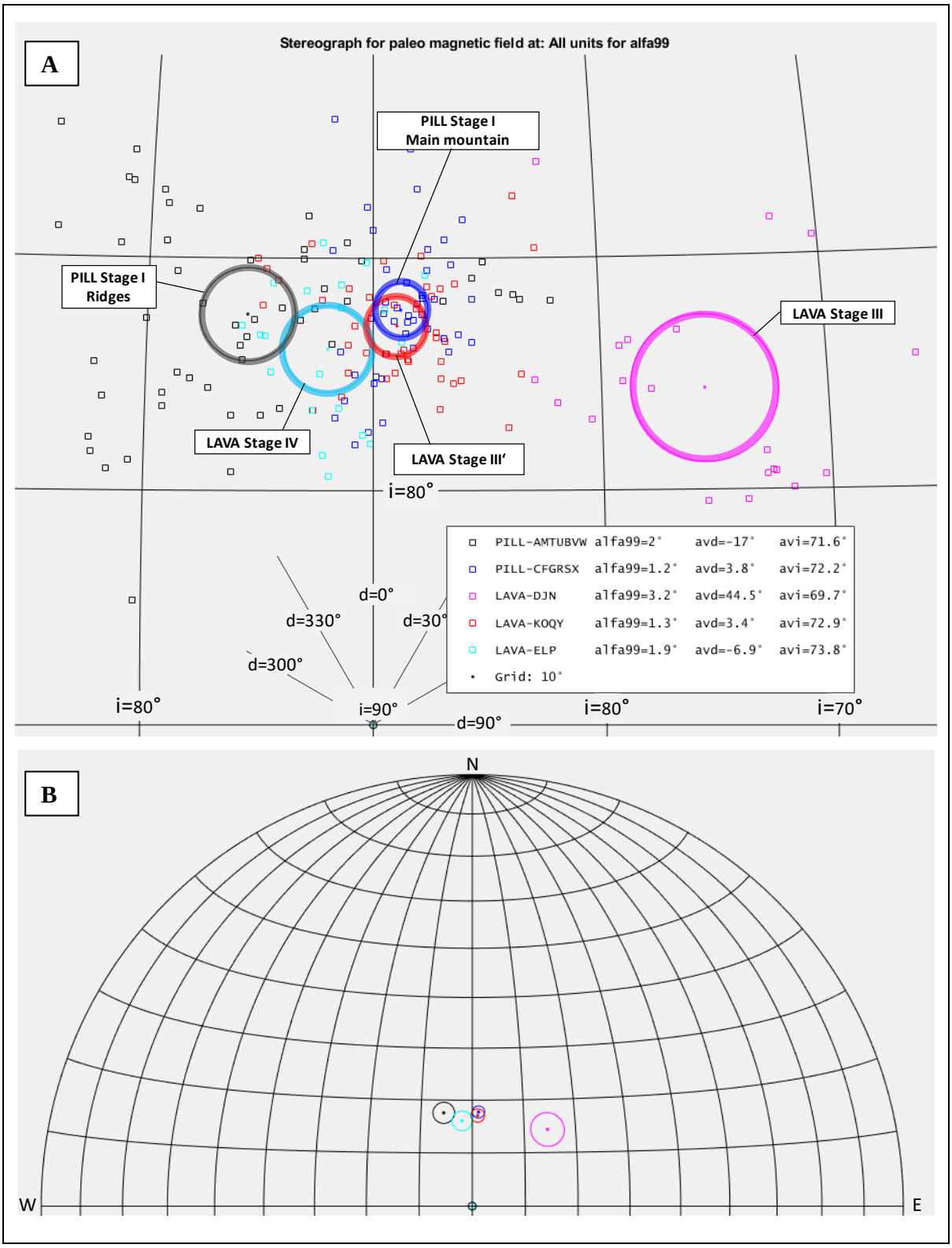

Figure 7-6. Overall result in a stereograph for all units in Hlöðufell. (A) Enlarged part of figure B showing all paleomagnetic field directions with alpha99 confidence circles. (B) Showing direction of the paleomagnetic field on large scale.

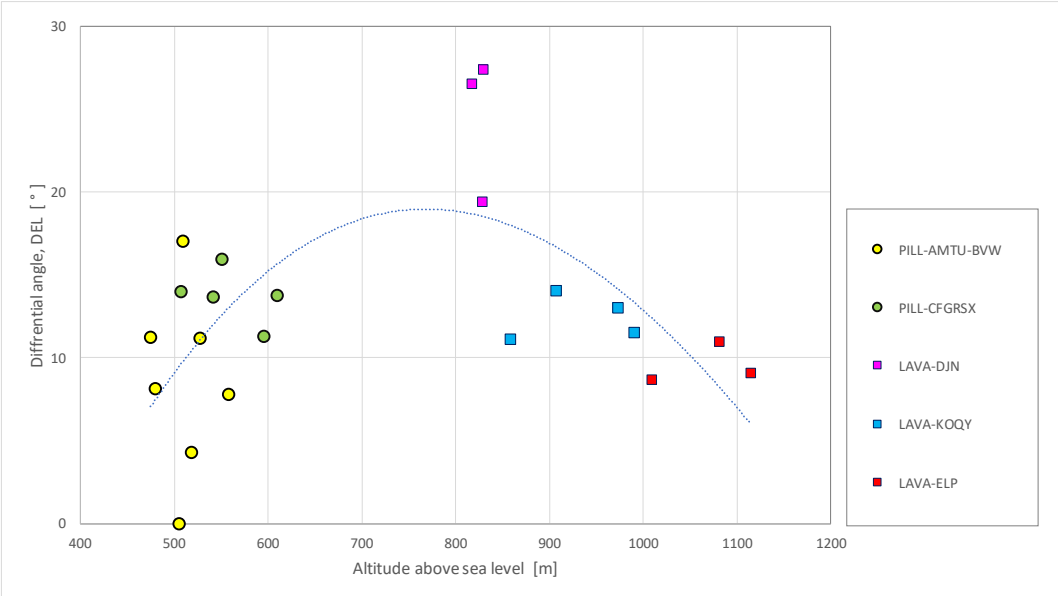

Figure 7-7. Diagrams showing the differential angle DEL for all sampling sites in Hlöðufell, differential angle from the sampling site with lowest declination angle, HF-W. The curve is 3rd degree polynomial fit for all sampling sites on the graph. Table for the data this diagram represents is in Appendix A.

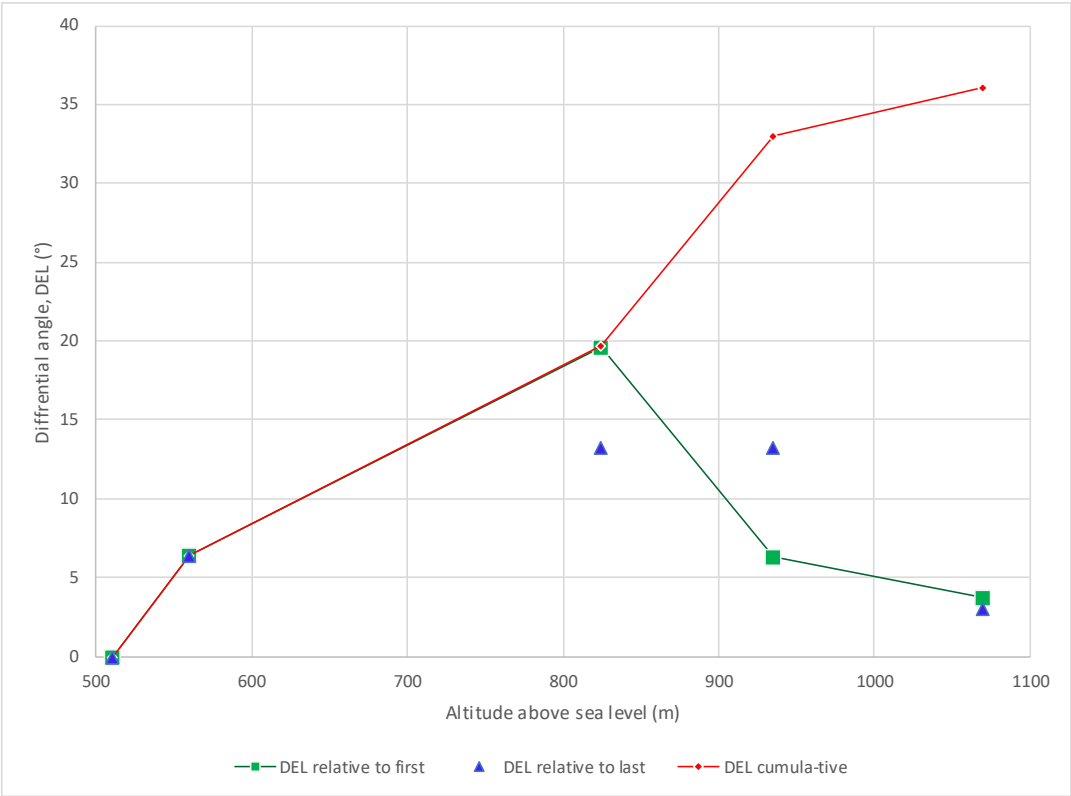

Figure 7-8. Diagrams showing differential angle, DEL for all units described in this chapter. The green squares are the angle difference between each unit and the pillow ridge units, PILL-AMTU-BVW in stage I. The blue triangles show the differential angle relative to the previous unit in the stratigraphy of the mountain. The red line and diamonds show the cumulative differential angle relative to the lowest unit, PILL-AMTU-BVW in stage I.

Þórólfsfell

The two sampling sites from Þórólfsfell do not fit together but they have both directions not far from the direction measured in Hlöðufell see Figure 7-10. The main results of Þórólfsfell is in Appendix K on page 156. Since there are only those two sampling sites and they are not fitting very well together, it is difficult to say much about them.

Measurements from year 2003

Three usable sampling sites are from the previous research made by Leo Kristjansson and Magnus Tumi Gudmundsson in year 2003, see Appendix C. Comparison of that research to this research is shown on a stereonet diagram, Figure 7-11.

Sampling site HL-2 is from stage III cap lava, not clearly located in the cliffs, close to the walking path in the upper part of Hlöðuvallagil. Some drill-holes were found in various places in the cliffs, leading to the assumption that the four samples from the sampling site are both from same rocks as the sampling sites HF-D;J;N but also from the different sampling site HF-Y. That would explain the large alpha95 confidence interval and also the paleomagnetic directions calculated between HF-D;J;N and HF-Y.

Sampling site HL-3 is from upper cap lava, Stage IV. It fits not badly with other samples from stage IV since the mean directions of HL-3 sampling site is within the 99% confidence circle of HF-ELP from all other samples of Stage IV.

Sampling site HL-4 does not fit as well into this research as other HL sampling sites. It should fall within the confidence level circle of pillow ridges (AMTUBVW) but it is closer to the pillow sites in the main mountain. Here should also be noted that HL-4 is not far from the main mountain and could be part of that, see Figure 7-12.

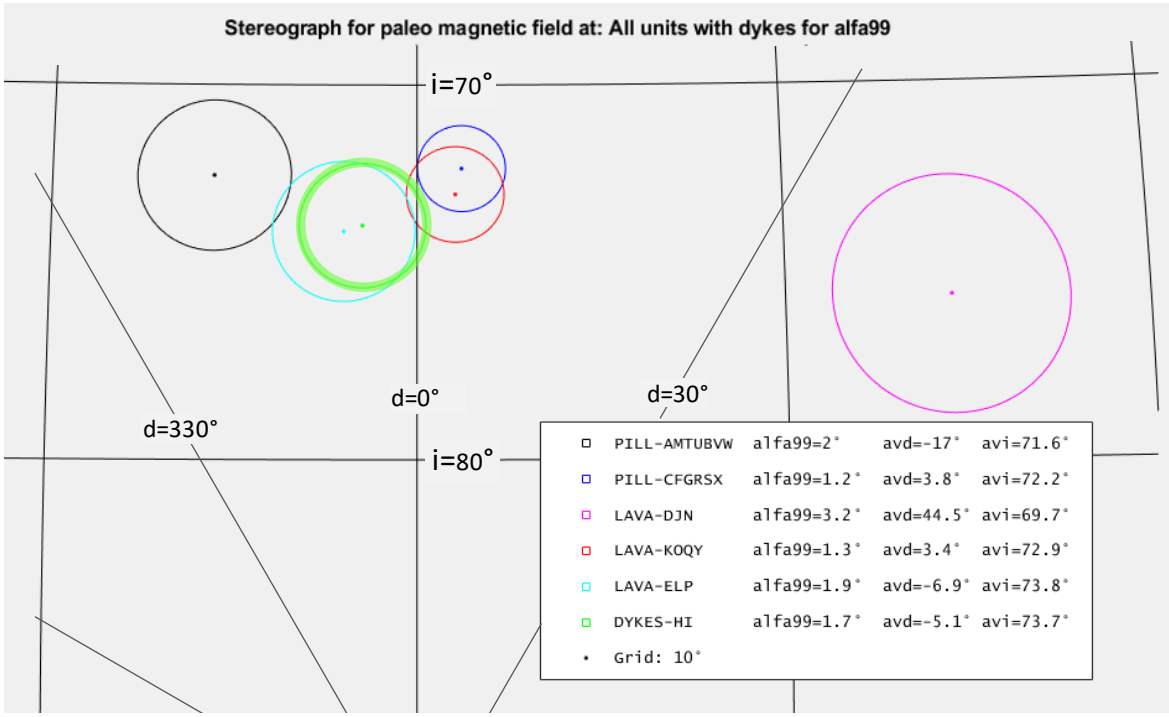

Figure 7-9. Comparison of the sampling sites of dykes with the units identified.

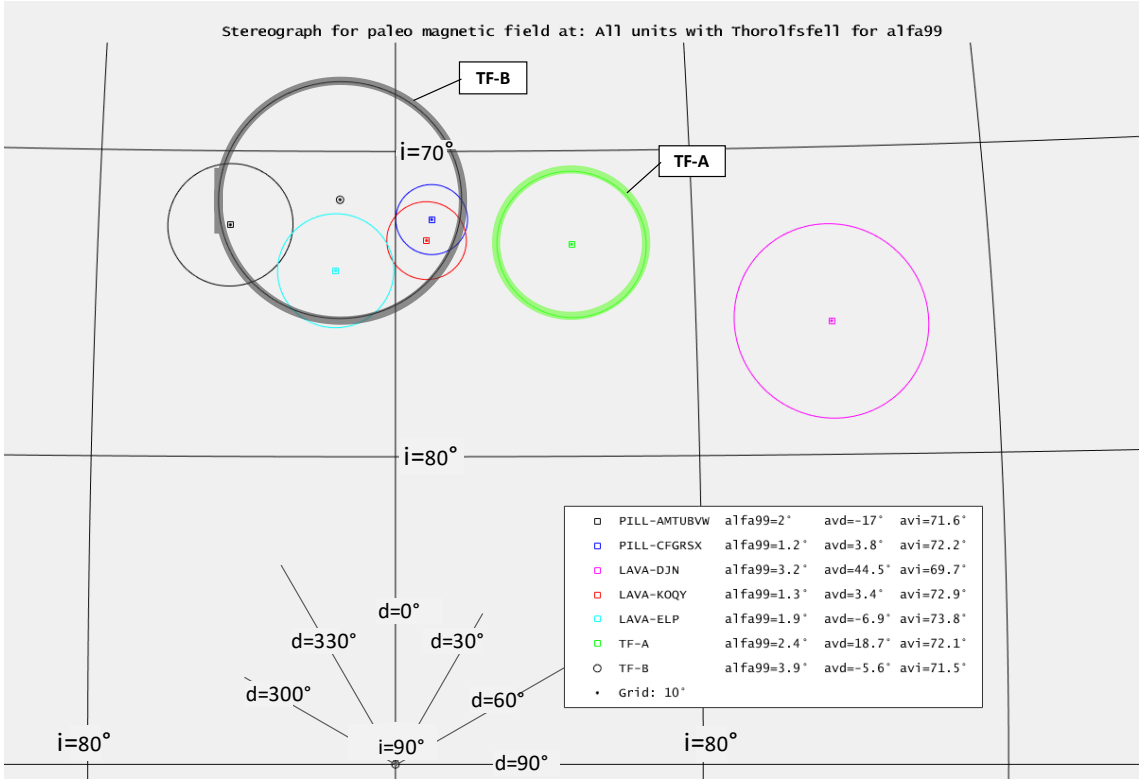

Figure 7-10. Comparison of the sampling sites in Þórólfsfell with the units identified.

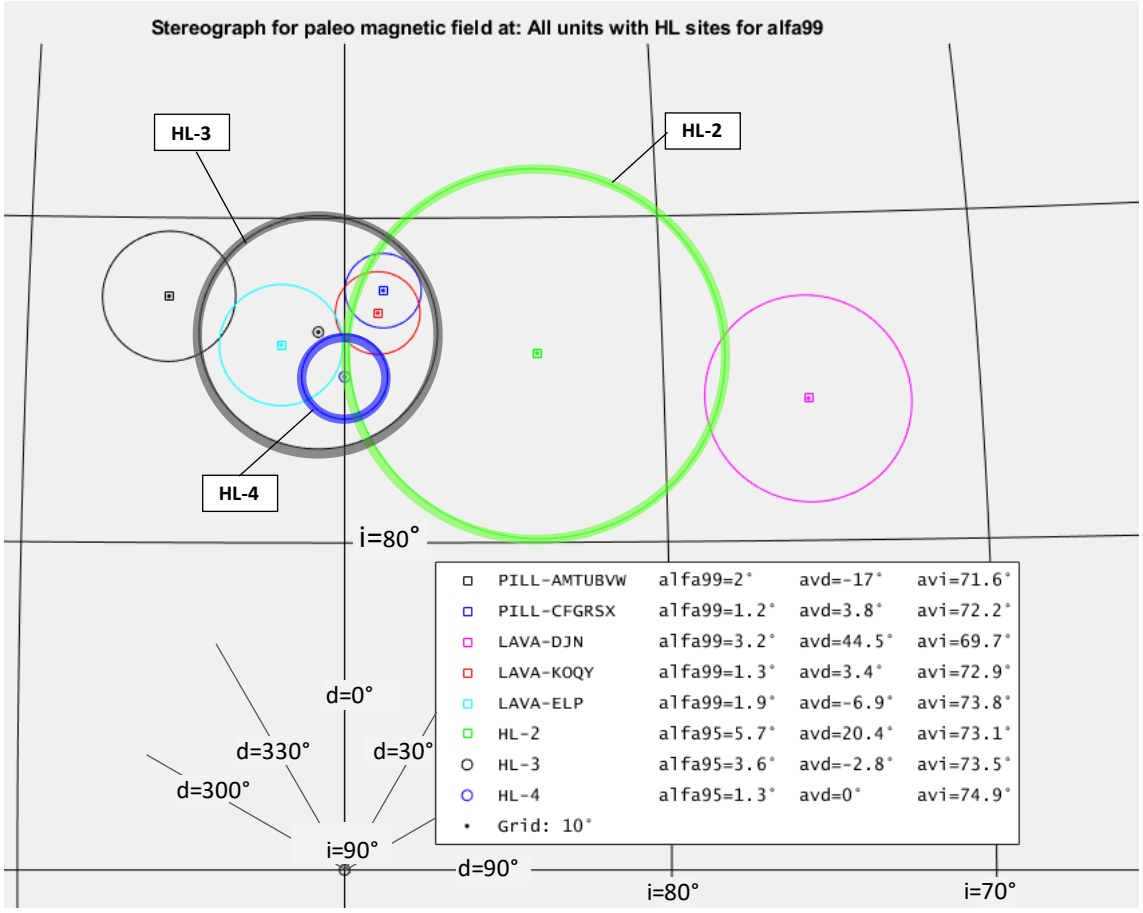

Figure 7-11. Comparison of the HL sampling sites from research in year 2003 with the units identified in this research.

Figure 7-12. Location of the sampling site HL-4 from the research of year 2003 showing the nearest sampling sites from this research, HF-U and HF-C in comparison. The sampling site HL-4 has more similar paleomagnetic directions as HF-C than HF-U.

8 Discussion

The original main idea behind this research was to find out whether it is possible to constrain the length of time it took for Hlöðufell to form by volcanic activity using paleomagnetism. The results of previous chapter indicate that the accumulated change in paleomagnetic direction (accumulated differential angle, DEL) from the stratigraphically oldest part (basal pillow lavas) to the youngest (top lava cap) was around 35° (Figure 7-8). If we compare that with the observations and models of change in paleomagnetic directions discussed in Chapter 2.3.3 we can expect the average change to be 5° per century. Thus, an accumulated change in paleomagnetic direction of 35° should need (if the average change in magnetic directions is 5° over 100 years), 700 years. Previous research of Hlöðufell (Skilling, 2009) did not suggest any gaps in the volcanic activity, these indications on eruption duration are higher than expected.

Below, three alternative scenarios explaining the observations are considered.

(1) The results should not be taken as an indication of real change in the paleomagnetic directions but are the result of tilting, rotation and other movement of the lavas measured and do not indicate information on the duration of the volcanic activity.

(2) Option one is wrong, and the data are a testimony of a long-lasting and continuous eruption.

(3) Formation took a long time as indicated but was characterized by several long gaps in the volcanic activity.

8.1 Three suggestions

8.1.1 First suggestion: the paleomagnetic measurements indicate tilting and rotation and do not indicate this long time of formation

It needs to be considered whether the measurements of different declination angles are due to inaccuracy in measurements and/or tilting or other local changes in the rocks measured.

The main argument against this suggestion is the fact that the difference of paleomagnetic directions is mostly in declination but not in inclination. If the difference in the angles was from tilting and rotation of the rocks, then it should be in both declination and inclination. Because of the northerly location of Iceland and that the magnetic poles wander around the geographical poles, then inclination angles in Iceland are usually not far from 70° as is the result of measured inclination angles in this research. Random or even systematic slumping and rotation should have more effect in the inclination than was measured in this research.

Inaccuracy in measurements is not considered to be likely since the results for all samples in each sampling site form a rather consistent cluster, leading to rather narrow confidence level for each sampling site. Inaccuracy would lead to more scatter in the results for each sampling site. Systematic error cannot be ruled out, but without any indications of such errors this is not likely.

The argument that the results simply indicate tilting and rotation of the lava blocs could possibly be supported by the fact that the main difference in paleomagnetic directions is observed in the lower part of the lower cap lava. That is stage III. If the three sampling sites HF-D;J;N were excluded from the research, then the total accumulated difference in paleomagnetic directions would be much reduced. Without the samples in here referred to as Stage III' that is

the three sampling sites: HF-D;J;N, the total cumulative change in paleomagnetic directions would be 10° but not 35°. Still, however, that change would need 200 years long time to take place. With notice of the confidence level then total change could have been less than 5° leading to an eruption time possible shorter than 100 years.

However, it is not assumed likely that the result simply indicate tilting and rotation of the lava blocks, but it is not possible to reject that suggestion completely. To determine that more definitely more measurements from the lower cap lava in stage III would be needed.

8.1.2 Second suggestion: One long lasting low-discharge eruption

If the formation of the mountain is the result of a single very long-lasting eruption, the basic question is if there are examples of other eruptions of that kind.

The total volume of the edifice at present has been estimated 3.3 km^3 (Appendix E). Since the mountain is partly eroded its original volume was somewhat greater soon after its formation. If we say that one fourth of the original volume has been eroded away, its original volume was 4.4 km^3. If this volume was erupted continuously over a 700 year period, the effusion rate would have been around 0.2 m^3/s.

If this is compared with other known eruptions, then for Surtsey 1963-1967, perhaps the longest lasting well known eruption in Iceland but still only of duration of 3.5 years with volume of 1.2 km^3 (Jakobsson, 1978). The result is an average effusion rate of about 10 m^3/s. Effusion rates in long-lasting Hawaiian eruptions are around 1 m^3/s with periods of effusion rates as low as 0.5m^3/s (Harris et al, 1998). Effusion rate of Etna 1975 was 0.3-0.5 m^3/s and lower effusions rates indicated above are not unknown but are more common in more silicic, higher viscosity lavas (Cas & Wright, 1988).

Since we are lacking real examples of long lasting (several hundreds of years) basaltic eruptions and there are no real examples of basaltic eruptions with that low effusion rate it is assumed unlikely to be the case in Hlöðufell.

8.1.3 Third suggestion: Activity occurred in several smaller eruptions

It is possible that the effusive activity was similar to that observed in e.g. Hawaii and Surtsey but was not active all the time. If using effusion rate of Hawaii (0.5-1 m^3/s), we have total eruption time for volume 4.4 km^3 as 130-260 years. That would mean we had eruption active for about 18-36% of the total 700 years' formation time. If using the eruption rate from Surtsey (10 m^3/s), the total eruption time would be about 13 years or less than 2% of the total 700 years.

A detailed estimate of the eruption behavior when Hlöðufell was forming and models for interaction with the glacier is out of scope of this research. However, some suggestions will be introduced. The morphology of Hlöðufell can be regarded as consistent with the idea of an eruption with some gaps or at least quiet periods during the formation of the mountain.

On the other hand, is also pointed out that volcanoes outside the central volcanoes in Iceland are usually not know to have multiple eruptions but only erupt once, each volcano. But it should also be noted that for the most prominent tuya in the North-East eruption zone in Iceland, Herðubreið its formation has been divided into separate eruptions with silent time gaps in between (Werner & Schmincke, 1999; Werner et al, 1996).

The reported age of Hlöðufell, 172 thousand years BP (Jakobsson et al., 2003), indicates that the eruption took place during the Saalian glaciation which lasted until the onset of the

warmer Eemian interglacial that began around 130 thousand years ago (Lauer & Weiss, 2018). This is consistent with conditions being favorable for the existence of an ice sheet in the region. Thus, an eruption may have lasted over for several hundreds or even thousands of years, with quiescence alternating with active volcanic periods. If the eruption was not steady all the time, the area was still covered with ice during the resting periods. Most likely, after an eruption in an ice age glacier icecap, the volcano would gradually be covered in several years or decades.

Terraces and lava benches

First, we have the terraces and lava benches in and between Stage III and Stage IV lavas. Previous research (Skilling, 2009) indicates 150 meters rise of water level between the passage zones of stage III stage IV lava cap. That would have needed a gap in activity. When the eruption started again after an eruption cessation the ice would have covered the volcano and the eruption had to melt the glacier again, In order to explain at higher water level we would at least need the depression from the previous eruption to be filled completely. How long time we need for that is not clear but evidence from Gjálp eruption in Grimsvotn 1996 indicates more than 10 years to fill the depression in the glacier around the volcano (Jarosch, Gudmundsson, Högnadóttir & Axelsson, 2008).

The lava benches on the south and on the north terraces of the mountain could also indicate some resting periods of the volcanic activity.

High values of difference in magnetic directions measured

Secondly, if the difference in measured paleomagnetic directions, between the lower part of the lower cap lava (stage III) and the upper part of it (stage III') is real, then the 13° change in magnetic direction measured there would need about 250 years to happen. The sampling sites with that difference in paleomagnetic directions only differs about 100 meters in altitude and the area of the mountain at that altitude is about 0.5 km^2. For a steady non-stopping eruption, that would mean about 0.05 km^3 of erupted material in 250 years or 0.006 m^3/s eruption rate which is not a realistic sustained flowrate.

8.2 Summary

In summary, it is not possible to exclude suggestion one completely, that the measured magnetic directions are due to rotation and/or slumping of the lava blocks. However, it is not supported by visual observations of these blocks. Suggestion two is considered unlikely since there are no known examples of 700 years long continuous basaltic eruptions with such low eruption rates. Therefore the third suggestion is assumed to be most likely. The implications of this are therefore considered briefly below, using the four stages already identified by Skilling (2009).

Stage I

The pillow ridges formed in the first part of the buildup of the mountain. Since the difference in magnetic direction from the pillow lava ridges to the pillows in the main mountain is measured as 6.5° we would need an eruption of about 100 years duration before the formation of the rest

of the pillows, the pillow lava in the main mountain. Here and below I assume that maximum directional change is 5° per century.

Stage II

Whether the hyaloclastite in stage II formed in the same eruption as the pillows in the main mountain is unclear from this research. It is also unclear if the hyaloclastite was formed in one eruption or how steady it was. There is however evidence of at least some fluctuations in that phase of the eruption to describe the subaerial lava in the west slope of the mountain.

Stage III

According to the measured changes in paleomagnetic directions (13°) from the pillow lava in the main mountain to the lowest cap lava in stage III we need 250 years. Where in the timeframe from end of stage I formation to beginning of stage III formation that was, is unclear from this research.

The upper part of stage III formation that have here been referred to as stage III' is again 13° back in magnetic directions, needing another 250 years between the start and the end of activity forming these units.

Stage IV

The difference in magnetic directions from the upper part of stage III, that is from stage III' to stage IV is 3° giving a minimum time of about 50 years to form this final part of the edifice.

9 Conclusions

- The measured paleomagnetic directions of the pillow lava (Stage I) in the ridges in the south part of Hlöðufell, Rani and the ridge at Hlöðuvellir, show 6,5° difference. Indicating at least 100 years long formation time, most likely in two separate eruptions.

- The difference in measured paleomagnetic directions in the lower part of Stage III cap lava in Hlöðufell from other parts of the mountain is 13°. That difference can be described with more than 200 years' time span from Stage I to Stage III and another 200 years' time span from Stage III to Stage III' or Stage IV. But that difference in measured paleomagnetic directions could also been described with indicate tilting and rotation of the lava blocs in that part of the mountain. More measurements from the Stage III cap lava in other places of the mountain could make more clear what the reason is.

- Several lava benches were identified both on the north terrace and on the south terrace of Hlöðufell. They could have formed by a rise in the water level, possibly accompanied by thickening of the glacier during the eruption, with or without discontinuity in eruptive activity during this possible rise in water level.

- A flow foot breccia seems to be within the cap lava previously referred to as Stage III but here referred to as Stage III and III' since the flow foot breccia should define two cap lavas.

- A subaerial lava was identified in the west side of Hlöðufell about 200 meters below the lowest cap lava of Stage III. When that lava was forming, the water level must have been much lower than when the lava and flow foot breccia of Stage III was forming.

- The paleomagnetic directions measured of two dikes through hyaloclastite formation (Stage II) of Hlöðufell were almost the same as measured in the highest cap lava of mountain, that is Stage IV.

Bibliography

Allmendinger, R.W., Cardozo, N. and Fisher, D.M. (2012). *Structural geology algorithms – Vectors and tensors*. Cambridge: University Press.

Bosi, F., Hålenius, U. and Skogby, H. (2009). Crystal chemistry of the magnetite-ulvöspinel series. *American Mineralogist, 94*, 181–189. doi: 10.2138/am.2009.3002

Branca, S., De Beni, E., and Proietti, C., (2013). The large and destructive 1669 AD eruption at Etna volcano: reconstruction of the lava flow field evolution and effusion rate trend. *Bull Volcanol, 75:694.* doi: 10.1007/s00445-013-0694-5

Cas, R.A.F. and Wright, J.V., 1988. *Volcanic Successions Modern and Ancient*. London, UK: Chapman & Hall.

Champion, D.E., Hodges, M.K.V., Davis, L.C., and Lanphere, M.A., (2011). *Paleomagnetic correlation of surface and subsurface basaltic lava flows and flow groups in the southern part of the Idaho National Laboratory, Idaho, with paleomagnetic data tables for drill cores*. U.S. Geological Survey Scientific Investigations Report 2011-5049, 34 p., 1 pl. (DOE/ID 22214).

Fisher, R. (1953). Dispersion on a sphere. *Proceedings of the Royal Society of London, 217*, 295-305.

Fisher, R.V. & Schmincke, H.-U. (1984). *Pyroclastic Rocks*. Berlin: Springer-Verlag.

Flóvenz, Ó.G., Hersir, G.P., Sæmundsson, K., Ármannsson, H. and Friðriksson, Þ. (2012*). Geothermal Energy Exploration Techniques. Comprehensive Renewable Energy*. Sayigh, A, (ed.), Vol 7, 51–95. Oxford: Elsevier.

Gasparov, L., Rush, A., Pekarek, T., Patel, N. and Berger, H. (2009). Raman studies of doped magnetite above and below the Verwey transition. *Journal of Applied Physics, 105*, 07E109, doi: 10.1063/1.3067858

Gudmundsson, M.T., Hognadottir, T. and Jakobsson, S.P., (2000). *Hraun og móbergsmyndanir sunnan Langjökuls, niðurstöður þyngdarmælinga* (RH-28-2000). Reykjavík: Raunvísindastofnun Háskólans.

Harris, A.J.L., Flynn, L.P., Keszthelyi, L., Mouginis-Mark, P.J., Rowland, S.K. and Resing, J.A. 1998. Calculation of lava effusion rates from Landsat TM data. *Bull Volcanol, 60*, 52-71.

Jakobsson, S.P. (1978). Environmental factors controlling the palagonitization of the Surtsey tephra, Iceland. *Bull. Geol. Soc. Denmark, 27*, Special Issue, 91–105.

Jakobsson, S.P., Gudmundsson, M.T. and Duncan, R.A. (2003). Eldvirkni í norðurhluta vestra gosbeltisins. Fyrstu niðurstöður aldursgreininga. Vorráðstefna JFÍ 23. apríl 2003. Unpublished.

Jakobsson, S.P. and Gudmundsson, M.T. (2008). Subglacial and intraglacial volcanic formations in Iceland. *Jökull, 58*, 179-196.

Jakobsson, S.P. and Gudmundsson, M.T. (2012). Móbergsmyndun og gos undir jöklum. *Náttúrufræðingurinn, 82*(1-4), 113-125.

Jakobsson, S.P. and Johnson, G.L. (2012). Intraglacial volcanism in the Western Volcanic Zone, Iceland. *Bull Volcano, 74*, 1141−1160. doi 10.1007/s00445-012-0589-x

Jarosch, A., Gudmundsson, M.T., Högnadóttir, T. and Axelsson, G. (2008). Progressive cooling of the hyaloclastite ridge at Gjálp, Iceland, 1996–2005. *Journal of Volcanology and Geothermal Research 170* (2008), 218–229.

Jicha, B.R., Kristjansson, L., Brown, M.C., Singer, B.S., Beard, B.L. and Johnson, C.M. (2011). New age for the Skálamælifell excursion and identification of a global geomagnetic event in the late Brunhes chron. *Earth and Planetary Science Letters. 310* (2011), 509–517. doi:10.1016/j.epsl.2011.08.007

Jones, J.G. (1968). Pillow lava and pahoehoe. *The Journal of Geology. 76*(4), 485-488.

Jones, J.G. (1969). Intraglacial volcanoes of the Laugarvatn region, south-west Iceland - I. *Q. Jl Geol. Soc. Lond., 124*, 197-211.

Jones, J.G. (1970). Intraglacial volcanoes of the Laugarvatn region, southwest Iceland - II. *Journal of Geology, 78*, 127-140.

Kearey, P., Brooks, M. and Hill, I. (2002). *An Introduction to Geophysical Exploration*. Malden, USA: Blackwell Publishing Company.

Korte, M., Constable, C. (2005). The geomagnetic dipole moment over the last 7000 years - new results from a global model. – *Earth and planetary science letters, 236*, 1-2, 348-358. DOI: 10.1016/j.epsl.2004.12.031

Kristjansson, L. (2002). Estimating properties of the paleomagnetic field from Icelandic lavas. *Physics and Chemistry of the Earth. 27*(25), 1205-1213. doi: 10.1016/S1474-7065(02)00122-5

Kristjansson, L. (2015). New evidence on an episode of geomagnetic instability, recorded in Middle Miocene lava flows in Northwest Iceland. *Studia Geophysica et Geodaetica, 59*(2), 309-324. doi: 10.1007/s11200-014-0910-6

Lanza, R. and Meloni, A. (2006). *The Earth's Magnetism - An Introduction for Geologists*. Berlin: Springer-Verlag Heidelberg.

Lauer, T. and Weiss, M. (2018). Timing of the Saalian- and Elsterian glacial cycles and the implications for Middle – Pleistocene hominin presence in central Europe. *Nature - Scientific Reports, 8:5111*. doi:10.1038/s41598-018-23541-w

Leirvogur Magnetic Results 2016, Science Institute, Reykjavik 2017, 127 pp.

Loughlin, S.C. (2002). Facies analysis of proximal subglacial and proglacial volcaniclastic successions at the Eyjafjallajökull central volcano, southern Iceland. Smellie, J.L. and Chapman, M. (eds.), *Volcano-ice Interaction on Earth and Mars* (pp. 149–178). London: The Geological Society.

Lowrie, W. (2007). *Fundamentals of Geophysics*. Cambridge, UK: University Press.

Luxey, P., Blondel, P. and Parson, L.M. (1997). Tectonic significance of the South Iceland Seismic Transform Zone. *Journal of Geophysical Research, 102*(B8), 17969-17960.

Mál og menning / Forlagið. (2009). *Kjölur, Langjökull, Kerlingarfjöll, Sérkort 3* [staðfræðikort, 1:100.000]. Reykjavík: Mál og menning / Forlagið.

Mankinen, E.A., Prévot, M., Grommé, C.S. and Coe, R.S. (1985). The Steens Mountain (Oregon) geomagnetic polarity transition 1. Directional history, duration of episodes, and rock magnetism. *Journal of Geophysical Research, 90*(B12), 10393-10416.

McElhinny, M.W. (1973). *Paleomagnetism and Plate Tectonics*. Cambridge, UK: Cambridge Univ. Press.

NOAA (2016). National centers for environmental information. National oceanic and atmospheric administration. http://www.ngdc.noaa.gov/geomag/GeomagneticPoles.shtml retrieved 15-May-2016.

Opdyke, N.D. and Channell, J.E.T. (1996). *Magnetic Stratigraphy*. San Diego USA: Academic Press.

Perkins, D. (2011). *Mineralogy*. New Jersey: Pearson Prentice Hall.

Pollock, M., Edwards, E., Hauksdóttir, S., Alcorn, R. and Bowman L. (2014). Geochemical and lithostratigraphic constraints on the formation of pillow-dominated tindars fromUndirhlíðar quarry, Reykjanes Peninsula, southwest Iceland. *Lithos 200–201*(2014), pp 317–333. doi:10.1016/j.lithos.2014.04.023

Reynolds, R.L., Rosenbaum, J.G., Hudson, M.R. and Fishman, N.S. (1990). Rock magnetism, the distribution of magnetic minerals in the Earth's crust, and aeromagnetic anomalies. Hanna, W.F. (ed.), *Geologic Application of modern Aeromagnetic Surveys*, pp 24-45. Lakewood, Colorado: U.S. Geological Survey Bulletin 1924.

Russell, J.K., Edwards, B.R., Porritt, L. and Ryane, C. (2014). Tuyas: a descriptive genetic classification. *Quaternary Science Reviews, 87*, 70-81. http://dx.doi.org/10.1016/j.quascirev.2014.01.001

Sharma, P.V. (1986). *Geophysical Methods in Geology 2nd ed*. New York: Elsevier Science Publishing Co.

Sigmundsson, F., Gudmundsson, M.T., Steinthorsson, S., Hoskuldsson, A., Larsen, G., Imsland, P., … Einarsson, P. (2013). Eldfjallavá. Solnes, J. (Ed.), *Náttúruvá á Íslandi* (pp. 73-175). Reykjavik: Viðlagatrygging Íslands/Háskólaútgáfan.

Sinton, J., Grönvold, K. and Sæmundsson, K. (2005). Postglacial eruptive history of the Western Volcanic Zone, Iceland. *Geochemistry, Geophysics, Geosystems, 6*(12) doi: 10.1029/2005GC001021

Skilling, I.P. (2009). Subglacial to emergent basaltic volcanism at Hlöðufell, south-west Iceland: A history of ice-confinement. *Journal of Volcanology and Geothermal Research 185*. 276–289. doi:10.1016/j.jvolgeores.2009.05.023

Sæmundsson, K., Kristjansson, L., McDougall, I. and Watkins, N.D. (1980) K-Ar dating, geological and paleomagnetic study of a 5-km lava succession in Northern Iceland. *Journal of Geophysical Research, 85*, 3628-3646.

Tauxe, L. (2010). *Essentials of Paleomagnetism*. Berkeley and Los Angeles, California: University of California Press.

Thordarson, T. and Höskuldsson, Á. (2008). Postglacial volcanism in Iceland. *Jökull, 58*, 197-228.

Thordarson, T. and Larsen, G. (2007). Volcanism in Iceland in historical time: Volcano types, eruption styles and eruptive history. *Journal of Geodynamics, 43*(1), 118-152. doi: 10.1016/j.jog.2006.09.005

Werner, R. and Schmincke, H.-U. (1999). Englacial vs lacustrine origin of volcanic table mountains: evidence from Iceland. *Bulletin of Volcanology, 60*(5). 335-354. doi: 10.1007/s004450050237

Werner, R., Schmincke, H.-U. and Sigvaldason, G. (1996). A new model for the evolution of table mountains; volcanological and petrological evidence from Herdubreid and Herdubreidartögl volcanoes (Iceland). *Geologische Rundschau, 85*(2), 390-397. doi: 10.1007/s005310050084

Appendix A: Magnetic directions - Data in tables

Tables are:

A1	All sampling sites:	List of all sampling sites with paleomagnetic information for each sampling site
A2	All units:	List of all units with paleomagnetic information for each unit
A3	All samples	List of all samples with paleomagnetic and other magnetic information for each sample

A1: All sampling sites

Name	Stage and location within the stage	Location (GPS)	Numb. of samples	DECL (°)	INCL (°)	Demag (mT)	Alpha95 (°)	Unit	Altitude [m]	VGP	Sampling date	Note
HF-A	Stage I: Pillow lava, south part	N64.40115 W20.55046	8	331	72.4	40	1.9	PILL-AMTU	518	74.6°N 237.0°E	08-Jul-14	
HF-B	Stage I: Pillow lava in Rani	N64.39941 W20.53045	7	352.3	70	20	1.1	PILL-BVW	475	78.8°N 183.4°E	20-Sep-14	
HF-C	Stage I: Pillow lava, south part.	N64.40331 W20.54896	7	8.7	73.3	35	1.7	CJB-C	610	84.1°N 118.0°E	29-Aug-15	
HF-D	Stage III: Lower cap lava, south part	N64.40654 W20.54755	7	58.5	70	20	1.3	LAVA-DJNY	849	59.5°N 61.3°E	30-Aug-15	
HF-E	Stage IV: Upper cap lava, southern part.	N64.41020 W20.54815	6	351.7	75.8	35	1.9	LAVA-ELP	1009	86.1°N 234.2°E	30-Aug-15	
HF-F	Stage I: Pillow lava, west side.	N64.43798 W20.55019	6	-2.5	76.8	30	1.0	PILL-FG	594	88.8°N 274.6°E	13-Sep-15	
HF-G	Stage I: Pillow lava, west side.	N64.43795 W20.55031	6	4.3	72.2	50	1.1	PILL-FG	596	82.6°N 140.9°E	13-Sep-15	
HF-H	Dyke: North-western part of Hlöðufell	N64.43658 W20.55424	5	-4.5	73.4	25	1.8	DYKE	636	84.4°N 183.5°E	13-Sep-15	
HF-I	Dyke: Western part of Hlöðufell.	N64.41526 W20.56618	7	-4.8	73.8	30	2.1	DYKE	724	85.0°N 188.3°E	18-Sep-15	
HF-J	Stage III: Lower cap lava, south part	N64.40662 W20.54813	6	29.8	72.4	15	1.7	LAVA-DJNY	857	72.7°N 78.0°E	10-Oct-15	
HF-K	Stage III-IV: Cap lava bench, south terrace	N64.40950 W20.54482	11	12.1	74.6	25	1.2	LAVA-K	908	83.6°N 95.0°E	10-Oct-15	
HF-L	Stage IV: Upper cap lava, southern part.	N64.41461 W20.53851	6	347.4	71.4	30	1.7	LAVA-ELP	1115	79.6°N 202.2°E	10-Oct-15	
HF-M	Stage I: Pillow lava, south part.	N64.40130 W20.54876	9	335.2	64.9	30	1.7	PILL-AMTU	527	67.9°N 209.0°E	18-Oct-15	
HF-N	Stage III: Lower cap lava, south part	N64.40644 W20.54791	8	38.1	65.4	20	4.7	LAVA-DJNY	839	63.5°N 90.5°E	18-Jul-16	
HF-O	Stage III-IV: Cap lava bench, north terrace	N64.43087 W20.54511	15	1.3	71.1	20	2.0	LAVA-OQ	974	81.2°N 154.6°E	18-Jul-16	
HF-P	Stage IV: Upper cap lava, north part.	N64.42490 W20.54816	8	-1.2	73.9	15	2.6	LAVA-ELP	1081	85.6°N 167.4°E	19-Jul-16	

Name	Stage and location within the stage	Location (GPS)	Numb. of samples	DECL (°)	INCL (°)	Demag (mT)	Alpha95 (°)	Unit	Altitude [m]	VGP	Sampling date	Note
HF-Q	Stage III-IV: Cap lava bench, north terrace	N64.42965 W20.54270	8	1	74.1	15	1.5	LAVA-OQ	991	85.8°N 152.5°E	19-Jul-16	
HF-R	Stage I: Pillow lava, west side	N64.43781 W20.55889	9	7	72.7	15	1.0	PILL-RS	543	82.8°N 128.8°E	29-Aug-16	
HF-S	Stage I: Pillow lava, west side	N64.40409 W20.55708	11	3.8	70.5	30	1.5	PILL-RS	507	80.1°N 146.4°E	29-Aug-16	
HF-T	Stage I: Pillow lava, south part.	N64.40130 W20.55296	8	15.8	70.7	25	1.2	PILL-AMTU	510	77.7°N 112.4°E	29-Sep-16	
HF-U	Stage I: Pillow lava, south part.	N64.40201 W20.54929	8	344.6	72.5	15	1.1	PILL-AMTU	558	80.1°N 213.3°E	29-Sep-16	
HF-V	Stage I: Pillow lava in Rani	N64.39875 W20.52769	7	342.1	70.6	25	3.4	PILL-BVW	480	76.9°N 210.9°E	30-Sep-16	
HF-W	Stage I: Pillow lava in Rani	N64.39687 W20.51954	7	317.7	74.4	30	2.6	PILL-BVW	505	70.5°N 258.4°E	30-Sep-16	
HF-X	Stage I: Pillow lava, east side of main mountain	N64.40567 W20.52242	5	3.6	67.5	10	3.8	PILL-X	551	76.7°N 149.3°E	30-Sep-16	
HF-Y	Lower cap lava, south part	N64.40719 W20.54816	7	-2.8	72.7	15	0.9	LAVA-DJNY	879	83.0°N 169.5°E	15-Oct-16	
HL-1	Stage I: Pillow lava, south part.	N64.40085 W20.55170	1-2	NA	NA	NA	NA	PILL-AMTU	500		year 2003	Not used directly in this research.
HL-2	Lower cap lava, south part	N64.40673 W20.54795	8	19.6	73.6	25	5.1	LAVA-DJN	850		year 2003	Not used directly in this research.
HL-3	Stage IV: Upper cap lava, southern part.	N64.41268 W20.54285	4	-2.8	73.5	25	3.6	LAVA-ELP	1035		year 2003	Not used directly in this research.
HL-4	Stage I: Pillow lava, south part.	N64.40242 W20.54883	4	0	74.9	25	1.3	PILL-AMTU	561		year 2003	Not used directly in this research.
TF-A	Pillow lava, Western side of Þórólfsfell	N64.44850 W20.51689	10	18.7	72.1	30	1.8	TFPILL	544	78.4°N 99.7°E	08-Jul-14	Not used directly in this research.
TF-B	Pillow lava, Southern side of Þórólfsfell	N64.44211 W20.51501	7	-5.6	71.5	60	2.9	TFPILL	536	81.3°N 180.8°E	20-Sep-14	Not used directly in this research.
		Average		1.3	72.1	26.2	2.0					
		Standard deviation		19.7	2.7	10.7	1.1					
		Min		-42	64.9	10	0.9					
		Max		59	76.8	60	5.1					
		Span		101	11.9	50	4.1					

A2: All units

No	Description	Code	Stage	Sampling sites	Location	Altitude [m]	Samples total	Decl [°]	Incl [°]	Alpha95 [°]	Demag [mT]	VGP	Sampling sites
1	Pillow lava in Rani	PILL-BVW	I	3	64.39875°N -20.52769°E	490	18	-23.0	72.1	2.5	30	76.7°N 226.8°E	HF-B;V;W
2	Pillow ridge at Hlöðuvallagil	PILL-AMTU	I	4+1	64.40115°N -20.55046°E	520	33	-14.3	71.2	5.1	30	78.8°N 205.3°E	HF-A;M;T;U; (HL-4)
3	Pillow lava main mountain	PILl-RSX	I	3	64.40409°N - 20.55708°E	534	25	4.4	71.0	1.1	30	80.7°N 143.7°E	
3B	Pillow lava main mountain, west	PILL-RS	I	2	64.40409°N - 20.55708°E	525	20	4.6	71.7	1.0	30	81.7°N 141.4°E	HF-R;S
3C	Pillow lava main mountain, east	PILL-X	I	1	64.40567°N - 20.52242°E	551	5	3.7	68.2	3.8	30	76.7°N 149.3°E	HF-X
4	Pillow lava main mountainn, west-higher	PILL-FG	I	2	64.43798°N -20.55019°E	588	12	1.5	74.9	1.4	20	87.1°N 145.1°E	HF-F; G
5	Cube joint lava in Hlöðuvallagil	CJB-C	I	1	64.41020°N -20.54815°E	617	7	7.8	73.7	1.7	35	84.1°N 118.0°E	HF-C
6	Lower cap lava without HF-Y	LAVA-DJN	III	3+1	64.40673°N -20.54795°E	848	18	44.5	69.7	2.5	20	65.3°N 74.3°E	HF-D;J;N; (HL-2)
6B	Lower cap lava with HF-Y	LAVA-DJNY	III	4+1	64.40673°N -20.54795°E	811	27	34.2	71.5	3.0	20	71.5°N 79.4°E	HF-D;J;N;Y; (HL-2)
6C	Lower cap lava, higher (HF-Y)	LAVA-Y	III	1	64.40719°N - 20.54816°E	879	7	-2.3	-2.3	72.3	15	83.0°N 169.5°E	HF-Y
7	Cap lava benches on south terrace	LAVA-K	III'	1	64.40950°N - 20.54482°E	910	11	12.1	74.6	1.2	25	83.6°N 95.0°E	HF-K
8	Cap lava benches on north terrace	LAVA-OQ	III'	2	64.42965°N -20.54270°E	987	23	1.6	72.2	1.5	20	82.8°N 152.4°E	HF-O;Q
9	Upper cap lava	LAVA-ELP	IV	3+1	64.41020°N -20.54815°E	1050	20	-6.9	73.8	1.5	30	84.4°N 197.3°E	HF-E;L;P; (HL-3)
10	Dykes	DYKES-HI	NA	2	NA	NA	12	-5.1	73.7	1.3	30	84.7°N 188.7°E	HF-H;I
11	Pillow lava in Þórólfsfell	TF-AB	NA	2	64.44850°N - 20.51689°E	NA	17	9.2	72.3	2.2	30	81.7°N 123.1°E	TF-A;B

A2: All samples

1) Calculation of susceptibility by volume in SI units:

$$\chi_{Vol\,SI} = Susceptibility_{\substack{By\,Vol \\ in\,cgs\,system}} \cdot 4\pi = \frac{Reading\ of\ instrument}{Volume\ in\ cm^3 \cdot 1000}\,4\pi$$

2) Induced magnetization J_i in [A/m] is calculated with instruction from Leo Kristjansson:

$$J_I = Susceptibility_{\substack{By\,Vol \\ in\,cgs\,system}} \cdot 0.5$$

3) Konigsberger ratio Q is calculated with instruction from Leo Kristjansson, from reading of the instrument in the following way, where $\boldsymbol{J_{NRM}}$ is measured natural remanent magnetization and $\boldsymbol{J_I}$ is induced magnetization:

$$Q = \frac{J_{NRM}}{J_I} = \frac{J_{NRM}}{\frac{Reading\ of\ instrument}{Vol_{cc} \cdot 1000}\,0.5 \cdot 1000}$$

4) MDF is the median demagnetizing field, that is the external alternating magnetic field strength needed to remove half of the original remanent magnetization of each sample in the demagnetization process.

5) Declination and inclination after the demagnetization in column 6.

6) Demagnetization in mT is the maximum external magnetic field in demagnetization used while calculating the declination and inclination angles.

		1)	2)		3)	4)	5)		6)
Sample	Vol cc	Susceptibility [SI by Vol]	J_i [A/m]	J (NRM) [A/m]	Q	MDF [mT]	Declination [°]	Inclination [°]	Demagnetization [mT]
HF-A-01	10.65	7.02E-03	0.28	7.19	25.7	10.9	336.1	+72.0	40
HF-A-02	10.83	6.46E-03	0.26	6.52	25.4	10.1	337.9	+71.5	40
HF-A-03	10.80	5.70E-03	0.23	6.51	28.7	12.9	336.3	+72.3	40
HF-A-04	10.66	5.18E-03	0.21	6.73	32.6	12.3	324.9	+69.0	40
HF-A-05	10.81	6.89E-03	0.27	7.00	25.5	9.7	324.8	+73.1	40
HF-A-06	10.58	6.52E-03	0.26	7.80	30.1	9.1	333.7	+76.5	40
HF-A-07	10.86	3.25E-03	0.13	7.87	60.9	18.0	332.0	+72.2	40
HF-A-08	10.53	2.45E-03	0.10	9.05	92.5	21.3	323.4	+72.1	40
HF-B-02	10.17	1.87E-03	0.07	12.1	161	54.6	351.5	+69.8	20
HF-B-03	10.45	2.08E-03	0.08	13.1	158	52.3	352.9	+71.0	20
HF-B-04	10.43	1.89E-03	0.08	12.3	163	53.4	355.5	+69.7	20
HF-B-06	10.58	1.74E-03	0.07	12.2	175	54.4	349.3	+71.2	20
HF-B-07	10.46	1.79E-03	0.07	12.1	170	51.2	350.9	+69.9	20
HF-B-08	10.39	1.81E-03	0.07	12.7	175	52.7	NA	NA	NA
HF-B-09	10.87	1.76E-03	0.07	11.5	163	53.7	353.5	+68.1	20
HF-C-02	10.82	9.65E-03	0.38	5.71	14.9	14.6	1.5	+76.3	35
HF-C-04	11.01	10.9E-03	0.43	6.42	14.8	15.1	13.4	+73.0	35

Sample	Vol cc	Susceptibility [SI by Vol]	J_i [A/m]	J (NRM) [A/m]	Q	MDF [mT]	Declination [°]	Inclination [°]	Demagnetization [mT]
HF-C-05	10.97	11.0E-03	0.44	6.52	14.8	15.1	7.5	+74.0	35
HF-C-06	10.88	10.7E-03	0.43	5.96	13.9	20.5	6.6	+74.1	35
HF-C-07	10.84	11.2E-03	0.45	6.10	13.7	14.1	7.3	+69.7	35
HF-C-08	11.30	12.3E-03	0.49	4.31	8.8	12.7	9.7	+73.9	35
HF-C-09	10.76	11.5E-03	0.46	4.40	9.6	12.0	7.4	+74.9	35
HF-D-01	10.62	7.37E-03	0.29	5.51	18.8	16.8	57.7	+69.5	20
HF-D-03	11.01	8.05E-03	0.32	6.11	19.0	17.8	60.9	+67.7	20
HF-D-04	10.58	65.2E-03	2.60	8.56	3.3	9.5	59.0	+71.2	20
HF-D-05	11.21	15.4E-03	0.62	7.39	12.0	12.5	57.4	+69.9	20
HF-D-06	10.69	9.90E-03	0.39	7.55	19.2	10.1	56.2	+72.7	20
HF-D-07	10.84	8.60E-03	0.34	5.72	16.7	15.3	57.5	+69.6	20
HF-D-08	8.87	11.1E-03	0.44	6.85	15.4	13.9	60.5	+69.2	20
HF-E-01	10.57	3.12E-03	0.12	10.9	87.4	13.5	344.5	+74.9	35
HF-E-04	10.58	3.20E-03	0.13	10.9	85.8	16.3	351.6	+75.5	35
HF-E-05	10.64	2.32E-03	0.09	7.91	85.4	17.1	355.2	+72.5	35
HF-E-06	10.48	2.84E-03	0.11	8.54	75.6	16.3	353.7	+77.0	35
HF-E-07	10.77	2.15E-03	0.09	5.64	65.7	20.9	356.0	+78.1	35
HF-E-08	10.60	3.08E-03	0.12	8.21	66.9	25.5	349.8	+76.6	35
HF-F-01	10.25	1.44E-03	0.06	11.0	191	66.5	6.0	+75.5	20
HF-F-02	10.96	3.09E-03	0.12	9.43	76.5	13.3	356.6	+76.0	20
HF-F-03	10.66	2.95E-03	0.12	7.81	66.4	21.7	351.2	+76.6	20
HF-F-04	10.59			9.40		19.1	358.7	+77.0	20
HF-F-05	10.30	2.39E-03	0.10	8.74	91.8	27.4	356.0	+77.9	20
HF-F-06	10.59	1.76E-03	0.07	10.6	151	38.9	358.0	+78.0	20
HF-G-01	10.81			8.68		46.2	9.1	+73.5	20
HF-G-03	10.96	1.77E-03	0.07	8.97	126	36.0	358.0	+74.0	20
HF-G-04	10.22	1.59E-03	0.06	8.90	139	46.3	3.2	+72.6	20
HF-G-05	10.77	1.92E-03	0.08	7.62	99.5	35.5	2.1	+72.8	20
HF-G-06	10.87	2.33E-03	0.09	8.30	89.4	25.2	5.0	+72.5	20
HF-G-07	10.25	1.70E-03	0.07	9.06	133	40.4	7.8	+71.6	20
HF-H-01	10.87	8.28E-03	0.33	11.3	34.1	10.4	352.5	+72.3	25
HF-H-02	10.72	8.47E-03	0.34	10.6	31.3	9.9	2.1	+73.2	25
HF-H-03	10.77	8.00E-03	0.32	14.5	45.5	9.7	358.9	+72.9	25
HF-H-04	10.84	8.07E-03	0.32	13.2	41.4	10.6	349.6	+75.4	25
HF-H-05	10.41	8.41E-03	0.33	11.8	35.2	10.8	353.9	+73.1	25
HF-I-01	10.93	7.58E-03	0.30	5.87	19.5	12.8	7.8	+74.9	30
HF-I-02	10.70	7.92E-03	0.32	9.41	29.8	11.8	354.9	+71.2	30
HF-I-03	10.72	7.81E-03	0.31	7.25	23.3	10.7	350.3	+75.0	30
HF-I-05	10.88	8.04E-03	0.32	11.1	34.6	8.6	356.4	+72.6	30
HF-I-06	10.83	8.36E-03	0.33	11.0	33.2	8.6	352.9	+72.3	30
HF-I-07	10.61	5.85E-03	0.23	7.25	31.1	13.7	344.6	+77.5	30
HF-I-08	9.99	6.17E-03	0.25	7.96	32.4	11.9	357.3	+72.9	30
HF-J-03	10.60	10.5E-03	0.42	5.66	13.5	8.8	36.8	+70.9	25

Sample	Vol cc	Suscepti-bility [SI by Vol]	J_i [A/m]	J (NRM) [A/m]	Q	MDF [mT]	Declin-ation [°]	Inclin-ation [°]	De-magneti-zation [mT]
HF-J-05	10.60	15.0E-03	0.60	5.51	9.2	8.3	37.8	+74.2	25
HF-J-06	10.27	13.9E-03	0.56	5.85	10.5	8.1	34.7	+71.4	25
HF-J-07	10.32	14.8E-03	0.59	5.86	9.9	8.3	29.1	+74.1	25
HF-J-08	10.70	11.3E-03	0.45	5.51	12.2	8.4	31.1	+70.3	25
HF-J-09	10.28	16.2E-03	0.65	5.95	9.2	7.8	29.0	+72.3	25
HF-K-01	10.83	8.78E-03	0.35	8.00	22.9	21.6	10.2	+74.4	25
HF-K-03	10.61	9.90E-03	0.39	8.39	21.3	25.0	3.8	+74.7	25
HF-K-04	10.89	10.2E-03	0.41	10.44	25.5	22.2	13.7	+75.1	25
HF-K-05	10.55	10.4E-03	0.41	10.39	25.1	22.1	10.7	+75.0	25
HF-K-06	10.50	10.1E-03	0.40	10.12	25.1	21.9	13.6	+75.8	25
HF-K-07	10.28	9.56E-03	0.38	9.52	25.0	21.9	14.6	+75.2	25
HF-K-08	10.27	14.1E-03	0.56	8.05	14.3	12.9	23.3	+75.8	25
HF-K-09	10.04	14.7E-03	0.59	8.70	14.8	13.7	5.1	+74.5	25
HF-K-10	10.04	12.7E-03	0.51	6.24	12.3	9.6	10.0	+73.8	25
HF-K-11	10.59	11.9E-03	0.48	6.27	13.2	11.8	6.0	+71.1	25
HF-K-12	10.78	10.8E-03	0.43	5.53	12.8	15.0	23.6	+73.8	25
HF-L-01	10.65	9.87E-03	0.39	14.0	35.6	17.4	343.9	+72.6	30
HF-L-02	10.75	10.8E-03	0.43	14.8	34.2	14.8	341.8	+72.0	30
HF-L-03	10.80	8.76E-03	0.35	10.6	30.3	26.3	344.4	+72.7	30
HF-L-04	10.88	10.0E-03	0.40	11.5	28.5	24.4	347.3	+70.6	30
HF-L-05	10.43	9.13E-03	0.36	11.3	31.2	23.2	354.1	+69.2	30
HF-L-06	10.65	8.83E-03	0.35	10.7	30.4	22.8	351.3	+71.2	30
HF-M-01	10.37	5.73E-03	0.23	13.4	58.7	9.4	337.7	+63.2	30
HF-M-02	10.51	5.51E-03	0.22	7.92	36.1	11.4	336.0	+64.2	30
HF-M-03	10.91	6.16E-03	0.25	6.85	27.9	15.6	336.7	+68.8	30
HF-M-04	10.83	9.13E-03	0.36	9.15	25.2	8.9	336.4	+64.4	30
HF-M-05	9.79	4.67E-03	0.19	13.2	71.0	12.3	332.6	+60.7	30
HF-M-06	10.19	4.66E-03	0.19	7.78	41.9	14.2	332.4	+66.6	30
HF-M-07	10.18	7.67E-03	0.31	7.66	25.1	9.7	338.8	+65.3	30
HF-M-08	10.84	6.88E-03	0.27	7.64	27.9	10.5	338.7	+65.9	30
HF-M-09	10.30	3.76E-03	0.15	11.7	77.8	15.2	327.8	+64.6	30
HF-N-01	10.69	43.1E-03	1.72	7.15	4.2	10.0	32.9	+70.6	20
HF-N-02	11.07	32.2E-03	1.29	5.48	4.3	9.7	37.4	+68.6	20
HF-N-03	10.60	21.6E-03	0.86	3.65	4.2	7.2	37.9	+62.2	20
HF-N-04	10.84	24.3E-03	0.97	8.10	8.4	8.8	16.1	+64.8	20
HF-N-05	10.59	7.28E-03	0.29	2.62	9.0	11.9	41.7	+61.6	20
HF-N-06	10.93	26.1E-03	1.04	14.2	13.7	31.3	55.5	+61.6	20
HF-N-08	10.93	23.1E-03	0.92	11.7	12.7	29.7	29.0	+60.3	20
HF-O-01	10.69	2.15E-03	0.09	1.36	15.9	25.2	9.1	+73.0	20
HF-O-02	10.73	2.90E-03	0.12	1.44	12.5	23.1	8.7	+71.1	20
HF-O-03	10.65	3.81E-03	0.15	2.75	18.1	21.6	10.4	+70.8	20
HF-O-04	10.78	13.8E-03	0.55	10.8	19.7	27.1	18.6	+68.4	20

Sample	Vol cc	Susceptibility [SI by Vol]	J_i [A/m]	J (NRM) [A/m]	Q	MDF [mT]	Declination [°]	Inclination [°]	Demagnetization [mT]
HF-O-05	10.93	11.4E-03	0.45	9.27	20.4	29.7	14.7	+66.5	20
HF-O-06	10.55	7.94E-03	0.32	7.31	23.1	45.8	352.7	+69.2	20
HF-O-07	10.69	10.3E-03	0.41	9.58	23.4	41.7	348.0	+70.5	20
HF-O-08	10.60	8.31E-03	0.33	7.33	22.2	37.7	346.9	+69.9	20
HF-O-09	11.17	14.3E-03	0.57	36.5	63.7	52.9	356.8	+71.3	20
HF-O-10	10.78	6.13E-03	0.24	9.39	38.5	39.4	346.2	+69.4	20
HF-O-11	10.78	7.82E-03	0.31	16.1	51.7	42.0	345.3	+71.4	20
HF-O-12	10.58	7.75E-03	0.31	5.45	17.6	34.7	5.8	+69.8	20
HF-O-13	10.69	7.55E-03	0.30	4.93	16.4	24.5	7.7	+71.5	20
HF-O-14	10.88	4.74E-03	0.19	3.26	17.3	30.4	5.3	+74.3	20
HF-O-17	10.69	16.2E-03	0.65	7.93	12.2	20.9	2.2	+75.2	20
HF-P-01	10.87	6.96E-03	0.28	6.63	23.9	12.8	348.9	+76.3	30
HF-P-02	10.69	3.43E-03	0.14	4.04	29.6	13.5	349.7	+79.2	30
HF-P-03	10.84	3.73E-03	0.15	5.15	34.7	10.2	357.9	+77.6	30
HF-P-04	11.01	4.46E-03	0.18	2.65	14.9	11.6	1.6	+72.2	30
HF-P-05	10.64	8.78E-03	0.35	6.10	17.4	7.7	4.3	+73.6	30
HF-P-06	10.49	13.7E-03	0.55	12.5	22.8	20.8	359.1	+70.2	30
HF-P-07	10.64	11.8E-03	0.47	10.3	21.9	13.4	355.9	+71.1	30
HF-P-08	10.83	9.66E-03	0.38	9.85	25.6	13.5	6.6	+70.6	30
HF-Q-01	10.73	4.54E-03	0.18	4.13	22.9	21.7	4.6	+74.3	15
HF-Q-02	10.77	3.79E-03	0.15	4.73	31.4	39.0	1.1	+74.0	15
HF-Q-03	10.50	4.95E-03	0.20	5.50	27.9	20.2	3.5	+73.4	15
HF-Q-06	10.48	4.86E-03	0.19	4.51	23.3	13.0	3.8	+72.8	15
HF-Q-07	10.83	5.12E-03	0.20	3.95	19.3	13.0	4.1	+72.3	15
HF-Q-08	10.77	8.03E-03	0.32	4.02	12.6	14.6	4.9	+73.0	15
HF-Q-10	10.97	5.81E-03	0.23	5.95	25.7	24.5	354.1	+75.6	15
HF-Q-11	10.74	5.93E-03	0.24	4.08	17.3	11.6	348.6	+76.5	15
HF-R-01	10.92	9.20E-03	0.37	7.55	20.6	11.6	11.8	+73.6	15
HF-R-02	10.77	7.51E-03	0.30	10.1	33.7	14.4	8.0	+71.2	15
HF-R-03	10.45	10.2E-03	0.41	6.63	16.2	11.6	9.9	+73.6	15
HF-R-04	10.43	10.0E-03	0.40	7.15	17.9	11.5	9.2	+72.8	15
HF-R-05	10.03	10.7E-03	0.43	9.69	22.7	9.4	4.1	+73.6	15
HF-R-06	10.88	9.08E-03	0.36	10.4	28.9	9.3	5.3	+70.8	15
HF-R-07	10.64	8.51E-03	0.34	8.32	24.6	35.9	6.2	+72.5	15
HF-R-08	10.78	7.45E-03	0.30	8.77	29.5	13.4	0.5	+74.0	15
HF-R-09	10.11	9.89E-03	0.39	6.05	15.4	9.3	7.5	+71.6	15
HF-S-01	9.90	1.77E-03	0.07	11.1	157	42.8	6.1	+73.8	30
HF-S-02	10.58	3.00E-03	0.12	13.1	109	20.2	1.5	+72.4	30
HF-S-03	10.58	4.27E-03	0.17	15.5	90.9	17.1	4.8	+73.2	30
HF-S-04	10.59	5.76E-03	0.23	15.9	69.3	13.0	359.4	+67.8	30
HF-S-05	10.53	5.94E-03	0.24	10.9	46.1	14.9	355.1	+69.6	30
HF-S-06	11.06	4.78E-03	0.19	15.6	82.0	15.2	8.2	+71.6	30

Sample	Vol cc	Suscepti-bility [SI by Vol]	J_i [A/m]	J (NRM) [A/m]	Q	MDF [mT]	Declin-ation [°]	Inclin-ation [°]	De-magneti-zation [mT]
HF-S-07	10.88	4.69E-03	0.19	14.1	75.6	14.5	8.3	+69.0	30
HF-S-08	10.19	5.15E-03	0.21	13.3	64.8	14.4	4.7	+66.9	30
HF-S-09	10.58	6.64E-03	0.26	13.3	50.3	13.2	360.0	+68.8	30
HF-S-10	10.88	1.28E-03	0.05	7.05	138	57.0	9.5	+70.0	30
HF-S-12	11.16	6.38E-03	0.25	12.52	49.3	13.7	5.9	+71.9	30
HF-T-01	10.36	10.6E-03	0.43	6.27	14.7	8.3	19.3	+69.9	25
HF-T-02	10.27	9.62E-03	0.38	7.04	18.4	9.8	21.3	+70.1	25
HF-T-03	10.25	8.65E-03	0.34	8.49	24.7	8.7	15.7	+71.4	25
HF-T-04	10.25	8.78E-03	0.35	6.14	17.6	9.9	21.6	+69.8	25
HF-T-05	10.31	7.09E-03	0.28	8.23	29.2	12.3	10.3	+70.3	25
HF-T-06	10.78	8.20E-03	0.33	9.45	28.9	10.4	12.2	+69.6	25
HF-T-07	10.68	9.13E-03	0.36	5.50	15.1	10.1	10.8	+71.8	25
HF-T-08	10.23	9.87E-03	0.39	6.05	15.4	9.4	14.3	+72.0	25
HF-U-01	10.59	2.36E-03	0.09	9.35	99.5	21.6	340.3	+72.7	20
HF-U-02	9.97	2.44E-03	0.10	10.1	104	19.5	348.2	+72.1	20
HF-U-03	10.84	5.89E-03	0.23	10.8	46.2	11.8	351.9	+71.1	20
HF-U-04	10.77	0.96E-03	0.04	4.44	115	67.2	340.2	+73.0	20
HF-U-05	10.17	2.28E-03	0.09	11.5	1256	22.5	353.2	+73.5	20
HF-U-06	10.60	3.56E-03	0.14	11.3	79.9	14.0	340.9	+71.6	20
HF-U-07	10.49	3.35E-03	0.13	10.3	77.3	16.9	343.3	+72.3	20
HF-U-08	10.50	4.98E-03	0.20	10.8	54.5	12.9	341.9	+72.4	20
HF-V-01	10.07	4.87E-03	0.19	14.8	76.4	23.7	338.2	+70.4	25
HF-V-02	10.31	5.15E-03	0.21	20.1	97.9	19.0	335.0	+75.4	25
HF-V-03	10.28	7.05E-03	0.28	16.3	57.9	16.8	356.8	+71.6	25
HF-V-04	9.39	4.17E-03	0.17	13.5	81.5	28.6	357.5	+70.7	25
HF-V-05	10.34	8.24E-03	0.33	12.5	38.0	15.2	329.6	+69.9	25
HF-V-06	10.50	4.05E-03	0.16	24.0	149	22.1	337.4	+67.7	25
HF-V-07	10.00	4.39E-03	0.18	18.2	103	19.1	341.1	+66.7	25
HF-W-01	10.69	5.02E-03	0.20	18.4	91.8	20.5	317.1	+74.5	30
HF-W-03	9.90	3.29E-03	0.13	14.3	109	34.5	313.8	+74.1	30
HF-W-04	9.93	5.16E-03	0.21	17.1	83.3	21.6	314.0	+73.1	30
HF-W-05	10.59	1.81E-03	0.07	11.8	163	55.7	297.4	+78.4	30
HF-W-06	10.53	4.89E-03	0.19	23.0	118	16.1	315.3	+72.6	30
HF-W-07	10.69	3.50E-03	0.14	15.4	110	31.4	332.1	+73.2	30
HF-W-08	10.82	3.51E-03	0.14	14.4	103	33.2	327.5	+73.1	30
HF-X-01	10.49	3.74E-03	0.15	12.4	82.8	14.1	1.7	+70.5	30
HF-X-02	10.03	4.92E-03	0.20	12.0	61.3	13.8	3.7	+65.2	30
HF-X-03	10.83	6.75E-03	0.27	11.3	42.0	8.6	356.4	+63.9	30
HF-X-04	10.41	4.17E-03	0.17	8.69	52.3	14.0	6.5	+69.5	30
HF-X-05	10.30	5.03E-03	0.20	10.7	53.3	13.2	13.0	+71.3	30
HF-Y-01	10.60	3.62E-03	0.14	5.83	40.4	16.7	0.2	+69.7	15
HF-Y-03	10.51	3.98E-03	0.16	4.30	27.2	9.9	357.5	+72.8	15

Sample	Vol cc	Susceptibility [SI by Vol]	J_i [A/m]	J (NRM) [A/m]	Q	MDF [mT]	Declination [°]	Inclination [°]	Demagnetization [mT]
HF-Y-04	10.23	3.99E-03	0.16	3.87	24.4	11.9	356.7	+73.5	15
HF-Y-05	10.18	4.25E-03	0.17	4.05	23.9	12.3	358.7	+73.6	15
HF-Y-07	10.33	3.40E-03	0.14	3.83	28.3	17.4	356.3	+73.3	15
HF-Y-08	10.64	5.77E-03	0.23	6.81	29.6	12.3	354.6	+71.6	15
HF-Y-09	10.31	4.52E-03	0.18	6.38	35.5	14.3	359.7	+71.5	15
TF-A-01	11.10	5.05E-03	0.20	16.1	79.9	14.3	21.6	+75.2	30
TF-A-02	10.51	5.23E-03	0.21	14.1	67.4	13.7	31.5	+69.7	30
TF-A-03	10.68	5.12E-03	0.20	14.1	69.4	14.9	16.3	+71.4	30
TF-A-04	11.14	5.48E-03	0.22	12.7	58.3	13.3	26.1	+71.7	30
TF-A-05	10.80	5.14E-03	0.20	12.6	61.3	15.3	21.0	+75.1	30
TF-A-06	10.06	5.44E-03	0.22	11.3	52.1	16.6	16.1	+74.7	30
TF-A-07	11.05	4.51E-03	0.18	22.0	122	15.3	14.8	+69.1	30
TF-A-08	10.28	4.08E-03	0.16	14.9	91.9	20.4	17.0	+70.4	30
TF-A-09	11.09	4.34E-03	0.17	22.3	129	16.1	12.2	+72.7	30
TF-A-10	11.01	3.95E-03	0.16	15.4	97.7	19.0	10.8	+70.0	30
TF-B-02	10.40	1.78E-03	0.07	12.9	181	53.8	351.1	+72.0	60
TF-B-03	9.90	1.90E-03	0.08	13.1	173	49.0	356.3	+73.1	60
TF-B-04	9.98	2.20E-03	0.09	14.0	159	44.0	9.9	+67.5	60
TF-B-05	10.63	1.71E-03	0.07	12.0	176	55.5	348.7	+72.1	60
TF-B-06	10.34	1.77E-03	0.07	12.6	179	55.8	348.9	+68.7	60
TF-B-07	11.05	1.58E-03	0.06	11.2	178	55.6	2.6	+73.5	60
TF-B-08	9.58	1.92E-03	0.08	13.2	172	50.2	341.0	+72.2	60

Appendix B: Demagnetization processes for all samples

In addition to the paleomagnetic directions, declination and inclination which are the main focus of this research, the results include some information on the magnetization properties from demagnetization measurements.

The MATLAB programs used in this research have the ability to do some analysis of the demagnetization process of the samples. Average curves for demagnetization have been drawn for each sampling site in Hlöðufell and are shown in Figure B-1. Both curves for the J/J_0 ratio and for measured J.

It could be noticed here is that there is some difference in behavior of demagnetization between the sampling sites. The pillow lavas in general seem to have stronger natural magnetization and more resistance against the external magnetic field used in the demagnetization process. Especially the samples that are from the glassy outer surface of the pillows. That is sampling site HF-B from Hlöðufell (see photos on page 115) and it is clear from Figure B-1 how slow the samples from that sampling site demagnetize. Demagnetization in 10 mT external field has almost no effect on the magnetization of the core. On Figure B-2 are demagnetization curves for all samples at HF-B and HF-D which is a cap lava.

Comparison of data for different kinds of sampling sites is in table B-1. The average MDF (median demagnetizing field, that is the external field needed to take out 50% of the original magnetization of the core, J_{RNM}) showing that the mean MDF for HF-B and TF-B is 52.6 mT while it is around 20 mT for all other sampling sites.

Similar pattern was for the demagnetization of samples in Undirhlíðar.

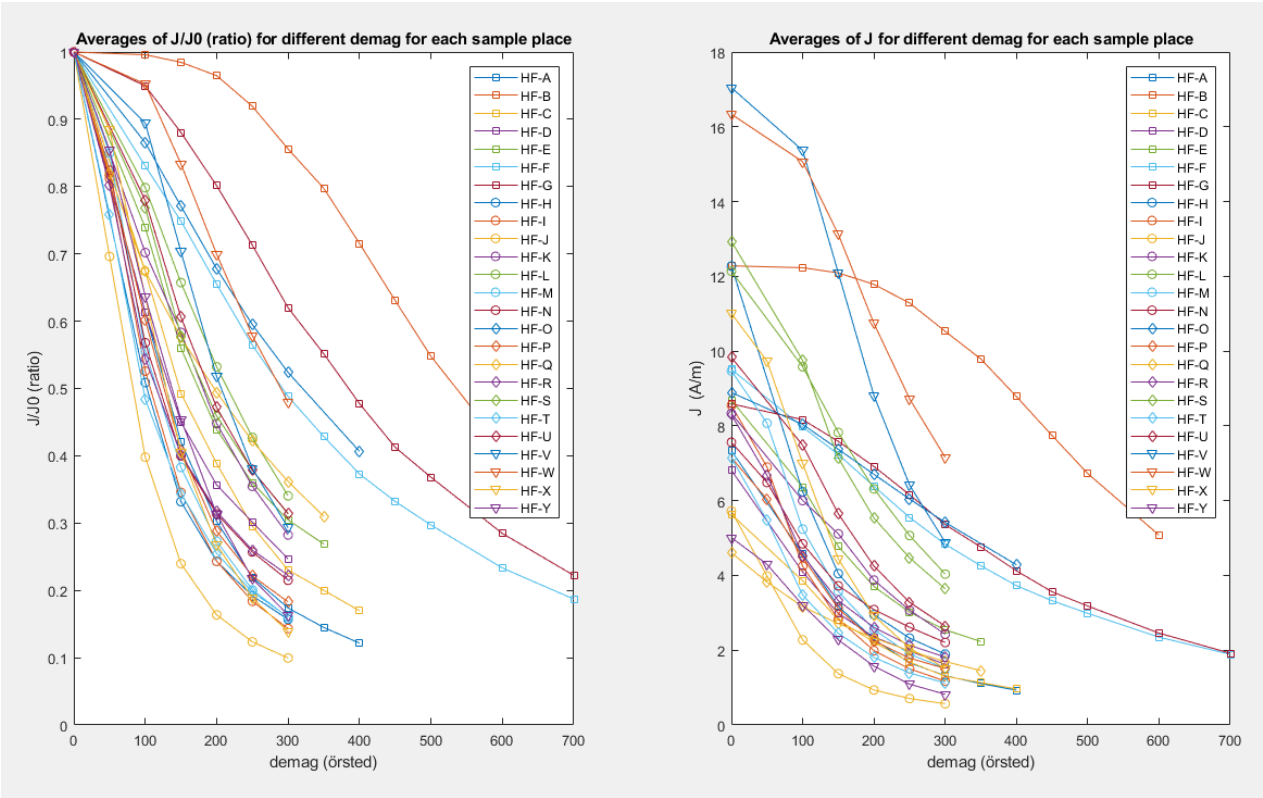

Figure B-1. Diagrams showing median demagnetization curve for each sampling site

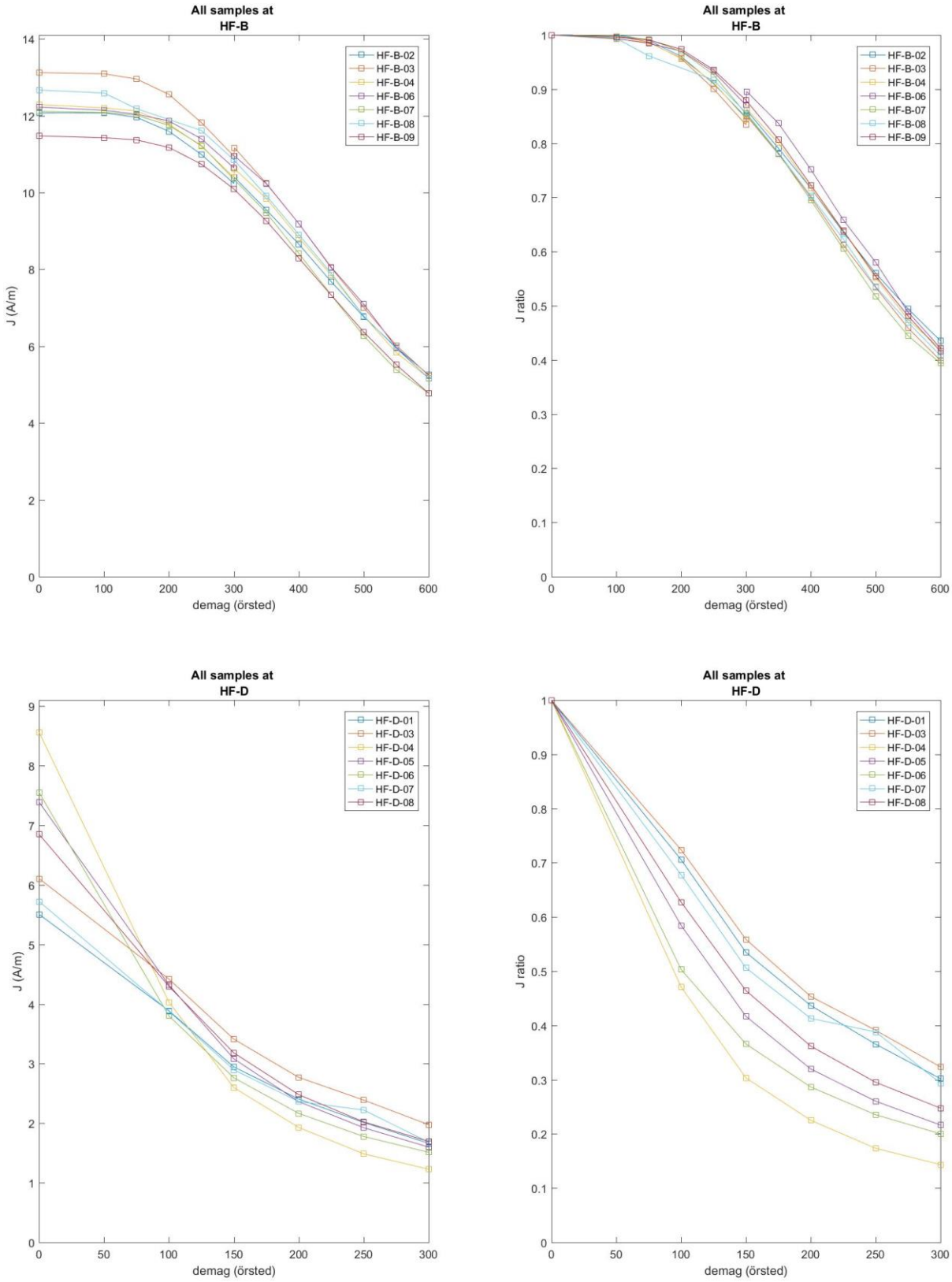

Figure B-2. Demagnetization curves for all samples at sampling sites HF-B and HF-D. Samples from sampling site HF-B are from the glassy outer surface of a pillow but HF-D is from a cap lava in stage III.

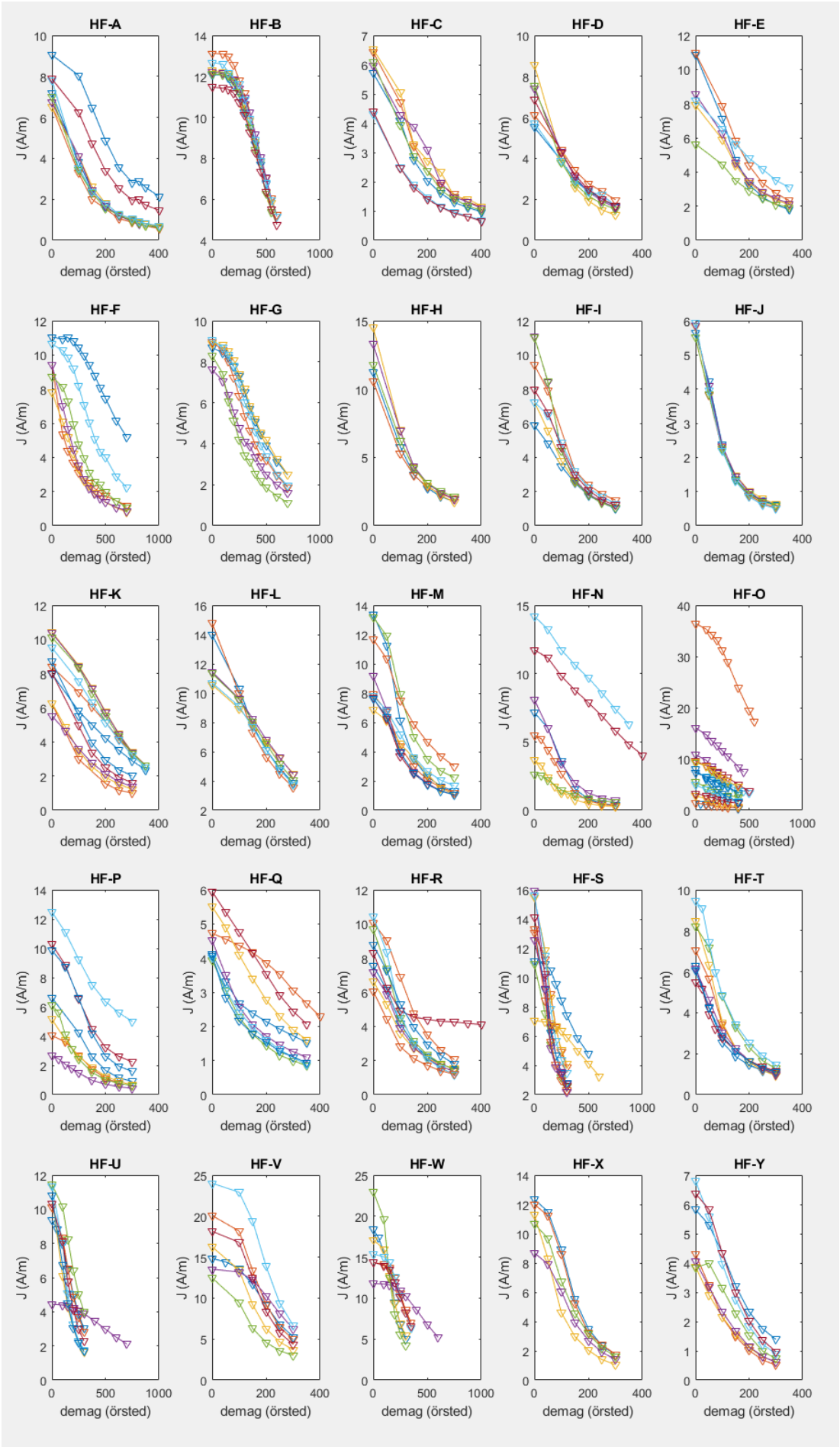

Figure B-3 Demagnetization curves for all samples for sampling sites in Hlöðufell. Remanent magnetization strength as a function of strength of demagnetizing field

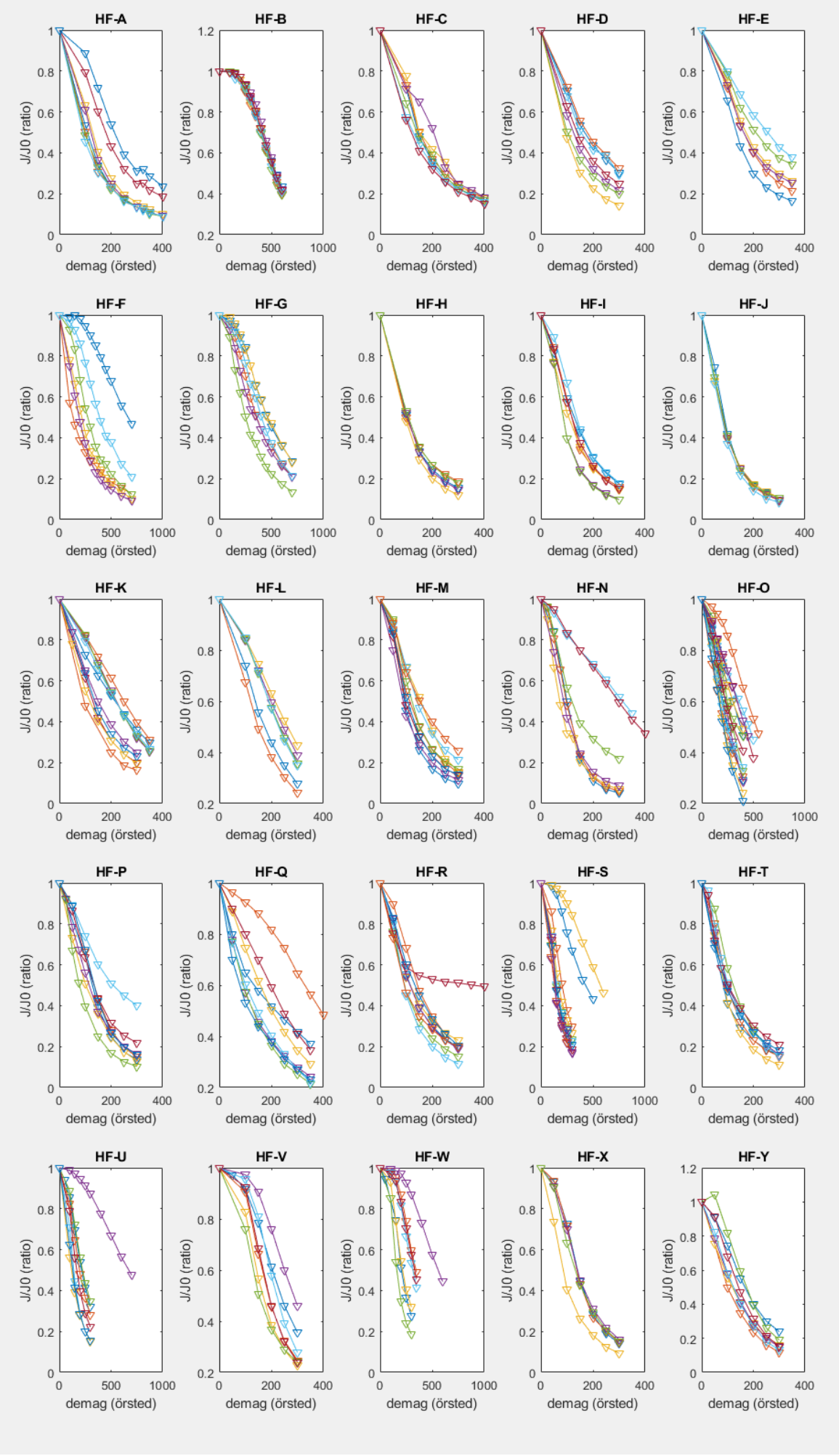

Figure B-4 Demagnetization curves for all samples for sampling sites in Hlöðufell. Remanent magnetization ratio as a function of strength of demagnetizing field

Table B-1. Comparison of demagnetization data of different types of sampling sites.

Sample	Ji [A/m]	J (NRM) [A/m]	J 10 mT [A/m]	J 20 mT [A/m]	J 30 mT [A/m]	Q	MDF [mT]	Number of samples
All samples, Hlöðufell and Þórólfsfell								
Mean	0.295	9.6	7.1	4.6	3.2	54.9	20.9	208
Lowest	0.039	1.4	1.1	0.5	0.3	3.3	7.2	208
Highest	2.597	36.4	35.3	33.2	28.8	191.8	67.2	208
Std	0.264	4.4	4.5	3.9	3.3	48.2	13.6	208
All pillow samples, Stage I and Þórólfsfell								
Mean	0.208	11.0	8.5	5.6	3.9	78.5	23.3	115
Lowest	0.039	4.3	2.5	1.4	0.9	8.8	8.3	115
Highest	0.490	24.0	22.9	13.9	11.2	191.8	67.2	115
Std	0.116	4.0	4.3	3.7	3.2	52.5	15.8	115
Pillow-outer core (HF-B and TF-B)								
Mean	0.074	12.5	12.5	12.1	10.7	170.4	52.6	14
Lowest	0.063	11.2	11.1	11.0	10.1	158.5	44.0	14
Highest	0.088	14.0	13.9	13.0	11.2	181.0	55.8	14
Std	0.006	0.7	0.7	0.6	0.4	7.5	3.1	14
Lava, stage III and IV								
Mean	0.413	7.6	5.4	3.6	2.6	25.3	19.0	82
Lowest	0.086	1.4	1.1	0.5	0.3	3.3	7.2	82
Highest	2.597	36.4	35.3	33.2	28.8	87.4	52.9	82
Std	0.362	4.4	4.4	4.1	3.5	18.0	9.8	82
Dykes, HF-H and HF-I								
Mean	0.308	10.1	5.2	2.4	1.5	32.6	10.8	12
Lowest	0.233	5.9	3.5	1.8	1.0	19.5	8.6	12
Highest	0.337	14.5	7.0	3.1	2.1	45.5	13.7	12
Std	0.033	2.5	1.1	0.5	0.4	6.6	1.5	12

Appendix C: Paleomagnetic measurements from year 2003: Leo Kristjansson

Leo Kristjansson and Magnus Tumi Gudmundsson went for magnetic core sampling in Hlöðufell the summer 2003. Measurable samples are from three places.

HL-1: Pillow lava in the pillow lava ridge at Hlöðuvellir. Stage I.

Location: N64.40085° W20.55170° (64° 24.051'N 20°33.102'E)
511m a.s.l.

D = 7.5 I = 73.1 Alpha95 > 10

Four samples taken but no reliable magnetic measurements of the cores were obtained due to lighting and not used in this research. The place was very close to HF-T.

HL-2: Lower cap lava. Stage III.

Location: N64.40673° W20.54795° (64° 24.404 'N 20° 32.877'E)
850 m a.s.l.

D = 19.6 I = 73.6 Alpha95 = 5

Four samples used.

HL-3: Upper cap lava, breccia. Stage IV.

Location: N ° W ° (64° 24,761'N 20° 32.574'E)
1050 m a.s.l.

D = 357.2 I = 73.5 Alpha95 = 3.6

Eight samples.

HL-4: Pillow lava in the ravine above Hlöðuvellir (Hlöðuvallagil). Stage I.

Location: N ° W ° (64° 24.153'N 20° 32.931'E)
m a.s.l.

D = 0.0 I = 74.9 Alpha95 = 2

Four samples. After 20 mT demagnetization:

Sample	Decl.	Incl.
1	2.8	+75.5
2	355.2	+74.4
3	358.3	+74.5
4	4.1	+75.0

On average with Fisher statistic: declination = 0.0, inclination = +74.9 and alpha95 less than 2°.

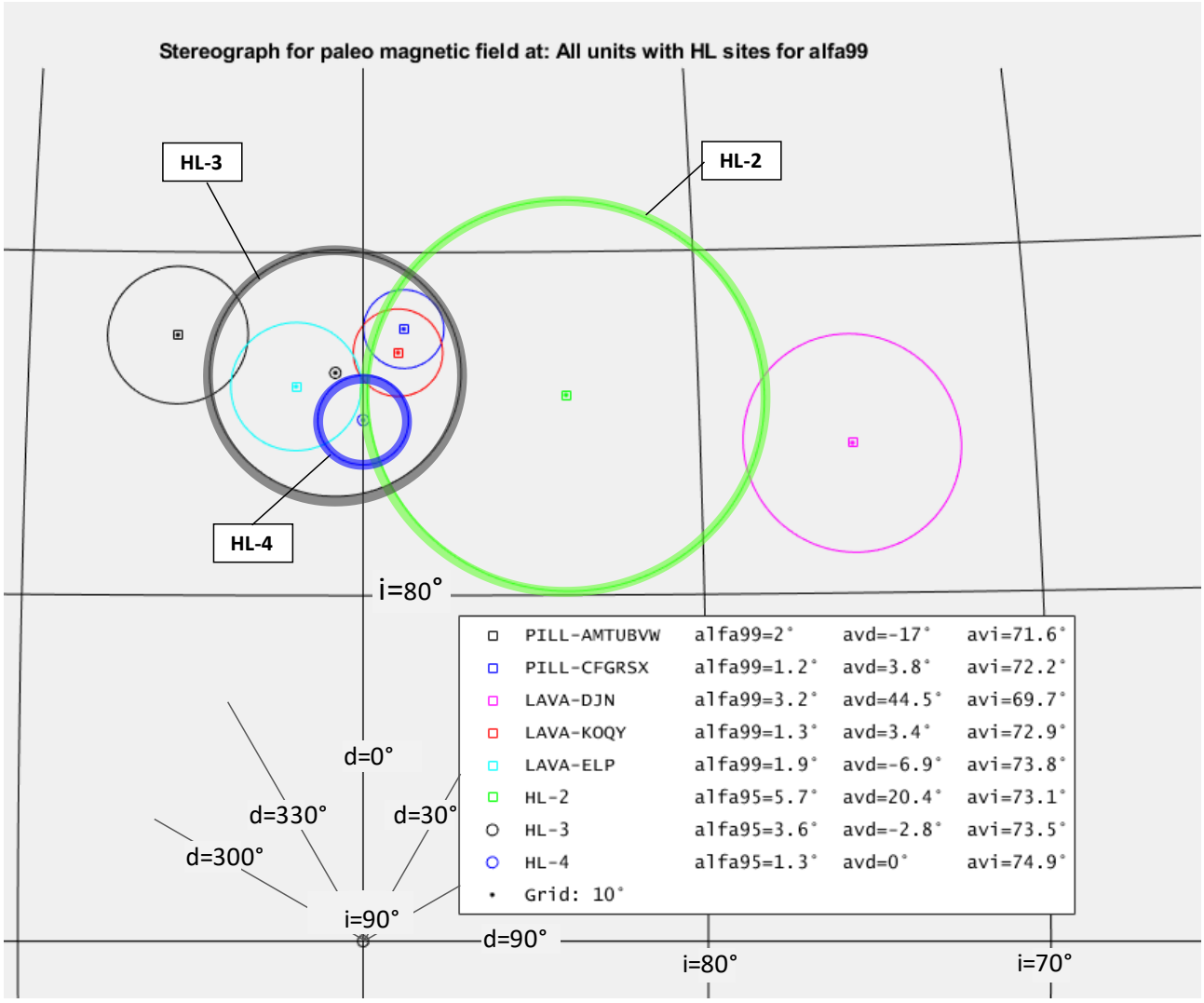

Paleomagnetic directions for HL samples from the research in year 2003 shown compared with average directions for all units recognized in this research.

Appendix D: Curie temperature

Curie temperature was measured for four samples in the paleomagnetic research room in Askja and the results is as is shown in the following table. The Curie temperature seem to be lower for the pillow lava samples (HF-C-09 and HF-A-05) than for the cap lava sample HF-J-06 and the sample HF-H-05 is from a dyke.

Sample	Description	Curie temperature
HF-C-09	Cube joint pillow lava, Stage I	93°C
HF-J-06	Cap lava, Stage III	125°C
HF-A-05	Pillow lava, Stage I	89°C
HF-H-05	Dyke	145°C

HF-C-09

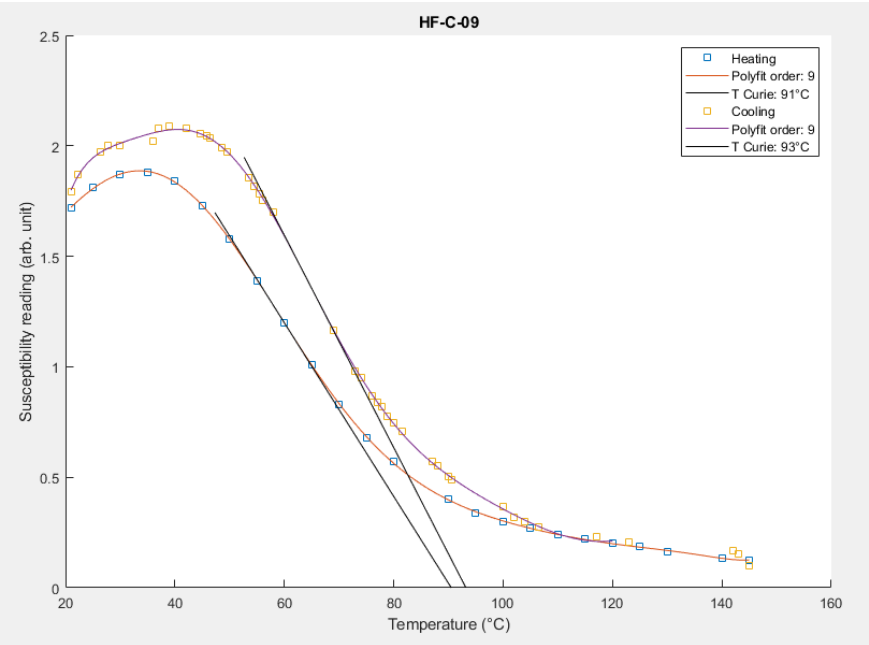


```
-----------------------------------------------------------------------------
DATAFILE: HF-C-09-warming.txt      for sample place: HF-C-09 / Heating
-----------------------------------------------------------------------------
     Legend on a graph                                    : Heating
     Curie temperature (intersection with x-axis)         : 90.52
     Curie temp. according to lowest measured susc        : 87.34
     Slope of tangent                                     : -0.039
     Intersection of tangent and polynomial               : 58.62
     Selected degree of best fitting polynomial           : 9
-----------------------------------------------------------------------------
Date of calculations: 21.02.2016   Time: 11:44

-----------------------------------------------------------------------------
DATAFILE: HF-C-09-cooling.txt      for sample place: HF-C-09 / Cooling
-----------------------------------------------------------------------------
     Legend on a graph                                    : Cooling
     Curie temperature (intersection with x-axis)         : 93.20
     Curie temp. according to lowest measured susc        : 91.12
     Slope of tangent                                     : -0.048
     Intersection of tangent and polynomial               : 64.31
     Selected degree of best fitting polynomial           : 9
-----------------------------------------------------------------------------
Date of calculations: 21.02.2016   Time: 11:45
```

HF-J-06

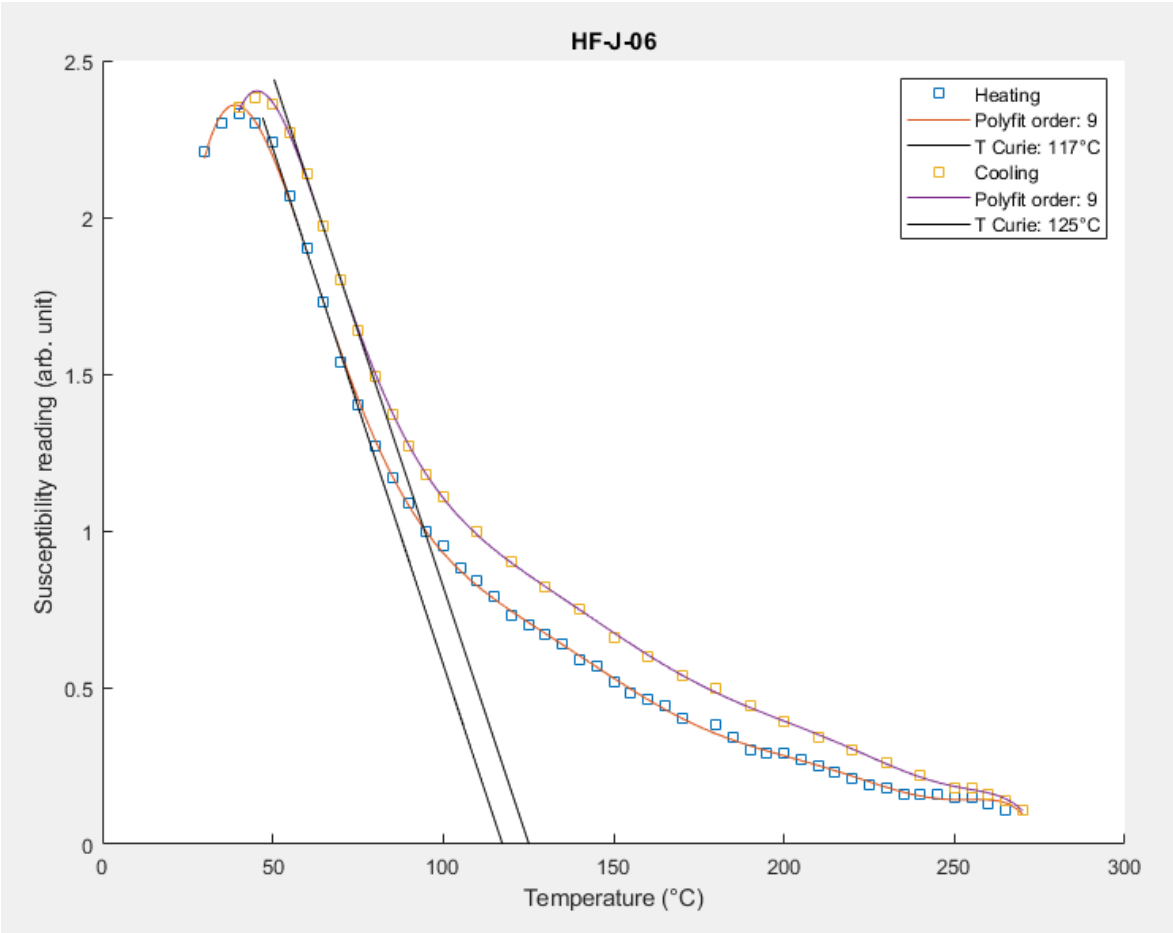


```
---------------------------------------------------------------------------
DATAFILE: HF-J-06-warming.txt      for sample place: HF-J-06 / Heating
---------------------------------------------------------------------------
     Legend on a graph                                  : Heating
     Curie temperature (intersection with x-axis)       : 117.40
     Curie temp. according to lowest measured susc      : 114.07
     Slope of tangent                                   : -0.033
     Intersection of tangent and polynomial             : 61.74
     Selected degree of best fitting polynomial         : 9
---------------------------------------------------------------------------
Date of calculations: 21.02.2016   Time: 11:49

---------------------------------------------------------------------------
DATAFILE: HF-J-06-cooling.txt      for sample place: HF-J-06 / Cooling
---------------------------------------------------------------------------
     Legend on a graph                                  : Cooling
     Curie temperature (intersection with x-axis)       : 125.17
     Curie temp. according to lowest measured susc      : 121.80
     Slope of tangent                                   : -0.033
     Intersection of tangent and polynomial             : 66.00
     Selected degree of best fitting polynomial         : 9
---------------------------------------------------------------------------
Date of calculations: 21.02.2016   Time: 11:49
```

HF-A-05

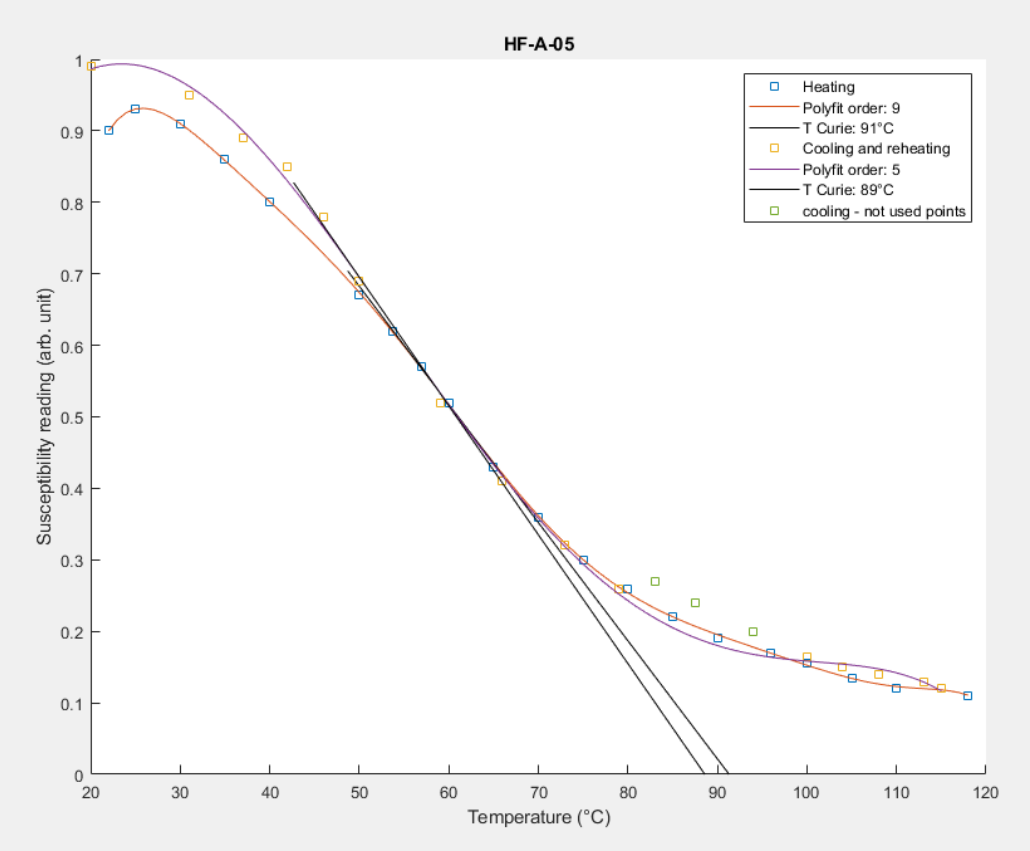


```
-----------------------------------------------------------------------------
DATAFILE: HF-A-05-warming.txt      for sample place: HF-A-05 / Heating
-----------------------------------------------------------------------------
     Legend on a graph                                    : Heating
     Curie temperature (intersection with x axis)         : 91.30
     Curie temp. according to lowest measured susc        : 84.65
     Slope of tangent                                     : -0.017
     Intersection of tangent and polynomial               : 60.11
     Selected degree of best fitting polynomial           : 9
-----------------------------------------------------------------------------
Date of calculations: 21.02.2016   Time: 12:44

-----------------------------------------------------------------------------
DATAFILE: HF-A-05-cooling-reheating-selection.txt      for sample place: HF-A-05 / Cooling
and reheating
-----------------------------------------------------------------------------
     Legend on a graph                                    : Cooling and reheating
     Curie temperature (intersection with x-axis)         : 88.59
     Curie temp. according to lowest measured susc        : 81.93
     Slope of tangent                                     : -0.018
     Intersection of tangent and polynomial               : 53.74
     Selected degree of best fitting polynomial           : 5
-----------------------------------------------------------------------------
Date of calculations: 21.02.2016   Time: 12:45
```

HF-H-05

Sample: HF-H-05				Date of measurement.: 18.02.2016 (hitun 3)
Tími	Afl	Hiti (°C)	Útslag	Athugasemdir
20:00	0	21.5	0.84	
	200	30.0	0.91	
		40.0	0.99	
		50.0	1.05	
		65.0	1.03	
		80.0	0.88	
		90.0	0.75	
		100.0	0.59	
		110.0	0.49	
		121.0	0.37	
		135.0	0.24	
		145.0	0.19	
		155.0	0.16	
		165.0	0.14	
		175.0	0.12	
		185.0	0.11	
		190.0	0.11	
		165.0	0.15	
		155.0	0.18	
		145.0	0.22	
		135.0	0.29	
		125.0	0.40	
		115.0	0.55	
		105.0	0.72	
		95.0	0.91	
		85.0	1.07	
		75.0	1.19	
20:05		26.0	1.00	Endurhitað 19.2 af Leó
	100	32.0	1.06	
		38.0	1.13	
		45.0	1.21	
20:10		53.0	1.22	
	0	60.0	1.23	
		65.0	1.22	

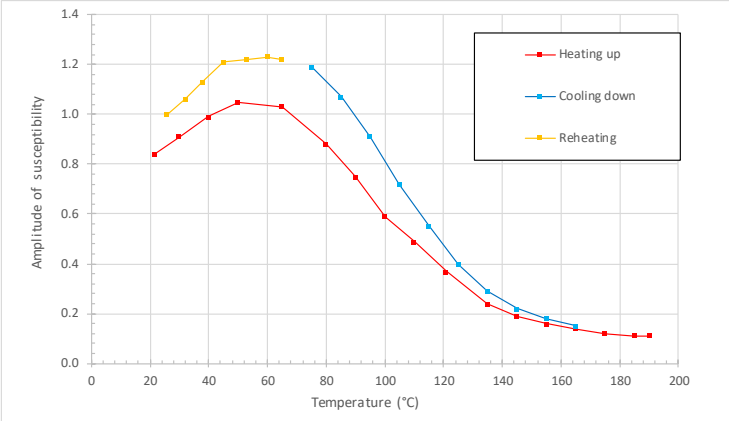

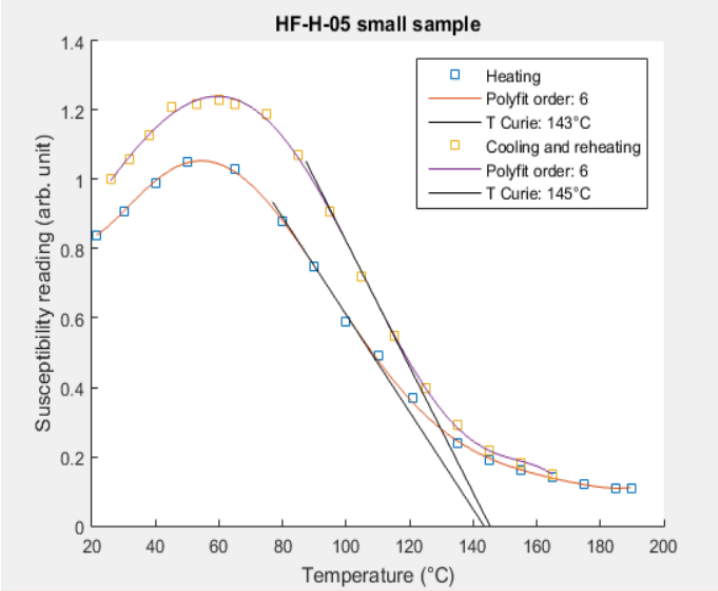


```
---------------------------------------------------------------------------
DATAFILE: HF-H-05-warming3.txt      for sample place: HF-H-05 small sample / Heating
---------------------------------------------------------------------------
     Legend on a graph                                  : Heating
     Curie temperature (intersection with x-axis)       : 143.39
     Curie temp. according to lowest measured susc      : 135.56
     Slope of tangent                                   : -0.014
     Intersection of tangent and polynomial             : 94.76
     Selected degree of best fitting polynomial         : 6
---------------------------------------------------------------------------
Date of calculations: 21.02.2016   Time: 12:25

---------------------------------------------------------------------------
DATAFILE: HF-H-05-cooling3-reheating.txt      for sample place: HF-H-05 small sample /
Cooling and reheating
---------------------------------------------------------------------------
     Legend on a graph                                  : Cooling and reheating
     Curie temperature (intersection with x-axis)       : 145.26
     Curie temp. according to lowest measured susc      : 137.01
     Slope of tangent                                   : -0.018
     Intersection of tangent and polynomial             : 105.47
     Selected degree of best fitting polynomial         : 6
---------------------------------------------------------------------------
Date of calculations: 21.02.2016   Time: 12:26
```

Appendix E: Estimate of volume of Hlöðufell

Estimate for volume of Hlöðufell **2.10.2016**

Height (km)	Area (km2)	Volume (km^3)
1.186	0.0	
1.1	1.0	0.04
1	2.3	0.17
0.9	4.0	0.32
0.8	5.0	0.45
0.7	6.2	0.56
0.6	7.9	0.71
0.5	12.4	1.02
	Total	**3.3**

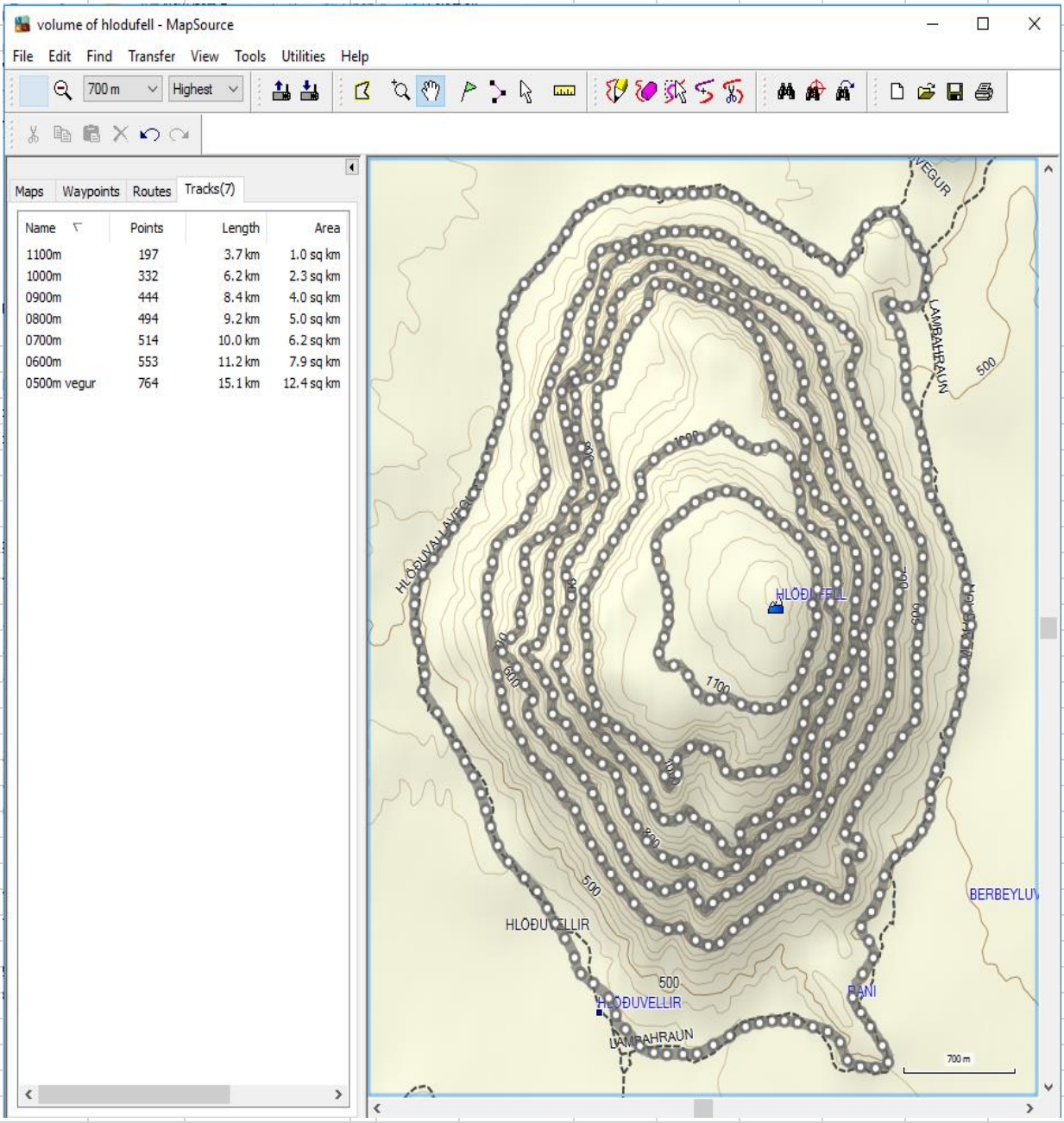

Appendix F: Direction of landforms in Hlöðufell area

Color	Name	Course
	Hlöðufell A	12° true
	Hlöðufell B	356° true
	Högnhöfði	30° true
	Kálfstindur	44° true
	Rauðafell	31° true
	Skefilfjöll	33° true
	Skriða	17° true
	Skriðutindar North part	31° true
	Skriðutindar South part	34° true
	Tindaskagi	34° true
	Þórólfsfell	7° true

Landforms in the area have some similarities in their elongate axes. On average for other mountains than Hlöðufell the direction is 29°, that is SSW-NNE, fitting to the general fissure swarm direction in the area. Standard deviation of the 9 axes is 10.8°.

The elongate axis direction of Hlöðufell is more difficult since the mountain is more circular than most other mountains in the area. Direction of the main elongate axis of Hlöðufell (dark yellow on the map), is -4° while there is another possible axis between the main vent on top of the mountain and a smaller vent in the south. That direction fits better with direction 12°.

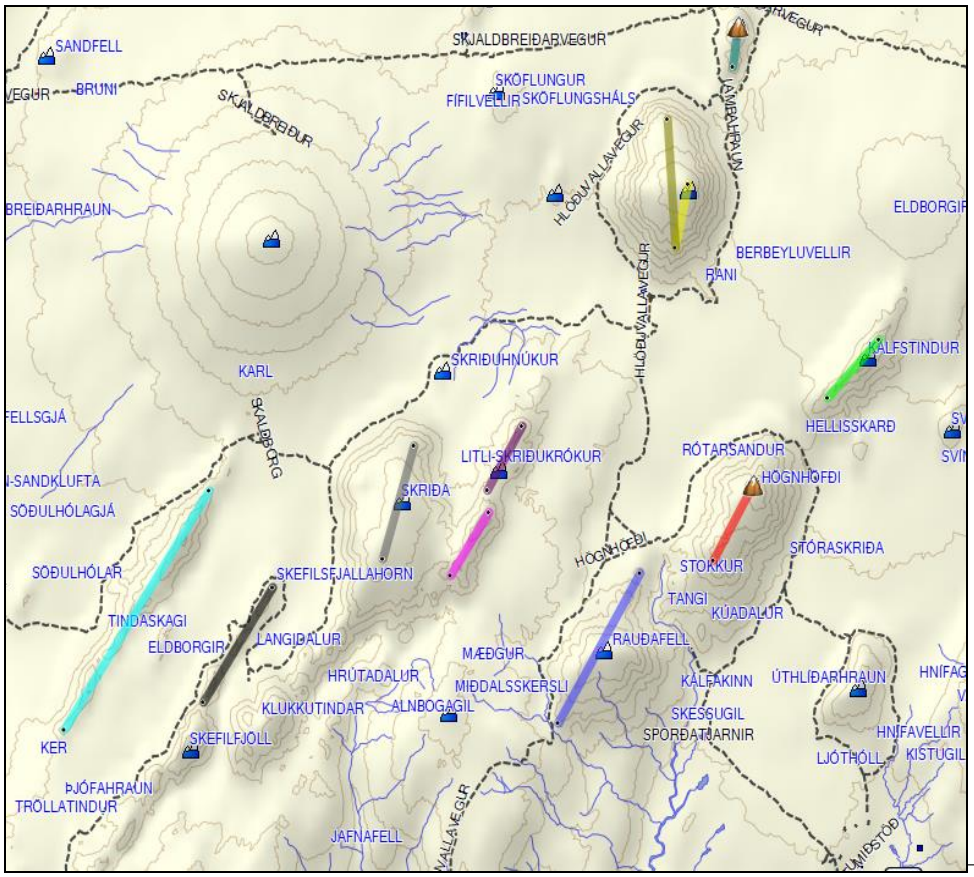

Map showing direction of landforms in Hlöðufell Area.

Appendix G: Glacial striae measured on top of Hlöðufell

Directions of glacial striae were measured when they were found in the field trips to the mountain, see table and map.

Note that most of the striae and all blue striae are pointing to top of the mountain and can then be represented as striae from a small glacier controlled by the form of Hlöðufell but was not formed by the Weichselian glacier.

Right hand side photo:
GPS 042 striae very clear in the evening sun.

Directions of glacial striae

Stria	Stage	Direction	Location	Date	Note
045	III	309°T	N64.43268 W20.55406	06-AUG-2016	907m asl (GPS)
TP1198	IV	313°T	N64.42377 W20.54612	06-AUG-2016	1106m asl (GPS)
016	IV	315°M	N64.42338 W20.54785	19-JUL-2016	1099m asl (GPS)
041	IV	268°T	N64.41919 W20.55198	27-JUL-2016	1092 m asl (GPS)
042	IV	243°T	N64.41684 W20.55462	27-JUL-2016	Very clear striae, see photo. 1079m asl (GPS)
015	IV	20°M	N64.41479 W20.54159	19-JUL-2016	1110 m asl (GPS)

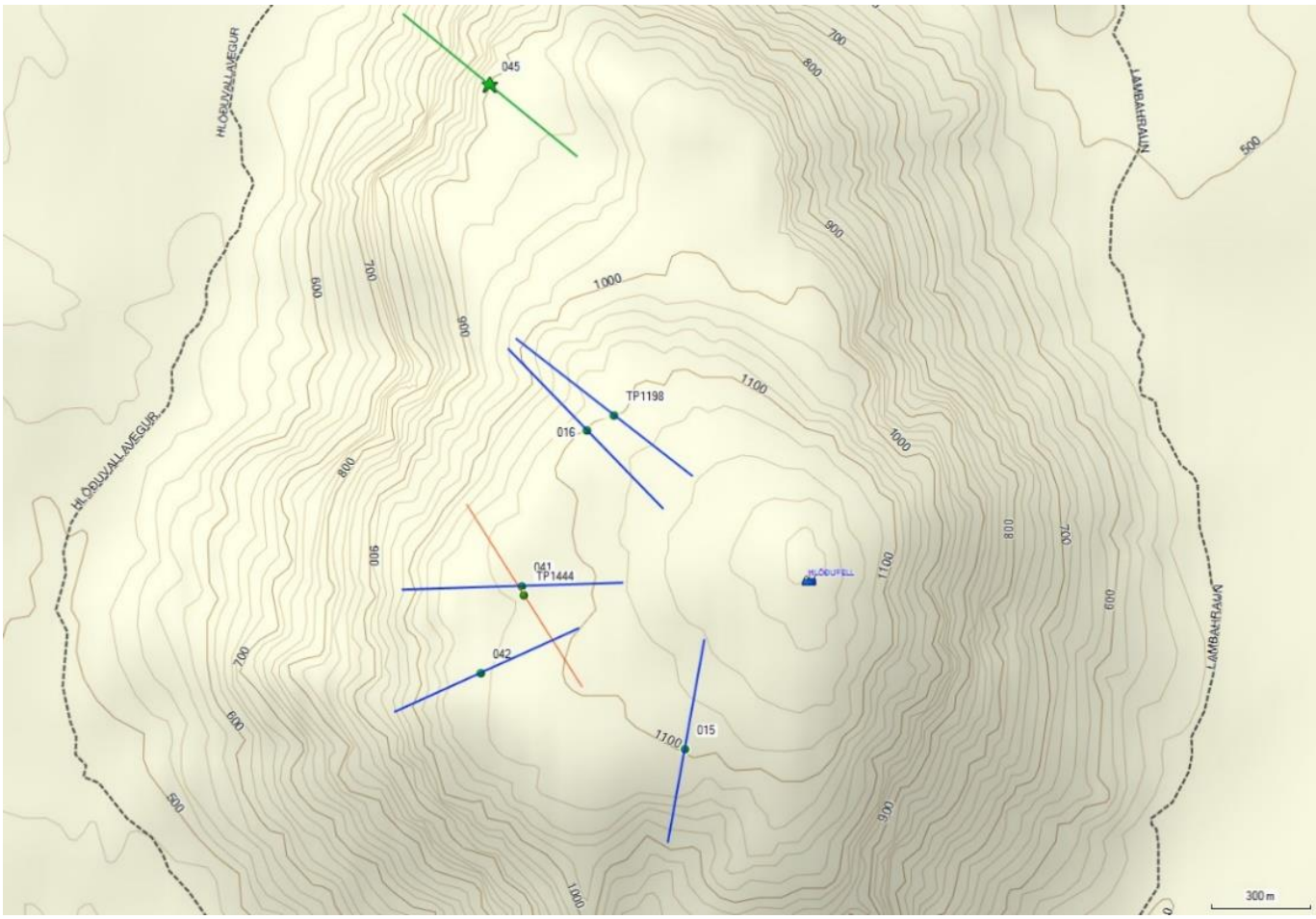

Map showing direction of glacial striae on pahoehoe lavas in Hlöðufell. Blue lines represents striae on top of Stage IV pahoehoe lava while the green line is the only stria found on the Stage III lava.

Appendix H: Field trips

This research was lasting for long time and quite many field trips where done to the area. Since the area is not so very far from Reykjavik, all the tours were relatively short and many of them just day-tours. Usually the plan was to take the opportunity when the weather was not so bad. Also, to mention here are the difficulties with the road to the area that is closed during winter and does usually not open until July.

It should be noted that the author broke his shoulder in end of July 2014 and was not able to do any proper fieldwork the following months and moreover, he broke his leg badly in January 2015 and was not able to do any field work until late summer 2015.

List of all field trips.

No	Description	Drilling of samples	Sampl. taken and oriented	Partici-pants	Date
01	General field exploration. Climbing the mountain but heavy fog above stage II. Driving around the mountain and shooting pictures.	HF-A	HF-A	ERS and GS	7-9 July 2014
02	Core sampling in Þórólfsfell and lower areas in Hlöðufell (Rani).	HF-B TF-A TF-B	HF-B TF-A TF-B	ERS, GS and HG	20 Sept. 2014
03	Core sampling. South part of Hlöðufell, Stage I, III and IV.	HF-C HF-D HF-E	HF-C HF-D HF-E	ERS and GS	29-30 August 2015
04	Core sampling. Pillow lava NW side of Hlöðufell and dykes.	HF-F HF-G HF-H	HF-F HF-G HF-H	ERS, GS and HG	13 Sept. 2015
05	Core sampling. Dyke in SW part of Hlöðufell. Problems with the drills that were appearing rather dull.	HF-I	HF-I	ERS and HB	18 Sept. 2015
06	Core sampling. South part of Hlöðufell, Stage III and IV. Fog in the area and not possible to orient the samples, so they were just drilled not taken away this time.	HF-J HF-K HF-L HF-Y	None	ERS and GS	25 Sept. 2015
07	Core sampling. Continued work from last trip. Cores from last trip oriented and taken. Snowy condition in the mountain, see photos below.	None	HF-J HF-K HF-L	ERS, GS and HG	10 Oct. 2015
08	Core sampling. The drill was not working properly, so only 2 cores.	HF-M	HF-M	ERS and GS	18 Oct 2015

Continued next page.

No	Description	Drilling of samples	Sampl. taken and oriented	Partici-pants	Date
09	Drilling in the south and northern parts of Hlöðufell in higher areas (Stage III and IV)	HF-N HF-K HF-O HF-P HF-Y	HF-N HF-K HF-O	ERS and GS	18-19 July 2016
10	Core sampling continued in north terrace, Stage III-IV.	HF-O HF-Q	HF-P HF-O HF-Q	ERS and GS	27 July 2016
11	Exploration of the higher areas of Hlöðufell. Walking more or less around the mountain on the edge. North bench explored better. Also, more exploration on my own of the lower areas to find new sites for core sampling.	None	None	ERS and GS	6 August 2016
12	Core sampling. Pillow lava various sites. HF-M continued from last year.	HF-R HF-S HF-T HF-M	HF-R HF-S HF-T HF-M	ERS	29 August 2016
13	Core sampling. Pillow lava various sites. Pillow ridge close to Hlöðuvellir, Rani area and east part of Hlöðufell. All in lower areas. Good progress in core sampling.	HF-T HF-U HF-V HF-W HF-X	HF-T HF-U HF-V HF-W HF-X	ERS	29-30 Sept. 2016
14	Core sampling and some exploration. Samples HF-Y that were drilled in some previous trips oriented and taken. Also, some more exploration of the south part of stage III/Stage IV	HF-M (addition)	HF-Y HF-M	ERS	15-16 Oct. 2016
15	A short photo tour to shoot some pictures that was assumed to be missing.	None	None	ERS	28 Oct. 2017

Participants did marvelous job in those field tours, especially in year 2015 when the author had broken his leg and was not able to carry any equipment up to the sampling sites.

GS: Gunnar Sigurðsson
HG: Haraldur Gunnarsson
HB: Höskuldur Björnsson

Melting of solidified dust from sample site HF-J while orienting and the snowy condition from sample site HF-L when the cores were oriented. Photos: Haraldur Gunnarsson.

See also more photos from field trips on next two pages.


© Einar Ragnar Sigurðsson 2015 / eirasi

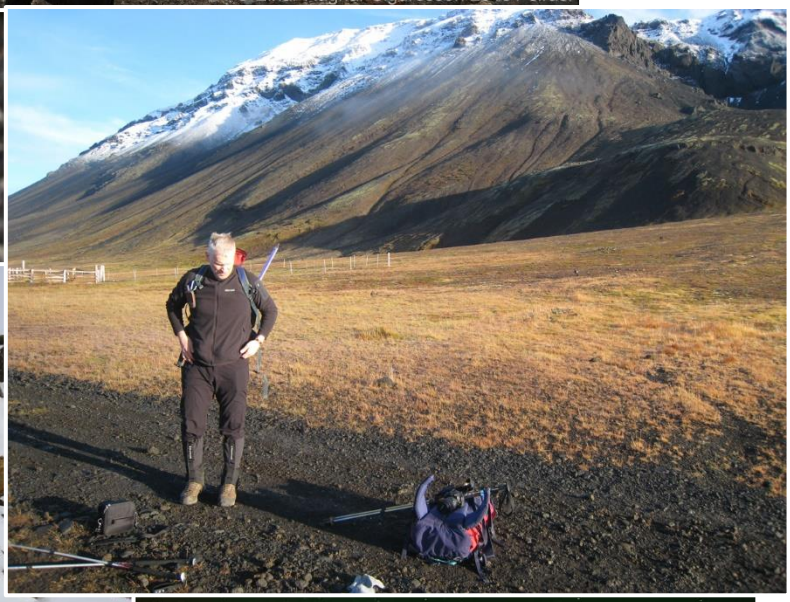

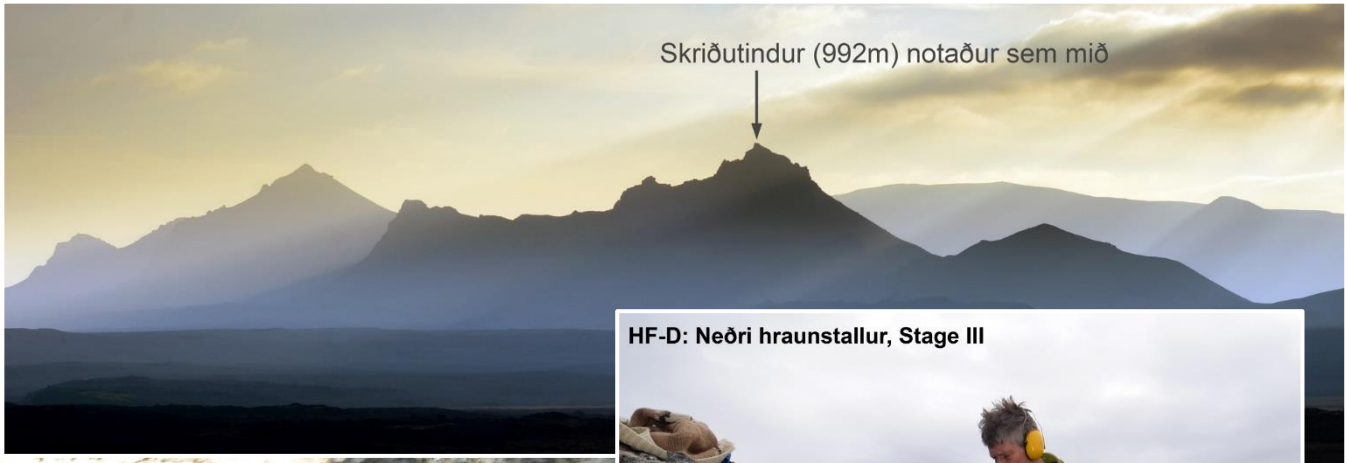
Skriðutindur (992m) notaður sem mið


HF-D: Neðri hraunstallur, Stage III

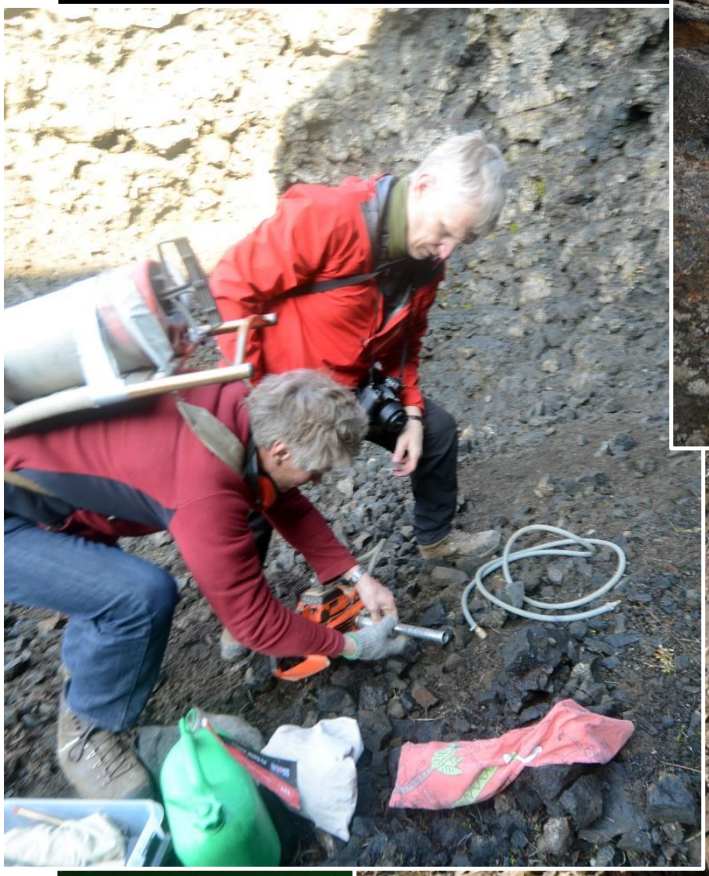

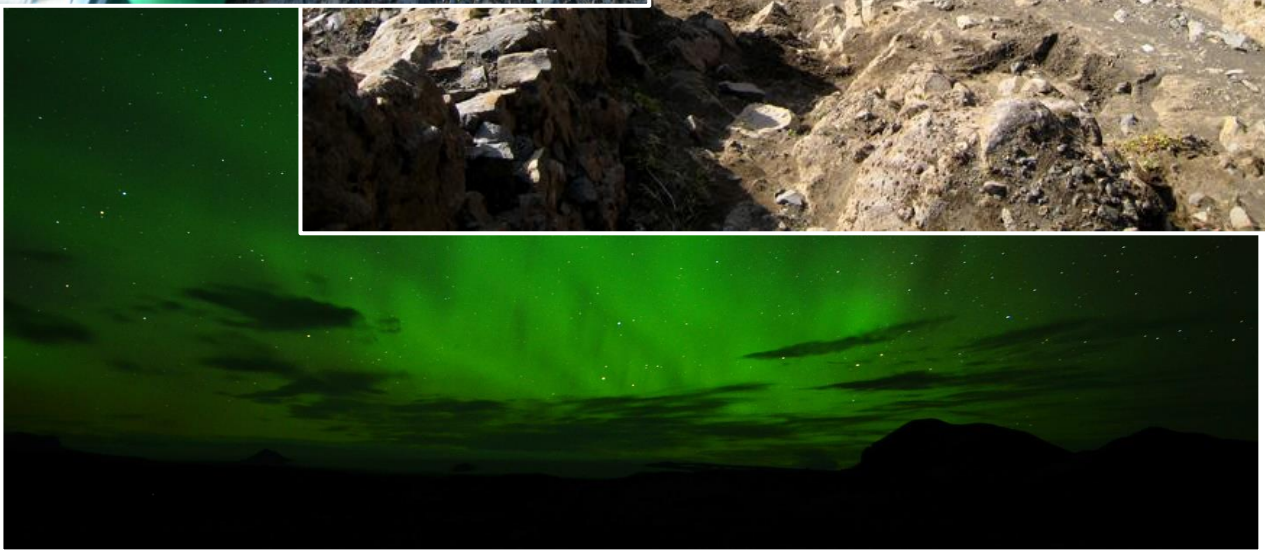

Appendix I: Terminology

In this research a system of terms is used to describe and refer to the paleomagnetic measurements carried out.

Sample: A sample core used in this research. Also referred to as "sample core". HF-A-01 is a sample number one from sampling site HF-A in the area Hlöðufell (HF). The part of a sample that is measured can also be referred to as a "*specimen*" or "*paleomagnetic specimen*".

Sampling site: A place where samples have been taken. HF-A is one sample site from Hlöðufell area. Paleomagnetic behavior of all samples from one sampling site should be the same. The sampling sites in this research are usually rather small representing just several meters or less area and they were defined in the field while drilling for the samples.

Unit: Part of the research area showing the same or similar paleomagnetic behavior. Each unit must seem to be geologically homogenious without any clear interfaces or boundaries. Units can also be referred to as "*geological units*".

Stage: One or more units in an area. The stages referred to in this research are from previous research made by Skilling (2009), dividing the formation of Hlöðufell into four stages that is: pillow lava as stage I, hyaloclastite formation as stage II, lower cap lava as Stage III and upper cap lava as Stage IV. Stages can also be referred to as "*stage formations*".

Area: Research area as Hlöðufell. Also referred to as "*research area*".

Appendix J: Sampling sites

See map for location of all sampling sites on page 44.

Sampling sites from Rani pillow ridge, Stage I

See location of all sampling sites in Rani on page 55.

HF-B

Sampling date (orientation):	20-09-2014	**Location:**	64.39941°N 20.5305°W
Description:	Pillow lava, all samples taken from the same pillow in a small area of the pillow. The samples are all from the outer surface of the pillow, undisrupted surface, that have most likely cooled very fast with direct contact to water. The samples are rather porous, color is dark and seem to be cryptocrystalline. The outer surface of the pillow was almost glassy.		

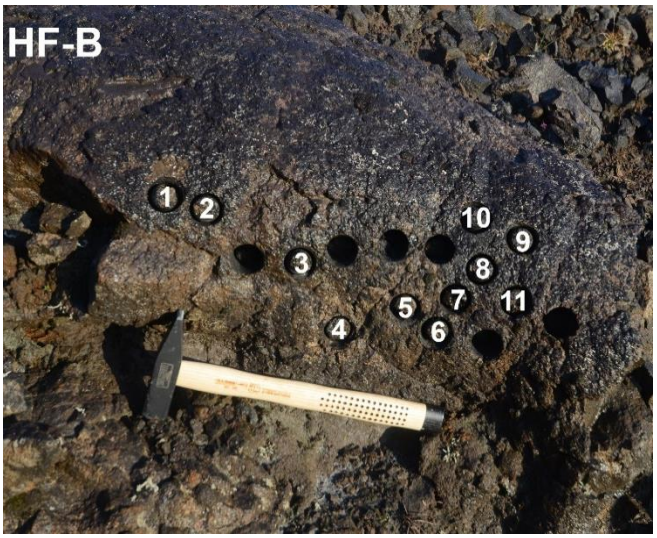

HF-V

Sampling date (orientation):	30.9.2016	**Location:**	64.39875°N 20.5277°W

Description:	The sampling site is a pillow lava outcrop Rani. The pillows were partly eroded, and the samples are from the interior of the pillows. The outcrop was partly a breccia but still some pillows possible to take samples from that looked undisrupted and not faulted. The pillows were small and not very good for sampling but however, some good samples were taken. The samples were porous and fine-grained with very few small crystal minerals not up to 1 mm, see photos.

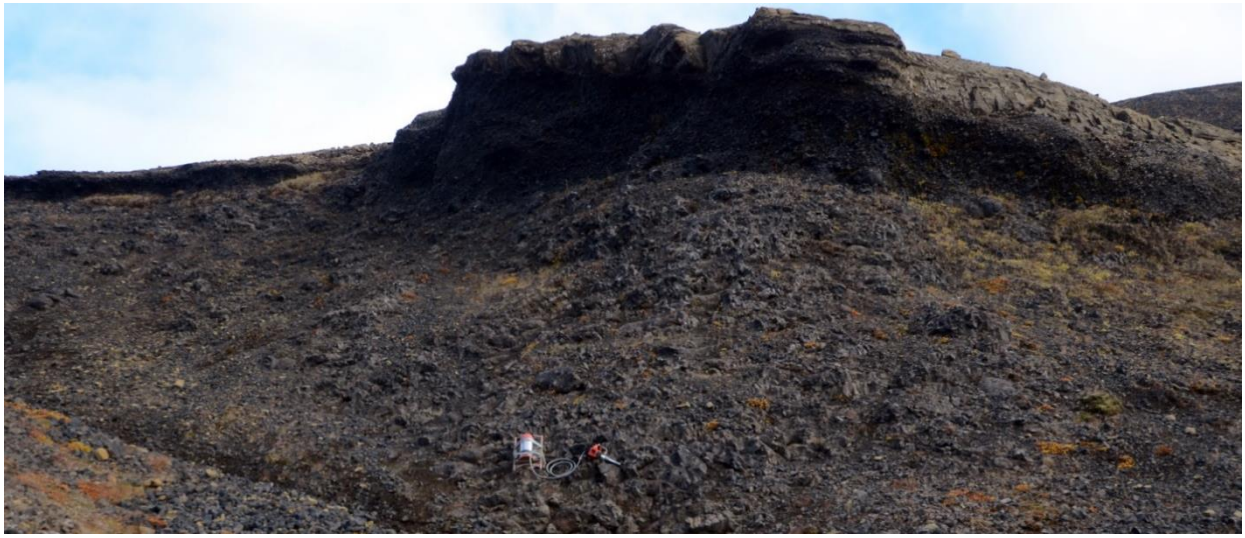

HF-W

Sampling date (orientation):	30.9.2016	**Location:**	64.39687°N 20.5195°W
Description:	The sampling site is a pillow lava outcrop from the end of Rani ridge. The pillows were partly eroded, and the samples are from the interior of the pillows. The outcrop was partly a breccia but still some pillows possible to take samples from that looked undisrupted and not faulted. The pillows were small and not very good for sampling but however, some good samples were taken. The samples were porous and fine-grained with few small crystal minerals. The hand samples taken were partly glassy.		

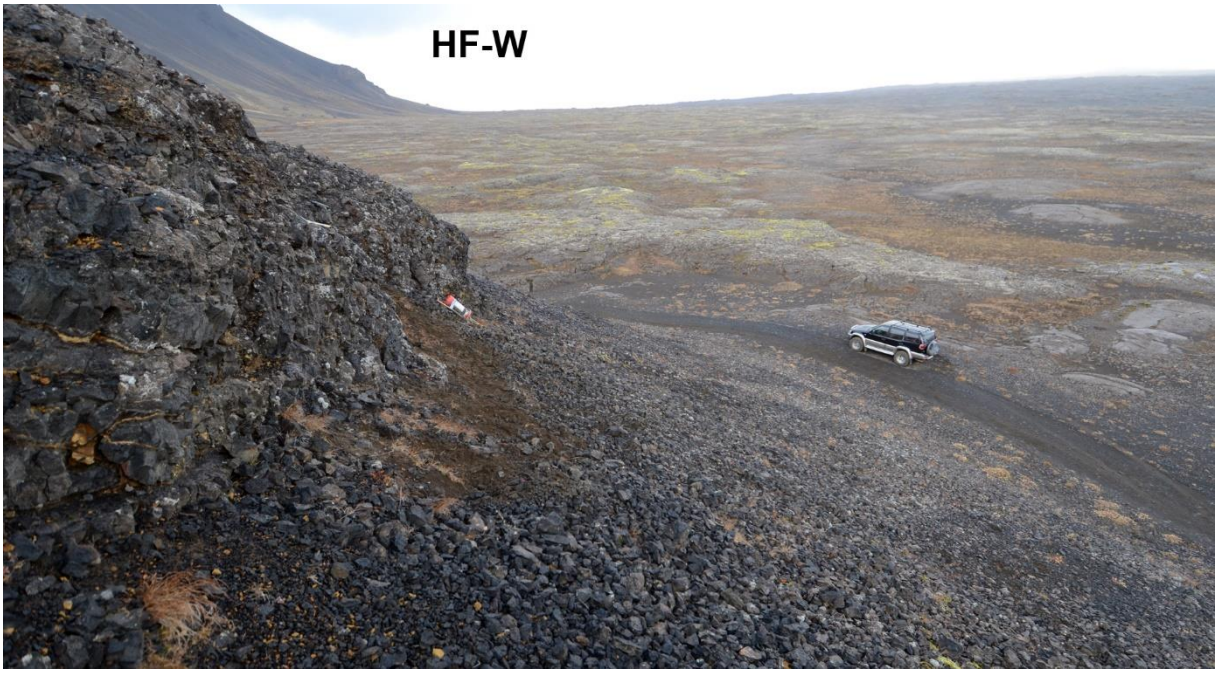

Sampling sites from pillow ridge at Hlöðuvallagil, Stage I

HF-A

Sampling date (orientation):	8.7.2014	**Location:**	64.40115°N 20.5505°W
Description:	The sampling site is a pillow lava outcrop in the pillow lava ridge at Hlöðuvellir. The pillows were partly eroded. The outcrop was partly a breccia but still some pillows possible to take samples from that looked undisrupted and not faulted. Conditions for sampling were not good and all samples were from the same pillow. The samples were slightly porous, fine-grained with large amount of white and olivine green crystal minerals up to 2 mm, see photos. The hand samples taken were partly glassy.		

HF-M

Sampling date (orientation):	18.10.2015 to 16.10.2016	**Location:**	64.4013°N 20.5488°W
Description:	The sampling site is a pillow lava outcrop in the pillow lava ridge at Hlöðuvellir. The pillows were partly eroded. The outcrop was in a breccia but still one pillows possible to take samples from that looked undisrupted and not faulted. Conditions for sampling were not good and all samples were from the same pillow. The samples were slightly porous, fine-grained with large amount of white and olivine green crystal minerals up to 2 mm. There were problems with the drills in year 2015 so only taking 2 samples at that time. Sampling finished in two attempts in year 2016.		

HF-T

Sampling date (orientation):	29.9.2016	**Location:**	64.4013°N 20.55296°W

Description:

The sampling site is an outcrop from the end of the pillow lava ridge at Hlöðuvellir. It was not clear pillow formation but still it looked more like a pillow lava than a normal subaerial lava flow.

Conditions for sampling were moderate and possible to distribute the samples somewhat over an area spanning couple of meters.

The samples were slightly porous, fine-grained with large amount of white and olivine green crystal minerals up to 2 mm. Some of the hand samples taken did not have many crystals.

Also, should be noted that the sampling site HF-T is close to HL-1 sampling site (Leo Kristjansson an Magnus Tumi Gudmundsson) year 2003 from where no magnetic results were obtained due to lightning problems.

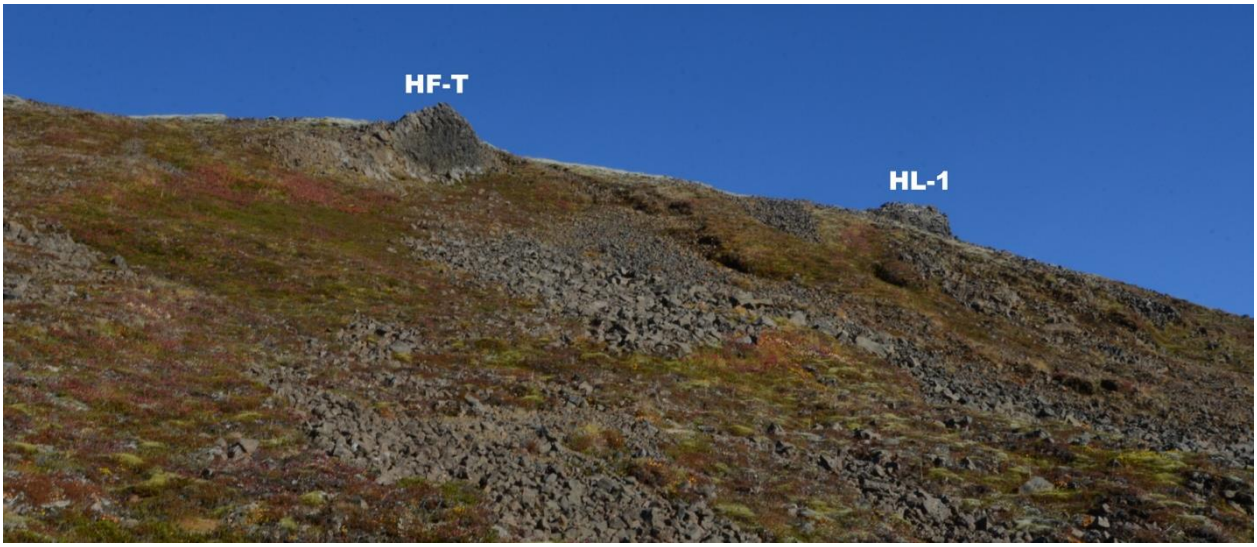

HF-U

Sampling date (orientation):	29.9.2016 and 16.10.2016	**Location:**	64.40201°N 20.54929°W
Description:	The sampling site is a pillow lava outcrop in the pillow lava ridge at Hlöðuvellir. This sampling site is close to the main mountain and it is facing the ravine at Hlöðuvellir, called Hlöðuvallagil. The pillows were only slightly eroded. Conditions for sampling were relatively good and it was possible to distribute the samples something over an area spanning several meters, see the photos. The samples were slightly porous, fine-grained with large amount of white and olivine green crystal minerals up to 2 mm.		

Sampling sites from pillow lava in the main mountain, Stage I

HF-C

Sampling date (orientation):	29.8.2015	**Location:**	64.4033°N 20.54896°W
Description:	The sampling site is from a cube-joint lava above the pillow ridge at Hlöðuvellir in Hlöðuvallagil. Although the sampling site is close to the pillow ridge at Hlöðuvellir, it seems to be more connected to the main mountain. It seemed possible that the formation was continuing at the other side of the Hlöðuvallagil, see white dotted line in the photo below. Due to steep slope of the mountain at this place, it was only possible to take samples from rather small area in the formation. The samples were almost non-porous, fine-grained with some amount of white and olivine green crystal minerals up to 1 mm in diameter.		

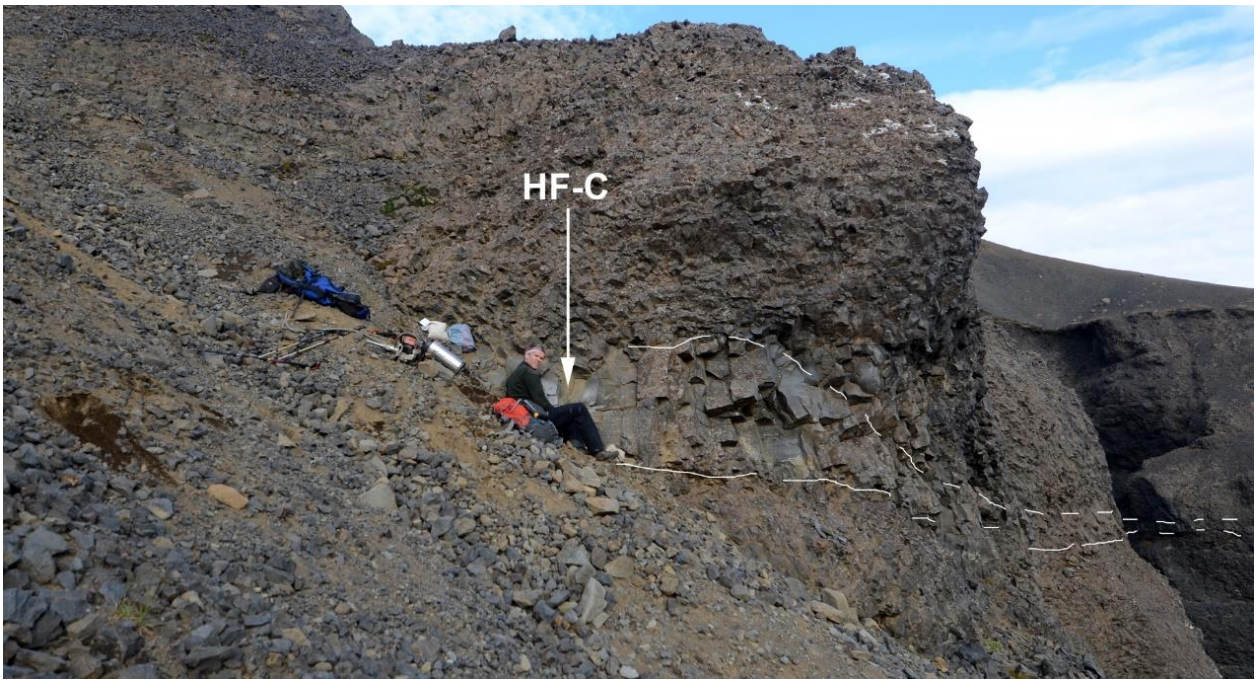

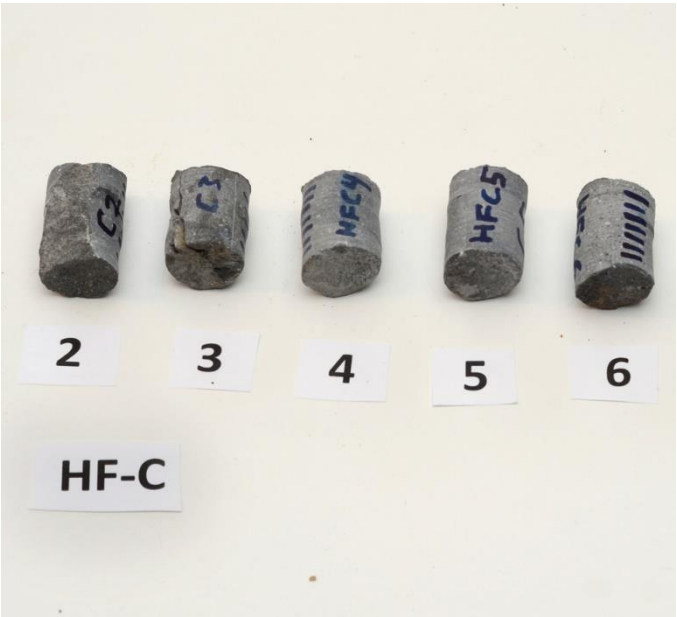

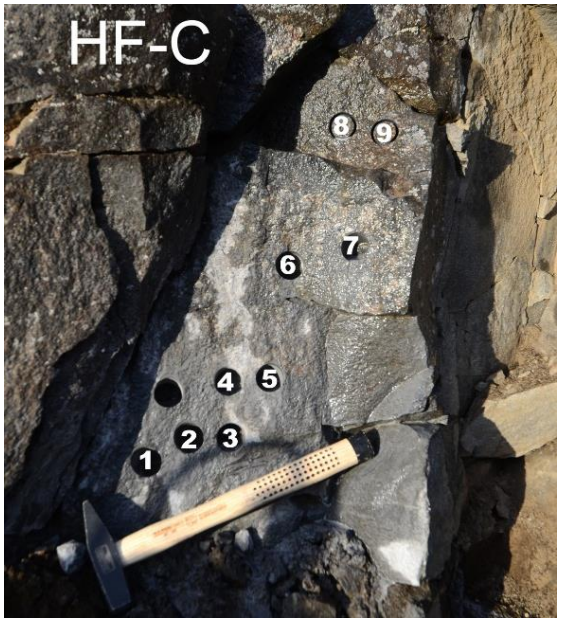

HF-FG

Sampling date (orientation):	13.09.2015	**Location:**	64.43795°N 20.55031°W
Description:	Sampling sites HF-F and HF-G are from the same remarkable formation which Skilling (2009) has described as formation solidifying around ice cubes. The samples were taken from the outer surface of two pillows, one pillow for each of the two sampling sites and since they are very close to each other they have been taken in this research as one sampling site. Distance between them is around 6 meters. The samples were only slightly porous, fine-grained with some amount of white and olivine green crystal minerals up to 1 mm in diameter.		

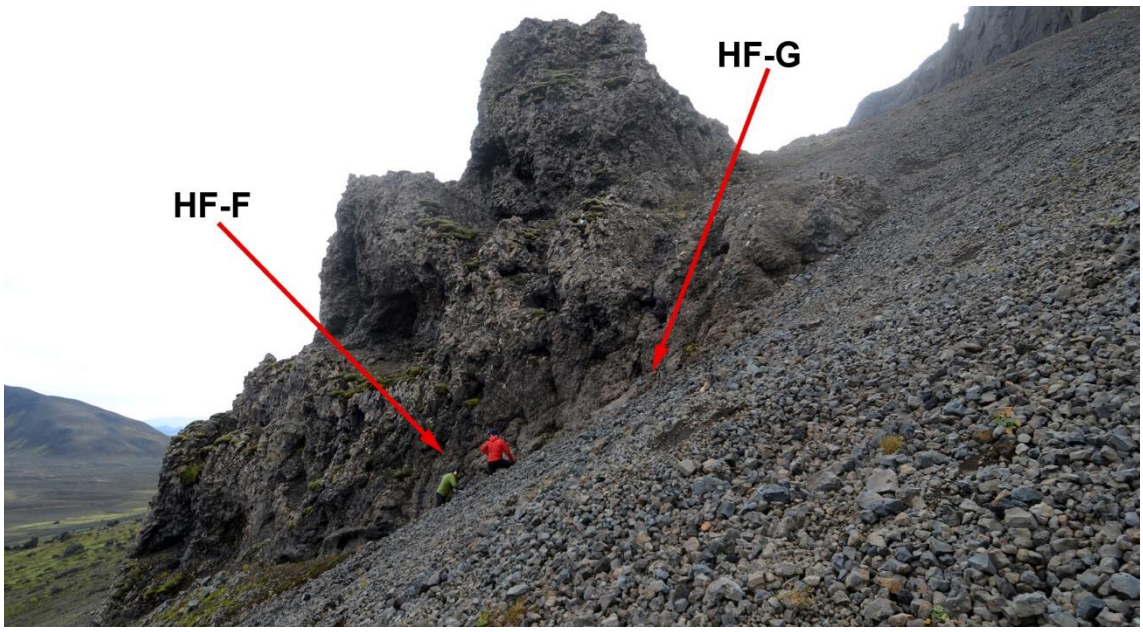

HF-R

Sampling date (orientation):	29.8.2016	**Location:**	64.43781°N 20.55889°W

Description:	The sampling site is a pillow like lava outcrop in the north-west part of Hlöðufell, main mountain. The rocks were somewhat eroded, and it was not possible to recognize regular pillows, but the formation was described as pillow like. The outcrop was rather well accessible with possibilities to take samples in a relatively wide area. The distance from sample HF-R-01 to HF-R-9 is close to 20 meters. Some of the samples were porous and some only slightly porous. They were fine-grained with some amount of white and olivine green crystal minerals up to 1 mm.

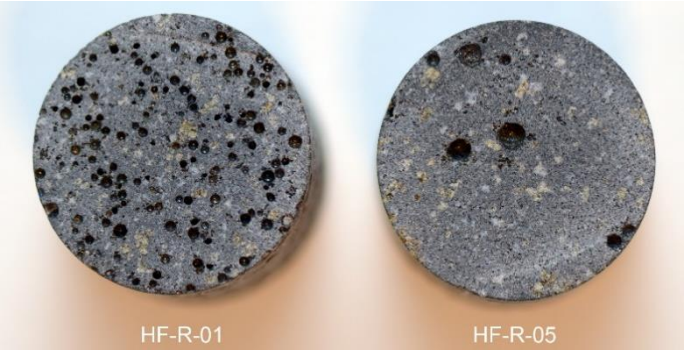

HF-S

Sampling date (orientation):	29.8.2016	**Location:**	64.40409°N 20.55708°W

Description:

The sampling site is a pillow like lava outcrop in the south-west part of Hlöðufell, main mountain. The rocks were somewhat eroded, and it was possible to recognize some regular pillows, and overall, the formation was described as pillow like.

The outcrop was rather well accessible with possibilities to take samples in a relatively wide area. The sampling area spanned more than 5 meters.

Few of the samples were porous and some only slightly porous. They were fine-grained with some amount of white and olivine green crystal minerals up to 1 mm. However, the amount of visible crystal minerals were less in this sampling site than most of the other pillow lava sampling sites.

HF-X

Sampling date (orientation):	30.9.2016	**Location:**	64.40567°N 20.52242°W
Description:	The sampling site is a pillow lava complex outcrop in a gully in the east part of Hlöðufell, main mountain. The pillows were very much eroded, but the samples were taken from undisrupted and not faulted pillows. The outcrop was small, but rather well accessible with possibilities to take samples a relatively wide area, see the photo below. The samples were taken late in evening in not very good weather conditions, so some inaccuracy might stem from that. The samples were slightly porous. They were fine-grained with average amount of white and olivine green crystal minerals up to 1 mm, mostly white.		

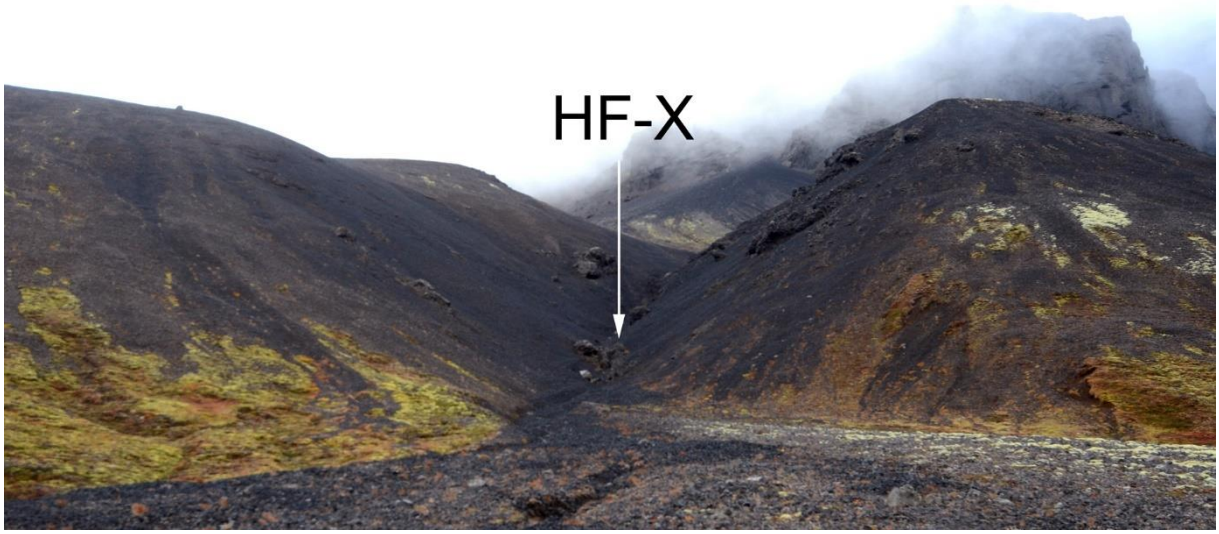

Sampling sites from lower cap lava, Stage III

HF-N

Sampling date (orientation):	18.07.2016	**Location:**	64.40644°N 20.54791°W
Elevation:	Measured elevation from GPS: 839. Elevation reading from a map (1:50.000) is just below 800 m and could be 795 m from that reading.		
Description:	The lowest sampling site from cap lava, unit III, lower lava bench. The sampling site is in the south part of the unit, about 30 meters east of the steep walking path to the summit of the mountain, west of the Hlöðuvallagil. The sampling site HF-N is the lowest sampling site taken in Stage III cap lava, just above the passage zone and the flow-foot breccia. The samples were taken from an area several meters wide, see photos below. The samples were very porous with large pores. They were fine-grained with average amount of white and olivine green crystal minerals up to 1 mm, more of them where white than olivine green.		

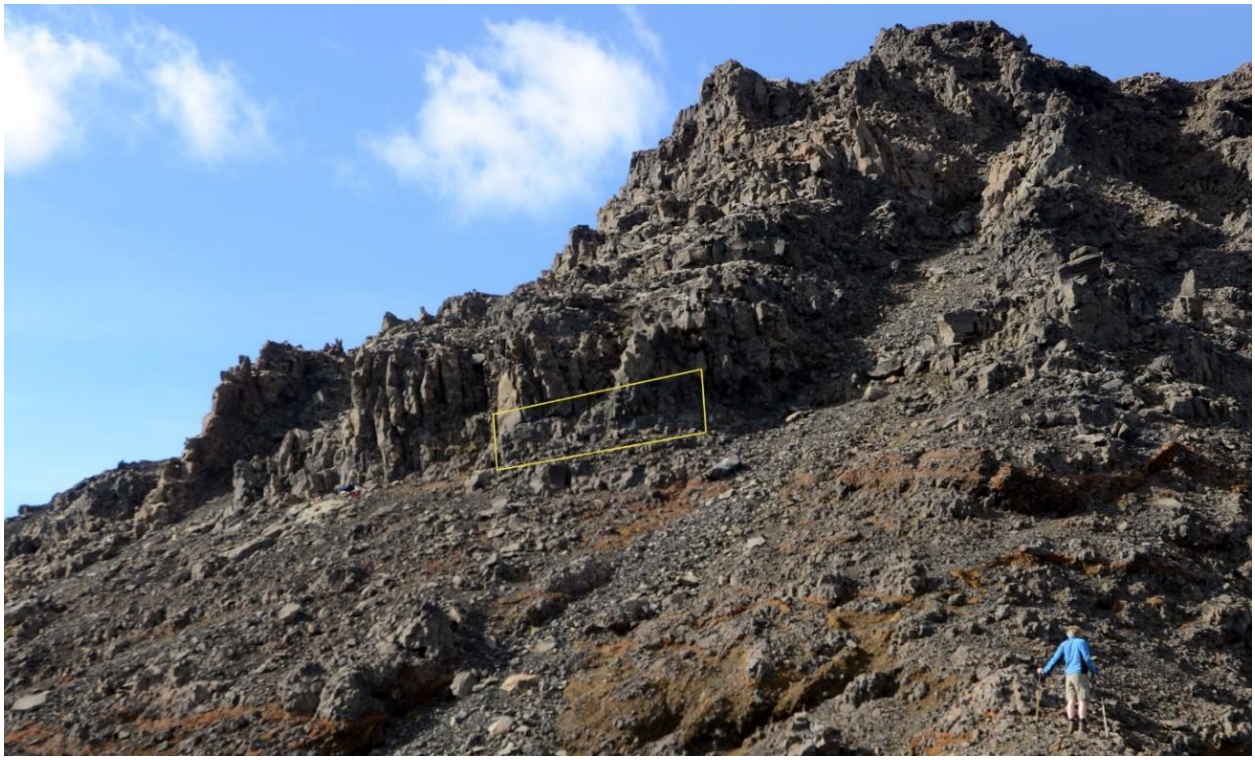

HF-J

Sampling date (orientation):	10-10-2015	**Location:**	64.40662°N 20.54813°W
Elevation:	Measured elevation from GPS: 857. Elevation reading from a map (1:50.000) is 800 m. This sampling site is for sure higher than HF-N but is in similar elevation as HF-D. From GPS reading this site is 8 m higher than HF-D but from the map reading, this site is 10 m lower than HF-D.		
Description:	Sampling site from cap lava, unit III, lower lava bench. The sampling site is in the south part of the unit, about 20 meters east of the steep walking path to the summit of the mountain, west of the Hlöðuvallagil. As seen in the photo, all samples are from very small area, about 1 m^2. The samples were almost non-porous. They were fine-grained with average amount of white and olivine green crystal minerals up to 1 mm. This is one of the last sampling sites from year 2015.The drilling was done in foggy weather in September and when orienting two weeks later we had difficult conditions in frost and snow. For orienting the sun was used for all samples since there was no view to nearby mountains.		

HF-D

Sampling date (orientation):	30.8.2015	**Location:**	64.40654°N 20.54755°W
Elevation:	Measured elevation from GPS: 849. Elevation reading from a map (1:50.000) is 810 m. This sampling site is for sure higher than HF-N but is in similar elevation as HF-J. From GPS reading this site is 10 m lower than HF-J but from the map reading, this site is 10 m higher than HF-J.		
Description:	Sampling site from cap lava, unit III, lower lava bench. The site is in the south part of the unit, about 50 meters east of the walking path to the summit of the mountain, west of the Hlöðuvallagil. As seen in the photo, all samples are from very small area, less than 0.5 m^2. The samples were very porous with large pores. They were fine-grained with some amount of white and olivine green crystal minerals up to 1 mm, more of them where white than olivine green.		

HF-Y

Sampling date (orientation):	15.10.2016	**Location:**	64.40719 °N 20.54816 °W
Elevation:	Measured elevation from GPS: 879. Elevation reading from a map (1:50.000) is 839 m. This sampling site is for sure higher than HF-D and HF-J.		
Description:	Sampling site from cap lava, unit III, lower lava bench. The site is in the south part of the unit, almost on the walking path to the summit of the mountain, west of the Hlöðuvallagil. This part of the cliffs in unit III was easily accessible since it is so close to the walking path. Drilling was done in several field trips, but orienting was done in the last one. Leo Kristjansson took samples in the same place in year 2003. The samples were distributed as much as possible over several meters area, see photo below. Samples were taken where the blue Pomeroy orienting tool is, and samples were also taken where the red helmet is lower down. The samples were rather porous. They were fine-grained with average amount of white and olivine green crystal minerals up to 1 mm, more of them where white than olivine green.		

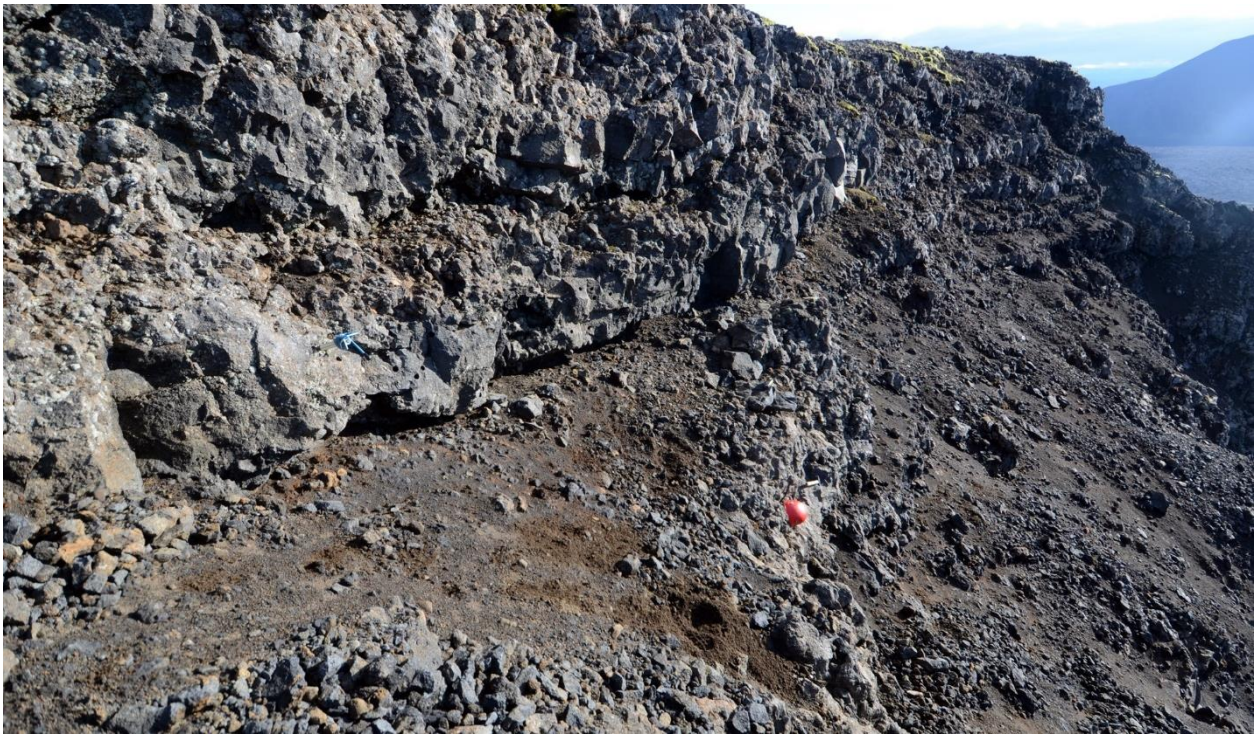

Middle cap lava

HF-K

Sampling date (orientation):	10.10.2015 and 18.7.2016	**Location:**	64.4095 °N 20.54482 °W
Elevation:	Measured elevation from GPS: 910 m. Elevation reading from a map (1:50.000) is 905 m.		
Description:	The sampling site HF-K is in the south part of Hlöðufell, above the lower cap lava in unit III but below the flow-foot breccia in unit IV. However, no flow foot-breccia was noticed between the sampling site HF-K and the lower lava bench, represented by the next sampling site, HF-Y, see Figure 6-10. Flow-foot breccia between HF-K and the lower lava cap could be covered by talus. The samples were partly well distributed over several meters area on the site, see the photos below.		

HF-O

Sampling date (orientation):	18.7.2016 and 27.7.2016	**Location:**	64.43087 °N 20.54511 °W
Elevation:	Measured elevation from GPS: 982 m. Elevation reading from a map (1:50.000) is 965 m.		
Description:	The sampling site HF-O is in the north part of Hlöðufell, above the lower cap lava in unit III but below the flow-foot breccia in unit IV. However, no flow foot-breccia was noticed between the sampling site HF-O and the lower lava bench. Flow-foot breccia between HF-O and the lower lava cap could be covered by talus, see Figure 5-1. Numerous samples were distributed over a large 50 m wide area.		

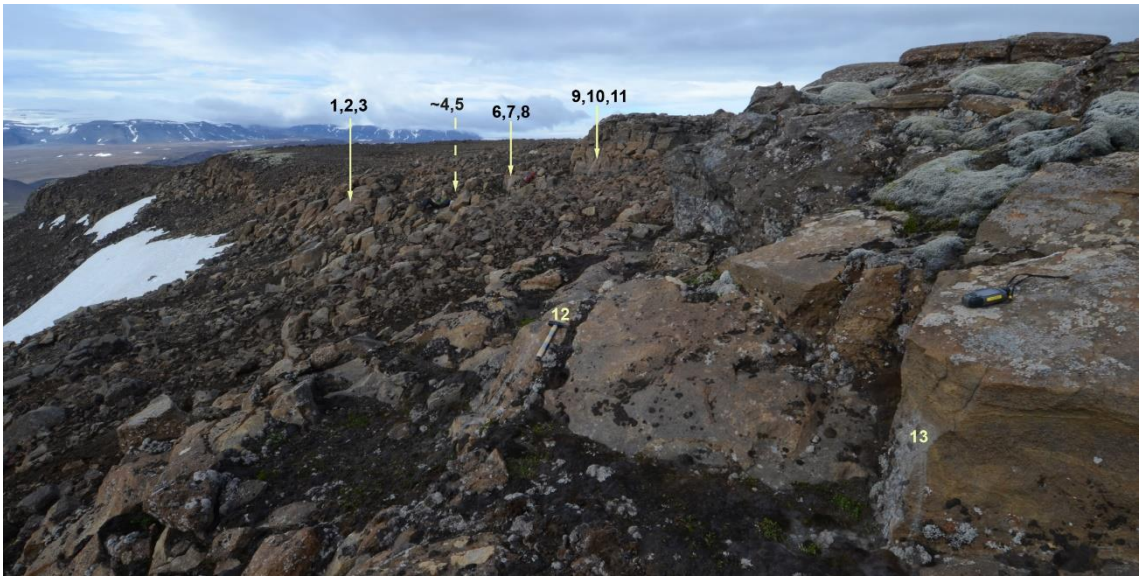

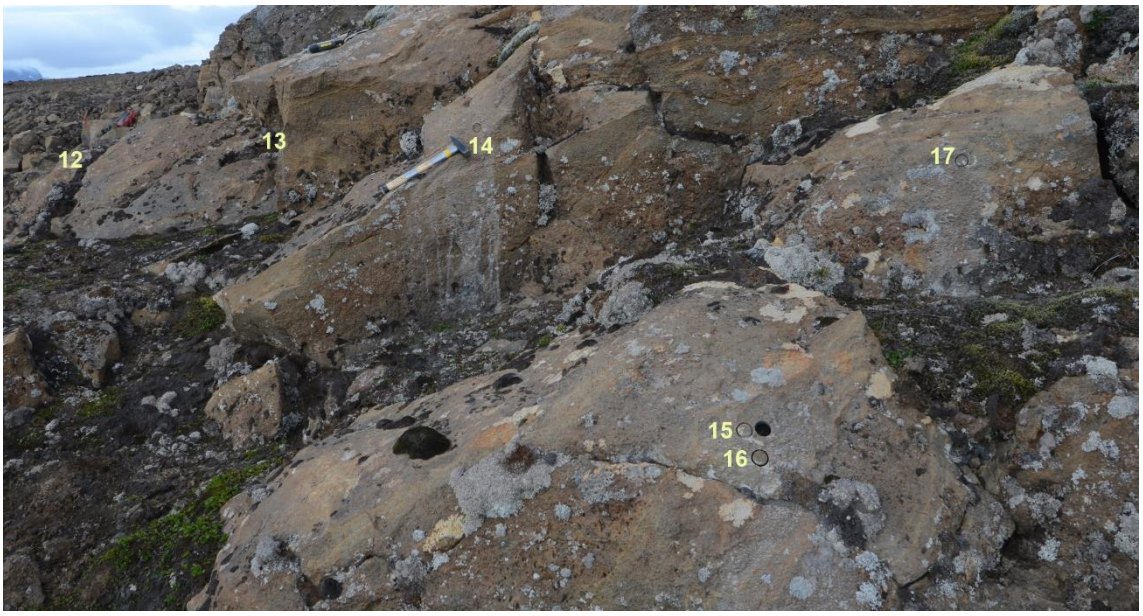

HF-Q

Sampling date (orientation):	27.07.2016	**Location:**	64.42965 °N 20.5427 °W
Elevation:	Measured elevation from GPS: 992 m. Elevation reading from a map (1:50.000) is 990 m.		
Description:	The sampling site HF-Q is in the north part of Hlöðufell, from a small lava bench above the more prominent lava bench where HF-O was taken. No flow foot-breccia was noticed between the sampling site HF-Q and the lava bench where HF-O. It is assumed very unlikely that a flow-foot breccia could exist there, covered by talus. Surroundings is shown in the figures below. The outcrop was rather small, so it was not possible to distribute the samples over a large area, see photo below.		

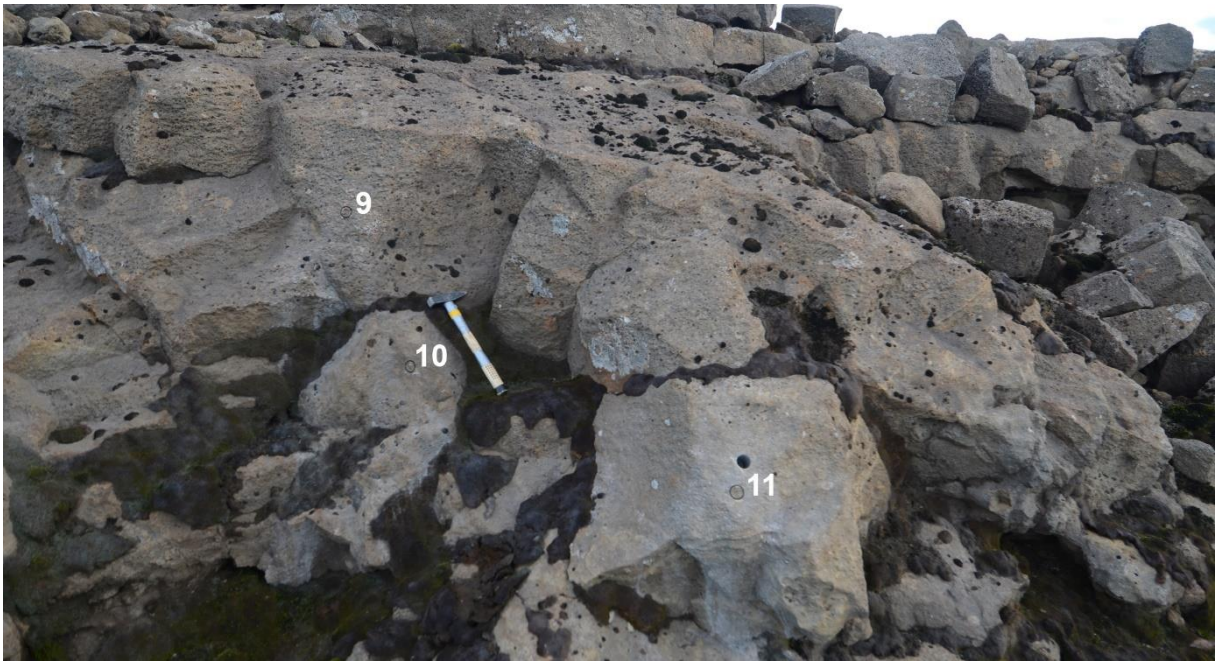

Upper cap lava, Stage IV

HF-E

Sampling date (orientation):	30.08.2015	**Location:**	64.42490°N 20.54816°W
Elevation:	Measured elevation from GPS: 1013 m. Elevation reading from a map (1:50.000) is 1005 m.		
Description:	The sampling site from south part of the upper cap lava, Unit IV, north part of it, not far from one of the walking paths to the summit. This was one of the first sampling sites in the project and unfortunately the samples were not distributed as they should have been, se photo below.		

HF-P

Sampling date (orientation):	19.07.2016	**Location:**	64.4249°N 20.54816°W
Elevation:	Measured elevation from GPS: 1081 m. Elevation reading from a map (1:50.000) is 1080 m.		
Description:	The sampling site from north part of the upper cap lava, Stage IV. The sampling site is on the edge of the cap lava. Below it is a talus that could be hiding the flow-foot breccia that is visible on the west side of the mountain in similar altitude. The samples were distributed somewhat but not very much, as is shown in the photos below.		

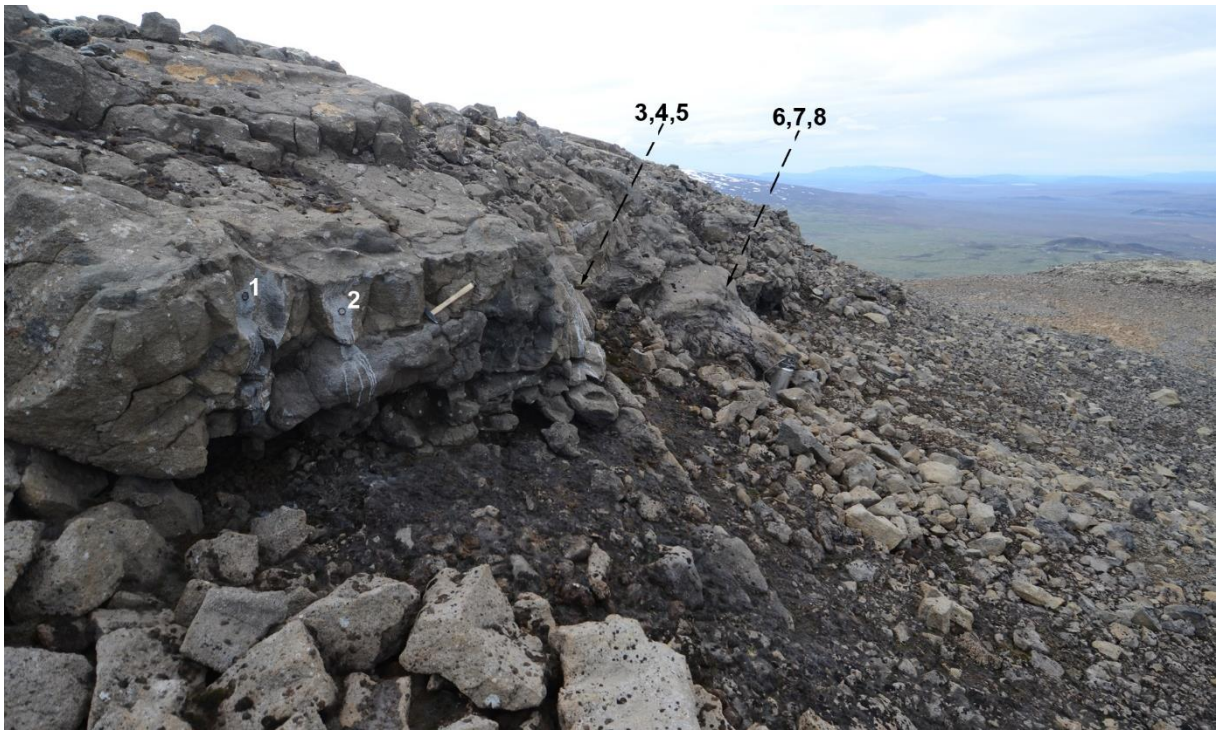

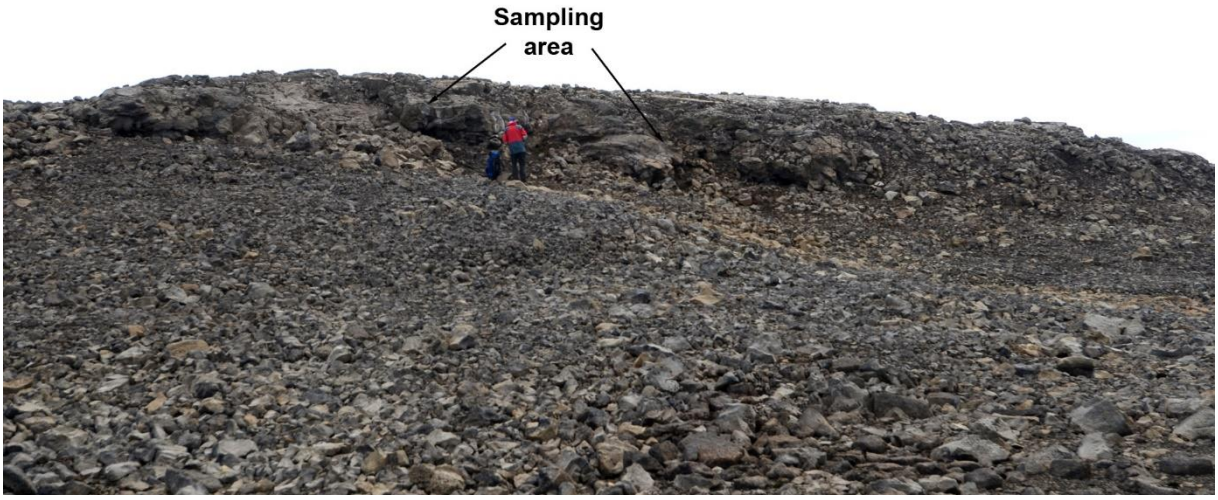

HF-L

Sampling date (orientation):	10.10.2015	**Location:**	64.41461°N 20.53851°W
Elevation:	Measured elevation from GPS: 1119 m. Elevation reading from a map (1:50.000) is 1110 m.		
Description:	This is the highest sampling site and it is from the top part of the cap lava, Stage IV. There were not many opportunities to take samples from the top of the mountain and this sampling site is from rather small vertical area there in the lava. When the drilling was done the weather was foggy, so it was not possible to orient. Orienting was done later and at that time we had snow in the area. The samples were very porous.		

Dykes

HF-H

Sampling date (orientation):	13.09.2015	**Location:**	64.43658°N 20.55424°W
Elevation:	Measured elevation from GPS: 636 m. Elevation reading from a map (1:50.000) is 690 m.		
Description:	Sampling site from a dyke in a ravine, north-west side of Hlöðufell. The samples were taken from a small area in the dyke but not distributed properly, see photo below.		

HF-I

Sampling date (orientation):	18.09.2015	**Location:**	64.41526°N 20.56618°W
Elevation:	Measured elevation from GPS: 728 m. Elevation reading from a map (1:50.000) is 720 m.		
Description:	Sampling site from a dyke in a dyke swarm (see photo below) in the south-west part of Hlöðufell. The samples were taken from a small area in the dyke but not distributed properly, see photo below. We had some difficulties in the drilling, not sure if it was because of the drill was dull or if the rock was more solid than in other places in the mountain. The samples were almost non-porous.		

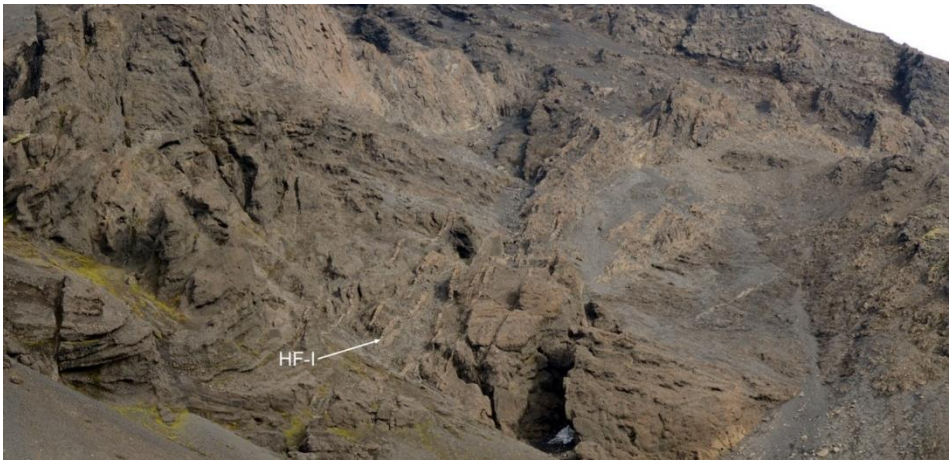

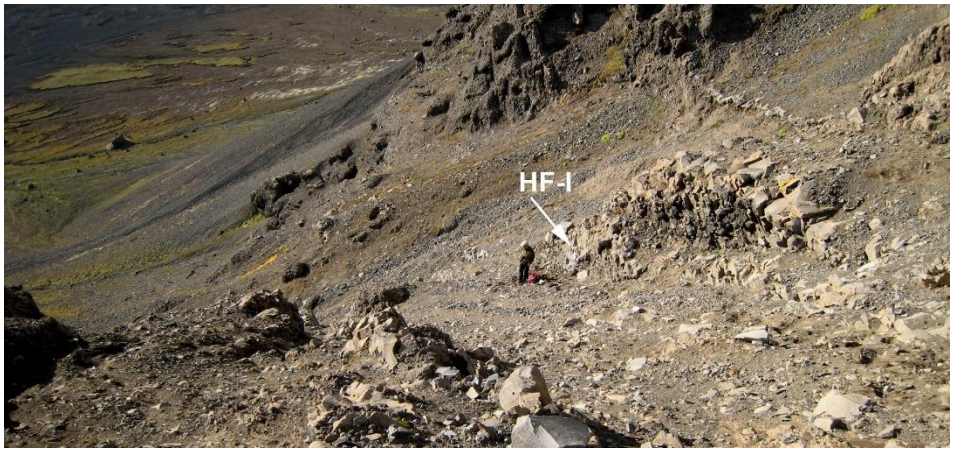

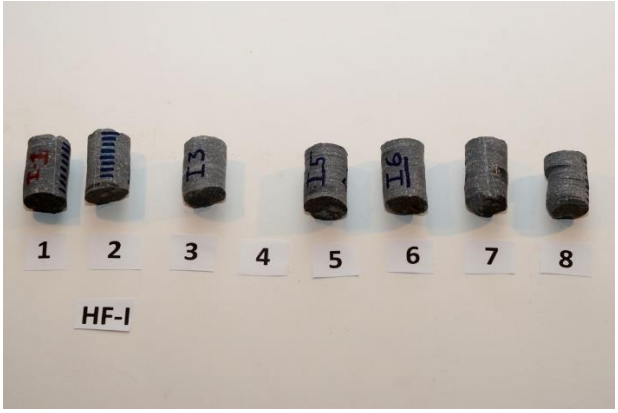

Þórólfsfell

TF-A

Sampling date (orientation):	20.09.2014	**Location:**	64.44850°N 20.51689°W
Elevation:	Measured elevation from GPS: 553 m. Elevation reading from a map (1:50.000) is 535 m.		
Description:	Sampling site from pillow lava outcrop in a ravine in west side of Þórólfsfell. The samples were not very much distributed and are all from the same pillow, see photo below.		

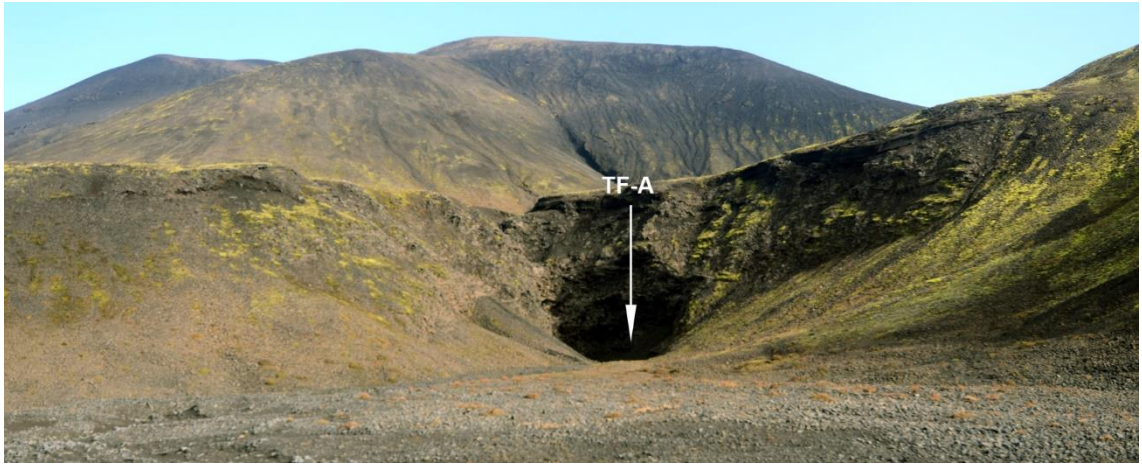

TF-B

Sampling date (orientation):	20.09.2014	**Location:**	64.44211°N 20.51501°W
Elevation:	Measured elevation from GPS: 542 m. Elevation reading from a map (1:50.000) is 530 m.		
Description:	Sampling site from pillow lava outcrop in a ravine in south part of Þórólfsfell. The cores are from the glassy outer surface of one pillow. The samples were not very much distributed and are all from the same pillow, see photo below.		

Appendix K: Paleomagnetic results for each unit described

In this appendix are more detail results for each sampling site and units than are in Chapter 7.

Stage I: Pillow lavas

The pillow ridge at Hlöðuvellir, sampling sites: HF-A, HF-M, HF-T and HF-U and HL-4 (PILL-AMTU)

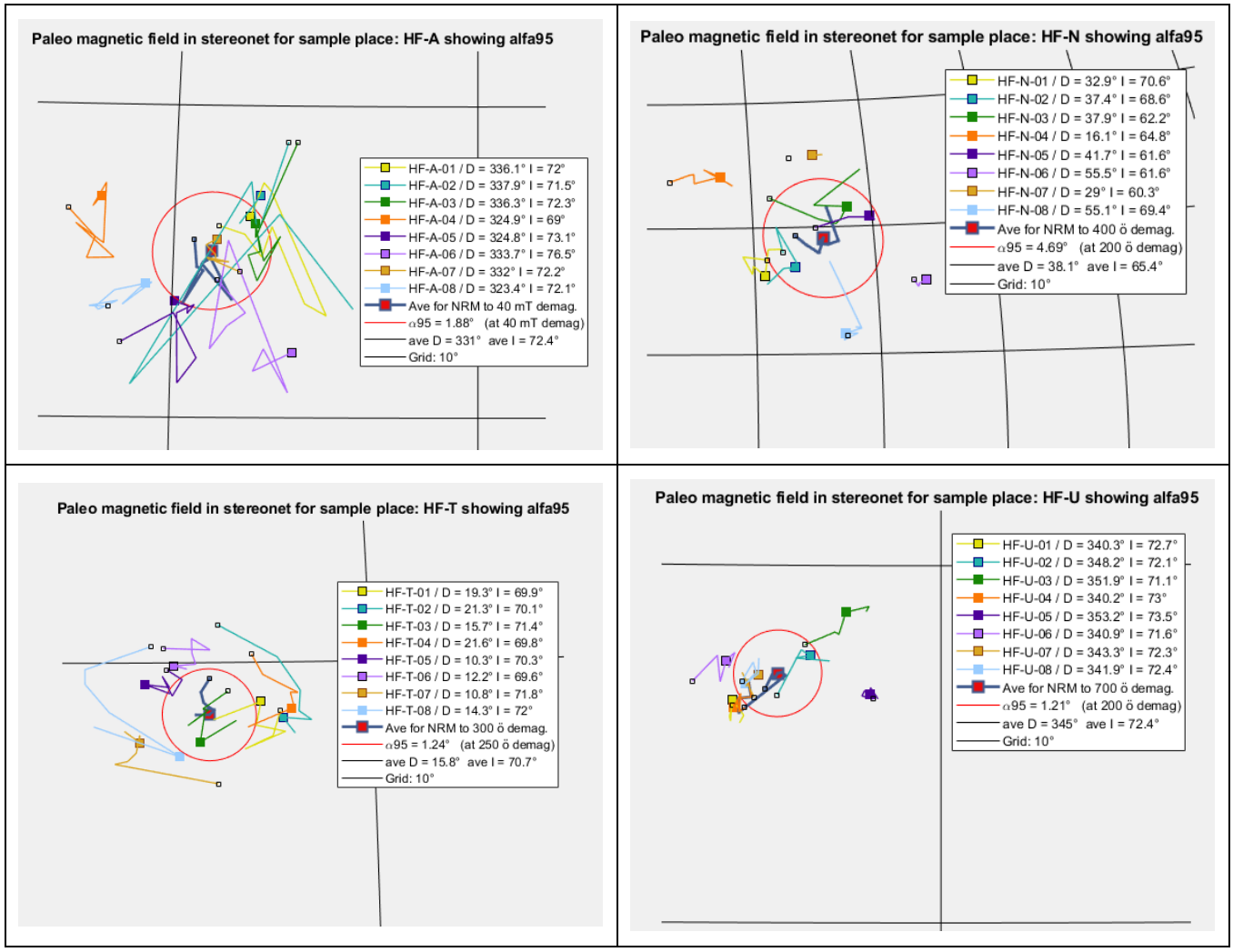

Stereonet diagrams showing the declination and the inclination for all samples in each sampling site in the unit through the demagnetization process for the samples.

From the pillow ridge in front of Hlöðuvallagil, we have four sampling sites of total 33 measured samples. Within each sampling site we have very good homogeneity with alpha95 values below 2.0° However, between the sampling sites we seem to have some discrepancy since the alpha95 value circles do not intersect each other and the samples are little bit clustered. There could have been some displacement, tilting, inhomogeneity in magnetization of the area or other reason for this. The result here is that the alpha95 confidence interval for the unit in total is most likely too low, representing the distribution of the data.

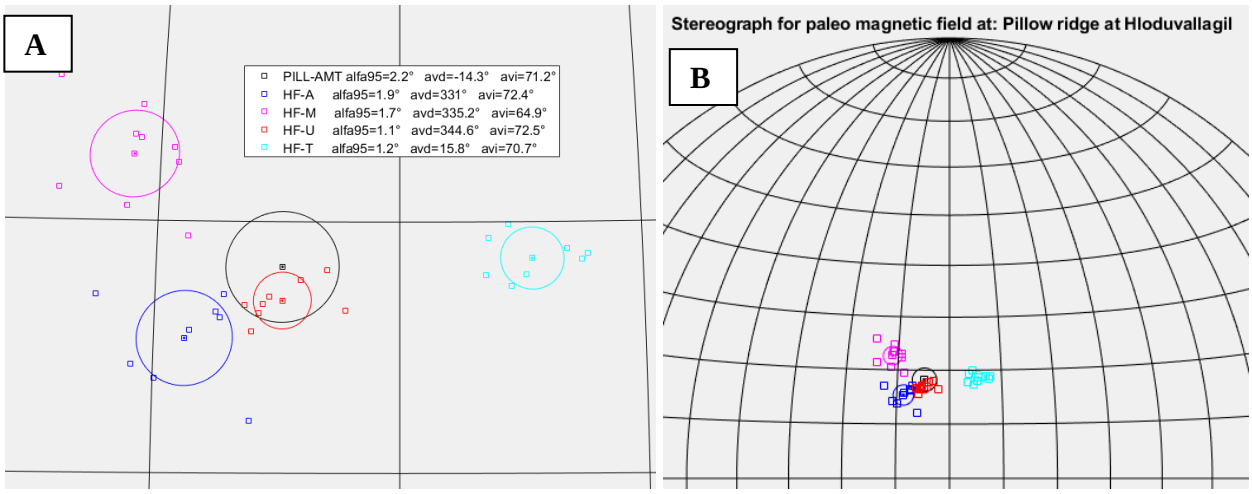

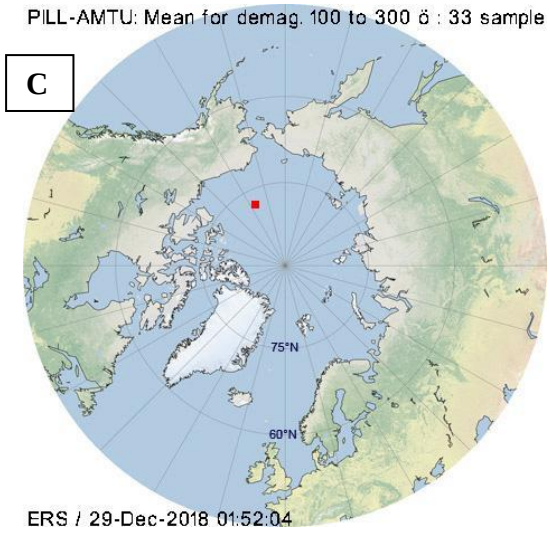

Diagrams showing results for pillow lava ridge at Hlöðuvallagil: HF-A, HF-M, HF-T and HF-U. (A) Sampling sites on stereograph, showing alpha95 confidence interval around mean values of all sample-points and also all samples. (B) Same as in A but smaller scale. (C) Paleo virtual geomagnetic dipole location.

More analysis of the sampling site HF-T

The sampling site, HF-T came out in the research as an outlier from other sampling sites in the same area of Stage I, pillow lava in the pillow lava ridge at Hlöðuvellir. Here is some more analysis of the samples from that sampling site.

First, the samples look very good as is shown on the following photo taken of the sample cores prior to sawing.

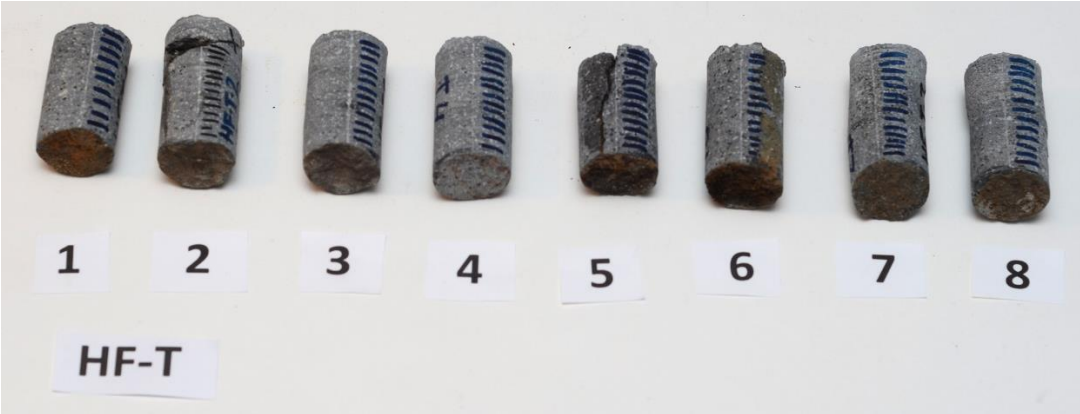

The sample cores from the sampling site HF-T, prior to sawing.

The suggestion about effects from a lightning can be analyzed somewhat with closer examination of the demagnetization process. In fact, those samples were demagnetizing very smoothly with no real change in the paleomagnetic directions, see stereonet diagrams on the next page. The directions do not change out of the alpha 95 circles and the lowest alpha 95 value is for 25 mT (or 250 oersted) demagnetization.

If the samples were indeed effected by a lightning, one should expect the remanent magnetization of the samples to be weak, that is easily removed through the demagnetization process and also changing more than in other samples. That was not the case with those samples.

The final suggestion is then rotation of the sampling site and that is always possible. Here is also noted that this sampling site is at the end of the ridge, see the photo below.

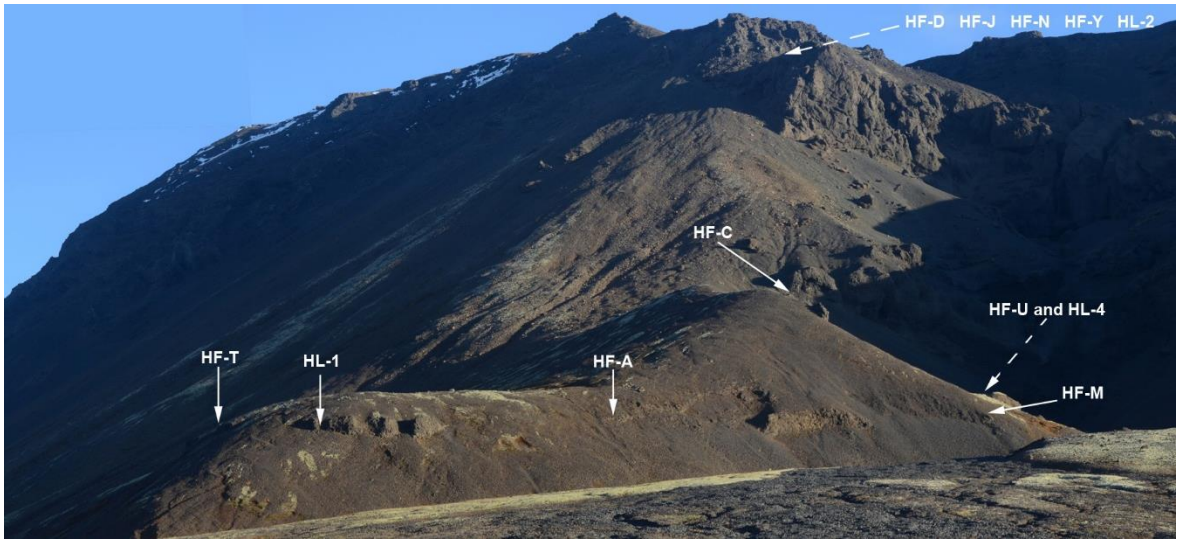

Photo showing the sampling site HF-T, HL-1 and other nearest sampling sites

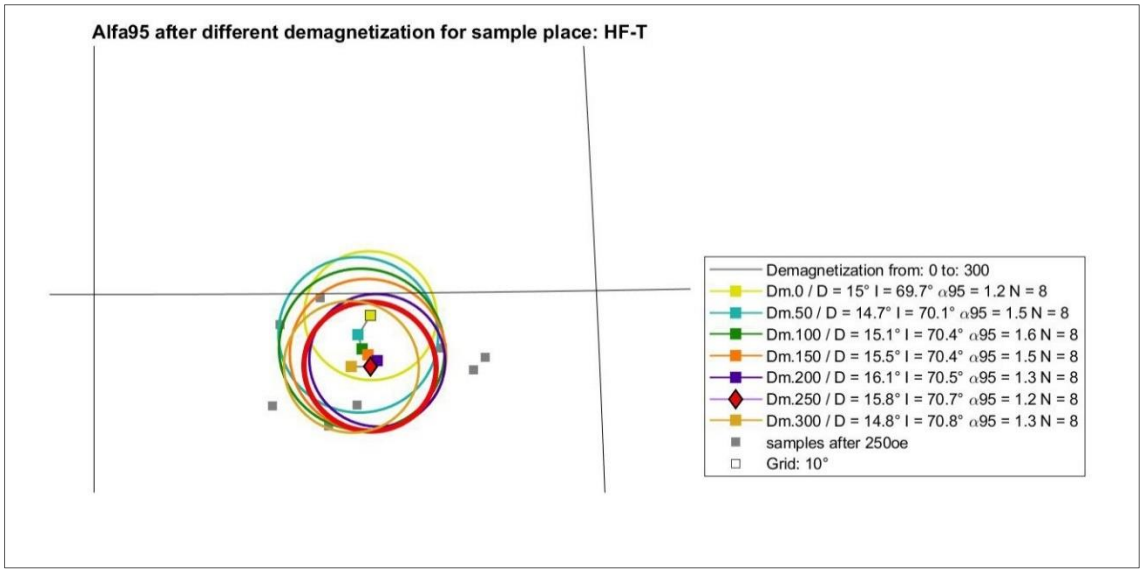

Paleomagnetic directions of the samples at HF-T through the demagnetization process shown on stereonet diagrams. From NRM to 30 mT (or 300 oersted) demagnetization.

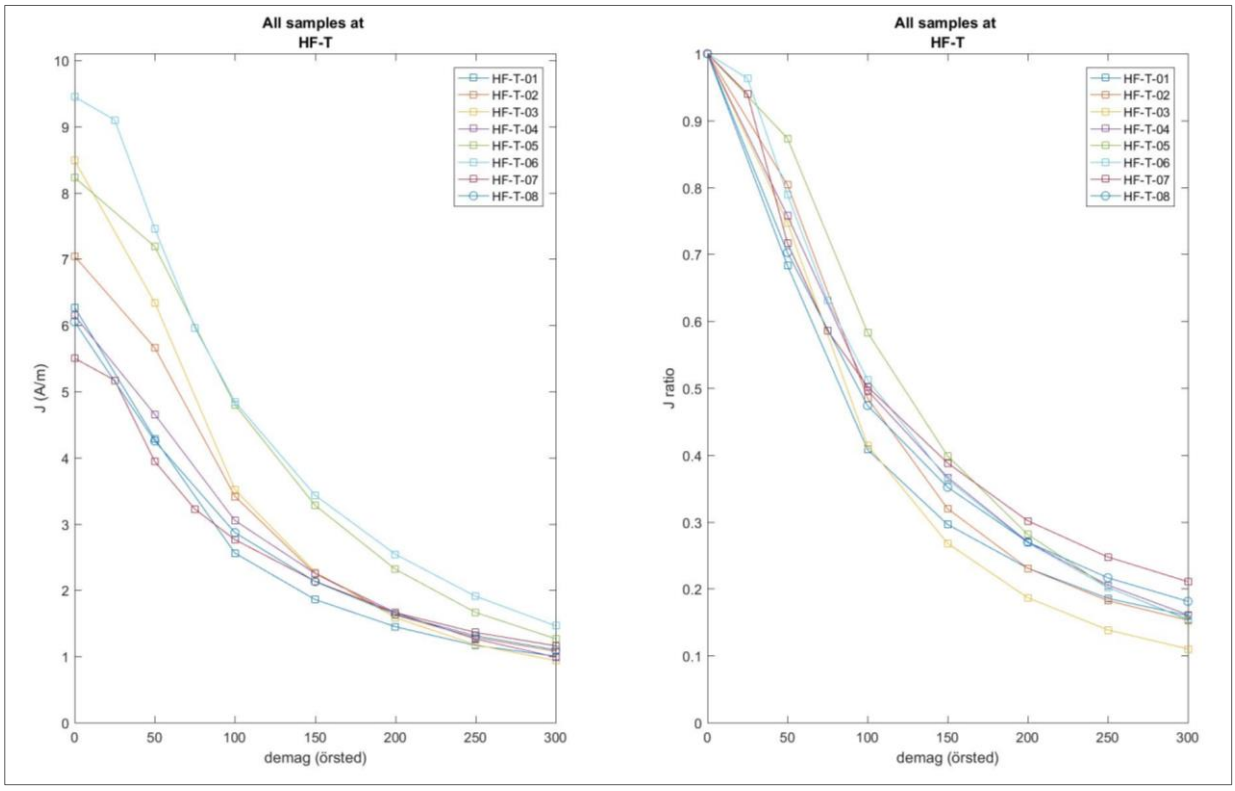

Demagnetization curves for all samples in HF-T.

Pillow lava in Rani: HF-B, HF-V AND HF-W

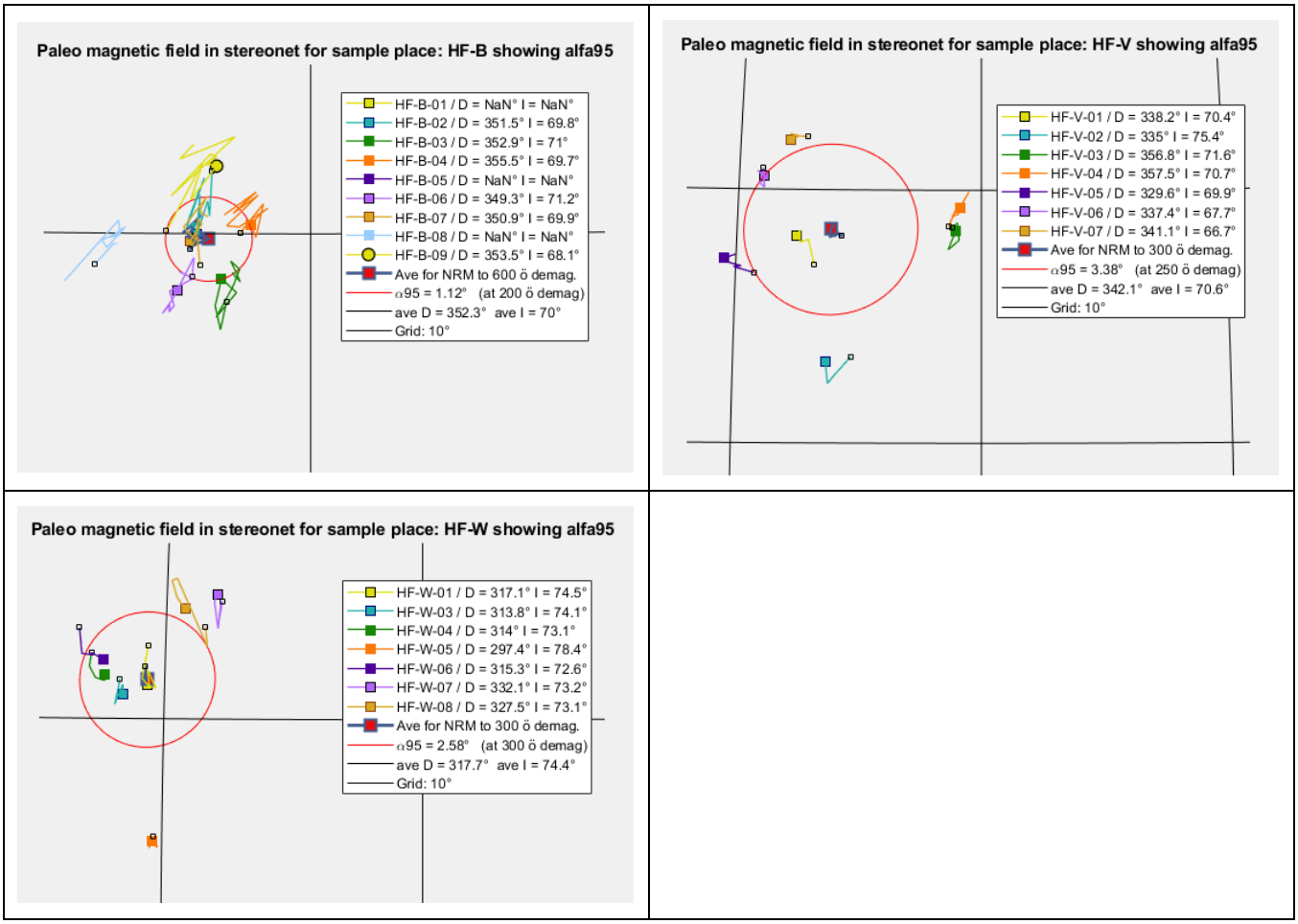

Stereonet diagrams showing the declination and the inclination for all samples in each sampling site in the unit through the demagnetization process for the samples.

The magnetic directions of the 21 sample cores from the three sampling sites in the unit Rani pillow ridge do not coincide very well since the alpha95 circles for the places do not intersect as shown in the figure below. This could be as is in the pillow ridge in Hlöðuvallagil because of different formation time or some minor different nudging of the sampling sites after cooling. But still, as in the pillow ridge at Hlöðuvallagil, there was no visible faulting.

However, for overall look of the samples in Rani area as shown in the figure below clustering of the samples is not obvious, so all samples are used for statistical analysis, giving alpha95 value of 2.3°.

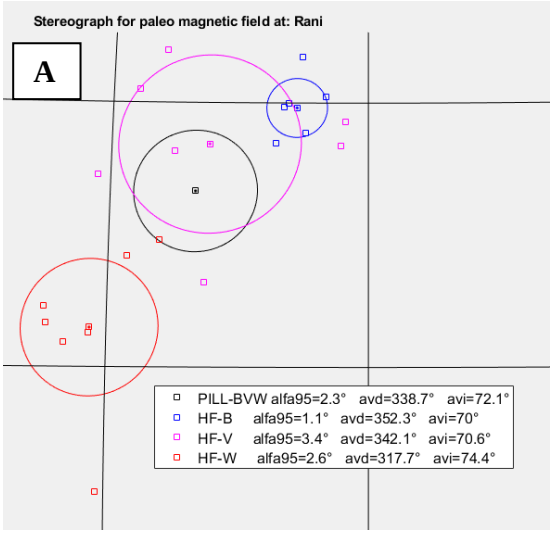

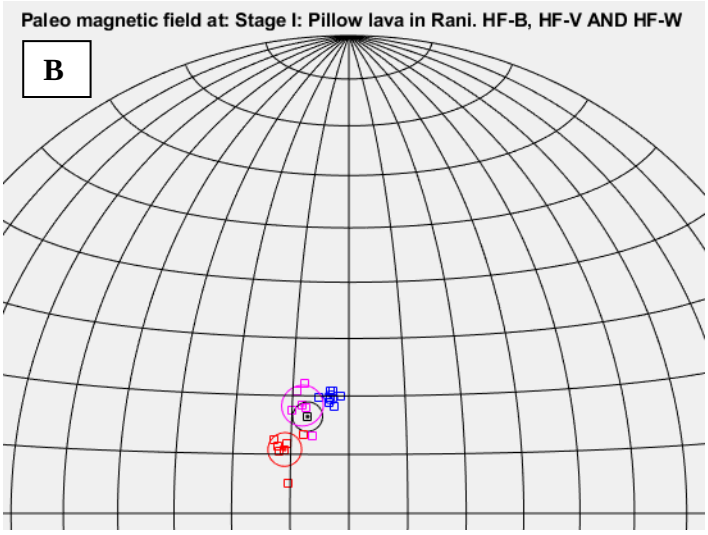

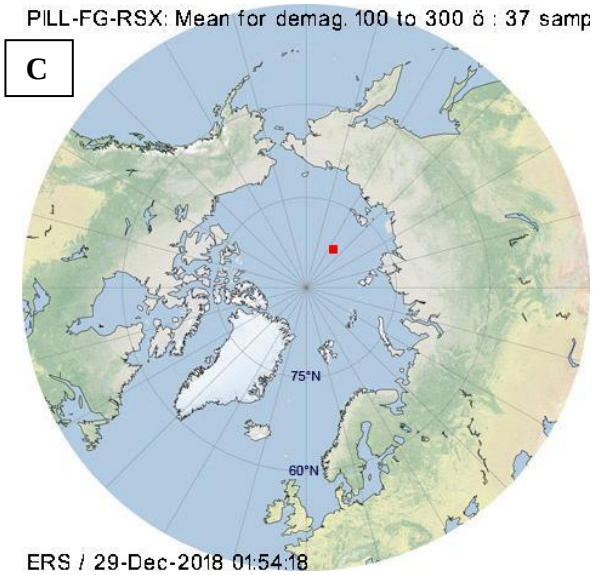

Diagrams showing results for pillow lava in Rani. (A) Sampling sites on stereograph, showing alpha95 confidence interval around mean values of all sample-points and also all samples. (B) Same as in A but smaller scale. (C) Paleo virtual geomagnetic dipole location.

Other pillow lava, west side and east side: HF-F, HF-G, (HF-FG), HF-R, HF-S and HF-X

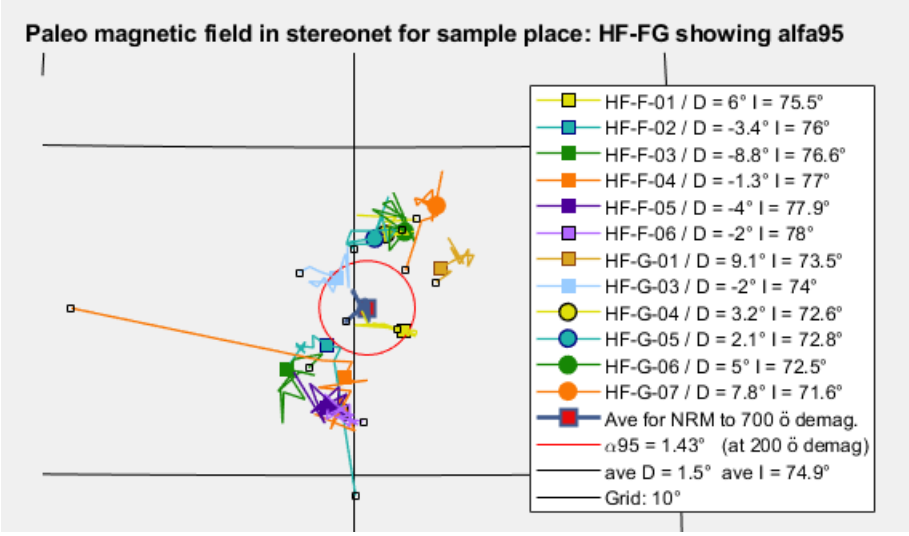

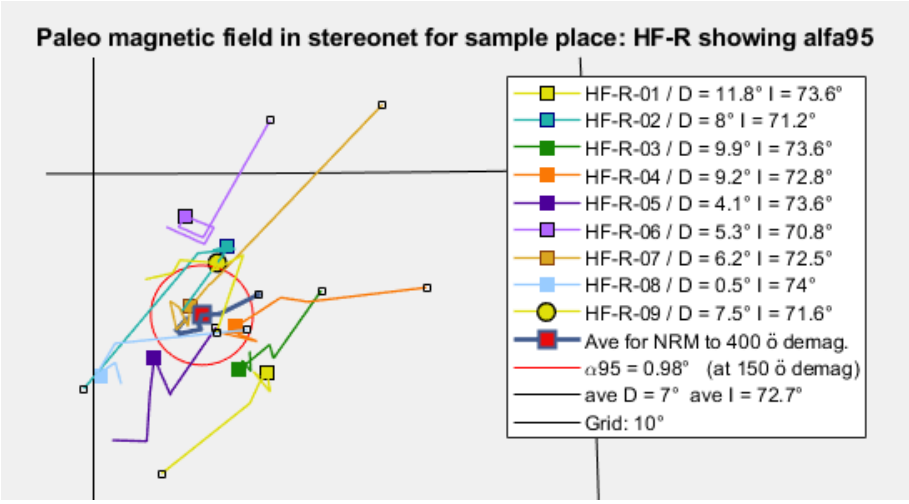

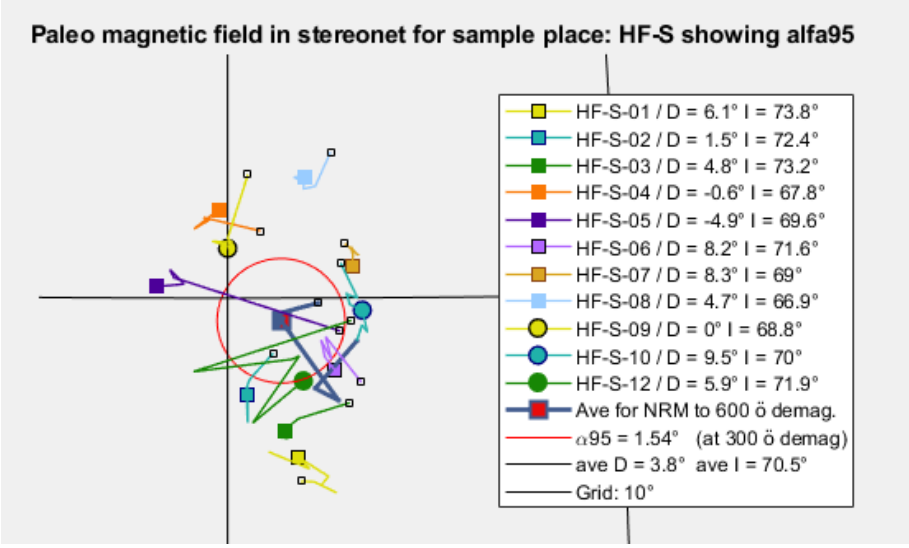

Stereonet diagrams showing the declination and the inclination for all samples in each sampling site in the unit through the demagnetization process for the samples.

The values for declination and inclination seem to coincide at least partly with each other. Those sampling sites are not very close to each other. HF-S and HF-X are on the opposite sides of the mountain but on similar altitudes. Sampling sites HF-R and HF-FG are close to each other in the north-west part of the mountain, while HF-FG are in higher altitude.

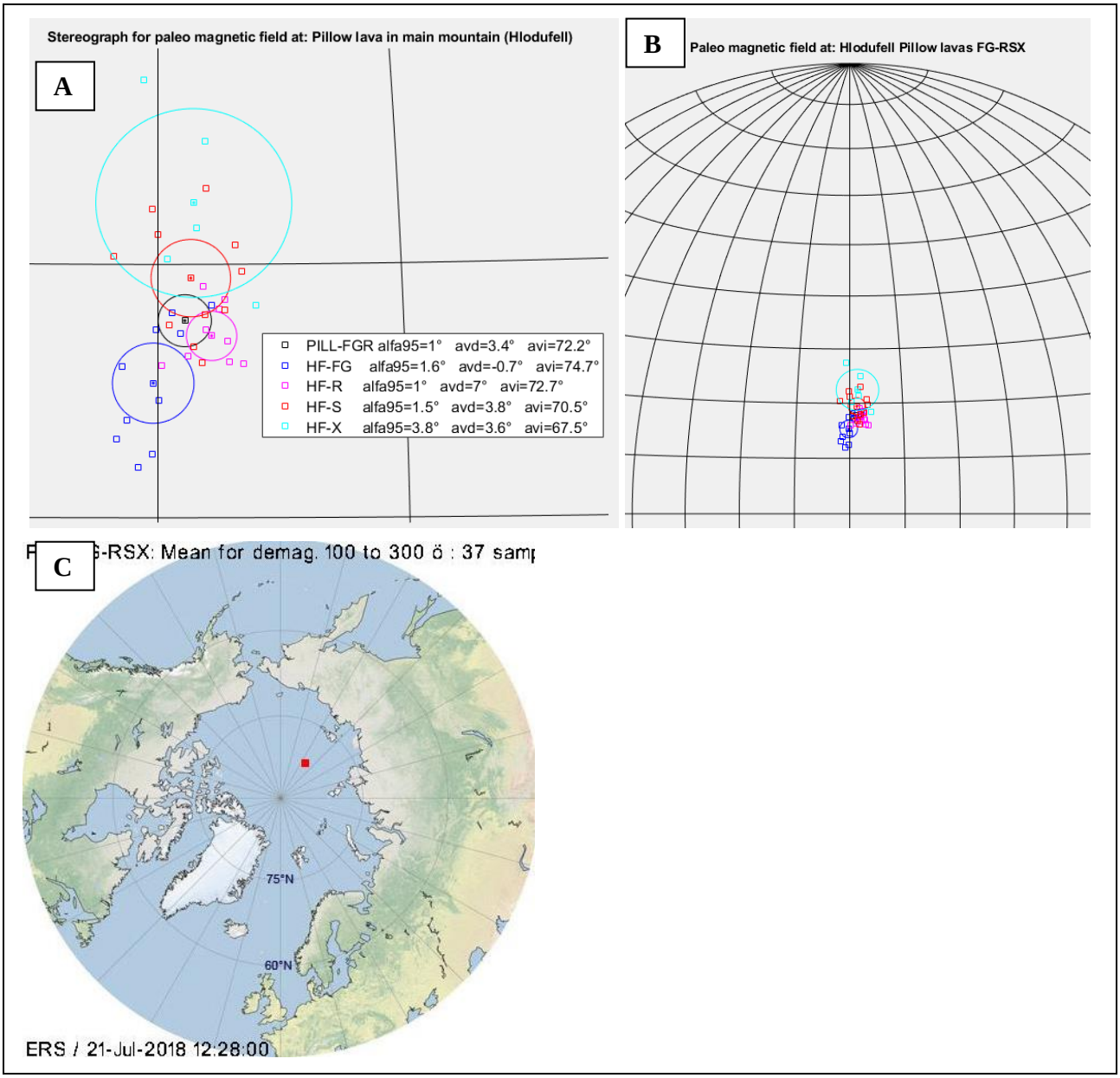

Diagrams showing results for pillows in Hlöðufell, other than Rani and pillow ridge at Hlöðuvallagil. (A) Sampling sites on stereograph, showing alpha95 confidence interval around mean values of all sample-points and also all samples. (B) Same as in A but smaller scale. (C) Paleo virtual geomagnetic dipole location.

Cube joint basalt formation above the pillow ridge at Hlöðuvellir: HF-C

The sampling site HF-C could be taken with the sampling sites unit in the pillow lava ridge at Hlöðuvallagil or with other stage I formations but since it is not exactly pillow lava, it is taken separated from the other formations. All samples in HF-C are were taken from rather small area so perhaps the value of alpha95 would have been higher if samples were taken from larger area. But here should also be noted that this sampling site was very difficult for core sampling due to steep slope of the hills and also danger of rock falling down from above.

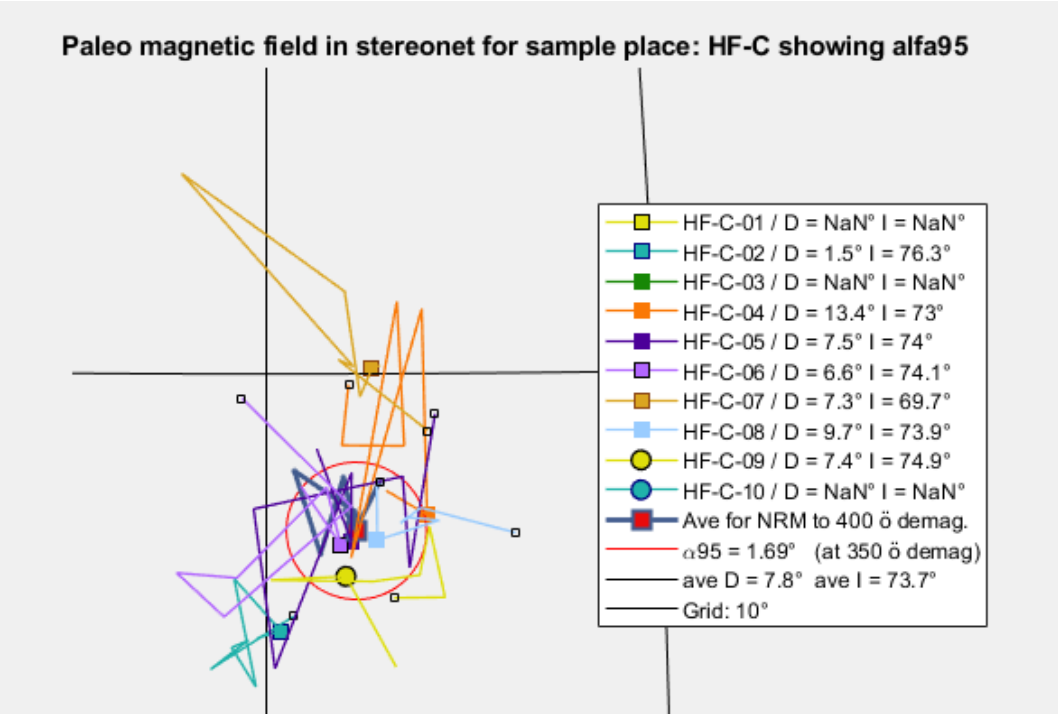

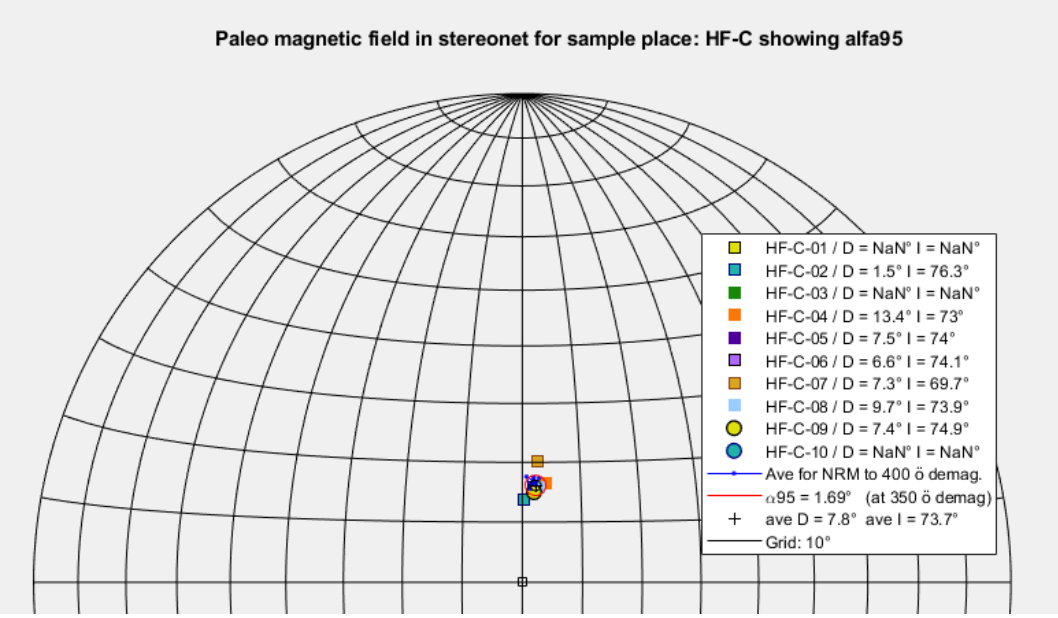

Stereonet diagrams showing the declination and the inclination for all samples in each sampling site in the unit through the demagnetization process for the samples.

Stage III: Lower cap lava

Lower cap lava, south part: HF-D, HF-J, HF-N

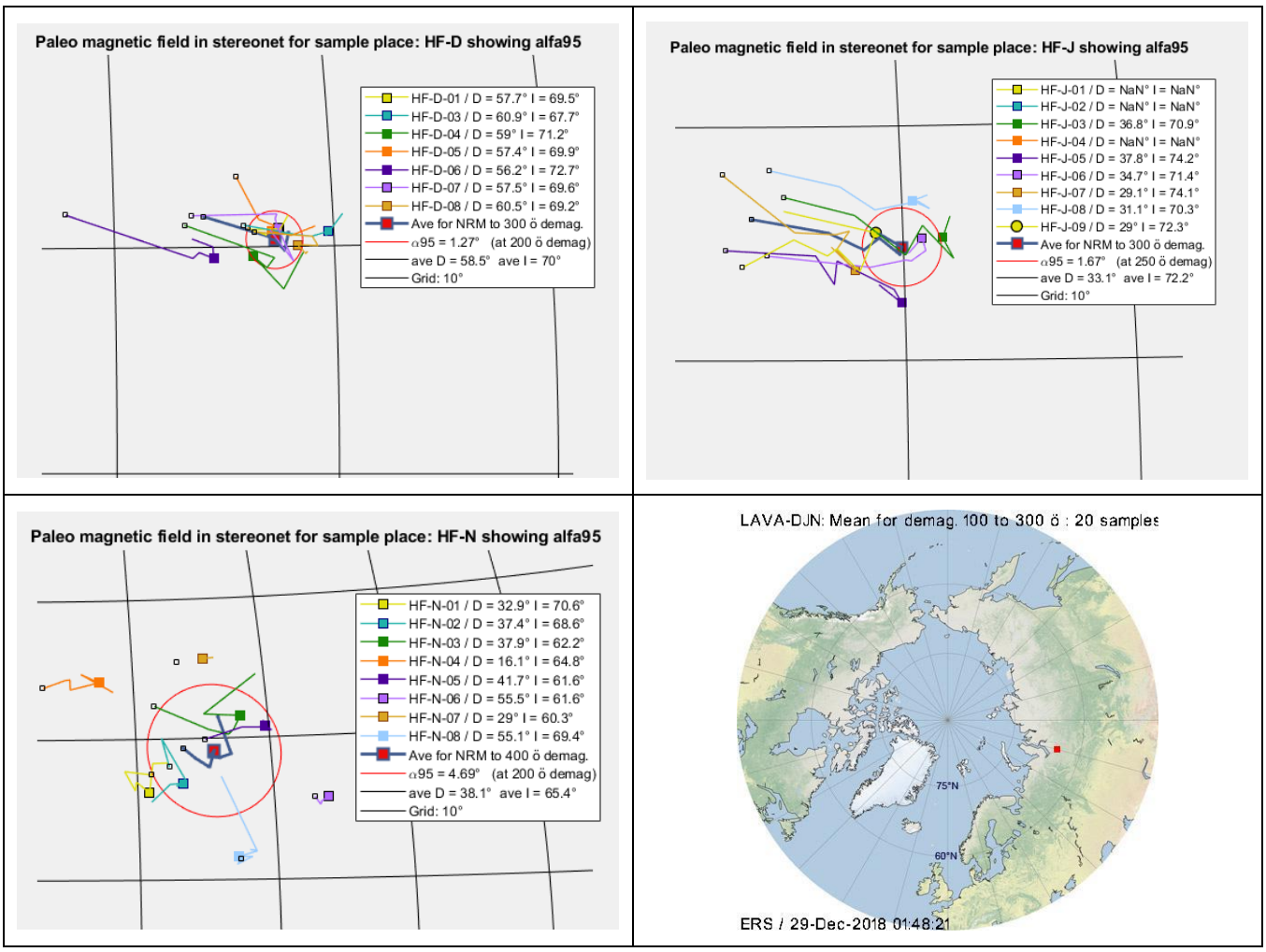

Stereonet diagrams showing the declination and the inclination for all samples in each sampling site in the unit through the demagnetization process for the samples. Also the virtual geomagnetic dipole location for the samples in the unit

Here should also be noted that the samples in sampling site HF-D and HF-J show the same pattern of changed paleomagnetic directions through the demagnetization process.

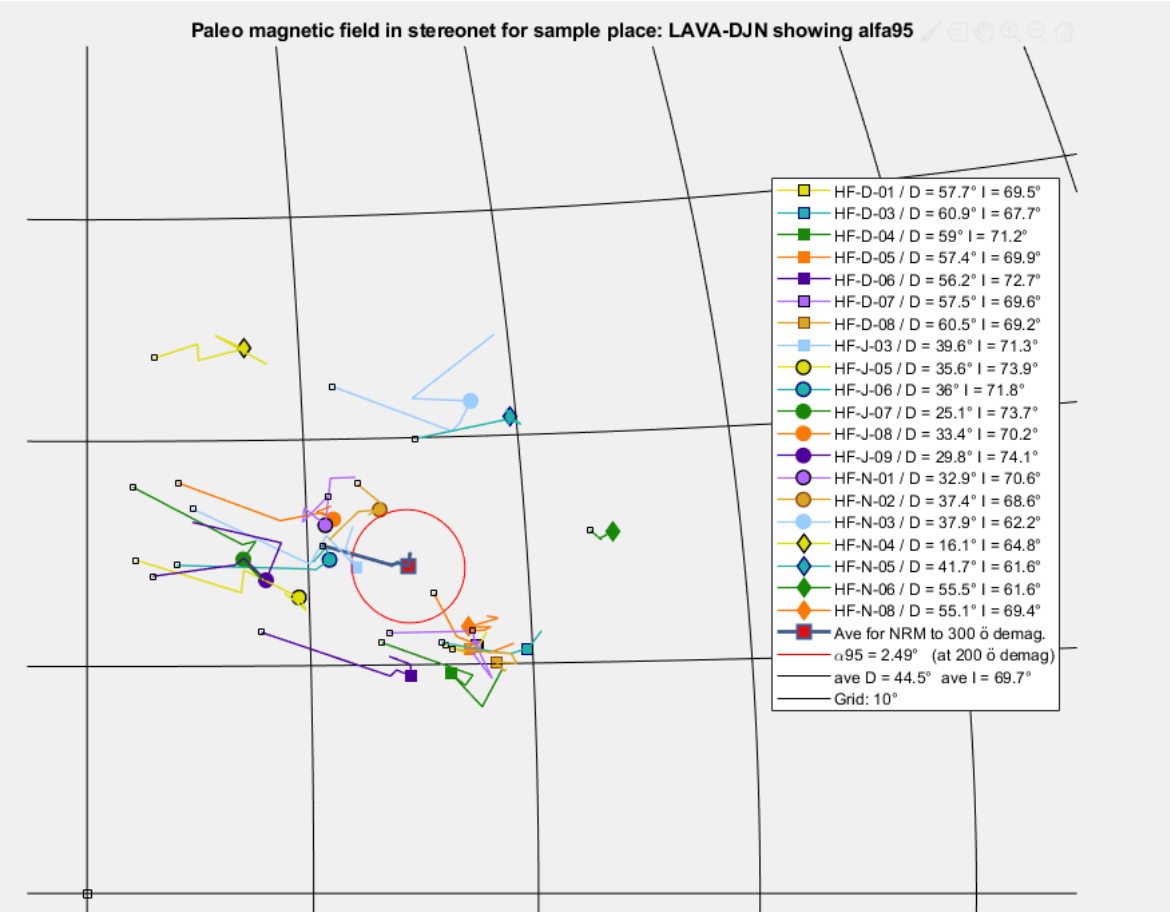

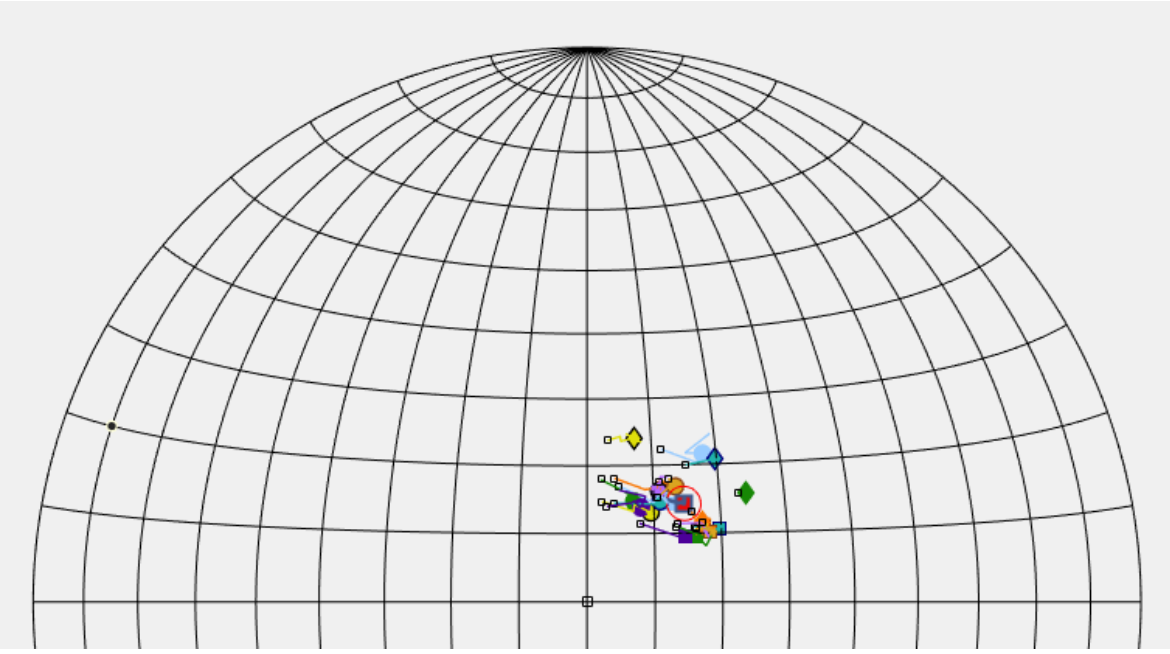

Stereonet diagrams showing the declination and the inclination for all samples unit through the demagnetization process.

Stage III': Middle cap lava

HF-K; HF-O, HF-Q, HF-Y

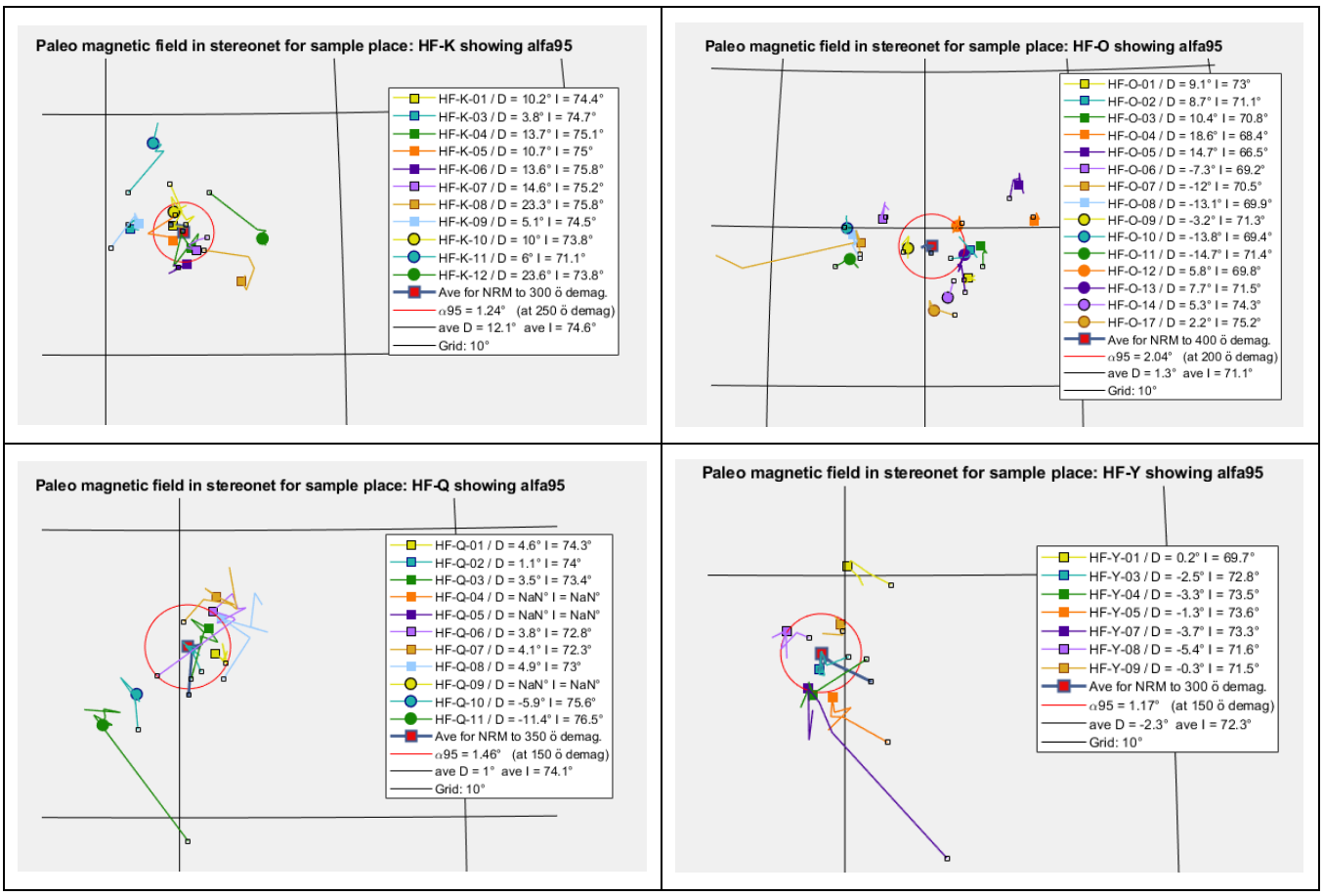

Stereonet diagrams showing the declination and the inclination for all samples in each sampling site in the unit through the demagnetization process for the samples.

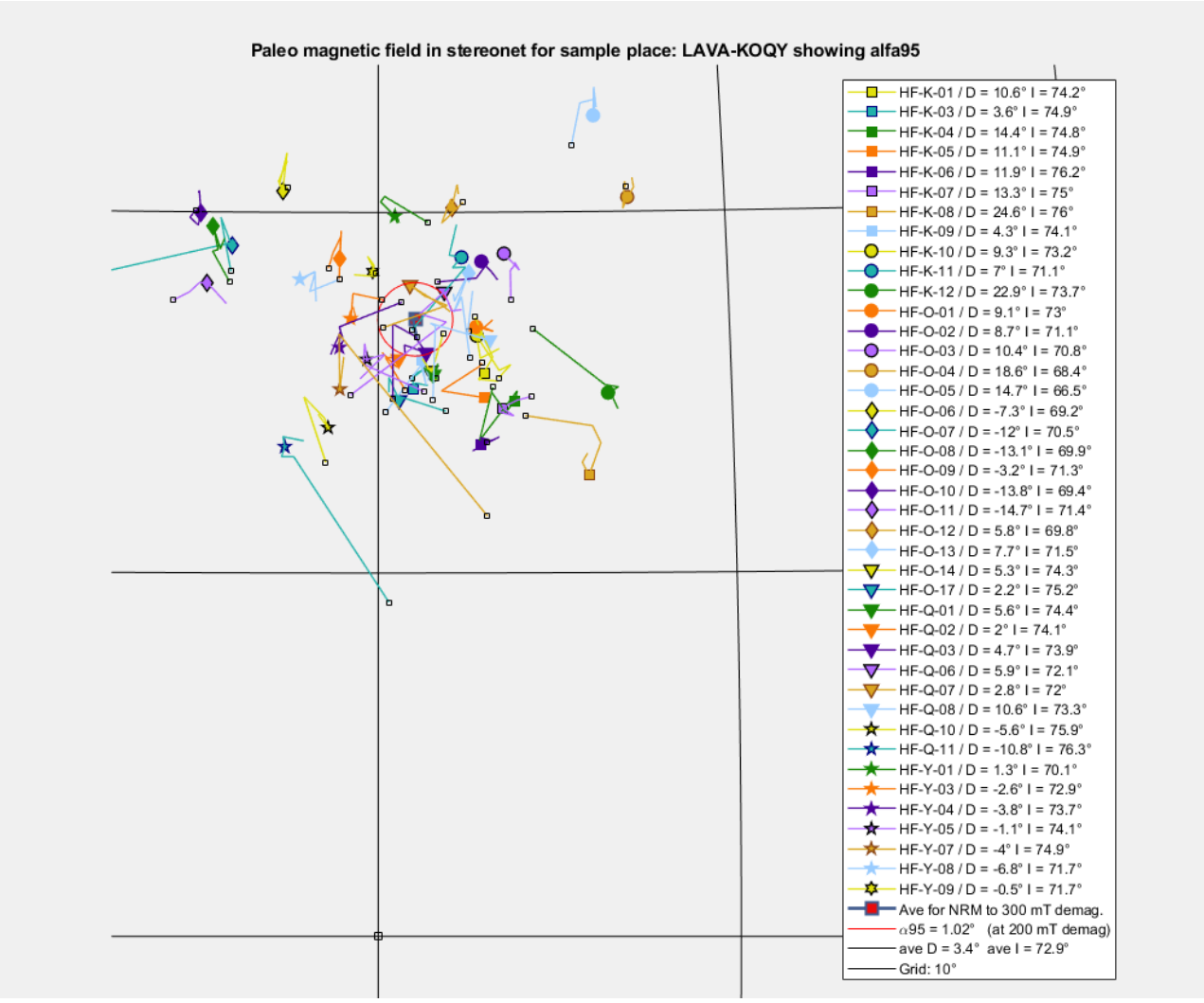

Stereonet diagrams showing the declination and the inclination for all samples unit through the demagnetization process.

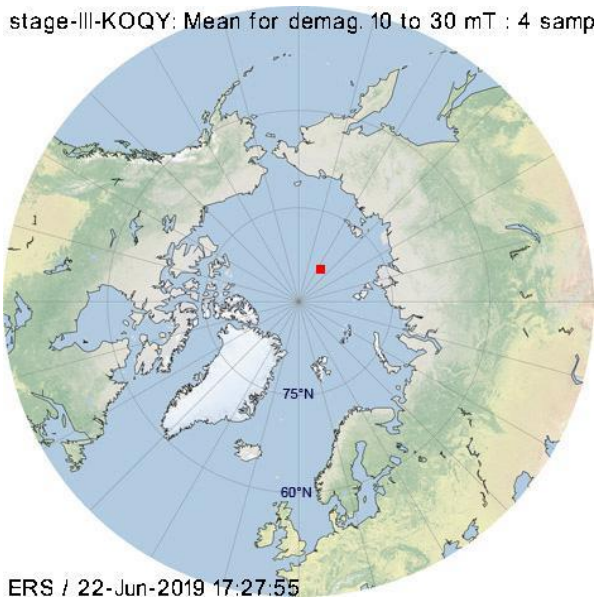

Paleo virtual geomagnetic dipole location.

Stage IV

HF-E; HF-L; HF-P

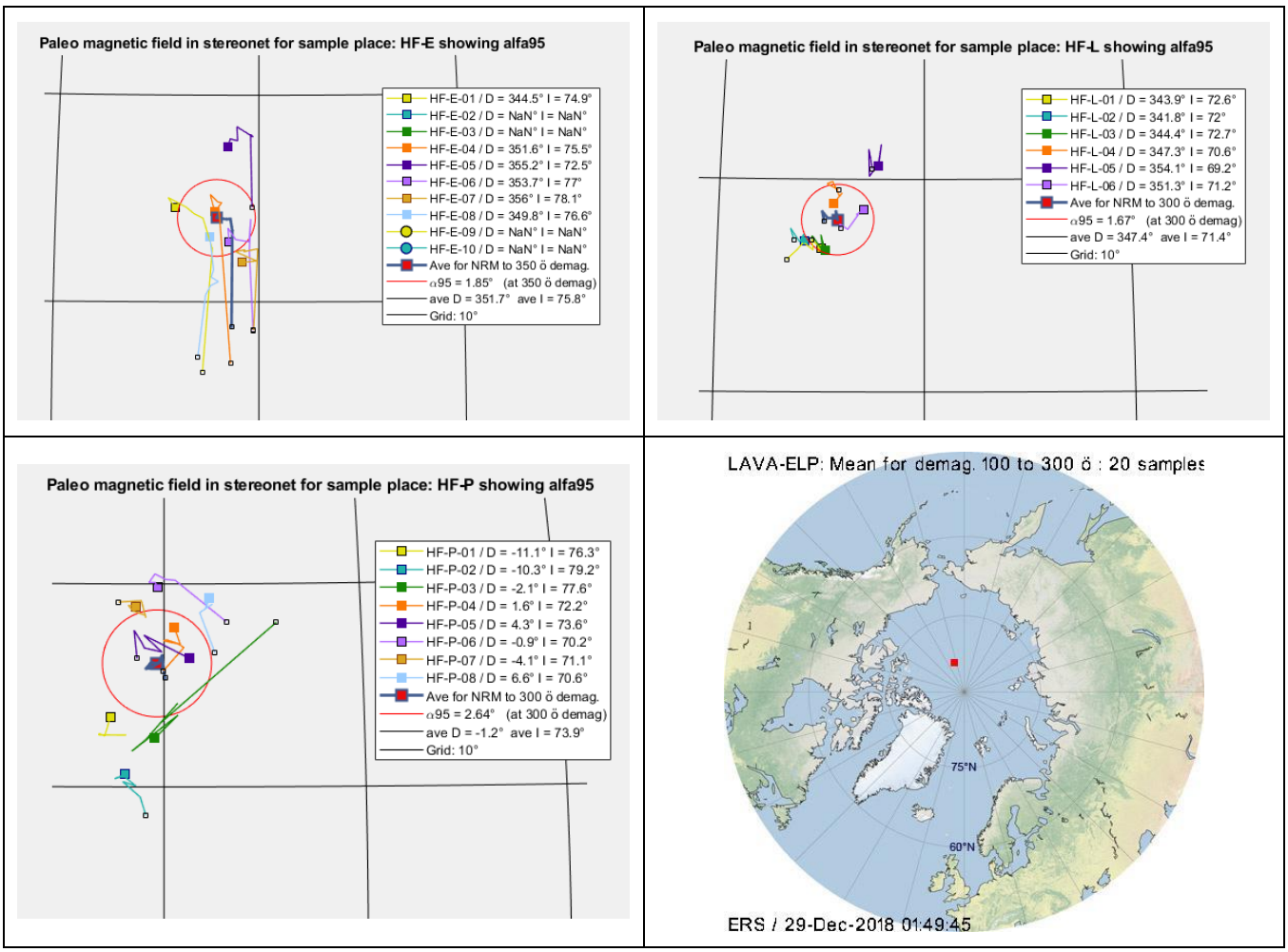

Stereonet diagrams showing the declination and the inclination for all samples in each sampling site in the unit through the demagnetization process for the samples. Also the paleo virtual geomagnetic dipole location.

Dykes

HF-H; HF-I

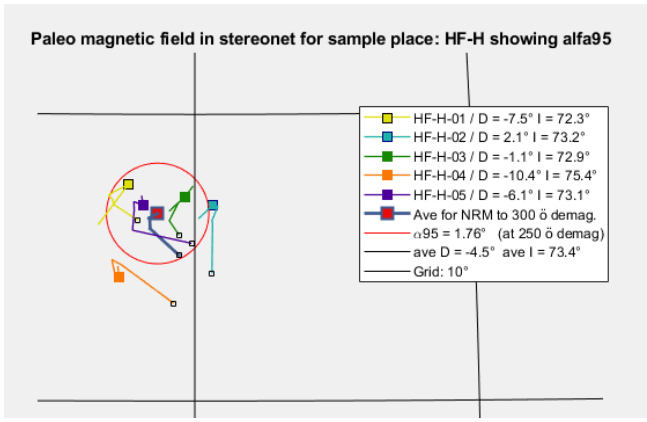

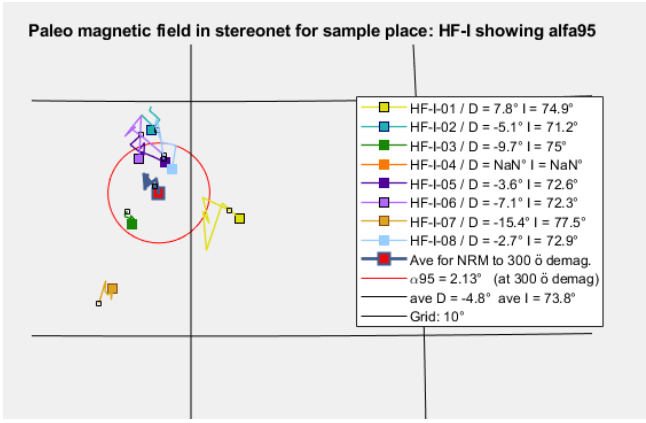

The sampling sites in dykes were about 730 m apart, see location in Figure 6-13. They give almost the same magnetic field directions and coincide completely with each other. The assumption is then that they have been formed at the same time.

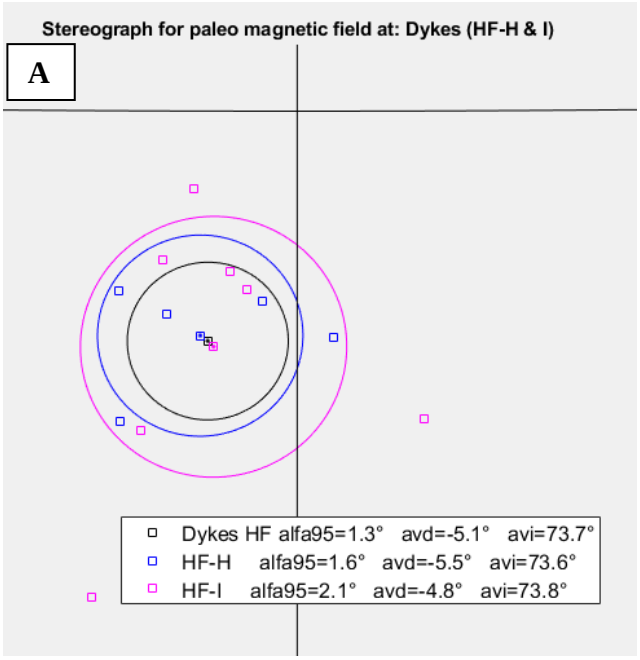

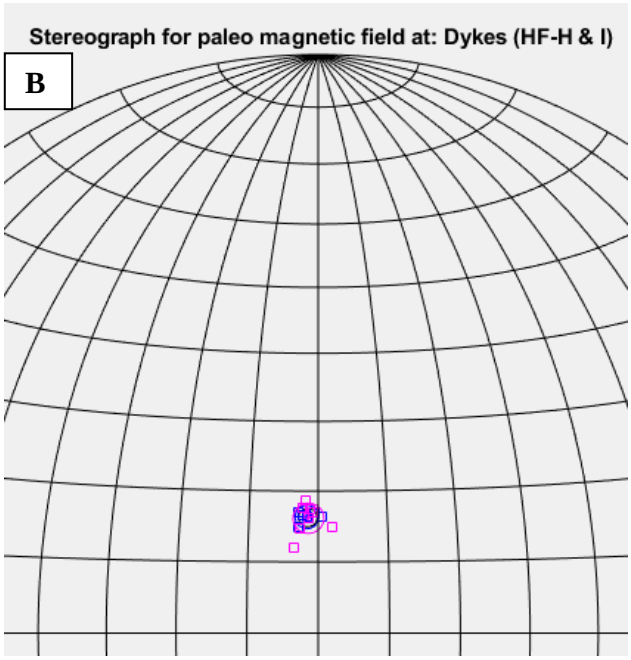

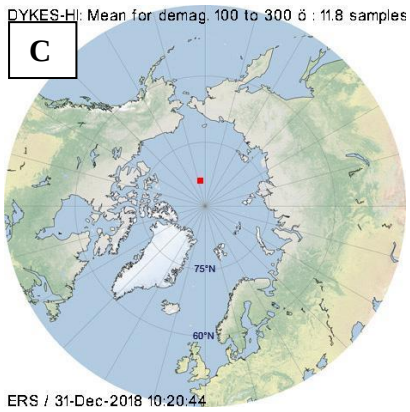

Diagrams showing results for dykes measured in Hlöðufell. (A) Sampling sites on stereograph, showing alpha95 confidence interval around mean values of all sample-points and also all samples. (B) Same as in A but smaller scale. (C) Paleo virtual geomagnetic dipole location.

Þórólfsfell

TF-A; TF-B

Two sampling sites were taken in Þórólfsfell.

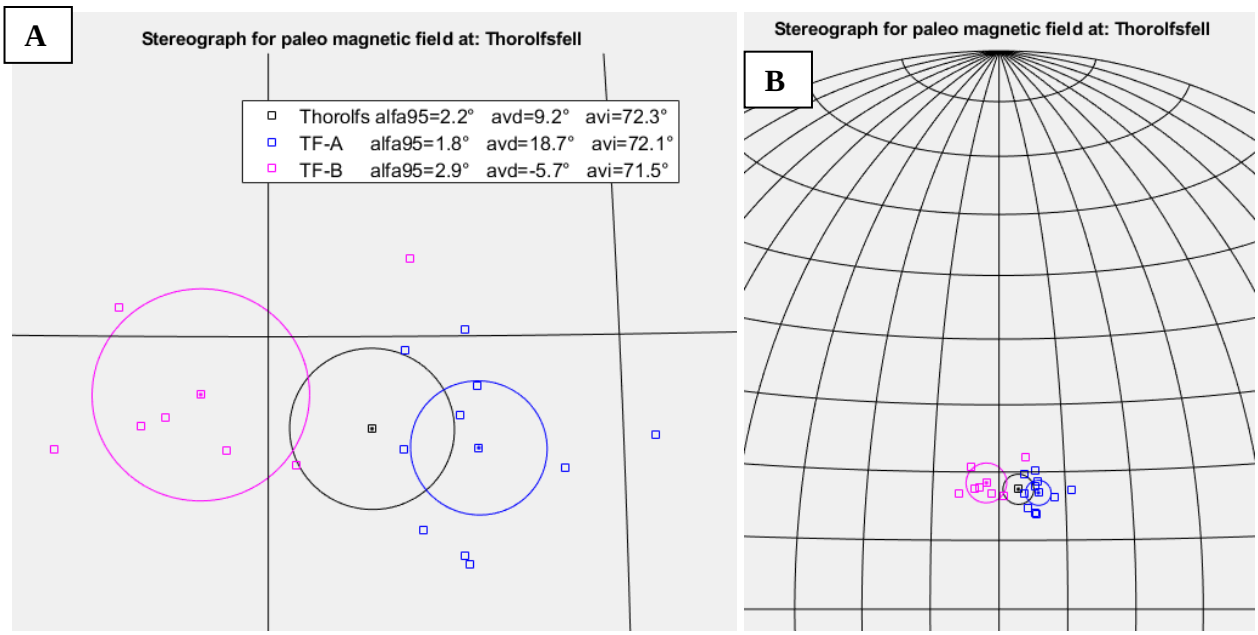

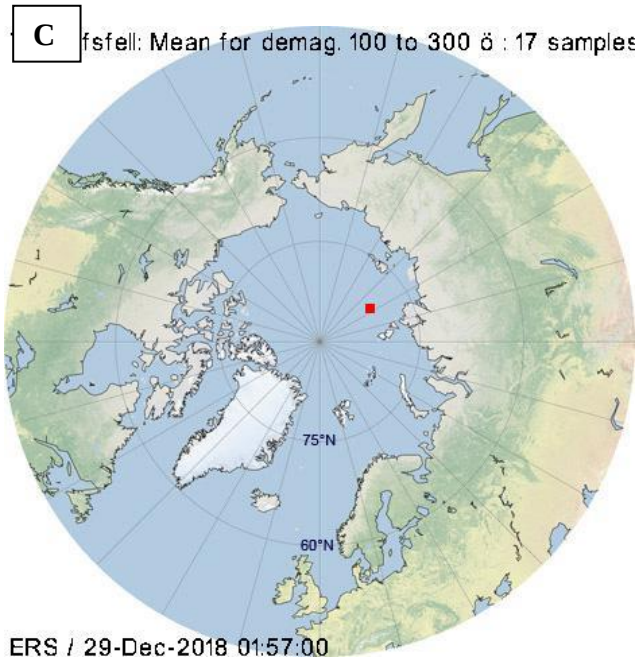

Diagrams showing results for the two sample points in Þórólfsfell. (A) Sampling sites on stereograph, showing alpha95 confidence interval around mean values of all sample-points and also all samples. (B) Same as in A but smaller scale. (C) Paleo virtual geomagnetic dipole location.

Appendix L: Undirhlíðar

L1 Introduction

A small project was organized in a quarry in Undirhlíðar on Reykjanes peninsula as a pre project, prior to the main project in Hlöðufell. The main purpose of the project in Undirhlíðar was to learn the basic methods of drilling and paleomagnetic core sampling and also learn how to calculate the paleomagnetic field directions from the sample cores. The project took place in the year 2014.

Figure L-1. Overview, showing a part of the quarry in Undirhlíðar. Most of the sampling sites taken in the quarry are visible in the photo.

L2 About the quarry in Undirhlíðar

Undirhlíðar is a pillow ridge in the Reykjanes Peninsula, close to Reykjavik (L-3 and Figure Figure L-3). The peninsula is in southwest Iceland and it connects the Western Volcanic Zone to the submarine portion of the slow-spreading Reykjanes Ridge. Undirhlíðar is a part of the Sveifluháls hyaloclastite ridge, which is part of the Krísuvik fissure system, which is one of several fissure systems in Reykjanes Peninsula. Glaciovolcanic eruptions along a ~7 km fissure produced the ~150 m thick pillow lava ridge, Undirhlíðar. The quarry used in this research is 0.6 km long and 0.25 wide and it is located at 63°59′46″ N and 21°53′24″ W. Regional mapping has assigned most of the volcanic ridge to be from early Weichselian time (118-10 kyr), with its northernmost end mapped as Early Weichselian (118-80kyr) (Pollock, Edwards, Hauksdottir, Alcorn & Bowman, 2014).

Several geological units were identified in the quarry in the research of Pollock et al. (2014) and they are used and referred to in this research. The main units that samples were from on this research are two pillow lava units, Lp1 and Lp2. They are separated with a hyaloclastite layer

(Figure L-4) and the pillow lava units are interpreted to be from two discrete eruptions (Pollock et al., 2014).

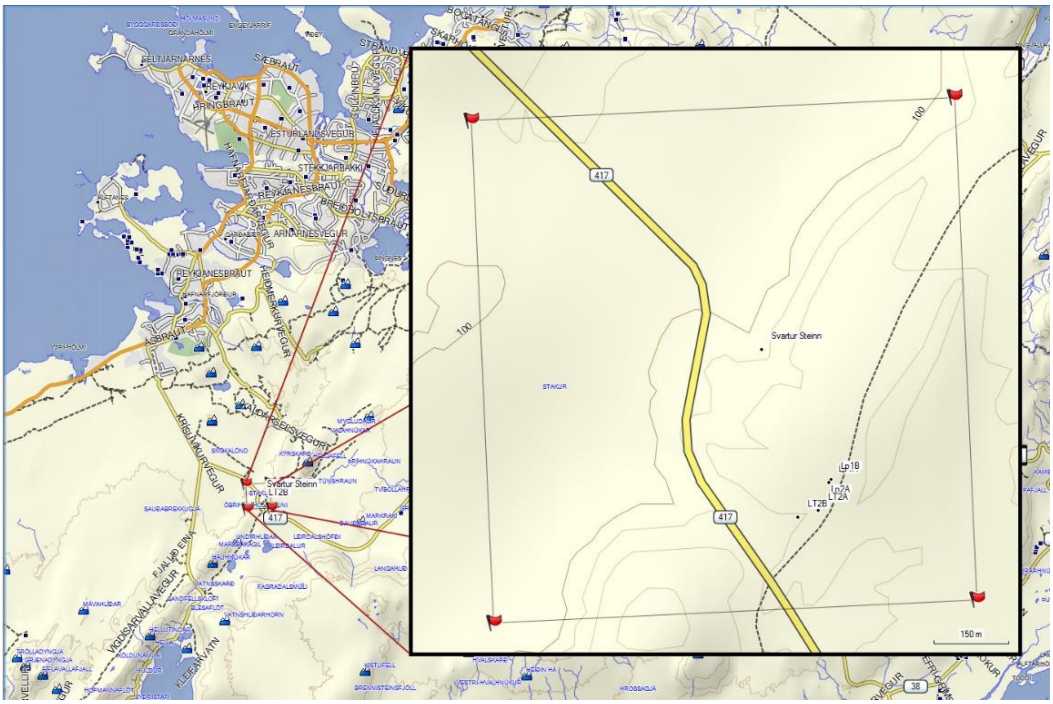

Figure L-2: A map showing the location of the quarry in Undirhlíðar, close to Reykjavik. The red flags on the inserted image shows the corner points of the map on Figure L-2. The location of the quarry is 63°59'46" N and 21°53'24" W.

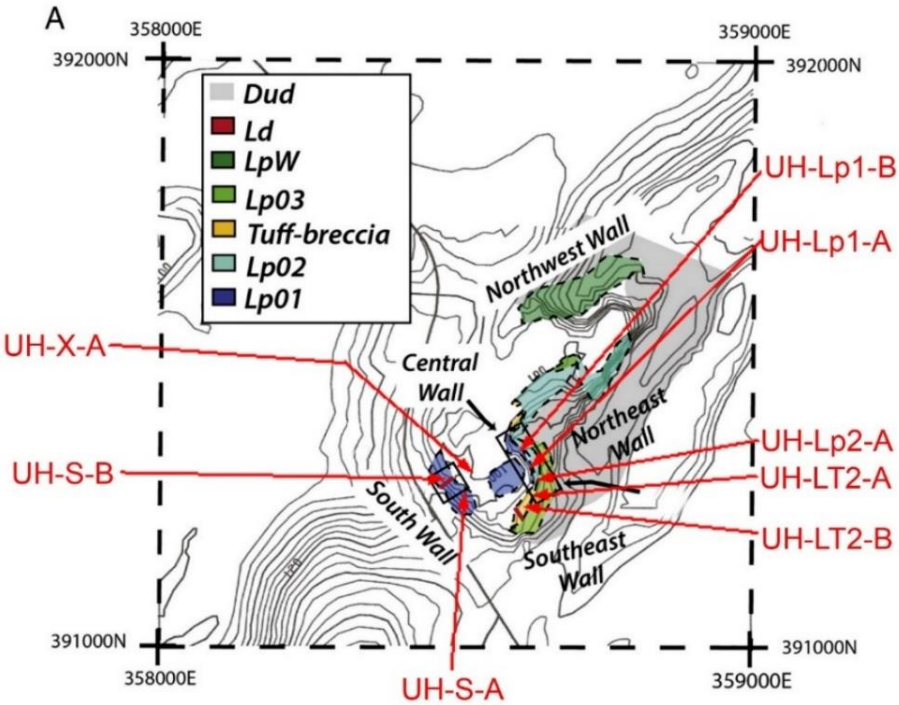

Figure L-3. Location of all sampling sites in Undirhlíðar quarry. Names of sampling sites in red text. Map modified from Pollock et al. (2014).

L3 Sampling sites and units in Undirhlíðar

The sampling sites in Undirhlíðar were all from the south part of the quarry that is the central wall, the southeast wall and the south wall (Figure L-3). Names of the sampling sites were taken from the names of the units the samples were from or connected to or from the walls. The name format for the sampling sites is: UH-Abc-D-0 where:

- UH stands for Undirhlíðar and is the same for all sampling sites in the research of Undirhlíðar
- Abc stands for the unit or the wall and is: Lp1, Lp2, LT2 for those units, S for south wall and X for a sampling site that was not connected to any unit or wall.
- D stands for what sampling site it is within the unit
- 0 is the number of the sample within in the sampling site.

Sample UH-Lp1-A-4 is then sample number for in the sampling site A within the unit Lp1 in Undirhlíðar.

L3.1 Sampling sites from the central wall

Three sampling sites are from the central wall (Figure L-3). Those sampling sites are from the lowest pillow lava unit, Lp1 and one sampling site is from the next pillow lava unit Lp2 which is above a lapilli tuff layer, LT (Figure L-4).

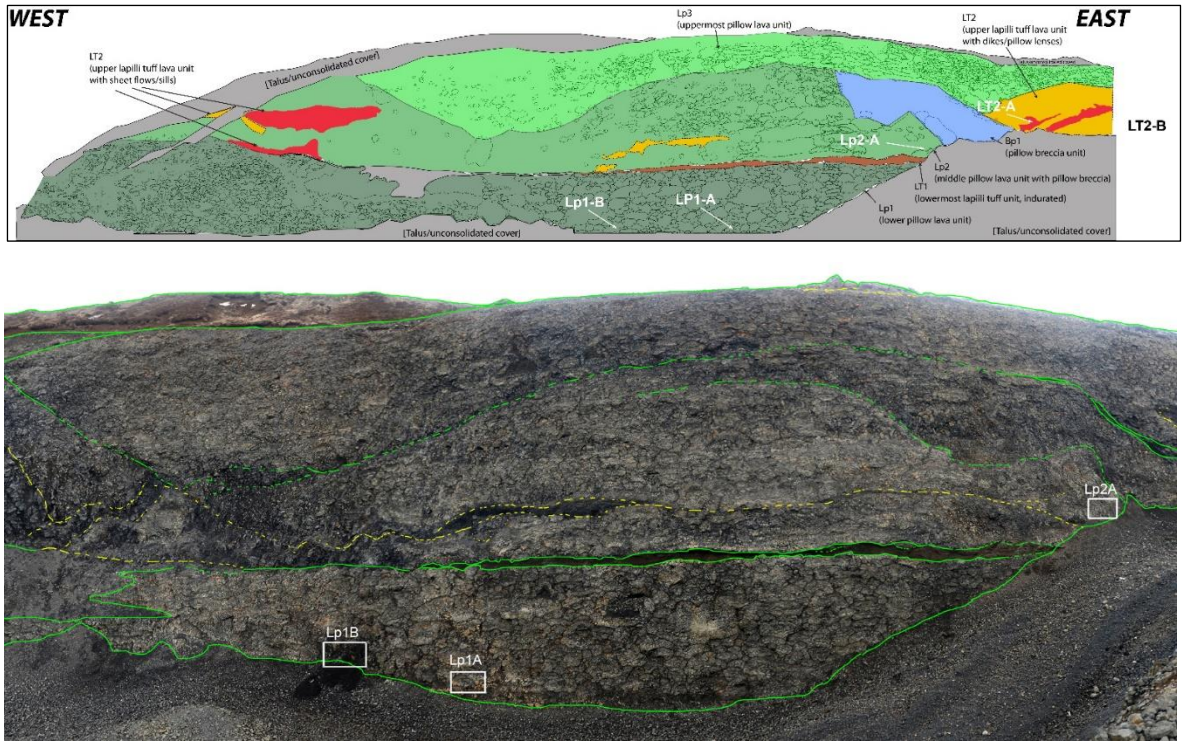

Figure L-4. The central Wall. (A) Annotated photomosaic of the central wall of Undirhlíðar showing interbedded pillow(Lp1 to Lp3) and tuff-breccia units (TB1, TB2/LT), modified from Pollock et al. (2014) (B) Photograph showing part of the same wall with markings for the sampling sites taken in this wall.

L3.2 Sampling sites from the southeast wall

Two sampling sites are from the southeast wall, referred to as LT2A and LT2B although they are not from the lapilli-tuff or breccia itself but from connected pillow lavas or intrusions into the lapilli unit (Figure L-5). The sampling site LT2A is most likely an intrusion but the LT2B sampling site could be from a pillow lava unit that has was not identified there by Pollock et al. (2014).

L3.3 Sampling sites from the south wall

Two sampling sites were from the south wall (Figure L-6). One sampling site is from the pillow lava unit in the wall (UH-S-A) and one sampling site is from a dyke through the wall (UH-S-B). According to Pollock et al. (2014), the pillow lava unit in the south wall is Lp1, which the same as the lowest one in the central wall (Figure L-4).

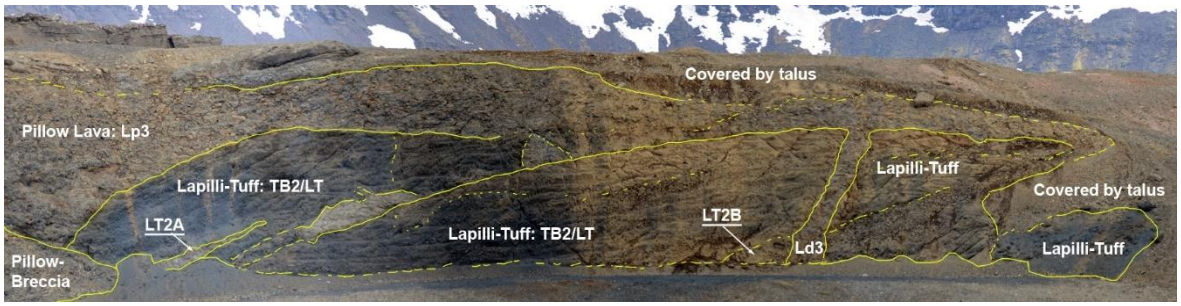

Figure L-5. The southeast wall of Undirhlíðar quarry. A photograph showing the lapilli tuff unit, LT2 and the sampling sites from the wall, LT2A and LT2B.

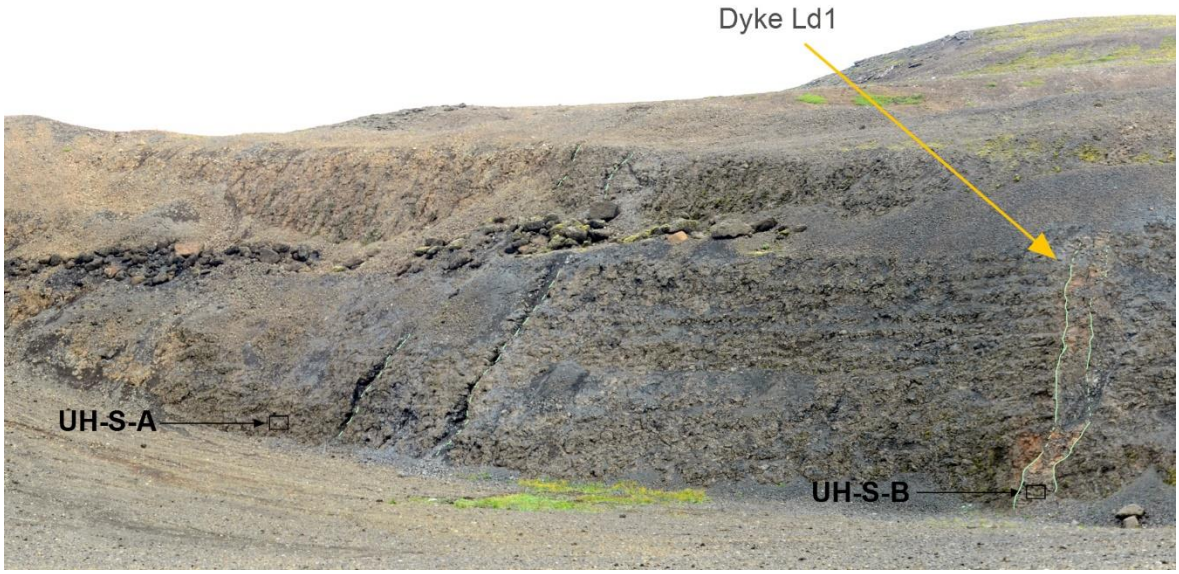

Figure L-6. Sampling sites in the south wall. The sampling site UH-S-A is from the pillow lava in the wall but UH-S-B is from the dyke Ld1.

L3.4 Other parts of the quarry

There was one other sampling site taken in the quarry, but was not part of any wall of it. That sampling site is from a cube joint lava which was inside the quarry (Figure L-7).

Figure L-7. The sampling site UH-X-A inside the quarry from a cube joint lava unit. The south wall is in the background.

L4 Results and discussion

The first overall result for all sampling sites is in Table L-1 and it is also represented on a stereonet image (Figure L-8). The sampling sites UH-Lp1-A and UH-Lp1-B should give same results and noted here is that their alpha95 circles intersects. Here is also noticed that the sampling site UH-LT2-B gives the same paleomagnetic directions as Lp1-A sampling site.

Table L-1 Undirhlíðar: Main result

Sampling site	No of samples	Demag (oe)	Alpha 95 (°)	Decl (°)	Incl (°)	VGP location (°N)	(°E)	J NRM (A/m)	J 100 (A/m)	MDF (oe)
UH-Lp1-A	11	300	1.6	356.6	70.2	80.1	169.9	17.7	11.4	132.0
UH-Lp1-B	4	200	3.6	7.1	68.2	76.8	138.4	14.0	8.2	125.6
UH-Lp2-A	8	250	2.6	344.0	63.2	68.7	190.7	24.8	18.7	148.9
UH-LT2-A	6	200	3.8	358.7	58.1	64.8	160.5	17.6	11.3	136.4
UH-LT2-B	6	200	4.1	6.2	68.2	77.0	140.6	18.5	13.3	141.9
UH-S-A	7	300	2.8	351.8	66.5	74.3	178.5	33.1	31.9	285.4
UH-S-B	9	200	1.5	345.3	51.7	57.0	181.3	6.4	4.0	145.6
UH-X-A	6	200	1.0	27.2	69.2	72.1	94.0	9.0	5.8	139.1

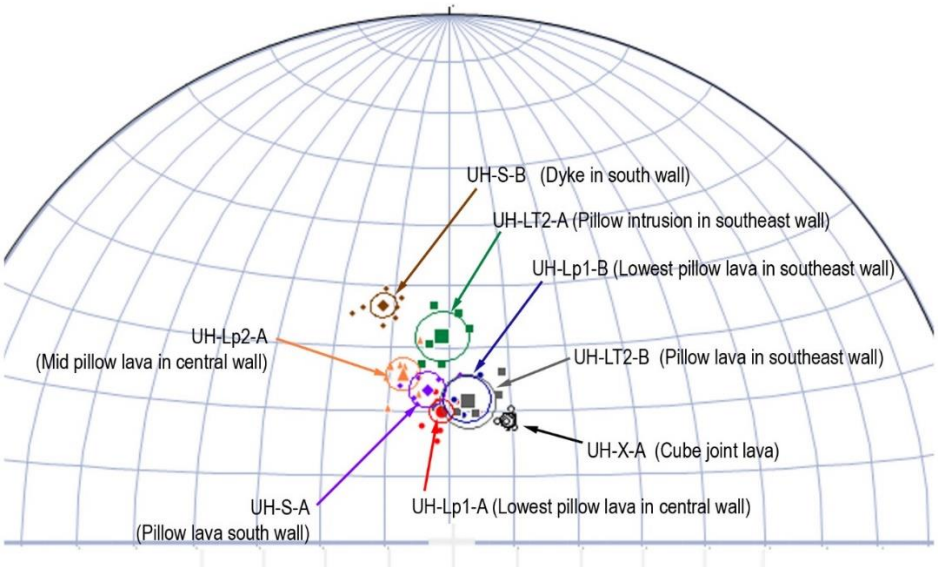

Figure L-8. Results for all sampling sites in Undirhlíðar on a stereonet diagram from the program Stereonet. Grid on the image is 10°.

This results could indicate some time gaps between different formations but more sampling is needed for any serious suggestion about that.

L4.3 Demagnetization process data

A clear pattern was visible when looking at the demagnetization process for the samples. Samples from the glassy outer edge of the pillows had much slower demagnetization process than other samples, see figures L-9 and L-11.

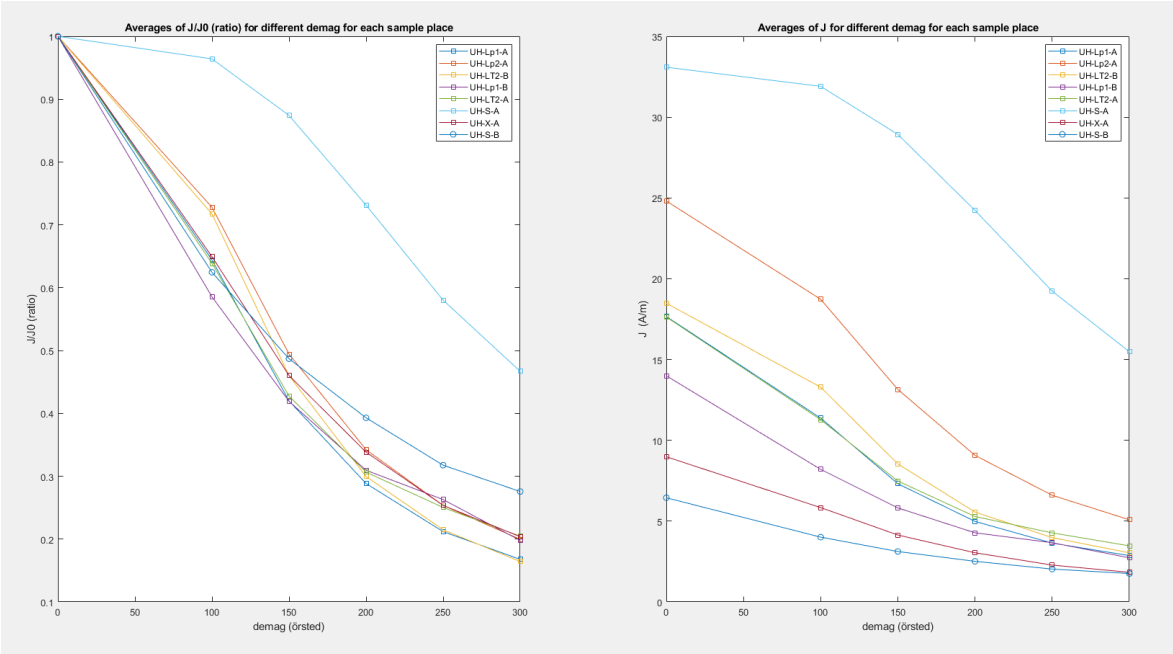

Figure L-9. The average demagnetization curves for all sampling sites in Undirhlíðar. Note how slowly the samples from UH-S-A demagnetizes.

Figure L-10. Sampling site UH-S-B from the glassy outer edge of a pillow. The samples from this sampling site showed much slower demagnetization than other samples in the research of Undirhlíðar.

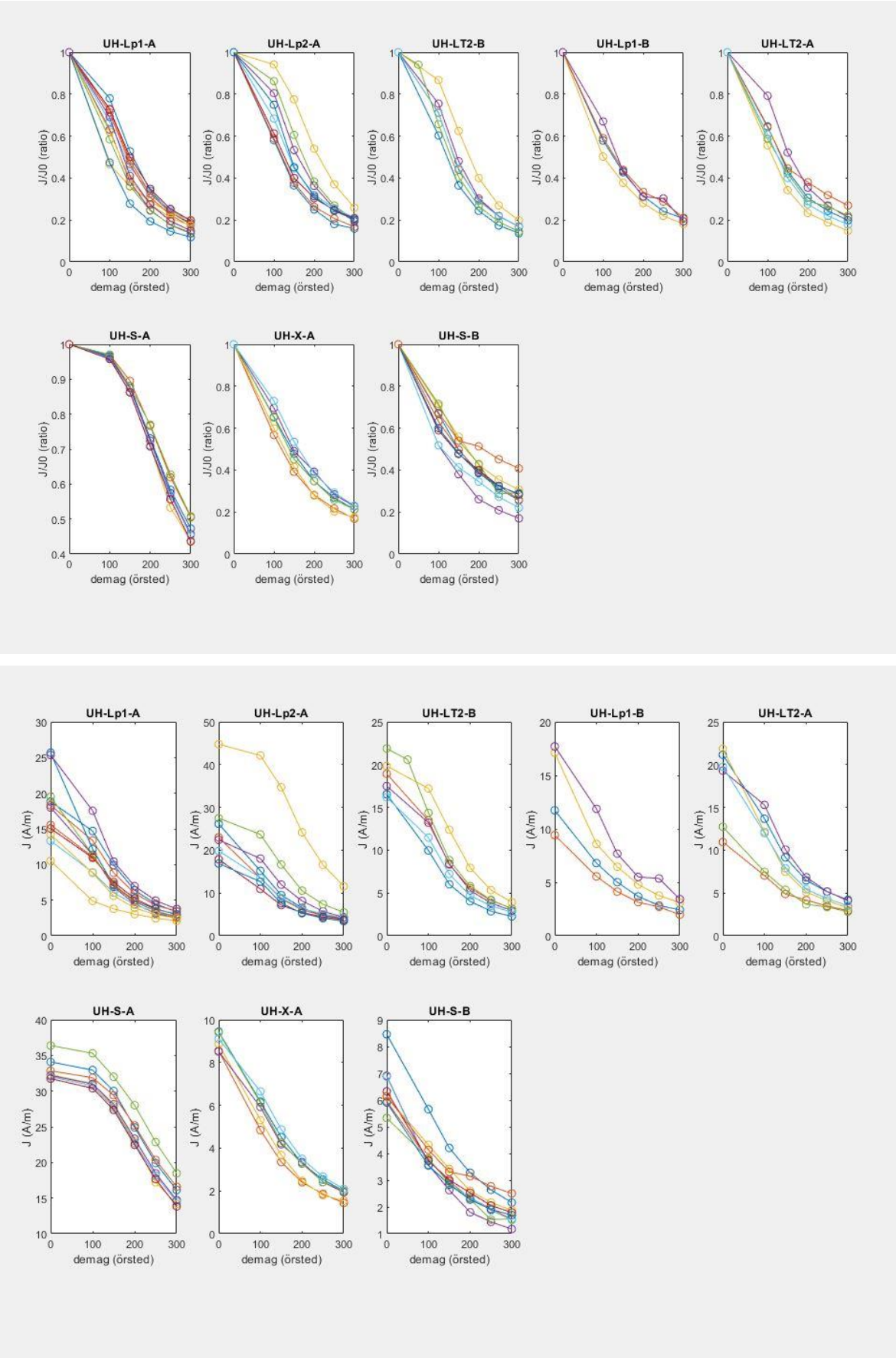

Figure L-12. Demagnetization processes for all samples in Undirhlíðar.

L5 Virtual geomagnetic poles

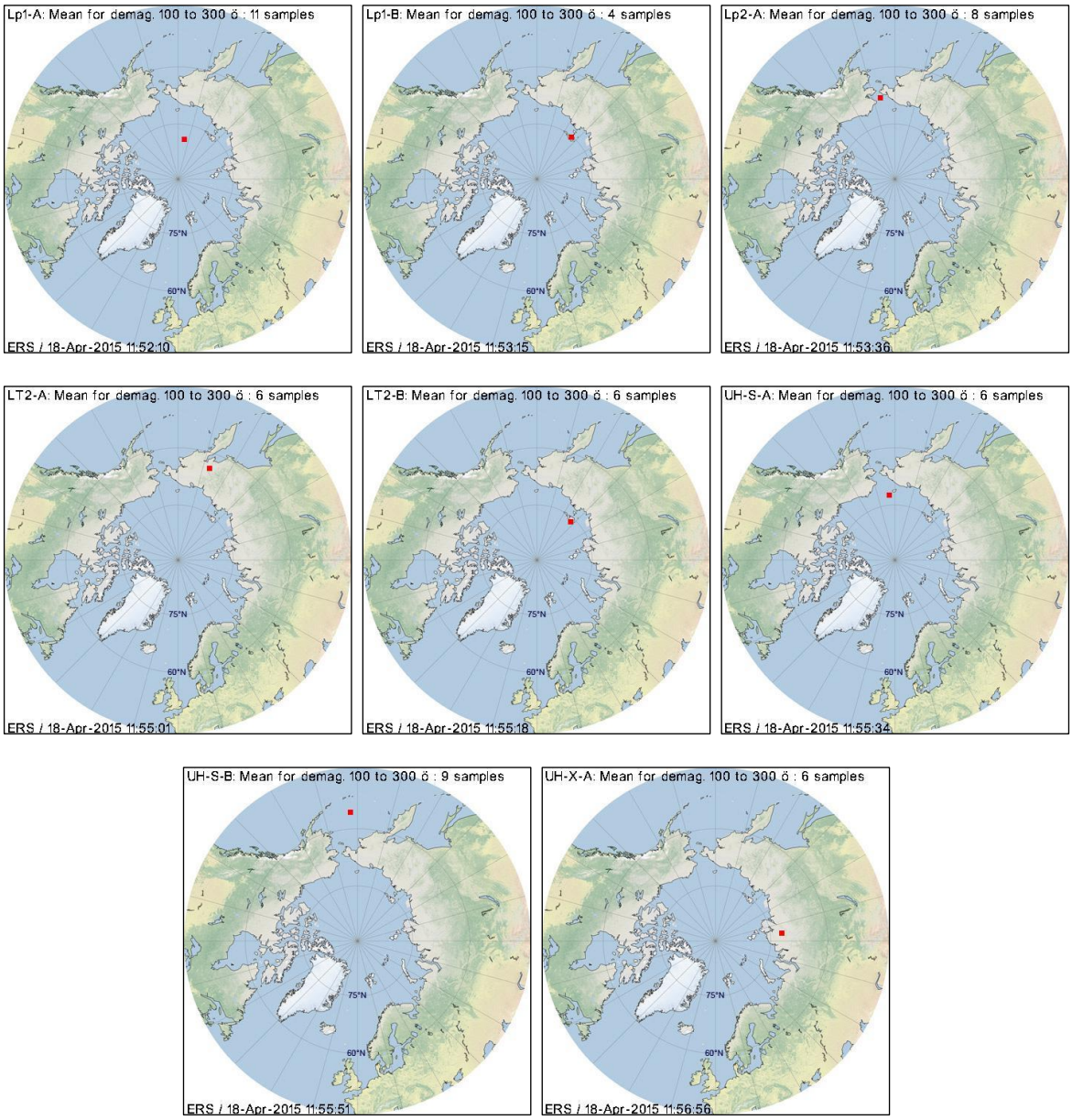

Figure L-13. Virtual geomagnetic pole, calculated from measured dipole field of the sampling sites in Undirhlíðar.